UNIVERSITY OF LONDON

Imperial College of Science and Technology

Department of Electrical Engineering

DESIGN OF IMPULSE-COMMUTATED THYRISTOR INVERTORS AND CALCULATION OF INDUCTION MOTOR PERFORMANCE UNDER VARIABLE SPEED OPERATION

Thesis submitted for the degree of

Doctor of Philosophy in Engineering

by

Sayeed Nurul Ghani

August 1968

ABSTRACT

This thesis describes the design of a three-phase variable-frequency thyristor invertor with single D.C-side impulse commutation, and the measurement and prediction of the performance of an invertor-fed induction motor. The motor performances when invertor fed and when fed from a sinusoidal source are compared.

The circuit configuration of the invertor is well known, but equations allowing design and parameter optimization have not been previously published. Such equations are derived and given in normalized form. The step-by-step design of an invertor according to a given specification is included.

Conventional no-load and locked-rotor tests were performed to enable evaluation of the induction motor equivalent circuit parameters which were used to predict the performance of the invertor-fed motor. The parameters were checked by performing load test with a variable-frequency sinusoidal excitation.

The induction motor losses under fixed-frequency sinusoidal excitation, calculated by known methods, are discussed, and extended to include the effects of airgap space harmonics on motor performance.

A known modification to the fixed-frequency conventional equivalent circuit enabling prediction of motor performance under variable-frequency fixed maximum torque operation, is given.

Because no prediction method for the motor performance including the effect of space harmonics under conditions of variable-frequency sinusoidal excitation had been published, the known variable frequency equivalent circuit was extended to account for space harmonics.

This equivalent circuit was further extended to include the effects of the time harmonics of the invertor supply. The effect of the invertor supply on the main flux path iron loss of the machine is also examined.

An original analysis, in the time domain, of the invertor-fed machine was carried out and the results are used for the invertor design.

ACKNOWLEDGMENTS

The investigation described in this thesis was carried out under the supervision of Mr. B.J. Cory, B.Sc. (Eng.), A.C.G.I., C. Eng., M.I.E.E., Senior Lecturer in Electrical Engineering, Imperial College of Science and Technology, London, S.W.7, and the author gratefully acknowledges his encouragement and guidance.

The author also expresses his gratitude to Mr. D.A.G. Pedder, M.Sc. (Eng.), D.I.C., C. Eng., M.I.E.E., for useful discussions and suggestions.

The author is very much indebted to the Kingston College of Technology, Kingston-upon-Thames, and especially to Mr. R.H. Ness, B.E.M. B.Sc. (Eng.), C. Eng., M.I.E.E., Head of the Department of Electrical Engineering for his encouragement and for allowing time for the preparation of this thesis.

Finally, the financial help given by The Burmah Oil Company is gratefully acknowledged.

INDEX

Abstract			2
Acknowledgments			4
Index			5
List of Symbols			14
CHAPTER 1	:	INTRODUCTION	31
		1.1. Basic electro-magnetic principles behind variable speed drives	31
		1.2. Methods of speed control	32
		1.2.1. Control of speed by variation of active voltage induced in a rotor winding	32
		1.2.2. Variable speed drive by field flux control	38
		1.2.3. Speed control through change of rotational speed of stator field	42
		1.3. The object of the investigation and the layout of the thesis	50
CHAPTER 2	:	THE INVERTOR	52
		2.1. Single D.C. side impulse commutated invertor	52
		2.2. Operation of the invertor	54
		2.3. Analysis of commutation circuit	58
		2.3.1. Bridge thyristor reverse bias time	63

2.3.2. Total commutation time t_c 67

2.3.3. Commutation circuit inductance and capacitance 68

2.3.4. Energy loss in the commutating line chokes 69

2.3.5. Peak flux-linkage of commutation chokes 70

2.3.6. Commutating thyristor i^2t_c rating 71

2.3.7. R.M.S. current of commutation thyristor 73

2.3.8. Average current of commutation thyristor 74

2.3.9. Power rating of auxiliary commutating supply 75

2.3.10 Commutation power supplied by the main D.C. supply 76

2.3.11 D.C. line clamping diode average current 77

2.4. Choice of commutation circuit parameter 77

2.4.1. Optimization for minimum commutation energy 78

2.4.2. Minimization of commutation choke flux-linkage 84

2.4.3. Choice of design variables 87

2.5. Capacity of supply reservoir capacitors 88

CHAPTER 3 : INVERTOR DESIGN 91

3.1. Specifications 92

3.2. Design of commutation circuit

3.2.1. Choice of the main supply voltage 92

3.2.2. Choice of auxiliary supply voltage 95

3.2.3. Commutation efficiency 97

3.2.4. Choice of inductance of D.C. line chokes 97

3.2.5. Choice of commutating capacity 98

3.2.6. Choice of capacity of supply reservoir capacitors 99

3.2.7. Total commutation time 101

3.2.8. Bridge thyristor reverse bias time 102

3.2.9. Choice of commutating thyristors 103

3.2.10 Choice of D.C. line diodes 105

3.3. Design of thyristor bridge 106

3.3.1. Voltage ratings of bridge thyristors 106

3.3.2. Current rating of bridge thyristors 107

3.4. Design of diode bridge 109

3.4.1. Voltage rating of bridge diodes 109

3.4.2. Current rating of bridge diodes 111

3.5. Protection of invertor 113

3.5.1. Transient over-voltage protection 113

3.5.2. Over-current protection 114

CHAPTER 4 : THE INDUCTION MOTOR AND EXPERIMENTAL DETERMINATION OF EQUIVALENT CIRCUIT PARAMETERS 118

4.1. Design details of the induction motor 118

4.2. Conventional constant frequency equivalent circuit 119

4.3. Variable frequency no-load test 122

4.4. Variable frequency locked rotor test 133

CHAPTER 5 : INDUCTION MOTOR LOSSES UNDER FIXED AND VARIABLE FREQUENCY SINUSOIDAL SUPPLY 142

5.1. Losses due to main flux 145

5.1.1. Hysteresis loss 145

5.1.2. Eddy-current loss 150

5.2. Stator copper loss 153

5.3. Rotor copper loss 153

5.3.1. Field harmonics in the airgap of induction motor 155

5.3.2. Extension of conventional fixed frequency equivalent circuit to include the effects of space harmonics 163

5.4. Losses due to slot openings 170

5.5. Variable frequency equivalent circuit accounting for space fundamental mmf only 173

5.6. Modification of the variable frequency equivalent circuit for constant maximum torque operation 181

5.7. Variable frequency supply voltage regulation 184

5.8. Performance calculations from variable frequency simple equivalent circuit 189

5.9. Variable frequency equivalent circuit for constant maximum torque operation accounting for space fundamental and space harmonic mmfs. 198

5.10. Performance calculations from variable frequency extended equivalent circuit 198

CHAPTER 6 : TIME HARMONIC ANALYSIS OF INVERTOR-FED INDUCTION MOTOR 203

6.1. Iron loss in the main flux path 204

6.1.1. Hysteresis loss 206

6.1.2. Eddy current loss 210

6.2. Effect of stator connection in star or delta on iron losses 212

6.3. Variable frequency equivalent circuit representing the contribution of arbitrary time harmonics on motor performance taking into account the space fundamental mmf only 214

6.4. Performance calculations for time harmonics and space fundamental mmf. 218

6.5. Equivalent circuit representing the contribution of time harmonics on motor performance taking into account the fundamental and higher space harmonics 223

6.6. Performance calculations taking into account the time fundamental and time harmonics of supply and space fundamental and space harmonics of machine air-gap mmf 223

CHAPTER 7 : TIME DOMAIN ANALYSIS OF INVERTOR-FED INDUCTION MOTOR 235

7.1. Assumptions 236

7.2. Representation of machine and machine equations 237

7.2.1. Representation of machine along the three-phase spatial rotor and stator holonomic reference frame (α frame; RYB and ryb) 237

7.2.2. Representation of machine along stator DQO and rotor dqo axes (α' frame) 238

7.2.3. Representation of machine along non-holonomic forward and backward revolving FBO and fbo axes (α'' frame) 248

7.3. Elimination of rotor axes 250

7.4. Evaluation of stator and rotor current along α' frame 258

7.5. The differential equations for currents 263

7.6. Evaluation of electro-magnetic torque 268

7.7. Generalization of the differential equations given stator and rotor sequence currents 270

7.8. Effect of stator connection (star or delta) on iron loss due to main flux 276

CHAPTER 8 : INDUCTION MOTOR LOAD TESTS 285

8.1. Windage and friction loss of the induction and D.C. loading motor 285

8.2. Variable frequency load test under sinusoidal excitation 286

8.2.1. Variation of stator current with slip for various constant values of supply frequency 290

8.2.2. Electro-magnetic power output 291

8.2.3. Electro-magnetic torque developed 293

8.2.4. Electric power input 296

8.2.5. Total electro-magnetic loss 296

8.2.6. Electro-magnetic efficiency 300

8.3. Variable frequency load test under invertor operation 300

8.3.1. Variation of stator current with slip for various constant values of supply frequency 303

8.3.2. Electro-magnetic torque developed 304

8.3.3. Electro-magnetic power output 338

8.3.4. Electric power input 338

8.3.5. Total electro-magnetic loss 344

8.3.6. Electro-magnetic efficiency 350

CHAPTER 9 : GENERAL CONCLUSIONS AND DISCUSSIONS 351

9.1. Applicability of the Invertor Design Equations to Other Types of Impulse-commutated Invertors 351

9.2. Performance Prediction and Measurement of the Motor when excited from sinusoidal source 354

9.3. Performance Prediction and Measurement of Invertor-fed Induction Motor 357

9.4. Torque Fluctuation of Invertor-fed Induction Motor 364

9.5. Bridge Thyristor and Bridge Diode Conduction Angle 365

9.6. Bridge Thyristor and Bridge Diode Peak Current 365

9.7. Considerations of Design for Invertor-fed Induction Motors 366

9.8. Further Discussions 367

9.9. Further Work 369

9.10. Final Summary 370

APPENDIX I : SOLUTION OF THE MACHINE DIFFERENTIAL EQUATION 373

AI.1. Response due to direct axis excitation only 373

AI.2. Response due to quadrature axis excitation only 381

APPENDIX II : HARMONIC ANALYSIS OF IDEALIZED INVERTOR OUTPUT VOLTAGE 384

AII.1. Line to line voltage 384

AII.2. Line to neutral voltage 386

AII.3. R.M.S. value of the idealized line to line voltage in terms of its step height 388

AII.4. R.M.S. value of the idealized line to line voltage in terms of the r.m.s. value of its time fundamental 388

AII.5. Average value of the idealized invertor line to line voltage in terms of its step height 389

AII.6. Form factor of idealized invertor line to line voltage 389

AII.7. R.M.S. value of invertor idealized line to neutral voltage in terms of line to line voltage step 389

AII.8. R.M.S. value of invertor idealized line to neutral voltage in terms of its time fundamental R.M.S. value 390

AII.9. Average value of invertor idealized line to neutral voltage in terms of idealized line to line voltage step 390

AII.10. Form factor of idealized invertor line to neutral output voltage. 391

REFERENCES : 392

SYMBOLS

Symbols are listed as they appear in the text.

CHAPTER 2

Th_1, Th_2, Th_3 .... Th_6	are the six bridge thyristors
Th_7 and Th_8	are the two commutation thyristors
D_1, D_2, D_3 .... D_6	are the six bridge diodes
D_7 and D_8	are the two D.C. line diodes
L_1 and L_2	are the two D.C. line chokes
C_A and C_B	are the two main supply reservoir capacitors
C_C and C_D	are the two auxiliary supply reservoir capacitors
C_3	is the commutating capacitor
V_1	is the main D.C. supply voltage
V_2	is the auxiliary D.C. supply voltage
I_o	is the current flowing in the thyristor bridge at the instant of commutation
t_o	is the bridge thyristor reverse bias time
t_c	is the total commutation time
I_p	is the peak current attained in the D.C. line chokes during commutation
r_1 and r_2	are the resistance of the D.C. line chokes

w_o	is the natural angular frequency of the commutation circuit
α	is the damping constant of the commutation circuit
w	is the damped angular frequency of the invertor at the instant of commutation
τ_c and τ_1	are the two commutation circuit time constants
x and k	are the invertor commutation circuit independent variables
$v_{c_3}(t)$	instantaneous voltage across the commutation capacitor
$v_{Xn}(t)$	instantaneous voltage of point X with respect to neutral n
$f_1(x, k)$	bridge thyristor reverse bias time function
$f_2(x, k)$	commutation energy loss function
$f_3(x, k)$	D.C. line choke peak flux linkage function
$f_4(x, k)$	D.C. line choke inductance function
$f_5(x, k)$	commutating capacity function
$f_6(x, k)$	commutating thyristor i^2t function
$C_{I_{RMS}}$	r.m.s. value of commutating thyristor current
f	frequency of invertor output voltage
$f_7(x, k)$	commutating thyristor r.m.s. current function

$C_{I_{AV}}$	average value of commutating thyristor current
f_8 (x, k)	commutating thyristor average current function
P_{CA}	auxiliary D.C. supply power rating
f_9 (x, k)	auxiliary D.C. supply power function
P_{CM}	commutation power supplied by the main D.C. supply
f_{10} (x, k)	main D.C. supply commutation power function
$D_{I_{AV}}$	average current of D.C. line clamping diodes
f_{11} (x, k)	D.C. line diode average current function
Q_C	charge delivered by the supply reservoir capacitors during commutation
$\frac{\Delta V}{V}$	allowable D.C. supply per unit variation during commutation

CHAPTER 3

$\hat{V}_{INV}$	the amplitude of idealized line to line invertor output voltage
$V_{1\ INV}^{RMS}$	r.m.s. value of time fundamental component of line to line invertor output voltage
P_{MAIN}	main D.C. supply power rating
η_{INV}	invertor efficiency
η_M	induction motor efficiency

CHAPTER 4

V_f	sinusoidal stator line to neutral supply voltage of frequency f
R_1	stator resistance
R_2	rotor resistance
X_{1f}	stator leakage reactance at frequency f
X_{2f}	rotor leakage reactance at frequency f
X_{Mf}	magnetizing reactance at frequency f
R_{Mf}	main flux path iron loss simulating resistance at frequency f
E_{gf}	air-gap voltage at frequency f
S	slip of rotor
P	number of poles
$NL_{P_{in}}$	stator power input under no load condition (at zero rotor slip)
I_{NL}	no load stator input current (zero rotor slip)
$P_{h.e}$	hysteresis and eddy current loss in main flux path
$\emptyset_{NL}$	no load (zero rotor slip) input power factor angle
V_{bl}	locked rotor stator line to neutral voltage at frequency f
I_{bl}	locked rotor stator input current at frequency f

R_{blf}	locked rotor input resistance at frequency f
X_{blf}	locked rotor input reactance at frequency f
P_{bl}	locked rotor input power
Z_{blf}	locked rotor input impedance at frequency f
l_1	stator leakage inductance
l_2	rotor leakage inductance
L_M	magnetizing inductance
N_s	synchronous speed in R.P.M.

CHAPTER 5

W_h	hysteresis loss
η_h, a, b	hysteresis loss coefficients
n	hysteresis loss exponent
B_m	flux density
A	area of flux path
R_h	hysteresis loss simulating resistance
ϕ_m	peak value of main flux
K_f	form factor of air-gap voltage
N_1	number of stator twins per phase
Kw_1	stator winding factor for space fundamental air-gap mmf
R_{h50}	hysteresis loss simulating resistance at 50 Hz

W_{h50}	hysteresis loss at 50 Hz
W_e	eddy current loss in main flux path
ρ_e	resistivity of the material in which eddy current flows
δ	thickness of laminations
R_e	eddy current loss simulating resistance
W_{e50}	eddy current loss in main flux path at 50 Hz
F_1	amplitude of space fundamental mmf
K_{d1}	winding distribution coefficient for space fundamental mmf
q_1	number of stator slots per pole per phase
K_{y1}	winding pitch factor coefficient for space fundamental mmf
y	winding pitch expressed as a fraction of full pitch
τ	space fundamental pole pitch
ν	order of stator space harmonic
K_1, K_2	any positive integer including zero
K_{1z}, K_{2z}	any positive integer excluding zero
ν_z	order of slot harmonics
S_1	stator slots
ν_b	order of belt harmonics
$K_{w\nu_b}$	winding distribution factor for ν_b^{th} space harmonic

$K_{y\nu_b}$	winding pitch factor for ν_b^{th} space harmonic
$K_{d\nu_z}$	winding distribution factor for ν_z^{th} space harmonic
$K_{y\nu_z}$	winding pitch factor for ν_z^{th} space harmonic
μ	order of rotor mmf space harmonics
q_2	number of rotor slots per pole per phase
S_2	total number of rotor slots
S_ν	slip of rotor with respect to ν^{th} stator field harmonic
R_M	core loss analogue resistance at normal supply frequency
$X_{M\nu}$	magnetising reactance due to ν^{th} space harmonic at normal supply frequency
$R_{2\nu}$, $X_{2\nu}$	rotor resistance and leakage reactance corresponding to ν^{th} space harmonic at normal supply frequency
$X_{M\nu_b}$	magnetising reactance corresponding ν_b^{th} belt harmonic at normal supply frequency
$X_{M\nu_z}$	magnetizing reactance corresponding to ν_z^{th} slot harmonic at normal supply frequency
p_s	half the amplitude of air-gap permeance variation
p_o	average value of air-gap permeance variation

$X_{2d\nu}$	differential harmonic leakage corresponding to ν^{th} space harmonic at normal supply frequency
K_{sdl}	a correction factor
$X_{sk\nu}$	skew leakage reactance for ν^{th} space harmonic
$K_{sk\nu}$	skew factor for ν^{th} space harmonic
τ'	pitch of the fundamental poles in terms of rotor slots
c'	pitch of rotor slots with respect to stator slots
$R_{2\nu}$	rotor resistance for ν^{th} space harmonic referred to stator
$R_{2\nu_b}$	rotor resistance for $\nu_b{}^{th}$ belt harmonic referred to stator
$R_{2\nu_z}$	rotor resistance for ν^{th} slot harmonic referred to stator
X_{2Sf}	stator referred rotor leakage reactance at slip frequency sf
E_{gn}	air-gap voltage at any normal frequency fn
E_{2Sf}	stator referred rotor induce voltage of slip frequency sf
I_1	stator current
I_2	rotor current referred to stator
I_m	magnetizing current
	ratio of any frequency to normal frequency

Z_1	stator leakage impedance
Z_2	stator referred rotor leakage impedance
Y_M	magnetizing admittance
m_2	number of rotor phases
N_{ns}	normal frequency synchronous speed
m_1	number of stator phases
P_{2in}	rotor input power
P_{cu2}	rotor copper loss
P_{2o}	rotor power output
P_{FE}	core loss
P_{cu1}	stator copper loss
T	electro-magnetic torque
$I_{2\nu}$	rotor current due to ν^{th} space harmonic
$P_{2in\ \nu}$	ν^{th} space harmonic rotor power input
$P_{cu2\nu}$	ν^{th} space harmonic rotor copper loss
$P_{2o\nu}$	ν^{th} space harmonic rotor power output
T_ν	electro-magnetic torque produced by ν^{th} space harmonic

CHAPTER 6

γ	order of time harmonics
$E_{g(non\sim)}$	r.m.s. value of non-sinusoidal air-gap voltage
E_{g1}	r.m.s. value of the time fundamental component of non-sinusoidal air-gap voltage
$W_{h(non\sim)}$	hysteresis loss due to non-sinusoidal excitation
$R_{h(non\sim)}$	hysteresis loss simulating resistance under non-sinusoidal excitation
C	a constant relating $E_{g(non\sim)}$ and E_{g1}
$W_{h(INV)}$	hysteresis loss under invertor operation
$W_{h(\sim)}$	hysteresis loss under sinusoidal excitation
$R_{h50(\sim)}$	hysteresis loss simulating resistance at 50 Hz sinusoidal excitation
$R_{h(INV)}$	hysteresis loss simulating resistance under invertor operation
$W_{e(non\sim)}$	eddy current loss under non-sinusoidal excitation
$W_{e50(\sim)}$	eddy current loss at 50Hz under sinusoidal excitation
V_{γ}	r.m.s. value of γ^{th} time harmonic of supply line to neutral voltage

$W_{hf(non\ \sim)}$	hysteresis loss at any frequency f under non-sinusoidal excitation
$E_{gf(non\sim)}$	r.m.s. air-gap voltage at any frequency f under non-sinusoidal excitation
$E_{gf\gamma}$	r.m.s. value of γ^{th} time harmonic of air-gap voltage at any frequency f
$R_{Mf(non\sim)}$	iron loss simulating resistance under non-sinusoidal excitation of frequency f
$R_{M\gamma}$	analogue iron loss simulating resistance for γ^{th} time harmonic
$R_{M(INV)}$	analogue iron loss simulating resistance under invertor operation at normal supply frequency
$Z_{1\gamma}$	analogue stator impedance to γ^{th} time harmonic
$Z_{2\gamma}$	analogue rotor impedance to γ^{th} time harmonic
$Y_{M\gamma}$	analogue admittance to γ^{th} time harmonic
$E_{g\gamma}$	γ^{th} time harmonic r.m.s. value of air-gap line to neutral analogue voltage
$I_{2\gamma}$	stator referred γ^{th} time harmonic r.m.s. rotor current
$I_{M\gamma}$	γ^{th} time harmonic magnetizing current
$I_{1\gamma}$	γ^{th} time harmonic stator current

$P_{2in\gamma}$	γ^{th} time harmonic rotor power input
$P_{cu2\gamma}$	γ^{th} time harmonic rotor copper loss
$P_{2o\gamma}$	γ^{th} time harmonic rotor output power
$P_{FE\gamma}$	γ^{th} time harmonic core loss
$P_{cu1\gamma}$	γ^{th} time harmonic stator copper loss
VA_{γ}	γ^{th} time harmonic stator volt-ampere input
T_{γ}	γ^{th} time harmonic electro-magnetic torque
$S_{\gamma\nu}$	slip of the rotor to ν^{th} space harmonic produced by γ^{th} time harmonic
$I_{2\gamma\nu}$	rotor ν^{th} space harmonic current due to γ^{th} time harmonic
$P_{2in\gamma\nu}$	ν^{th} space harmonic rotor power input due to γ^{th} time harmonic
$P_{cu2\gamma\nu}$	ν^{th} space harmonic rotor copper loss due to γ^{th} time harmonic
$P_{2o\gamma\nu}$	ν^{th} space harmonic rotor power output due to γ^{th} time harmonic
$T_{\gamma\nu}$	electro-magnetic torque produced by γ^{th} time and ν^{th} space harmonic

CHAPTER 7

α, α', α^{*}	three different machine reference frames
$Z_{\alpha'}$	machine impedance tensors for α' reference frame

$\hat{L_V}_{INV}$	peak value of idealized line to line invertor output voltage
$\hat{P_V}_{INV}$	peak value of idealized line to neutral invertor output voltage
$INV_{v_{RY}}$, $INV_{v_{YB}}$, $INV_{v_{BR}}$	instantaneous invertor three phase line to line output voltages
$INV_{v_{RN}}$, $INV_{v_{YN}}$, $INV_{v_{BN}}$	instantaneous invertor three phase line to neutral voltages
v_R, v_Y, v_B, v_r, v_y, v_b	instantaneous voltages impressed on stator R, Y, B and rotor r, y, b coils of α reference frame
v_D, v_Q, v_d, v_q	instantaneous voltages impressed on stator D, Q and rotor d, q coils of α' reference frame
i^R, i^Y, i^B, i^r, i^y, i^b	instantaneous currents flowing in stator R, Y, B and rotor r, y, b coils of α reference frame
i^D, i^Q, i^d, i^q	instantaneous currents flowing in stator D, Q and rotor d, q coils of α' reference frame
v_F, v_B, v_f, v_b	instantaneous voltages impressed on stator F, B and rotor f, b coils of α'' reference frame
i^F, i^B, i^f, i^b	instantaneous currents flowing in stator F, B and rotor f, b coils of α'' reference frame

$Y^{3\alpha''}$	machine reference frame admittance tensors for α'' reference frame
$C^{\alpha'}_{\alpha''}$	transformation tensors relating quantities to α' quantities α''
$v_{\alpha''}$	voltage along α'' reference frame
$v_{\alpha'}$	voltage along α' reference frame
$Z_{\alpha'\beta''}$	machine impedance tensors along α'' reference frame
$i^{\alpha''}$	machine currents along α'' reference frame
M	stator rotor mutual inductance
L_s	stator self inductance
L_r	rotor self inductance
p	d/dt
$p\theta = w_r$	rotor angular velocity
$B_{\alpha''}$	the air-gap flux density along α'' reference frame
$G_{\alpha''\beta''}$	torque tensors
τ_s	stator time constant
τ_r	rotor time constant
σ	leakage factor
B_F, B_B, C_F, C_B, D_F, D_B, K_s, D_f, K_r, B, C, D, K	are the various constants

CHAPTER 8

V_A	D.C. voltage across the armature of the loading machine
I_A	D.C. current flowing in the armature of the loading machine
R_A	resistance of D.C. loading machine armature
P_{W+F}	windage and friction loss of the induction motor and the loading D.C. machine
N	rotor speed in R.P.M.

APPENDIX I

R_a, R_b	roots of the differential equation
$V_{DO}(s)$	Laplace transform of direct axis axis voltage for one cycle only
$I_D(s)$	Laplace transform of direct axis current
$I_{DO}(s)$	Laplace transform of direct axis current for one cycle only
$A_D(s)_{s = R_a}$, $A_D(s)_{s = R_b}$	principle terms of the Laurant's expansion about the poles $s = R_a$ and $s = R_b$ (for direct axis)
$A_D(s)_{s = R_a, R_b}$	sum of $A_D(s)_{s = R_a}$ and $A_D(s)_{s = R_b}$ (for direct axis)
K_D	height of direct axis voltage step
T	period of invertor output voltage

$T_{DO}(s)$	a factor which relates the wave-form of direct axis exciting voltage for one cycle
A_1, B_1, C_1	residues of Laurant's expansion
$H(s)$	impulse response
$V_{QO}(s)$	Laplace transform of quadrature axis voltage for one cycle only
$I_Q(s)$	Laplace transform of quadrature axis current
$I_{QO}(s)$	Laplace transform of quadrature axis current for one cycle only
K_Q	height of each step of quadrature axis voltage
$T_{QO}(s)$	a factor which relates the wave-form of direct axis exciting voltage
$A_Q(s)_{s = R_a}$, $A_Q(s)_{s = R_b}$	principle terms of the Laurant's expansion about the poles $s = R_a$ and $s = R_b$ (for quadrature axis)
$A_Q(s)_{s = R_a, R_b}$	sum of $A_Q(s)_{s = R_a}$ and $A_Q(s)_{s = R_b}$

APPENDIX II

θ	angle
b_1, b_2, b_3 .... b_7	coefficients of the fourier expansion
$L_{V_{INV}}^{RMS}$	r.m.s. value of line to line invertor output voltage
$L_{V_{1\ INV}}^{RMS}$	r.m.s. value of the time fundamental component of invertor output voltage

$L_{V_{INV}}^{AV}$	average value of invertor line to line output voltage
$L_{K_{f\ INV}}$	form-factor of invertor line to line output voltage
$P_{V_{INV}}^{RMS}$	r.m.s. value of line to neutral invertor output voltage
$P_{V_{1\ INV}}^{RMS}$	r.m.s. value of the time fundamental component of invertor line to neutral output voltage
$P_{V_{INV}}^{AV}$	average value of invertor line to neutral output voltage
$P_{K_{f\ INV}}$	form-factor of invertor line to neutral output voltage

CHAPTER 1

INTRODUCTION

In recent years there has been a rapid increase in demand for variable speed electrical drives in almost all industries and public services. Although many different arrangements utilizing various types of machine have been devised in order to obtain variable speed drive, most are based on a few fundamental principles of electro-mechanical energy conversion.

It is considered appropriate, therefore, that a brief review of the methods by which speed control may be achieved with electrical machines should be given.

1.1 Basic Electro-magnetic Principles behind Variable Speed Drives

The basic principles on which the speed variation of electrical machines depend are

(a) The voltage applied to any machine winding must balance both the active and the passive voltage of the winding.

(b) The active voltage generated in a rotor winding is proportional to the flux penetrating the winding and the relative speed of the winding to the flux.

This active voltage is popularly termed the back emf.

Back emf = machine constant x flux x relative speed.

The machine constant contains the design terms such as number of poles, number of rotor conductors, etc. (The only exception is the pole-change motor.)

The above equation indicates that speed variation can be obtained by controlling individually or by any suitable combination the following three quantities :

1) Machine constant.

2) Flux.

3) Back emf.

1.2 Methods of Speed Control

The various well known methods of speed control will now be reviewed in light of the basic electro-magnetic principles stated in section 1.1.

1.2.1 Control of Speed by Variation of Active Voltage induced in a Rotor Winding

There are two basic methods of varying the voltage induced in a rotor winding, (a) resistance regulation, and (b) regulation of the voltage applied to the rotor from an external source of supply.

(a) Resistance regulation

In this method external resistance is introduced in the rotor circuit so that flow of current through this resistance creates a passive voltage drop and hence brings about a change in the voltage induced in the rotor. This method of speed control as applied to a D.C. and an A.C. motor is shown in figures 1.1 and 1.2. The speed-torque characteristics for this method of speed control are shown in figure 1.14.

Although simple this method suffers from certain disadvantages. A power loss proportional to the reduction of speed occurs in the resistance. Any change in current causes a change in the passive voltage drop in the resistance, amounting to the change in speed. This method therefore suffers from large speed variation with load.

Resistance regulation has limited application. It is used intermittently for crane motors and for traction. It also finds application in controlling currents and torques, where high efficiency is not of prime importance.

(b) Regulation of voltage applied to the rotor from an external source of supply

In this method an external voltage, nearly independent of current, is applied to the rotor. A

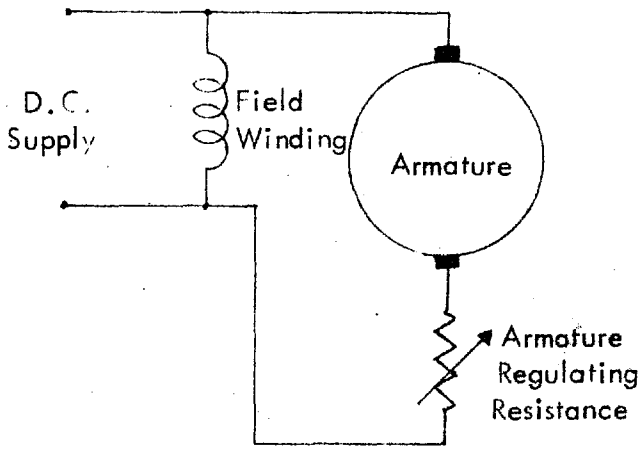

igure 1.1 Speed Variation By Rotor Resistance:- D.C. Motor.

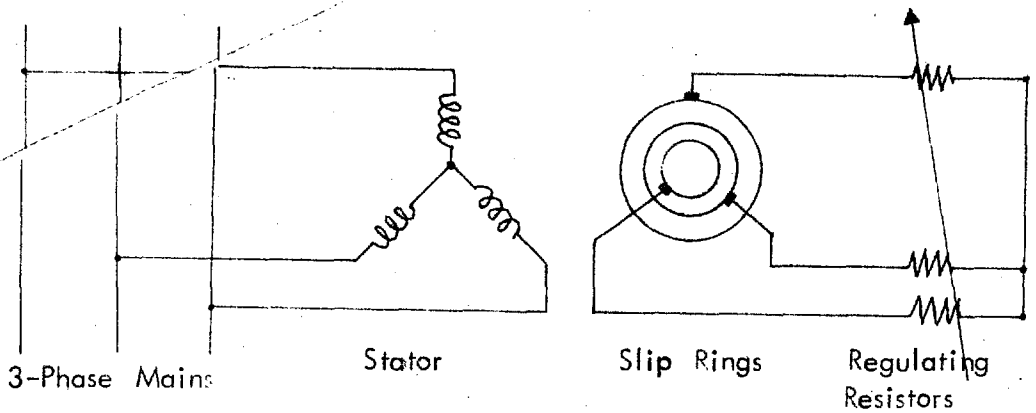

A.C. Slip Ring Machine

Figure1.2 Speed Variation By Rotor Resistance:- A.C. Slip Ring Machine.

machine controlled this way exhibits a constant torque-speed characteristic. Once the speed of operation has been selected loading has little effect on speed.

Four schemes, two for D.C. machines and two for A.C. machines, in which this method is applied are shown in figures 1.3 to 1.6.

Figure 1.3 shows the popular Ward-Leonard system using three phase as the main supply. The A.C. driving motor is mechanically coupled to a D.C. exciter and a D.C. generator. The D.C. generator output voltage is varied by control of field current. The variable output voltage of the generator is fed to the armature of the variable speed D.C. motor.

Figure 1.4 shows a variation of the Ward-Leonard system where the main supply voltage is unidirectional. This system employs positive and negative booster so connected that it either adds or subtracts its voltage from the main D.C. supply and the resultant variable D.C. voltage is applied across the variable speed D.C. motor armature.

Figure 1.5 shows the application of this method to a three-phase slip ring machine. Since the voltage at the slip rings has, (in general), a frequency different from that of the main supply, a variable frequency convertor

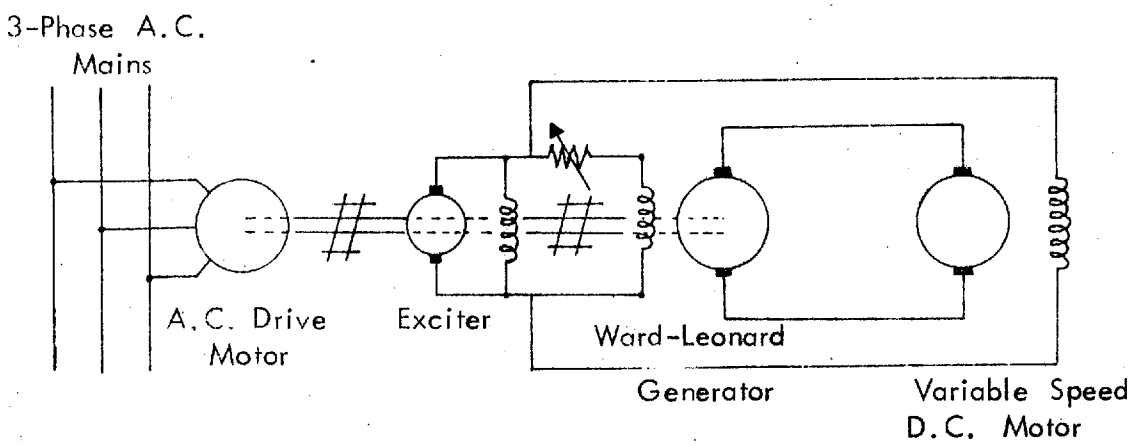

Figure 1.3 Ward-Leonard Variable Speed Drive:- Main Power Supply A.C.

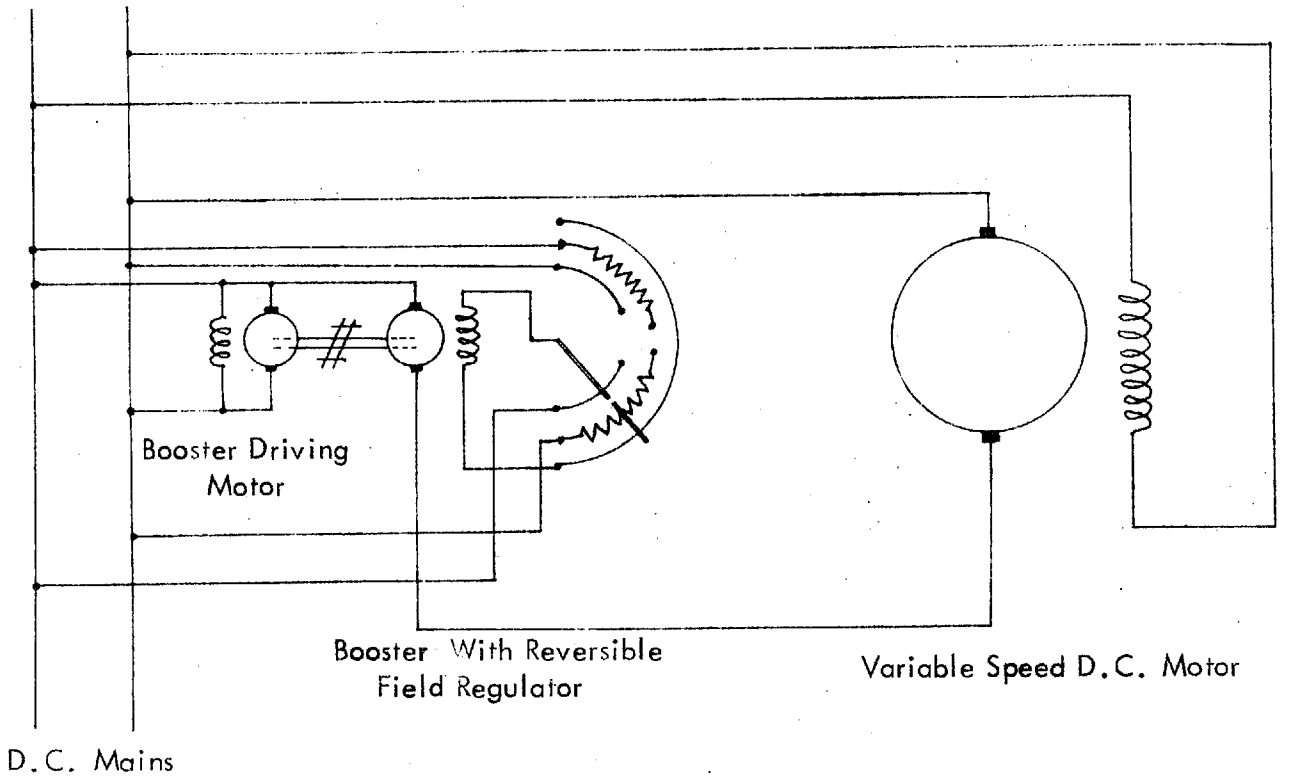

Figure 1.4 Ward-Leonard Variable Speed Drive:- Main Power Supply D.C.

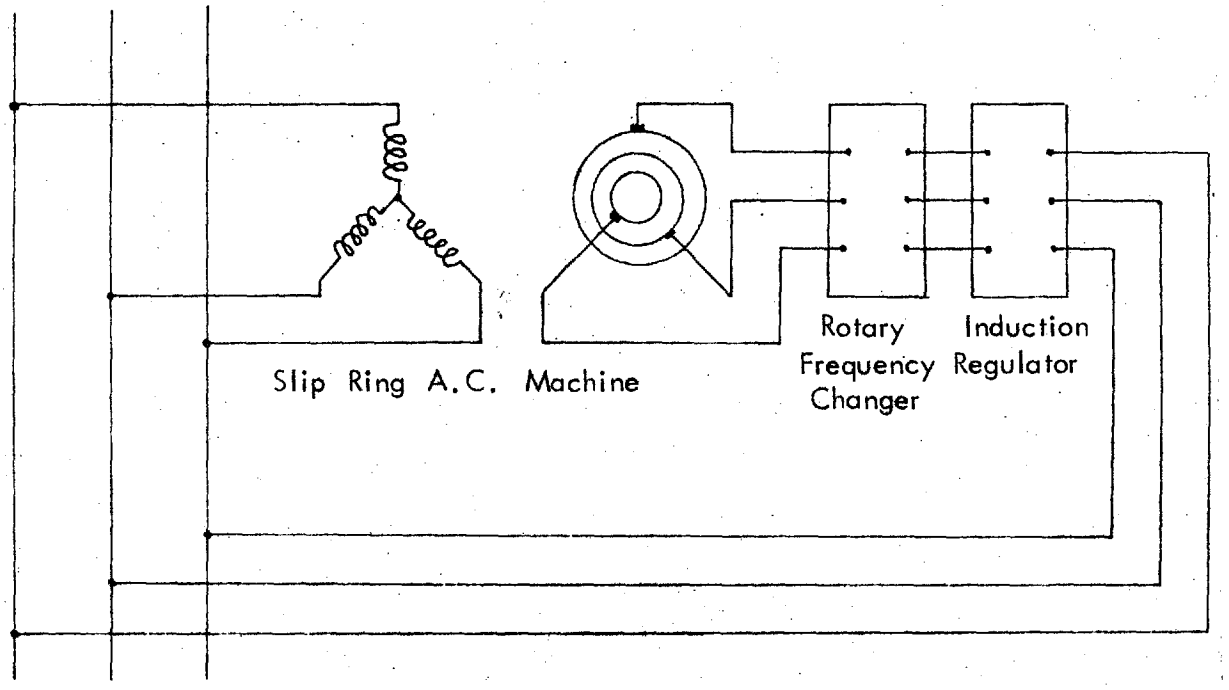

Figure 1.5 Speed Variation By Rotor Voltage Injection:- Slip Ring Machine

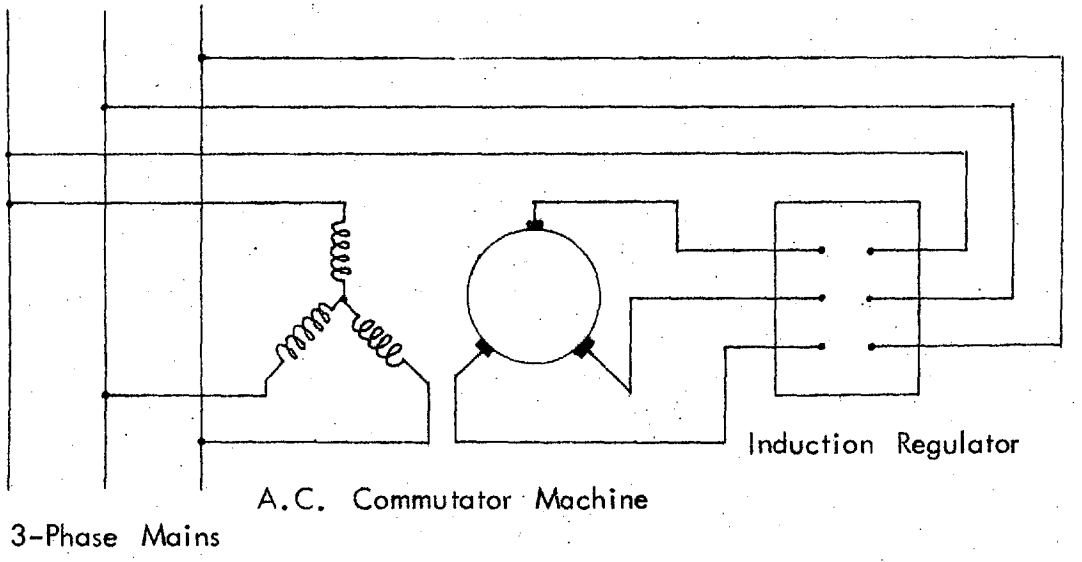

Figure 1.6 Speed Variation By Rotor Voltage Injection:- A.C. Commutator Machine.

and a variable voltage source are required to impart variable speed to the slip ring machine. Among several other alternatives, a Scherbius machine may be used for the frequency convertor.

The requirement of an additional rotating machine has caused the decline of this method for speed control which in practice is restricted to very large sets.

Replacement of slip rings by a commutator converts the variable rotor frequency to the supply frequency. Speed control of A.C. machines with commutators can be achieved by feeding the brushes with variable voltage of supply frequency.

This system, as shown in figure 1.6, has a shunt torque-speed characteristic and is widely used.

The speed-torque characteristics of this method of speed control are shown in figure 1.15.

1.2.2. Variable speed drive by field flux control

Application of this principle to series field (D.C. and A.C. motors) and shunt field (D.C. and A.C. motors) will be discussed.

(a) Series field motors

Figure 1.7 shows a simple D.C. series motor with a variable resistance connected in shunt with the field

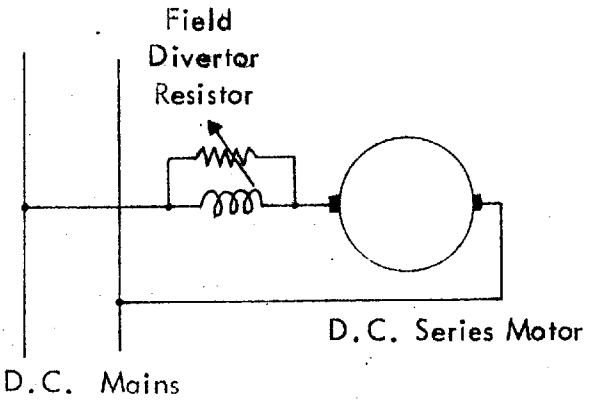

Figure 1.7 Speed Control By Field Flux Variation:- D.C. Series Motor.

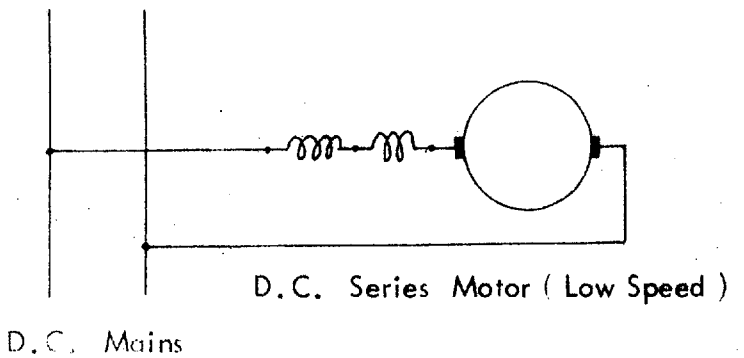

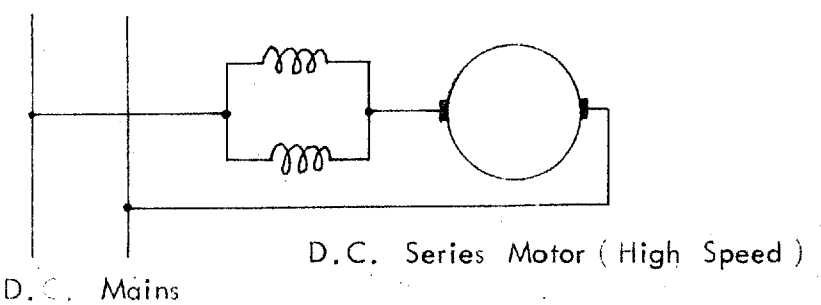

Figure 1.8 Speed Control By Field Flux Variation:- D.C. Series Motor.

winding. Adjustment of this resistance, popularly known as diverter resistance, causes the field flux to decrease and the speed to increase.

Figure 1.8 shows another method of speed control where arrangements are made for connecting the field coils, in series, for low speeds, and in parallel, for high speeds.

The armature winding of a D.C. series motor is usually designed to allow the full supply voltage to be applied to it. In the case of A.C. motors (Figure 1.9) it is in general necessary to couple the stator and the rotor winding through a transformer. For a given turns ratio of the transformer the currents in the rotor and the stator is always proportional.

Speed control is obtained by adjustment of phase position between stator and rotor current which is achieved by the brush gear shift.

If the intermediate transformer is replaced by an induction regulator, it is possible to obtain speed control without resorting to brush shift.

The speed-torque characteristics of such methods of speed control are shown in figure 1.16.

(b) Shunt motors

Adjustment of the field current of a D.C. shunt

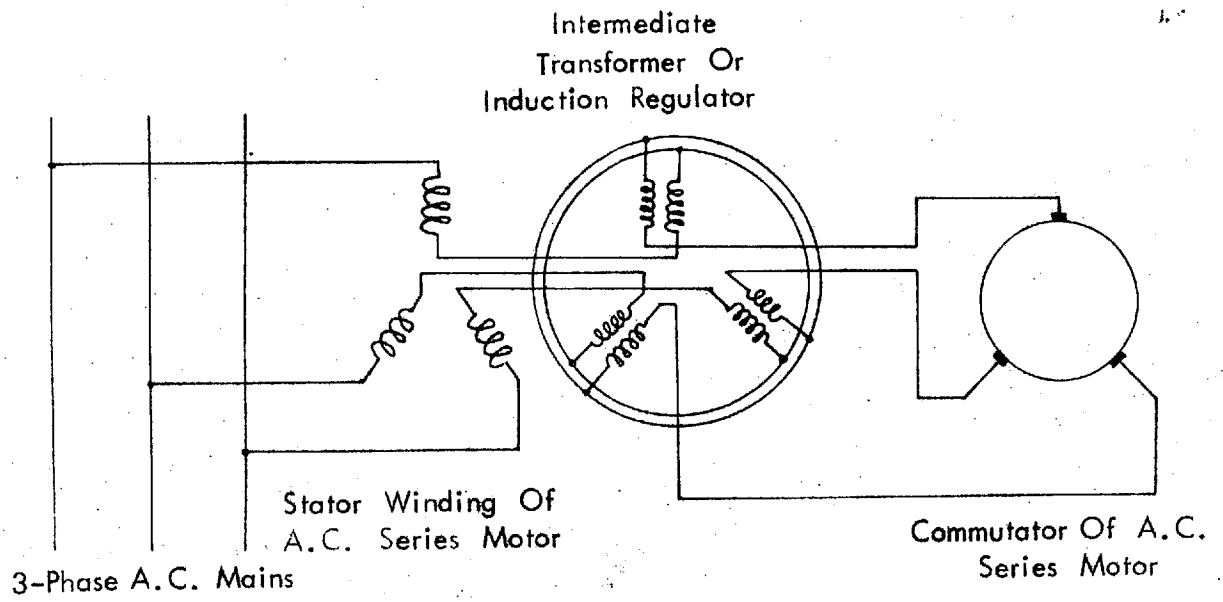

Figure 1.9 Speed Variation By Field Flux Control:- A.C. Series Motor.

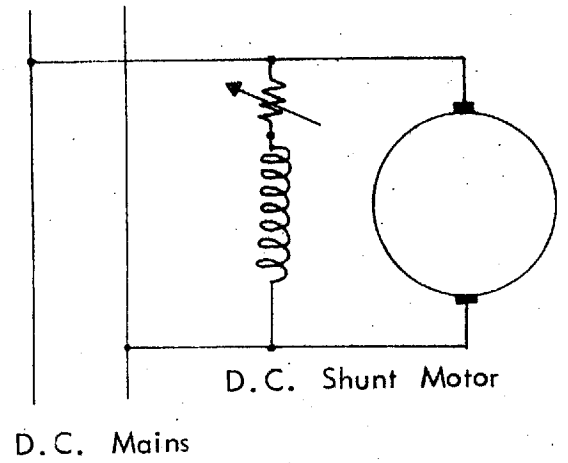

Figure 1.10 Speed Variation By Field Flux Control:- D.C. Shunt Motor.

machine for imparting variable speed is well known (Figure 1.10).

Speed control ofan A.C. shunt motor can be similarly attained but control is effective only if the machine operates at a speed different from the synchronous speed of the machine.

Speed control of A.C. shunt motors by stator voltage regulation is carried out in conjunction with a rotor voltage regulation (Figure 1.11). This is similar to the Ward-Leonard control scheme with field control of the main variable speed D.C. motor.

It can be seen from figure 1.11 that it is possible to reduce the flux of the motor with reducing speed by introducing a bucking voltage in the stator circuit. By this means a useful improvement of the performance, efficiency and power factor can be obtained in connection with drives which require low torques at low speeds, as in fans and pumps, for example.

The speed-torque characteristics of field-controlled shunt motors are shown in figure 1.17.

1.2.3. Speed control through change of rotational speed of stator field

This method of speed control is only applicable to A.C. motors. The speed of rotation of the stator field

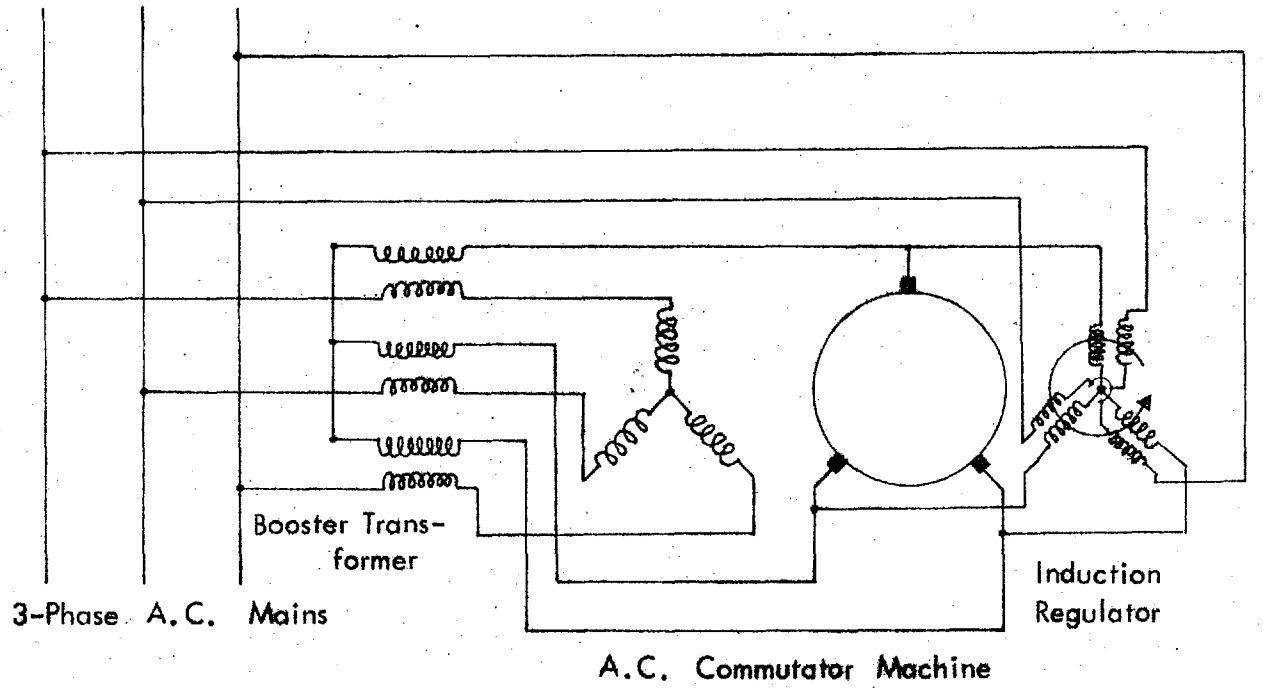

Figure 1.11 Speed Variation By Field Flux Control:- A.C. Shunt Commutator Motor.

is directly proportional to the number of poles and the frequency of the stator supply. Variation of either the number of poles or supply frequency can give a variable speed drive.

(a) Pole change motor

Motors of this type are usually constructed by providing the stator with two or more separate windings corresponding to two or more different number of pole pairs. These windings can be individually connected to the supply causing the rotor to rotate at different speeds.

A single winding could be used to provide different numbers of pole pairs by a suitable switching scheme.

Combination of the above two methods can be used to obtain more than two speeds. The system suffers from the disadvantage that only a limited number of fixed speeds can be obtained and infinitely variable speed control cannot be achieved.

(b) Speed control by supply frequency variation

This method is perhaps the most flexible of all other methods and has the advantage that it can be used in machines with cage rotors.

There are various schemes which give variable frequency supplies.

Perhaps the most direct method is to drive an alternator at a variable speed so that a variable-frequency voltage is generated in the alternator A.C. windings.

If only a fixed frequency three-phase A.C. supply is available a variable speed frequency changer set, driven by a variable speed A.C. commutator motor, can be used to supply variable frequency voltage to the induction motor or motors as shown in figure 1.12.

An alternative but more efficient and economical method of obtaining variable frequency is to use a three-phase variable speed A.C. commutator machine with slip rings (Figure 1.13). This results in a self-propelled frequency convertor as opposed to the externally propelled frequency changer mentioned above. This system, disregarding the induction motors connected to its slip rings, functions exactly as a light running commutator machine. The adjustment of speed is carried out by means of an induction regulator connected to the commutator brushes. The frequency obtainable at the slip rings depends on the difference between the actual and synchronous speeds.

The advantage of the system is that the slip ring and commutator currents tend to cancel one another as in a rotary convertor. The system possesses high efficiency and small size. The speed-torque characteristics of this

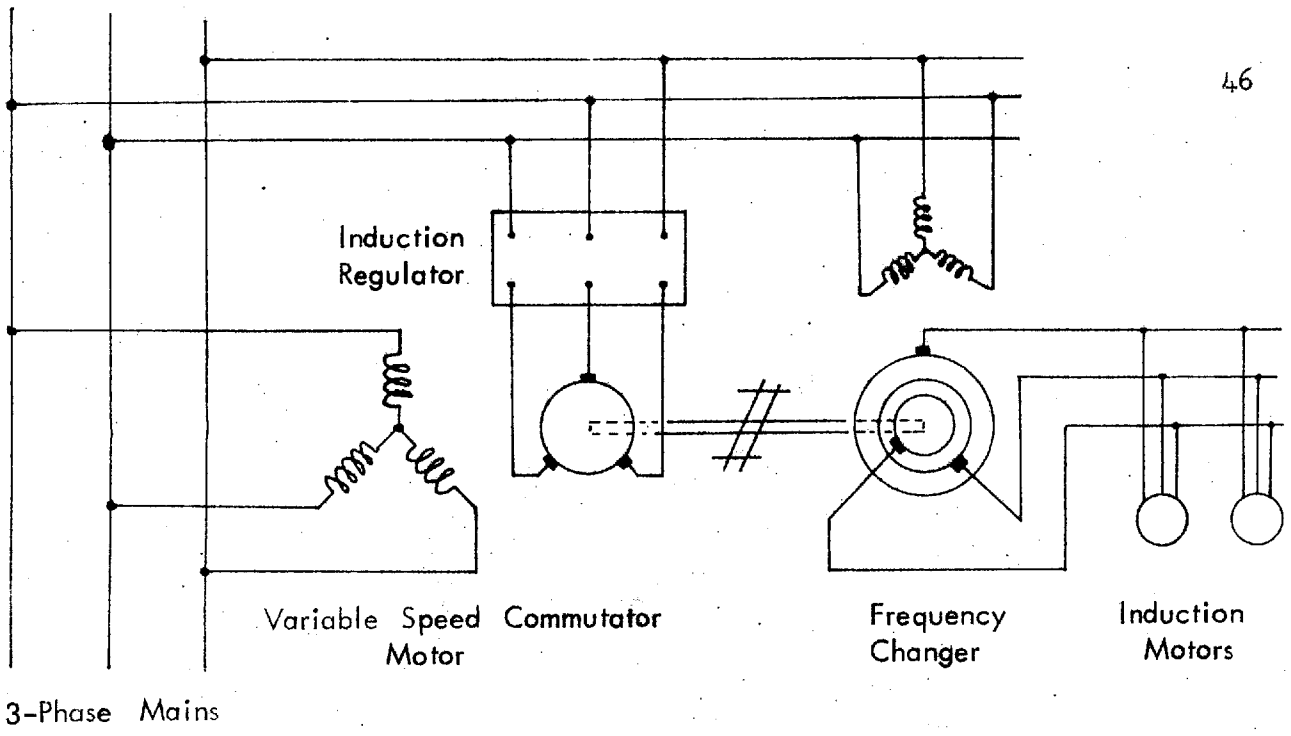

Figure 1.12 Variable Speed By Frequency Control Via Frequency Changer.

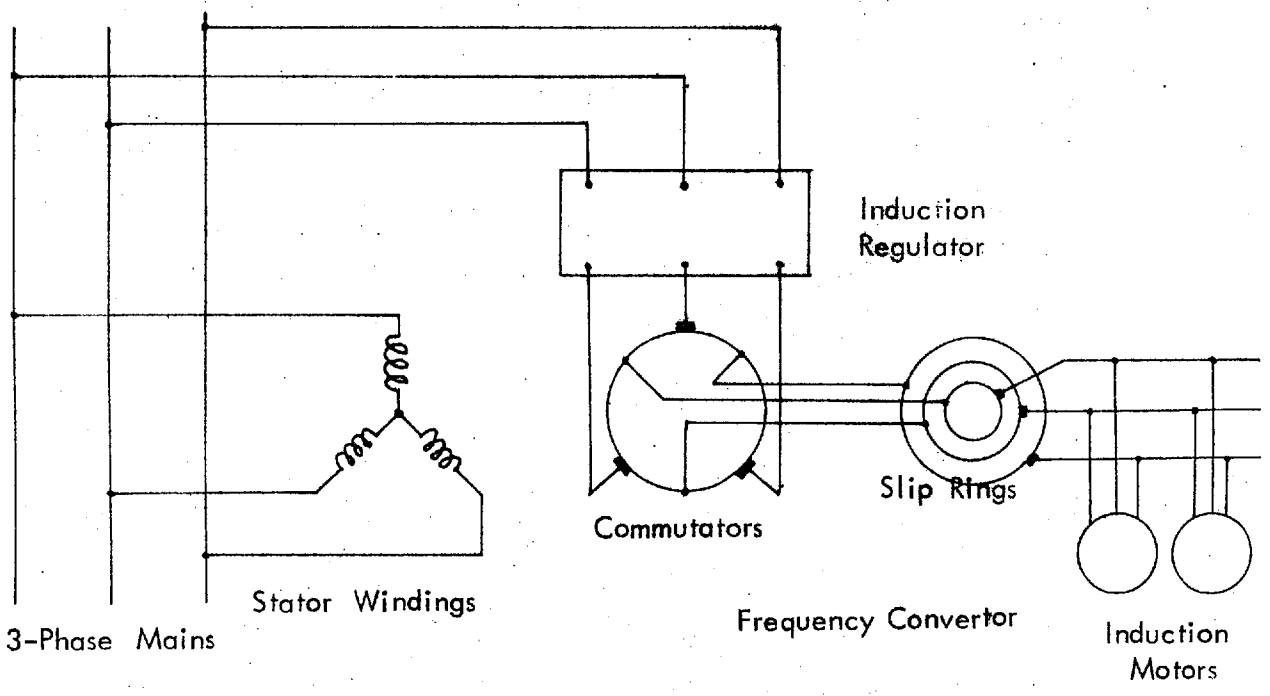

Figure 1.13 Variable Speed By Frequency Control Via Frequency Converter.

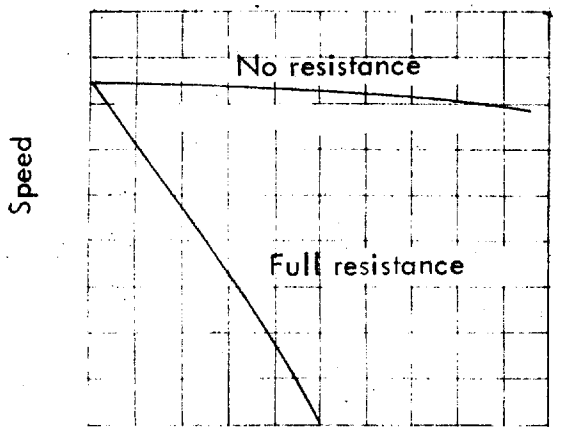

A. C. Slip Ring Machine
(Induction Motor)

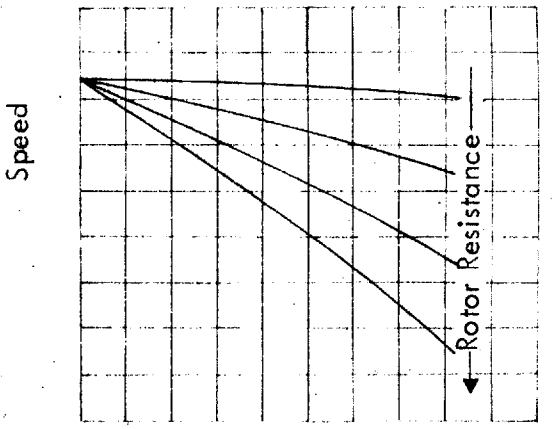

D. C. Shunt Motor

Figure 1.14 Speed Variation By Rotor Resistance.

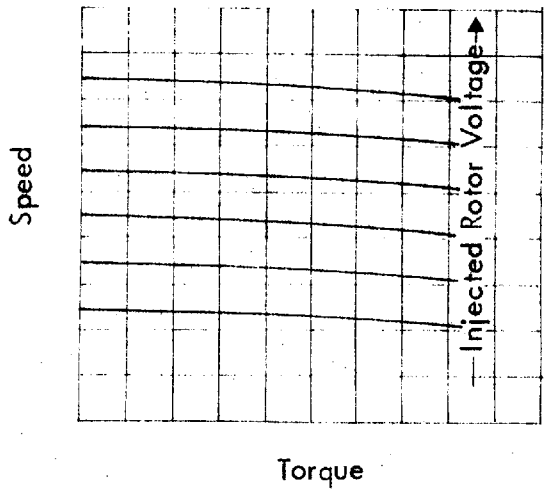

Figure 1.15 Speed Control By Rotor Voltage Injection
(A. C. & D. C. Shunt Machines)

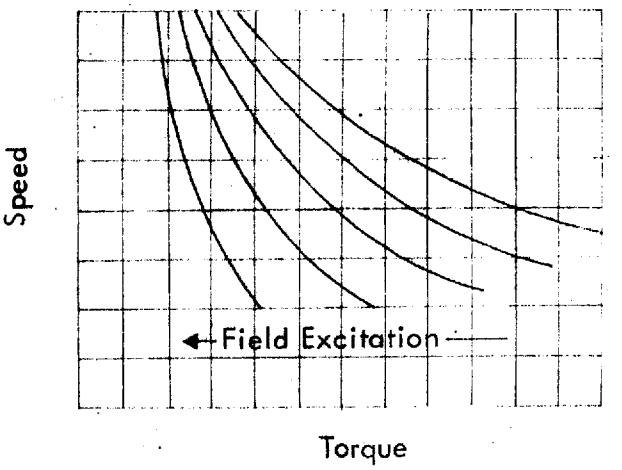

Figure 1.16 Speed Control By Field Flux Control
(A. C. & D. C. Series Motors)

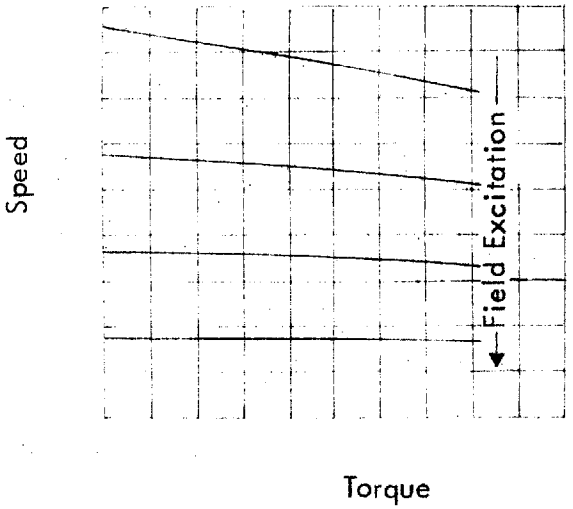

Figure 1.17 Speed Control By Field Flux Control.
(A.C. & D.C. Shunt Motor)

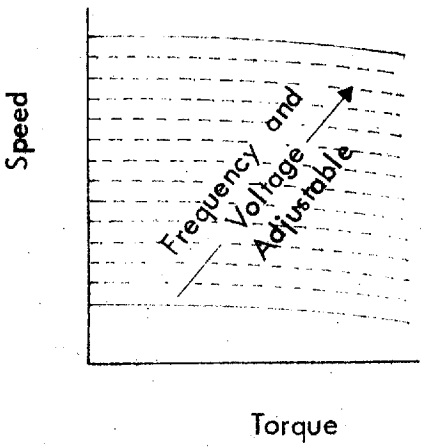

Figure 1.18 Speed Control By Frequency Control.

method of speed control are shown in figure 1.18.

This and similar arrangements have found their applications in cases where high speeds are required at the final motor shaft, as at high speeds it is easier to construct a cage-rotor machine than a commutator machine.

Any number of induction motors can be connected to the system and this creates the possibility of obtaining simultaneous speed control of cage-rotor machines over a wide speed range.

Amongst the various systems, the arrangement involving the self-propelled frequency convertor, is frequently adopted where variable-speed group drives are required.

The greatest weakness of the speed control systems described above lies in the presence of a commutator somewhere in the link. The commutator with its associated brush gear requires considerable maintainance. Conditions of maximum speed, voltage and temperature rise are imposed on the machine by the commutator.

With the advent of high power thyristors, static variable frequency invertors and cyclo-convertors are rapidly entering the field of variable speed drives. Efficient and compact invertors and cyclo-convertors can be constructed. Invertor-driven motors with suitable feed-

back control systems have flexibility and can produce any desired torque-speed characteristic within the limits of the machine. Although semi-conductor devices used in invertors are susceptible to over-loads, invertors can be designed and constructed so that external failures do not cause internal damage.

Invertors with sinusoidal output voltage are available, but are seldom used for variable speed motor drives on economic grounds.

Invertors used for variable speed motor drives are comparatively cheaper than those with sinusoidal output but deliver non-sinusoidal output voltages.

1.3. The Object of the Investigation and the Lay-out of the Thesis

The project undertaken involved the design of an invertor and the measurement and prediction of the performance of an induction motor when invertor-fed.

The general description and the design equations of an invertor are given in chapter 2. Chapter 3 deals with the design of an invertor to a given specification. Details of the experimental determination of an induction motor equivalent circuit parameters are given in chapter 4. The nature of variation of these parameters with frequency is also examined. Chapter 5 is devoted to induction motor

losses under fixed and variable frequency sinusoidal excitation. The effects of the space harmonics of the machine air-gap mmf are also discussed. The contribution of the time-harmonics of the invertor supply to induction motor performance is examined in chapter 6. Chapter 7 deals with the prediction of current wave-form and instantaneous torque of an invertor-fed machine. The prediction of the stator line current wave-form bears a direct relation to the invertor design. The measured motor performance under sinusoidal excitation and when fed from the invertor is described in chapter 8. The general conclusions from the investigation are given in chapter 9.

CHAPTER 2

THE INVERTOR

Three-phase thyristor invertors may be classified according to the method of commutation which may be carried out on the D.C. side or the A.C. side. D.C. side commutation may be further subdivided into single or double side commutated invertor since the thyristor connected to either or both the D.C. lines may be switched off during commutation. An invertor employing single D.C. side commutation was used on grounds of simplicity and cost.

2.1. Single D.C. Side Impulse Commutated Invertor

Figure 2.1. is the circuit diagram of a single D.C. side commutated invertor which was built from six thyristors Th_1 to Th_6 used in bridge configuration to switch the D.C. supply to the load in a pre-determined fashion, so as to produce three-phase alternating voltage wave-form at the load terminals. The commutation circuit consists of two chokes L_1 and L_2 in the positive and negative D.C. lines, two D.C. line diodes D_7 and D_8 and the commutating capacitor C_3. Capacitor C_A, C_B, C_C and C_D are the D.C. supply reservoir capacitors. V_1 is the main D.C. supply and V_2 the auxiliary D.C. supply voltage

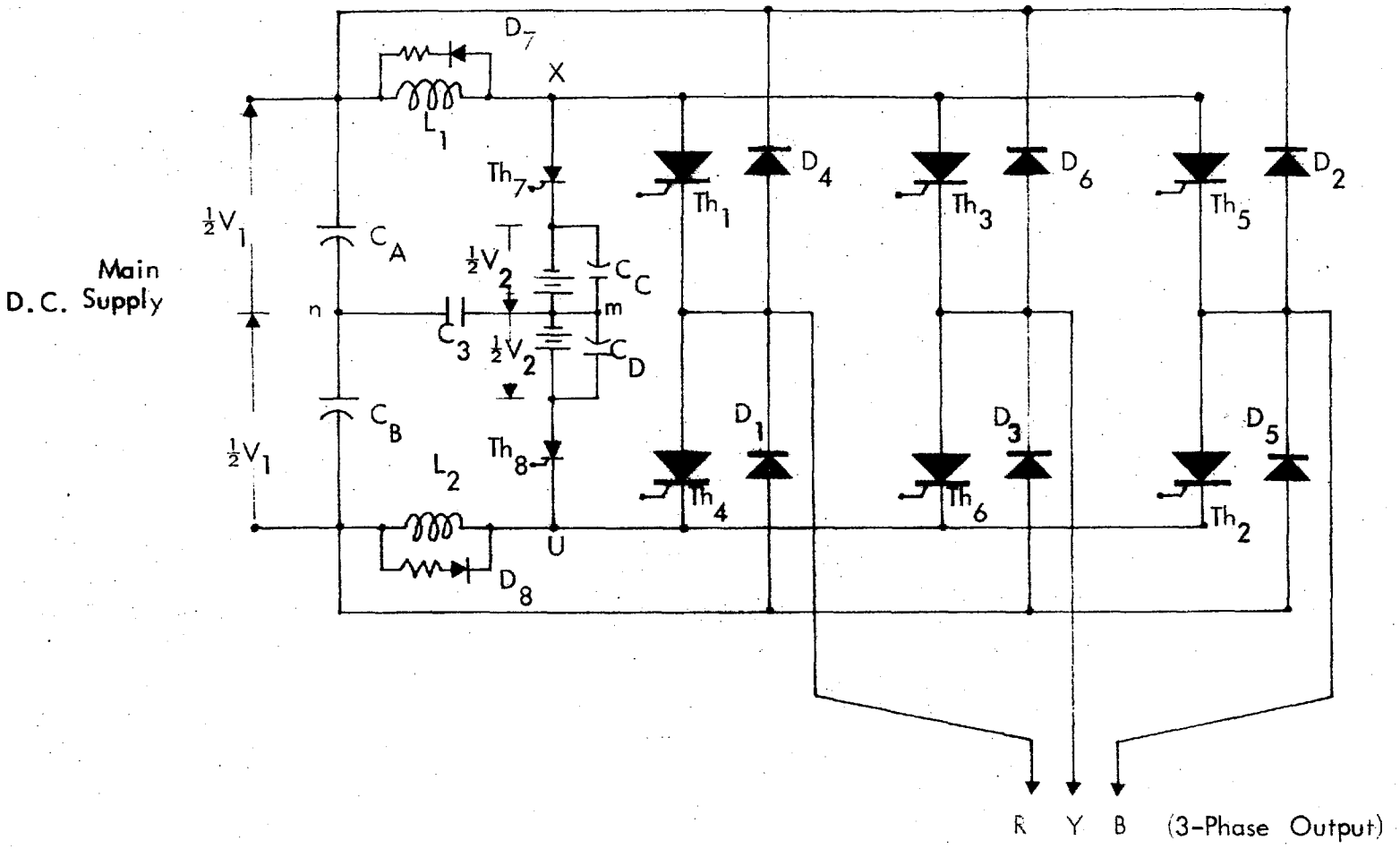

Figure 2.1 Single D.C. Side Impulse Commutated Invertor.

for commutation. Diodes D_1 to D_6 in the bridge arrangement are provided for energy stored in the load to be fed back to the main D.C. supply.

2.2. Operation of the Invertor

The gating sequence of the thyristors and the line to line output voltage of the invertor is shown in figure 2.2. The main bridge thyristors were gated for 180° conduction, but the actual angle of conduction of these thyristors depended on load conditions. The sum of conduction angles of any bridge thyristor and its complementary diode (e.g. Th_5 and D_5) is always 180°.

The operation of the invertor is as follows. Referring to figures 2.1 and 2.2, and starting from the instant when thyristors Th_6, Th_1 and Th_2 are conducting, current flows into the R terminal and out of the Y and B terminals of the load. The commutating capacitor C_3 is charged to $\frac{1}{2}(V_1+V_2)$ volts with the point m (Figure 2.1) positive with respect to the neutral n. All potentials referred to hereafter are with respect to the neutral point n. Thyristor Th_8 is then fired which causes the negative rail of the thyristor bridge to rise to a voltage $(\frac{1}{2} V_1+V_2)$ volts. The negative D.C. rail of the thyristor bridge is now more positive than that of the positive terminal of the main D.C. supply. Since the diodes D_6 and D_2 clamps the anodes

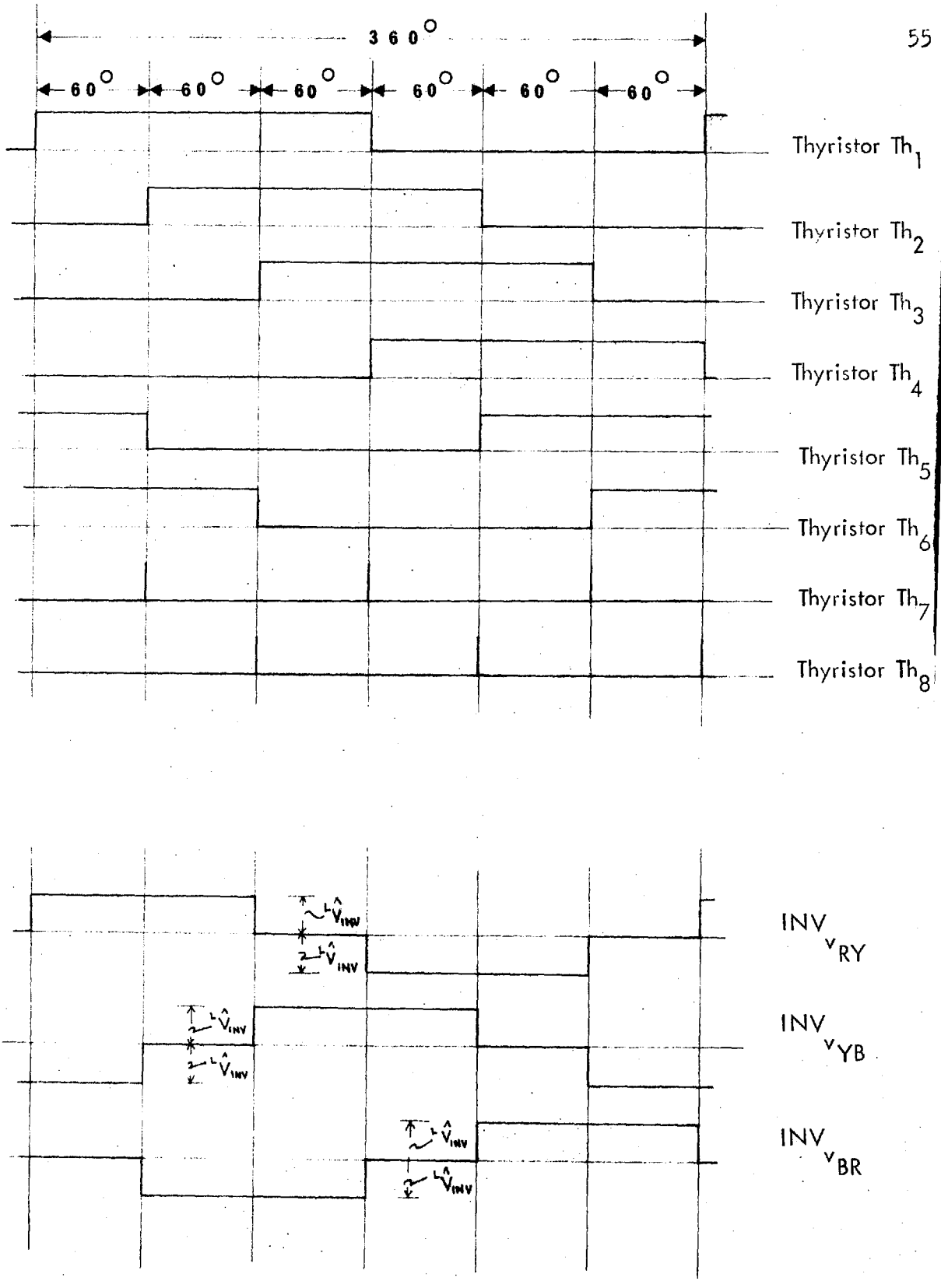

Figure 2.2 Firing Pattern of The Invertor Thyristors And The Instanteneous Line To Line Output Voltages

of thyristors Th_6 and Th_2 at a potential of $\frac{1}{2}V_1$ volts, the two thyristors are reversed biased by V_2 (auxiliary supply voltage) volts and hence ceases to conduct. The commutation circuit constants are chosen so that the thyristors are reversed biased for sufficient time to recover the forward blocking capability. For an inductive load the currents from the Y and B terminals now flows to the positive terminal of the main D.C. supply, via diodes D_6 and D_2.

During the commutation process the terminal m of the commutating capacitor C_3 becomes negative and the current I_o flowing in the choke L_2, at the instant of commutation, increases. The potential of the point U (Figure 2.1) on the negative D.C. rail of the thyristor bridge falls from $(\frac{1}{2}V_1+V_2)$ volts, and when the potential of this point becomes $\frac{1}{2}V_1$, the thyristors Th_6 and Th_2 loose their reverse bias and then on they progressively receive positive voltage. The rate of increase of forward voltage across the thyristors must be less than their "$\frac{dv}{dt}$" capability. The time interval between the gating of thyristor Th_8 and the instant when thyristors Th_6 and Th_2 becomes forward biased is denoted by t_o and this time should be greater than the rated turn-off time of the thyristors. After a time t_c the potential of point U becomes $-\frac{1}{2}V_1$ and the current

through the choke L_2 reaches its peak value I_p. As this current cannot suddenly cease to flow, the capacitor C_3 tends to charge to a higher potential difference. This causes the potential of the point U to fall below $-\frac{1}{2}V_1$ but the fall is limited by the diode D_8. The current I_p now ceases to flow through the commutating thyristor Th_8 and diverts through diode D_8. During this process the commutating capacitor C_3 is charged to the correct potential and polarity to ensure the next commutation of the positive rail thyristors.

Thyristors Th_1, and and Th_3 are now gated. As thyristor Th_1 was not affected during the negative rail commutation, current readily flows into the R terminal of the load. As current was flowing out of B terminal of the load thyristor Th_2 readily takes up this current. But thyristor Th_3 cannot readily build up the current since it flows out of Y phase into the positive terminal of the main D.C. supply through diode D_6. It may be noted that this Y phase current is in a decaying mode and sooner or later falls to zero. A build up of current in Y phase then takes place through thyristor Th_3. The current reversal in Y phase is thus achieved. A similar process takes place for the other two phases, causing a three-phase alternating current to flow into the load.

2.3 Analysis of Commutation Circuit

From the instant when the top commutating thyristor Th_7 is fired, to the instant when it switches off the commutating circuit configuration is as shown in figure 2.3. It is assumed that at the instant when thyristor Th_7 is fired the current flowing through the choke L_1 is I_o. The time interval between the switching "on" of thyristor Th_7 and its switching "off", denoted by "t_c", is the total commutation interval. The voltage to which the capacitor C_3 is charged initially is $\frac{1}{2}(V_1+V_2)$ volts.

The Laplace equivalent of the commutation circuit (Figure 2.3) is shown in figure 2.4. The current response of the circuit is given by

$$I(s) = \frac{(V_1+V_2)/s + L_1 I_o}{sL_1 + r_1 + \frac{1}{sC_3}} \qquad (2.1)$$

Inverting

$$i(t) = \frac{(V_1+V_2)}{wL_1} e^{-\alpha t} \sin wt - I_o \frac{w_o}{w} e^{-\alpha t} \sin (wt-\phi) \qquad (2.2)$$

where

$$w = (w_o^2 - \alpha^2)^{\frac{1}{2}}$$

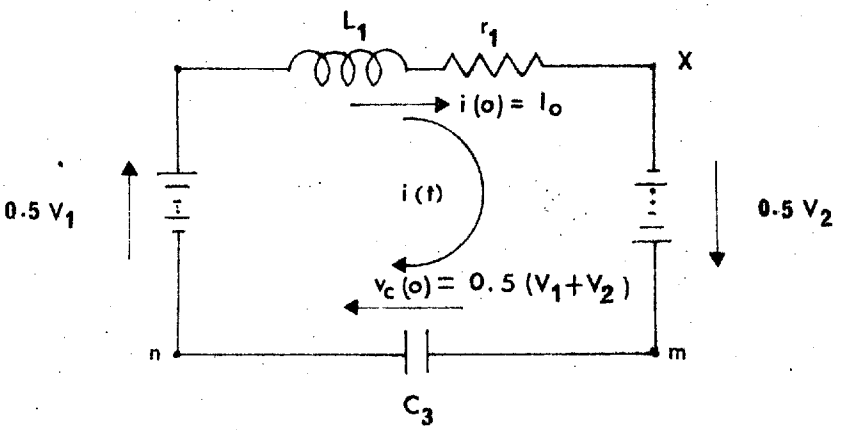

Figure 2.3 Commutation Circuit Configuration When The Positive D.C. Line Commutating Thyristor Is Fired.

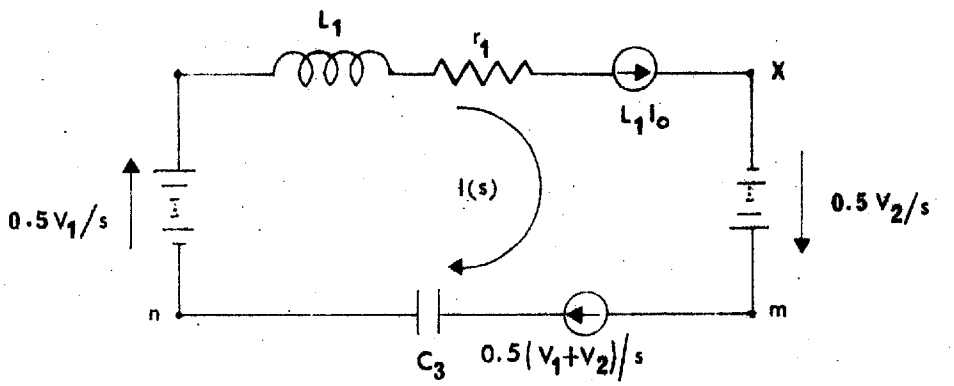

Figure 2.4 Laplace Equivalent Circuit Of Figure 2.3.

$$\tan \phi = w/\alpha \tag{2.4}$$

$$w_o = 1/(L_1 C_3)^{\frac{1}{2}} \tag{2.5}$$

$$\alpha = r_1/2L_1 \tag{2.6}$$

With realistic values of $r_1/2L_1$ the response computed for a quarter cycle from equation 2.2 is hardly any different from that computed from the same equation with $\alpha = 0$.

(With $r_1 = 0.5$, $L_1 = 123\mu H$, $C_3 = 20\mu F$, $V_1 = 160$ V and $V_2 = 120$ V (Chapter 3), the current i(t) at the end of quarter cycle from equation 2.2 is 109.4 A and that from equation 2.8 is 114 A)

Hence with the assumption $\alpha = 0$

$$w = w_o \tag{2.7}$$

and

$$i(t) = \frac{V_1 + V_2}{w_o L_1} \sin w_o t_o - I_o \sin(w_o t_o - \frac{\pi}{2})$$

$$= \frac{V_1+V_2}{w_o L_1} \sin w_o t - I_o \cos(w_o t) \qquad (2.8)$$

Substituting

$$I_p \sin \theta = (V_1+V_2)/(w_o L_1) \qquad (2.9)$$

$$I_p \cos \theta = I_o \qquad (2.10)$$

it can be derived that

$$i(t) = I_p \cos(w_o t - \theta) \qquad (2.11)$$

where

$$I_p = \left[I_o^2 + \left\{ (V_1+V_2)/(w_o L_1) \right\}^2 \right]^{\frac{1}{2}}$$

$$= I_o \left[1 + \left\{ \left(1+\frac{V_2}{V_1} \right) V_1/(I_o w_o L_1) \right\}^2 \right]^{\frac{1}{2}} \qquad (2.12)$$

and

$$\tan \theta = \left(1+\frac{V_2}{V_1}\right) V_1/(I_o w_o L_1) \qquad (2.13)$$

At the instant of commutation the current flowing from the supply was I_o and as such the quantity $\frac{V_1}{I_o}$ may be treated as dynamic D.C. input resistance of the invertor at the instant of commutation.

$$R_{in} = V_1/I_o \tag{2.14}$$

Substituting equation 2.14 in equation 2.12

$$I_p/I_o = \left[1+\left\{R_{in}(1+V_2/V_1)/(w_oL)\right\}^2\right]^{\frac{1}{2}}$$

$$= \left[1+\left\{(\tau_c/\tau_1)^{\frac{1}{2}}\ (1+V_2/V_1)\right\}^2\right]^{\frac{1}{2}} \tag{2.15}$$

where

$$\tau_c = R_{in}\ C_3 \tag{2.16}$$

$$\tau_1 = L_1/R_{in} \tag{2.17}$$

Further substituting

$$k = 1/(1+V_2/V_1) \tag{2.18}$$

in equation 2.15

$$I_p/I_o = \left[1+\left\{(\tau_c/\tau_1)^{\frac{1}{2}}/k\right\}^2\right]^{\frac{1}{2}} \tag{2.19}$$

Defining

$$x = \left[(I_p/I_o)^2 - 1\right]^{\frac{1}{2}} \tag{2.20}$$

a variable, it can be obtained from equation 2.19

$$xk = (\tau_c/\tau_1)^{\frac{1}{2}} \tag{2.21}$$

From equation 2.13

$$\tan\theta = V_1(1+V_2/V_1)/(w_oL_1I_o)$$

$$= R_{in}\,(C_3/L_1)^{\frac{1}{2}}/k$$

$$= (\tau_c/\tau_1)^{\frac{1}{2}}/k$$

$$= x \qquad (2.22)$$

The quantity "k" is a measure of the ratio of the auxiliary supply voltage V_2 to the main supply voltage and may be treated as an independent design variable. The quantity x is a measure of the current rise due to commutation and may also be treated as another independent design variable. Equation 2.21 is a measure of the required ratio of C_3 and L_1 for given values of x and k.

2.3.1. Bridge thyristor reverse bias time

The voltage across the commutating capacitor is given by

$$V_{c_3}(s) = -\tfrac{1}{2}(V_1+V_2)/s + i(s)/(sC_3)$$

$$= -\tfrac{1}{2}(V_1+V_2)/s + \frac{(V_1+V_2)/(sL_1C_3) + I_o/C_3}{s^2 + r_1/L_1 + 1/(L_1C_3)}$$

Inverting

$$v_{c_3}(t) = \tfrac{1}{2}(V_1+V_2) - \left[w(V_1+V_2)/w_o\right] e^{-\alpha t} \sin(wt-\phi)$$

$$+ \left[I_o/(wC_3)\right] e^{-\alpha t} \sin wt$$

With $r/L_1 \ll 1$

$$v_{c_3}(t) = \tfrac{1}{2}(V_1+V_2) - (V_1+V_2)\sin(w_o t+\pi/2) + I_o/(w_o C_3)\sin w_o t$$

$$= \tfrac{1}{2}(V_1+V_2) - (V_1+V_2)\cos w_o t + I_o/(w_o C_3)\sin w_o t \qquad (2.23)$$

The voltage of the point X with respect to the neutral n (Figures 2.1 and 2.5)

$$v_{Xn}(t) = v_{c_3}(t) - \tfrac{1}{2}V_2$$

$$= \tfrac{1}{2}V_1 - (V_1+V_2)\cos w_o t + I_o/(w_o C_3)\sin w_o t \qquad (2.24)$$

At the instant of commutation

$$v_{Xn}(0) = -(\tfrac{1}{2}V_1+V_2) \qquad (2.25)$$

Reverse bias on the top bridge thyristor ends when the potential of the point X reaches the value $-\frac{1}{2}V_1$

$$-\tfrac{1}{2}V_1 = \tfrac{1}{2}V_1 - (V_1+V_2)\cos w_o t_o + I_o/(w_o C_3)\sin w_o t_o$$

$$V_1 w_o C_3/I_o - \{V_1 w_o C_3(1+V_2/V_1)/I_o\}\cos w_o t_o + \sin w_o t_o = 0$$

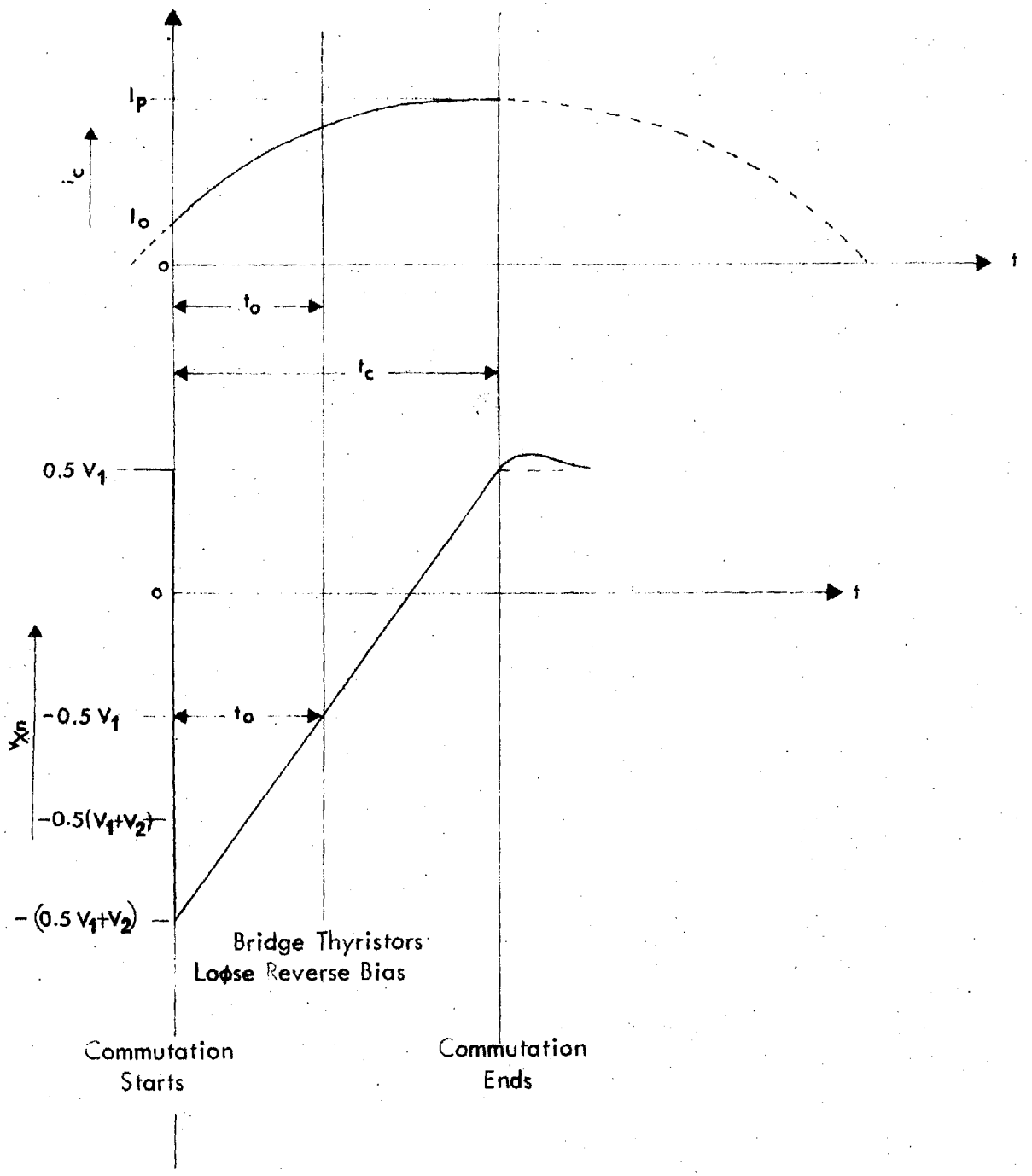

Figure 2.5 Commutation Circuit Current And Thyristor Bridge Positive D.C. Line Potential During Commutation.

Substituting in the above equation

$$V_1/I_o = R_{in} \qquad \text{(Equation 2.14)}$$

and

$$1/(1+V_2/V_1) = k \qquad \text{(Equation 2.18)}$$

$$R_{in}(C_3/L_1)^{\frac{1}{2}} - \{R_{in}(C_3/L_1)^{\frac{1}{2}}/k\} \cos w_o t_o + \sin w_o t_o = 0$$

$$kx - x \cos w_o t_o + \sin w_o t_o = 0 \qquad (2.26)$$

because

$$xk = (\tau_c/\tau_1)^{\frac{1}{2}} = R_{in}(C_3/L_1)^{\frac{1}{2}}$$

(Equations 2.21, 2.16, 2.17)

Equation 2.26 is now rewritten as $x \cos w_o t_o - \sin w_o t_o = kx$ (2.27)

Substituting

$$x = R \sin \theta$$

and

$$1 = R \cos \theta$$

$$R = (x^2+1)^{\frac{1}{2}} \quad \text{and} \quad \tan \theta = x$$

Therefore equation 2.27 becomes

$$(x^2+1)^{\frac{1}{2}} \sin(\theta - w_o t_o) = kx$$

$$\sin(\theta - w_o t_o) = kx/(x^2+1)^{\frac{1}{2}}$$

$$\tan(\theta - w_o t_o) = kx/\{1+x^2(1-k^2)\}^{\frac{1}{2}}$$

$$w_o t_o = -\tan^{-1}\left[kx/\{1+x^2(1-k^2)\}^{\frac{1}{2}}\right] + \tan^{-1}x$$

$$t_o/(\tau_c \tau_1)^{\frac{1}{2}} = \tan^{-1}x - \tan^{-1}\left[kx/\{1+x^2(1-k^2)\}^{\frac{1}{2}}\right]$$

The above equation gives the product of the time of reverse bias t_o and the natural angular frequency w_o of the commutation circuit as a function of the independent variables x and k. Let a dependent design variable $f_1(x, k)$ be defined as

$$f_1(x, k) = w_o t_o$$

$$= t_o/(\tau_c \tau_1)^{\frac{1}{2}}$$

$$= \tan^{-1}x - \tan^{-1}\left[kx/\{1+x^2(1-k^2)\}^{\frac{1}{2}}\right] \qquad (2.28)$$

2.3.2. Total commutation time t_c

Total commutation time t_c is defined as the time required for the point X to reach a potential of $\frac{1}{2}V_1$ (Figures 2.1 and 2.5).

Substituting $t = t_c$ in equation 2.24

$$\tfrac{1}{2}V_1 = \tfrac{1}{2}V_1 - (V_1+V_2)\cos w_o t_c + I_o/(w_o C_3)\sin w_o t_c$$

$$\therefore \tan w_o t_c = V_1(1+V_2/V_1)w_o C_3/I_o$$

Substituting equations 2.14 and 2.18 in the above equation

$$\tan w_o t_c = R_{in}(C_3/L_1)^{\frac{1}{2}}/k$$

$$= (\tau_c/\tau_1)^{\frac{1}{2}}/k$$

$$= x \qquad \text{(Equation 2.22)}$$

$$\therefore w_o t_c = \tan^{-1} x \qquad (2.29)$$

The expression of current during commutation interval is given by

$$i(t) = I_p \cos(w_o t-\theta) \qquad \text{(Equation 2.11)}$$

At the end of the commutation inverval t_c, the current has risen from its initial value I_o to I_p. The current through the commutating capacitor C_3 and the voltage of point X during the commutation of a positive rail thyristor is shown in figure 2.5.

2.3.3. Commutation circuit inductance and capacitance

The commutation circuit inductance L_1, and L_2

($L_1 = L_2$) and capacitance C_3 are expressed in non-dimensional form as function of x and k, in order to derive a set of curves applicable to all invertors of the type considered.

Rewriting equations 2.21 and 2.23 for convenience

$$xk = (\tau_c/\tau_1)^{\frac{1}{2}}$$

$$f_1(x, k) = t_o/(\tau_c \tau_1)^{\frac{1}{2}}$$

it can be shown that

$$f_4(x, k) = \tau_1/t_o .$$

$$= 1/\{xkf_1(x, k)\} \qquad (2.30)$$

and

$$f_5(x, k) = \tau_c/t_o$$

$$= xk/f_1(x, k) \qquad (2.31)$$

where $f_4(x, k)$ and $f_5(x, k)$ are inductance and capacitance functions respectively.

2.3.4. Energy loss in the commutating line chokes

The energy gained by the commutation choke during the commutation inverval

$$\mathcal{E}_c = \tfrac{1}{2}L_1(I_p^2 - I_o^2) \qquad (2.32)$$

The commutation energy required per joule of diverted D.C. rail energy

$$f_2(x, k) = \tfrac{1}{2}L_1 I_o^2\{(I_p/I_o)^2 - 1\}/(V_1 I_o t_o)$$

$$= \tfrac{1}{2}L_1 x^2/(R_{in} t_o)$$

$$= \tfrac{1}{2}\tau_1 x^2/t_o \qquad (2.33)$$

But

$$\tau_1/t_o = 1/\{xkf_1(x, k)\} \qquad \text{(Equation 2.30)}$$

So that commutation energy loss function, defined as

$$f_2(x, k) = \mathcal{E}_c/(V_1 I_o t_o)$$

$$= \tfrac{1}{2}x/\{kf_1(x, k)\} \qquad (2.34)$$

2.3.5. Peak flux linkage of commutation chokes

The peak flux-linkage produced is an important factor concerning the cost of the commutation chokes. It will be shown that minimum flux-linkage and maximum commutation efficiency are conflicting requirements. The peak flux-linkage is given by $L_1 I_p$. The D.C. main supply voltage V_1 is fixed by the A.C. output voltage consideration.

The reverse bias time t_o of the bridge thyristors is fixed by the manufacturer. The peak flux-linkage function $f_3(x, k)$ is given by

$$\begin{aligned} f_3(x, k) &= L_1 I_p/(V_1 t_o) \\ &= L_1 I_o (1+x^2)^{\frac{1}{2}}/(V_1 t_o) \\ &= L_1 (1+x^2)^{\frac{1}{2}}/(R_{in} t_o) \\ &= \tau_1 (1+x^2)^{\frac{1}{2}}/t_o \end{aligned}$$

Substituting equation 2.30 in the above equation

$$\begin{aligned} f_3(x, k) &= L_1 I_p/(V_1 t_o) \\ &= (1+x^2)^{\frac{1}{2}}/\{xkf_1(x, k)\} \end{aligned} \qquad (2.35)$$

2.3.6. Commutating thyristor i^2t rating

This rating is important for the choice of the commutating thyristors which carry heavy current pulses of very short duration t_c (about 100 μsec).

The commutating thyristors carry current for an inverval t_c (time for commutation), with initial current I_o and the final current I_p, according to the relation

$$i(t) = I_p \cos(w_o t-\theta) \qquad \text{(Equation 2.11)}$$

where

$$I_p = I\,(1+x^2)^{\frac{1}{2}} \qquad \text{(Equation 2.20)}$$

$$w_o = 1/(L_1C_3)^{\frac{1}{2}} \qquad \text{(Equation 2.5)}$$

$$\theta = \tan^{-1}x \qquad \text{(Equation 2.22)}$$

$$= w_o t_c \qquad \text{(Equation 2.29)}$$

$$\therefore \int_0^{t_c} i^2 dt = \int_0^{t_c} I_p{}^2 \cos^2(w_o t-\theta)\, dt$$

$$= \tfrac{1}{2}I_p{}^2\left\{t+\tfrac{1}{2}\sin 2(w_o t-\theta)\right\}/w_o\Big|_0^{t_c}$$

From equation 2.29 when $t = t_c$, i.e. at the end of commutation $w_o t_c = \theta$

$$\therefore \int_0^{t_c} i^2 dt = \tfrac{1}{2}I_p{}^2\left\{t_c-\tfrac{1}{2}\sin 2\theta\right\}/w_o$$

$$= \tfrac{1}{2}I_p{}^2(\tan^{-1}x-\sin\theta\cos\theta)/w_o$$

From equation 2.22

$$\sin\theta\cos\theta = x/(1+x^2)$$

$$\therefore \int_0^{t_c} i^2 dt = \tfrac{1}{2}I_p{}^2\left\{\tan^{-1}x-x/(1+x^2)\right\}/w_o$$

Substituting the value of w_o from equation 2.28 in the above equation

$$\int_0^{t_c} i^2 dt = \tfrac{1}{2} I_p{}^2 t_o \{\tan^{-1}x - x/(1+x^2)\}/f_1(x, k)$$

Replacing I_p in terms of I_o from equation 2.20

$$\int_0^{t_c} i^2 dt = \tfrac{1}{2} I_o{}^2 t_o (1+x^2)\{\tan^{-1}x - x/(1+x^2)\}/f_1(x, k)$$

$$= \tfrac{1}{2} I_o{}^2 t_o \{(x^2+1)\tan^{-1}x - x\}/f_1(x, k)$$

Commutating thyristor i^2t function defined as

$$f_6(x, k) = \int_0^{t_c} i^2 dt/(I_o{}^2 t_o)$$

$$= \tfrac{1}{2}\{(x^2+1)\tan^{-1}x - x\}/f_1(x, k) \qquad (2.36)$$

This equation gives the ratio of i^2t flowing through the commutation thyristor to $I_o{}^2 t_o$ during commutation process.

2.3.7. R.M.S. current of commutation thyristor

At an invertor output frequency of f Hz, the interval between commutations of either positive line or negative D.C. line thyristor is given by $\frac{1}{3}f$. The r.m.s.

commutation thyristor current is given by

$$C_{I_{RMS}} = (3f)^{\frac{1}{2}}\left[\int_0^{t_c} i^2 dt\right]^{\frac{1}{2}}$$

From equation 2.36

$$C_{I_{RMS}} = (3f)^{\frac{1}{2}}\left[\tfrac{1}{2}I_o{}^2 t_o\{(x^2+1)\tan^{-1}x-x\}/f_1(x, k)\right]^{\frac{1}{2}}$$

and we can define, for future use.

$$f_7(x, k) = C_{I_{RMS}}/\{(3ft_o)^{\frac{1}{2}}I_o\}$$

$$= \left[\tfrac{1}{2}\{(x^2+1)\tan^{-1}x-x\}/f_1(x, k)\right]^{\frac{1}{2}} \qquad (2.37)$$

2.3.8. Average current of commutation thyristor

The commutation thyristor current during the commutation interval t_c is given by

$$i = I_p \cos(w_o t-\theta) \qquad (2.11)$$

$$\therefore \int_0^{t_c} i\,dt = I_p \sin(w_o t-\theta)/w_o \Big|_0^{t_c}$$

when

$$t = t_c,\ w_o t_c = \theta \qquad \text{(Equations 2.29 and 2.22)}$$

$$\therefore \int_0^{t_c} i\,dt = I_p \sin\theta/w_o$$

Substituting equation 2.22 in the above equation

$$\int_0^{t_c} i\,dt = I_p x/\{w_o(x^2+1)^{\frac{1}{2}}\}$$

$$= I_o x/w_o \qquad \text{(From equation 2.20)}$$

$$= I_o t_o x/f_1(x, k) \qquad \text{(From equation 2.28)}$$

Therefore average commutation thyristor current

$$^{C}I_{AV} = 3f\int_0^{t_c} i\,dt$$

$$= 3fI_o t_o x/f_1(x, k)$$

We define another quantity, for future use.

$$f_8(x, k) = {}^{C}I_{AV}/(3fI_o t_o)$$

$$= x/f_1(x, k) \qquad (2.39)$$

2.3.9. Power rating of auxiliary commutating supply

The power rating of the centre-tapped auxiliary supply is given by (for each half section)

$$P_{CA} = {}^{C}I_{AV}V_2/2$$

Substituting the value of $^{C}I_{AV}$ from equation 2.39

$$P_{CA} = 3ft_o I_o V_2 x/\{2f_1(x, k)\}$$

The power supplied by the main D.C. supply at the instant of commutation is $V_1 I_o$

$$\frac{P_{CA}}{V_1 I_o} = 3ft_o V_2 x / \{V_1 2f_1(x, k)\}$$

But

$$V_2/V_1 = (1-k)/k \text{ from equation 2.18}$$

$$\therefore P_{CA}/V_1 I_o = 3ft_o x(1-k)/\{2kf_1(x, k)\}$$

and we define auxiliary commutating supply power function (for each section)

$$f_9(x, k) = P_{CA}/(3ft_o V_1 I_o)$$

$$= \tfrac{1}{2}x(1-k)/\{kf_1(x, k)\} \qquad (2.40)$$

2.3.10 Commutation power supplied by the main D.C. supply

The commutation power supplied by the main D.C. supply is given by

$$P_{CM} = \tfrac{1}{2} {}^{C}I_{AV} V_1$$

Substituting the value of ${}^{C}I_{AV}$ from equation 2.39

$$P_{CM} = 3ft_o I_o V_1 x/\{2f_1(x, k)\}$$

The power supplied by the main D.C. power source at the instant of commutation is $V_o I_o$

$$P_{CM}/V_1 I_o = 3ft_o x/\{2f_1(x, k)\}$$

and we define

$$f_{10}(x, k) = P_{CM}/(3ft_oV_1I_o)$$

$$= \tfrac{1}{2}x/f_1(x, k) \qquad (2.41)$$

2.3.11 D.C. line clamping diode average current

The D.C. line clamping diodes carry the peak current (I_p) at the end of the commutation interval. As soon as the bridge thyristors are fired this current falls to (I_p-I_o) and decays to zero when next commutation on the same side is due.

Assuming a linear decay from (I_p-I_o) to zero, the average diode current

$$^{D}I_{AV} = \tfrac{1}{2}(I_p-I_o)$$

$$= \tfrac{1}{2}I_o(x^2+1)^{\frac{1}{2}} - \tfrac{1}{2}I_o$$

we define

$$f_{11}(x, k) = {}^{D}I_{AV}/I_o$$

$$= \tfrac{1}{2}\{(x^2+1)^{\frac{1}{2}} - 1\} \qquad (2.42)$$

2.4. Choice of Commutation Circuit Parameters

The two design independent variables for the commutation circuit are

$$x = \left\{(I_p/I_o)^2 - 1\right\}^{\frac{1}{2}} \qquad \text{(Equation 2.20)}$$

and

$$k = 1/(1+V_2/V_1) \qquad \text{(Equation 2.18)}$$

The commutation energy loss function $f_2(x, k)$ and the peak flux-linkage function $f_3(x, k)$ are dependent on the two independent variables x and k. The commutation supply voltage V_2, the capacitor C_3, the inductances L_1, L_2; for given main D.C. supply voltage V_1, current to be commutated I_o, and reverse bias time t_o, should be chosen so that the commutation energy loss and peak flux-linkage of the D.C. line chokes be a minima.

2.4.1. Optimization for minimum commutation $\mathcal{E}_c$ for a given value of τ_1 and τ_c

The reverse bias time function has previously been defined

$$f_1(x, k) = t_o/(\tau_c \tau_1)^{\frac{1}{2}}$$

$$= \tan^{-1}x - \tan^{-1}\left[xk/\left\{1+x^2(1-k^2)\right\}^{\frac{1}{2}}\right]$$

(Equation 2.28)

For a given value of τ_c and τ_1

$$xk = (\tau_c/\tau_1)^{\frac{1}{2}} \qquad \text{(Equation 2.21)}$$

$$= \text{a constant } C_1$$

Let $(\tau_c \tau_1)^{\frac{1}{2}}$ be another constant C_2

Equation 2.28 can therefore be written as

$$f_1(k) = t_o/C_2$$

$$= \tan^{-1}(C_1/k) - \tan^{-1}\left[C_1/\{1+(C_1/k)^2 - C_1^2\}^{\frac{1}{2}}\right] \qquad (2.43)$$

Commutation energy function $f_2(x, k)$, rewritten for convenience

$$f_2(x, k) = \mathcal{E}_c/V_1 I_o t_o$$

$$= \tfrac{1}{2}x/\{kf_1(x, k)\} \qquad \text{(Equation 2.34)}$$

For given values of τ_c and τ_1, $f_2(x, k)$ reduces to

$$f_2(k) = \tfrac{1}{2}C_1/\{k^2 f_1(k)\} \qquad (2.44)$$

For the commutation energy to be a minimum k should be so chosen that

$\frac{d}{dk}\{f_2(k)\}$ should be zero.

Therefore differentiating $f_2(k)$ with respect be k and equating to zero

$$\tfrac{1}{2}C_1\Big[-2f_1(k)k^{-3} + k^{-2}C_1\Big\{1 + C_1^{\,2}/(k^2+C_1^{\,2}-C_1^{\,2}k^2)^{\frac{1}{2}}\Big\}/$$

$$(C_1^{\,2}+k^2)\Big]\Big/f_1(k)^{\,2} = 0$$

$$\therefore\quad k^{-2}C_1\Big\{1+C_1^{\,2}/(C_1^{\,2}+k^2-C_1^{\,2}k^2)^{\frac{1}{2}}\Big\}/(C_1^{\,2}+k^2) = 2k^{-3}f_1(k)$$

$$\therefore\quad f_1(k) = kC_1\Big\{1+C_1^{\,2}/(k^2+C_1^{\,2}-C_1^{\,2}k^2)^{\frac{1}{2}}\Big\}/\Big\{2(C_1^{\,2}+k^2)\Big\} \qquad (2.45)$$

The above relation gives the value of the reverse bias time-function for minimum commutation energy involved.

Substituting this value of $f_1(k)$ in equation 2.42 the minimum value of commutation energy function is obtained

$$f_2(k)/_{min} = (C_1^{\,2}+k^2)/\Big[k^3.\Big\{1+C_1^{\,2}/(k^2+C_1^{\,2}-k^2C_1^{\,2})^{\frac{1}{2}}\Big\}\Big] \qquad (2.46)$$

The value of k was not calculated from equation 2.45 because the equation is of the transcendental type and because as shown in section 2.5.2. that the minimum values of commutation energy and commutation chokes peak flux-linkage do not occur at the same value of k. Equation 2.44 was evaluated for a range of values of k for various constant values of C_1. This is shown in graphical form in figure 2.6. The region of interest is plotted to a larger scale in figure 2.7. The value of k for minimum commutation energy lies, for realizable values

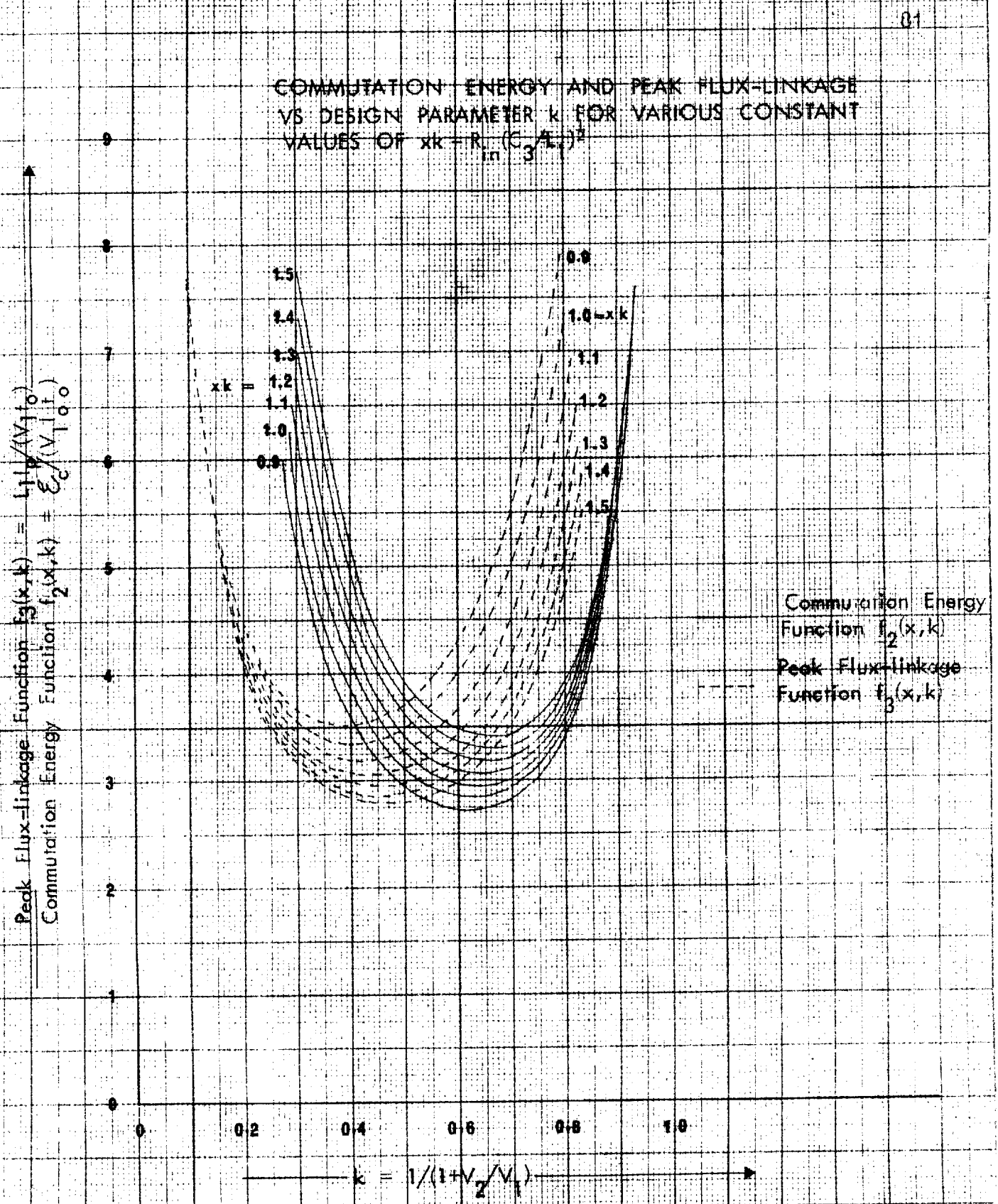

FIGURE 2.6 INVERTOR COMMUTATION CIRCUIT DESIGN CURVES.

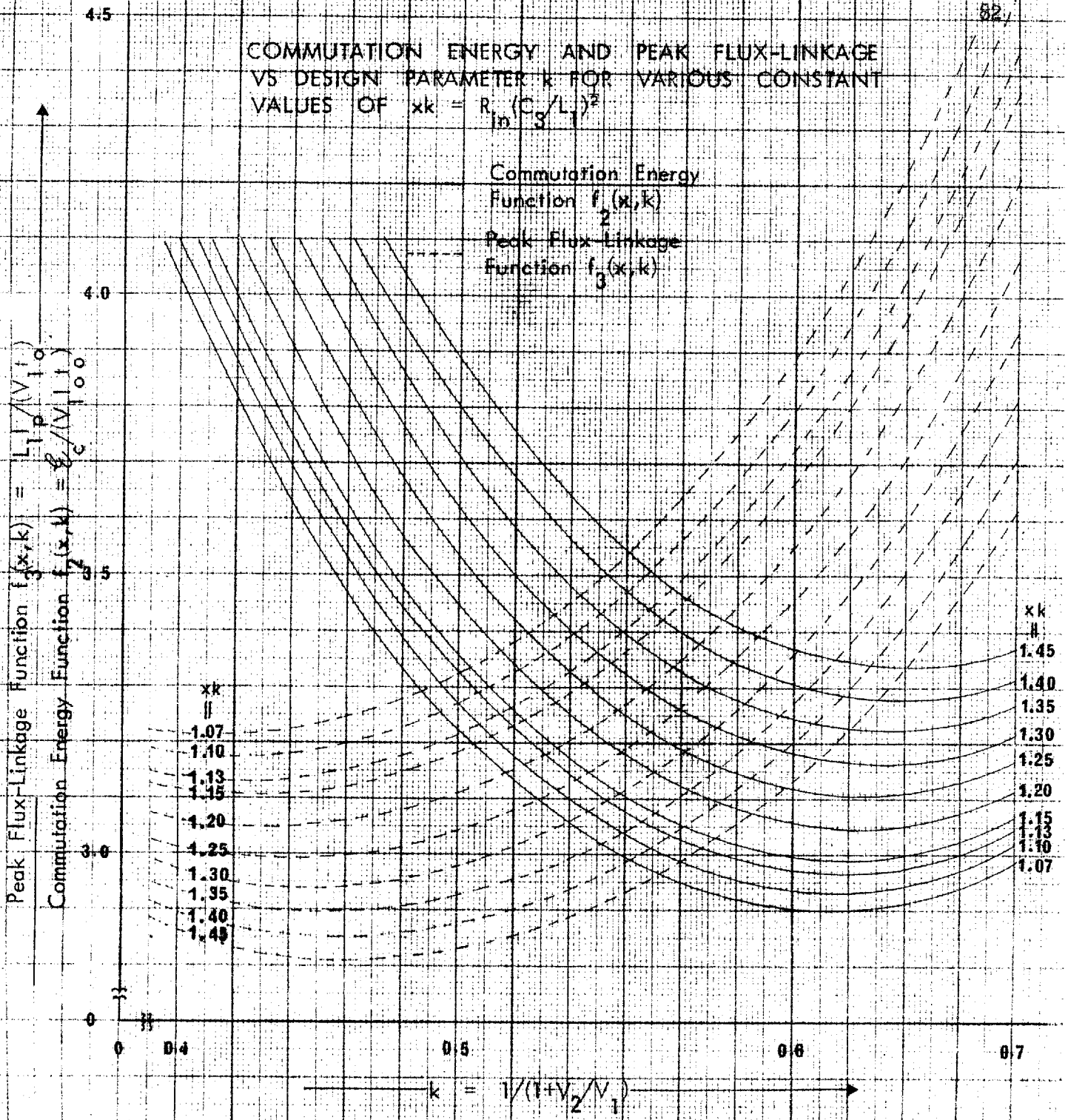

FIGURE 2.7 INVERTOR COMMUTATION CIRCUIT DESIGN CURVES.

of τ_1, within the range of 0.55 to 0.7. The "high" values of k correspond to low values of commutation line choke inductance.

For a given value of k, minimum commutation energy occurs when $C_1 = 0$ indicating that the D.C. line choke inductance is infinite. This can be verified by differentiating equation 2.46 with respect to C_1, equating the result to zero and evaluating the value of C_1. The value of k which results in a further minima can be found as follows

Under the condition of minimum commutation energy equations 2.43 and 2.45 can be written as

$$f_1(k) = \tan^{-1}(C_1/k) - \tan^{-1}\left[C_1/\left\{1+(C_1/k)^2 - C_1^2\right\}^{\frac{1}{2}}\right]$$

$$= \tfrac{1}{2}kC_1\left\{1+C_1^2/(C_1^2+k^2-C_1^2k^2)^{\frac{1}{2}}\right\}/(C_1^2+k^2)$$

or

$$\tan^{-1}\frac{\left[C_1/k - C_1/\left\{1+(C_1/k)^2 - C_1^2\right\}^{\frac{1}{2}}\right]}{k\left\{C_1^2 + (k^2+C_1^2-C_1^2k^2)^{\frac{1}{2}}\right\}}$$

$$= \tfrac{1}{2}kC_1\left\{1+C_1^2/(C_1^2+k^2-C_1^2k^2)^{\frac{1}{2}}\right\}/(C_1^2+k^2)$$

when $C_1 \longrightarrow 0$

$$C_1\left\{(k^2+C_1^2-C_1^2k^2)^{\frac{1}{2}} - k^2\right\}/\left[k\left\{C_1^2+(k+C_1^2-C_1^2k^2)^{\frac{1}{2}}\right\}\right]$$

$$= \tfrac{1}{2}kC_1\left\{1+C_1^2/(C_1^2+k^2-C_1^2k^2)^{\frac{1}{2}}\right\}/(C_1^2+k^2)$$

or

$$1/(2k) = (1-k)/k \quad \text{or} \quad k = 0.5$$

Complete minimum of commutation energy occurs when $C_1 = 0$, or the line choke inductance is infinity and k is 0.5.

2.4.2. Minimization of commutation choke flux-linkage

It has been shown that the commutation choke peak flux-linkage is given by

$$f_3(x, k) = (1+x^2)^{\frac{1}{2}}/\{xkf_1(x, k)\} \quad \text{(Equation 2.35)}$$

Since

$$xk = (\tau_c/\tau_1)^{\frac{1}{2}} \quad \text{(Equation 2.21)}$$

For given value of τ_c and τ_1

$$xk = \text{a constant } C_1$$

Equation 2.35 can be written as

$$f_3(k) = \{1+(C_1/k)^2\}^{\frac{1}{2}}/\{C_1 f_1(k)\} \quad (2.47)$$

Minimum peak flux-linkage occurs when

$$\frac{d}{dk}\{f_3(k)\} = 0$$

Therefore for a minima

$$(1/C_1)\left[f_1(k)\,\tfrac{1}{2}\left\{1+(C_1/k)^2\right\}^{\frac{1}{2}}C_1{}^2k^{-3}(-2)-\left\{1+(C_1/k)^2\right\}^{\frac{1}{2}}\frac{d}{dk}\left\{f_1(k)\right\}\right]/f_1{}^2(k) = 0$$

or

$$C_1{}^2f_1(k)/\left[k^3\left\{1+(C_1/k)^2\right\}^{\frac{1}{2}}\right] = \left\{1+(C_1/k)^2\right\}\left\{C_1/(C_1{}^2+k^2)\right\}\left\{1+C_1{}^2/(C_1{}^2+k^2-C_1{}^2k^2)^{\frac{1}{2}}\right\}$$

or

$$f_1(k) = k\left\{1+C_1{}^2/(C_1{}^2+k^2-C_1{}^2k^2)^{\frac{1}{2}}\right\}/C_1 \qquad (2.48)$$

The minimum value of peak flux-linkage of commutation line chokes can be found by substituting equation 2.48 in equation 2.47

$$f_3(k)\Big|_{\min} = (k^2+C_1{}^2)^{\frac{1}{2}}/\left[k^2\left\{k+C_1{}^2/(C_1{}^2+k^2-C_1{}^{-2}k^2)^{\frac{1}{2}}\right\}\right] \qquad (2.49)$$

Equation 2.48 is of transcendental type, and therefore the value of k, for minimum peak flux-linkage of commutation chokes, could not be evaluated from it directly. Equation 2.47 was evaluated for a range of values of k for

various constant values of C_1. These are shown in graphical form in figures 2.6 and 2.7. It may be seen from these graphs that for realizable values of τ_1, the value of k for minimum peak flux-linkage of commutation chokes, lies within the range of 0.4 to 0.5, and that the upper values of k correspond to lower values of τ_1.

When C_1 can be freely chosen the value of k for minimum commutation choke peak flux-linkage is of interest.

Expressing $f_3(x, k)$, (Equation 2.35), as a function of C_1 (k becomes a fixed parameter), and differentiating the function with respect to C_1 and equating to zero, yields, for a given k, the value of C_1 for which the peak flux-linkage of the commutation chokes is a minimum. This value of C_1 is infinity meaning $\tau_1 = 0$ or the inductance of the D.C. line chokes is zero. This result is what could be deduced intuitively. Equation 2.48 is rewritten for minimum flux-linkage

$$f_1(k) = \tan^{-1} \frac{C_1\left[C_1\left\{(k/C_1)^2 + 1 - k^2\right\}^{\frac{1}{2}} - k^2\right]}{k\left[C_1^2 + C_1\left\{(k_1/C_1)^2 + 1 - k^2\right\}^{\frac{1}{2}}\right]}$$

$$= k\left[1 + C_1^2 / \left\{k^2 + C_1 - C_1^2 k^2\right\}^{\frac{1}{2}}\right] / C_1$$

or

$$\tan^{-1} \frac{C_1^2\left[\left\{(k/C_1)^2 + 1 - k^2\right\}^{\frac{1}{2}} - (k/C_1)^2\right]}{kC_1^2\left[1 + \left\{1 - k^2 + (k/C_1)^2\right\}^{\frac{1}{2}} / C_1\right]}$$

$$= k\left[1+C_1/\left\{(k/C_1)^2 + 1 - k^2\right\}^{\frac{1}{2}}\right]/C_1$$

when $C_1 \longrightarrow \infty$

$$\tan^{-1}\left\{(1-k^2)^{\frac{1}{2}}/k\right\} = k/(1-k^2)^{\frac{1}{2}}$$

or

$$\tan\left\{k/(1-k^2)^{\frac{1}{2}}\right\} = (1-k^2)^{\frac{1}{2}}/k$$

The solution of the above transcendental equation yields that for optimum condition the value of k should be 0.657 when the D.C. line choke inductance is zero.

2.4.3. Choice of design variables

It is shown in sections 2.4.1. and 2.4.3. that for a given value of C_1 the value of k for minimum commutation energy and for minimum peak flux-linkage in the commutation chokes are not the same. Further, minimum peak flux-linkage in the commutation chokes occurs when k = 0.657 and $C_1 = \infty$ (zero inductance for line chokes). On the contrary minimum commutation energy occurs when k = 0.5 and C_1 = 0 (infinite inductance of line chokes). Moreover, as C_1 is increased (i.e. line choke inductance is decreased) I_p is increased. This means that large capacity main and auxiliary D.C. supply reservoir capacitors C_A, C_B, C_C and C_D (Figure 2.1) are required since a large

variation of the D.C. supply voltage is unwanted. Further, large values of I_p are to be avoided because each capacitor has a definite current capability and, if exceeded, the capacitor bank may fail. Increase of C_1 has further derogatory aspects in that it causes the ratings of the commutation thyristor and the auxiliary supply to be increased.

The value of C_1 may be chosen after giving due consideration to the economics involved. As this involves market research no attempt is made here to determine the optimal value of C_1 and k. Graphs (Figures 2.6 and 2.7) are given so that designers can have a wide range of C_1 and k here available and can decide on the value of C_1 and k by engineering judgement.

2.5. Capacity of Supply Reservoir

The reservoir capacitors C_A, C_B and C_C, C_D are required to supply the high current pulse during the commutation interval t_c. Inherent supply inductance renders the D.C. supplies unable to provide the current pulses. The capacity of these capacitors is best calculated from the amount of charge consumed during the commutation interval t_c and the acceptable voltage drop. Finally, the size of the capacitor should be such that it

can safely supply the peak current I_p at the end of the commutation interval.

The total charge required by the invertor during the commutation interval t_c is

$$Q_C = \int_0^{t_c} i\,dt$$

$$= I_o t_o x / f_1(x, k) \qquad \text{(Equation 2.38)}$$

If the acceptable voltage change is ΔV

$$C\Delta V = Q_C$$

$$C(\Delta V/V) = Q_C/V$$

$C = (Q_C/V)\,(V/\Delta V)$ where $\frac{\Delta V}{V}$ is the per unit voltage drop.

Substituting the value of Q_C from equation 2.38 in the above equation

$$C = I_o t_o x(V/\Delta V)/\{V f_1(x, k)\} \qquad (2.50)$$

The main supply reservoir capacitors C_A and C_B must be determined under worst case conditions, that is when the main supply voltage V_1 and the invertor frequency are low.

On the contrary, the commutation circuit components must be calculated for the highest supply voltage V_1 at the

highest operating frequency.

CHAPTER 3

DESIGN OF THE INVERTOR

The design of the invertor may be classified as illustrated below. With reference to figure 2.1.

i) The design of the commutation circuit involving the determination of :

(a) the inductance of the D.C. line chokes, L_1 and L_2;

(b) the commutation capacitor C_3 and its voltage rating;

(c) the main and auxiliary supply voltages V_1 and V_2 and their ratings;

(d) the current and voltage ratings of the D.C. line clamping diodes D_7 and D_8;

(e) the current and voltage ratings of the commutating thyristors Th_7 and Th_8;

(f) the capacitance values and the voltage ratings of D.C. supply reservoir capacitors C_A, C_B, C_C and C_D;

(g) the design of the thyristor bridge involving the determination of the voltage and current ratings of the thyristors Th_1 to Th_6;

(h) the design of the diode bridge involving the choice of the voltage and current ratings of the diodes D_1 to D_6;

(i) the protection against over-voltage and over-current.

The design equations derived in chapter 2 are listed in table 3.1 for convenience.

3.1. Specification

The specification usually provides sufficient constraints for circuit design to be possible. In this project an invertor was required to supply a 110 volt (at 50 Hz), 4 pole, 3 phase, 5 H.P. induction motor, with a frequency ranging from 10 Hz to 55 Hz.

3.2. Design of the Commutation Circuit

3.2.1. Choice of the main supply voltage

Considering the air-gap flux of the motor to be constant, the time fundamental component of supply voltage at 55 Hz, the highest frequency of operation, must be

$$110 \times \frac{55}{50} = 121 \text{ volts r.m.s.}$$

From appendix II, section AII-4, the amplitude of the idealized line to line output voltage of the invertor $\hat{V}_{INV}$ is related to the r.m.s. value of its time fundamental

Table 3.1 COMMUTATION CIRCUIT DESIGN TABLE

Functions of Design Variables x & k	Physical Quantity Represented by the Function	Functions in Terms of Design Variables x & k	Equation Number
Current Function x	$\{(I_p/I_o)^2 - 1\}^{\frac{1}{2}}$	x	2.20
Voltage Parameter k	$1/(1+V_2/V_1)$	k	2.18
Reverse Bias Time Function $f_1(x, k)$	$w_o t_o$	$\tan^{-1}x - \tan^{-1}\dfrac{kx}{\{1+x^2(1-k^2)\}^{\frac{1}{2}}}$	2.28
Commutation Energy Function $f(x, k)$	$\mathcal{E}_c/(V_1 I_o t_o)$	$\frac{1}{2}x/\{kf_1(x, k)\}$	2.34
Flux-linkage Function $f_3(x, k)$	$L_1 I_p/(V_1 t_o)$	$(1+x^2)^{\frac{1}{2}}/\{xkf_1(x, k)\}$	2.35
Inductance Function $f_4(x, k)$	$\tau_1/t_o = L_1 I_o/(V_1 t_o)$	$1/\{xkf(x, k)\}$	2.30
Capacitance Function $f_5(x, k)$	$\tau_c/t_o = V_1 C_3/(I_o t_o)$	$xk/f_1(x, k)$	2.31
Commutating thyristor Repetative i^2t Function $f_6(x, k)$	$(\int_0^{t_c} i^2 dt)/(I_o{}^2 t_o)$	$\dfrac{\frac{1}{2}\{(x^2+1)\tan^{-1}x - x\}}{f_1(x, k)}$	2.36
Commutating Thyristor R.M.S. Current $f_7(x, k)$	$I_{RMS}/\{(3ft_o)^{\frac{1}{2}} I_o\}$	$\left\{\dfrac{(x^2+1)\tan^{-1}x - x}{2f_1(x, k)}\right\}^{\frac{1}{2}}$	2.37

Functions of Design Variables x & k	Physical Quantity Represented by the Function	Functions in Terms of Design Variables x & k	Equation Number
Commutating Thyristor Average Current $f_8(x, k)$	$C_{I_{AV}}/(3fI_o t_o)$	$x/f_1(x, k)$	2.39
Auxiliary Commutating Supply Power Rating $f_9(x, k)$	$P_{CA}/(3fV_1 I_o t_o)$	$\frac{1}{2}x(1-k)/\{kf_1(x, k)\}$	2.40
Main D.C. Supply Supply Commutation Power Function $f_{10}(x, k)$	$P_{CM}/(3fV_1 I_o t_o)$	$\frac{1}{2}x/f_1(x, k)$	2.41
D.C. Line Clamping Diode Average Current Function $f_{11}(x, k)$	D_{I_A}/I_o	$\frac{1}{2}\{(x^2+1)^{\frac{1}{2}} - 1\}$	2.42
Total Commutation Time Function $f_{12}(x, k)$	$w_o t_c$	$\tan^{-1}x$	2.29
Reservoir Capacitance C	C_A, C_B, C_C, C_D	$\frac{I_o t_o x(V/\Delta V)}{Vf_1(x, k)}$	2.50

$L_{V_{1\ INV}}^{RMS}$ by

$$L\hat{V}_{INV} = \pi/(6)^{\frac{1}{2}}\ L_{V_{1\ INV}}^{RMS}$$

Therefore the required amplitude of the invertor output voltage is

$$L_{V_{INV}} = \pi 121/(6)^{\frac{1}{2}} = 150 \text{ volts.}$$

Allowing for thyristor and line voltage drop, a supply voltage of 160 V would be suitable.

Hence

V_1 = 160 V D.C. was assumed.

As the losses in the invertor are unknown, the power rating of the main D.C. supply P_{MAIN} was determined by estimating the invertor efficiency.

Assuming invertor efficiency η_{INV} to be 90% and the motor efficiency η_M to be 80% the output power of the main D.C. supply should be

$$P_{MAIN} = 0.746 \times H.P./(\eta_M \times \eta_{INV})$$

$$= 0.746 \times 5/(0.9 \times 0.8) = 5.18 \text{ KW}$$

3.2.2. Choice of auxiliary supply voltage

The auxiliary supply voltage V_2 depends on the choice

of the design variable k. Referring to figures 2.6 and 2.7, the value of k was chosen to be 0.57.

Substituting this value of k in equation 2.18 gave a value of 0.755 for the ratio of V_2 to V_1. Since V_1 is 160 volts (Section 3.2.1.) the auxiliary supply voltage V_2 should be 120V.

The power rating of the auxiliary commutating supply for a given value of frequency f, bridge thyristor reverse bias time t_o and main D.C. supply power at the instant of commutation V_1I_o, depends on the choice of the design variable x (Equation 2.40). The auxiliary commutating supply delivers maximum power when the operating frequency is high.

Choosing the value of x to be 1.25/0.57 from figures 2.6 and 2.7, the value of $P_{CA}/(3ft_oV_1I_o)$ calculated from equation 2.40 was 1.38. The highest operating frequency required was 55 Hz (Section 3.1.), the recommended bridge thyristor reverse bias time is 30 μsec (quoted by the thyristor manufacturer) and the power supplied by the main supply at the instant of commutation was V_1I_o = 8,320 watts (I_o is the D.C. link current during commutation, 52A from figure 3.1.). Using the above mentioned values the power rating of the auxiliary commutating supply was calculated from equation 2.40 to be 57 watts.

3.2.3 Commutation Efficiency

The total commutation power consists of that supplied by the auxiliary commutating supply P_{CA} (Sec. 3.2.2.), and that supplied by the main D.C. supply, P_{CM}. The values of x, k, V_1, I_o, f and t_o as given in section 3.2.2. when substituted in equation 2.41. provide the value of P_{CM} of 75 watt.

The total commutation power is therefore 132 watt. D.C. power supplied to the thyristor bridge at the instant of commutation is 8,320 watt. ($= V_1 I_o = 160 \times 52$).

If the commutation efficiency is defined as the ratio of the power to be diverted from the thyristor bridge to the total power involved at the instant of commutation, then the commutation efficiency in this design is 98.2%.

3.2.4 Inductance of D.C. Line Chokes

The inductance required for the D.C. line chokes was calculated by first finding the value of τ_1, for a given value of t_o, x and k from equation 2.30. Since the "worst case" for the commutation inductance occurs when the invertor is operating at highest voltage and frequency, using the values of x, k and t_o as given in section 3.2.2., the value of τ_1 was calculated to be 39.9×10^{-6} sec.

τ_1 is the ratio of the D.C. line choke inductance L_1 to the dynamic input resistance R_{in} (Equation 2.17). R_{in} is the ratio of the main supply voltage V_1 to the D.C. link

current I_o at the instant of commutation (Equation 2.14).

With voltage V_1 equal to 160 volt and I_o equal to 52 Ampere, L_1 was calculated to be 123 μH. By symmetry of the commutation circuit L_2 and L_1 are equal.

The chokes were rated to carry a direct current of 52 Amp (I_o) and at the end of commutation period t_c, a peak current of 126 Amp (I_p from equation 2.20).

The peak flux-linkage $L_1 I_p$ at the end of the period t_c was determined from equation 2.35. Substituting the values of x, k, V_1 and t_o, $L_1 I_p$ so calculated was 15.45 mWb-turn.

3.2.5. Choice of commutating capacitance

The commutating capacitance required can be determined for a given value of x and k from the capacitance function $f_5(x, k)$ (Equation 2.31). Since the capacitance function $f_5(x, k)$ gives the ratio of τ_c to t_o, then knowing t_o, τ_c can be calculated. τ_c is the product of the commutating capacitance C_3 and the dynamic input resistance R_{in} at the instance of commutation (Equation 2.16), and R_{in} is the ratio of the main supply voltage V_1 to the D.C. link current at the instant of commutation I_o (Equation 2.14). The "worst case" occurs when the invertor is delivering full power at the highest frequency of operation. Using the values of x, k, V_1, I_o, t_o under such operating conditions, and equations

2.31, 2.16 and 2.14, the value of C_3 was calculated to be 20.3 μF.

The maximum voltage applied to the capacitor is $\frac{1}{2}(V_1+V_2)$ Volt The capacitor voltage rating should therefore exceed 140 volt. It should also have a peak current rating of 126 Amp (I_p at the end of commutation).

3.2.6. Choice of size of supply reservoir capacitors

The supply reservoir capacitors C_A, C_B, C_C and C_D can be determined from equation 2.48, rewritten for convenience.

$$C = I_o t_o f_1(x, k)\left(\frac{V}{\Delta V}\right)\left(\frac{1}{V}\right) \qquad \text{(Equation 2.48)}$$

"Worst case" for C_A and C_B occurs when the main supply voltage is a minimum. Assuming that the minimum main supply voltage is 10 volts at a minimum invertor frequency of 10 Hz, the new value of k calculated from equation 2.18 was 0.0769.

Further

$$xk = (\tau_c/\tau_1)^{\frac{1}{2}} \qquad \text{(Equation 2.21)}$$

$$\tau_c = R_{in}C_3 \qquad \text{(Equation 2.16)}$$

$$\tau_1 = C_3/R_{in} \qquad \text{(Equation 2.17)}$$

$$R_{in} = V_1/I_o \qquad \text{(Equation 2.14)}$$

$$xk = V_1(C_3/L_1)^{\frac{1}{2}}/I_o$$

Since C_3, L_1 and I_o have been already fixed

$$xk \propto V_1$$

xk for lowest frequency

$$= \text{xk for highest frequency} \cdot \frac{V_1 \text{ at low-frequency}}{V_1 \text{ at high-frequency}}$$

The new value of xk so calculated was 0.078. Since the new value of k calculated earlier was 0.0769, the new value of x is 1.015.

Substituting these new values of x and k in equation 2.28, the new value of $f_1(x, k)$ was obtained to be 0.715. In the limit when the main supply voltage V_1 tends to zero, x tends to unity and $f_1(x, k)$ tends to 45^o or 0.785 radians.

Substituting the new values of x, k, $f_1(x, k)$, V_1 together with the values of I_o, t_o (Section 3.2.2.) in equation 2.50, the worst case capacity required for the main supply, can be determined provided the ratio of $(V_1/\Delta V_1)$ can be decided upon. Taking the allowable percentage change of the main supply voltage 100 $(\Delta V_1/V_1)$ as 5%, the main supply reservoir capacitance was calculated to be 4,440 μF. Since the main supply reservoir capacitor consists of two capacitors C_A and C_B in series, then $C_A = C_B = 10,000$ μF were used.

The main supply voltage V_1 is impressed across these two equal valued capacitors in series and therefore the voltage rating of each of them should exceed half of the main supply voltage. The "worst case" from the voltage and current rating point of view occurs when the invertor is operating at the highest voltage and frequency. The voltage rating of these capacitors should therefore exceed 80 volts D.C. These capacitors should also be able to supply peak currents of 126 Ampere at the highest frequency of operation.

For the auxiliary supply reservoir capacitors C_C and C_D, the worst case occurs when the main supply voltage is at its highest corresponding to the highest frequency of operation. Using the values of x, k, I_o, t_o, V_2 given in section 3.2.2. and the allowable percentage variation of commutating supply voltage of 5%, the capacitance of the commutating supply capacitors C_C and C_D was calculated from equation 2.50 to be 1,900 μF each. Two capacitor banks each of 2,000 μF capacity were used.

The voltage rating of each bank should be greater than $V_2/2$ or 60 volts and should also be able to deliver the peak current of 126 Ampere at the highest frequency of operation.

3.2.7. Total commutation time

The total commutation time t_c was obtained from equations 2.29 and 2.5

where

$$t_c = (L_1 C_3)^{\frac{1}{2}} \tan^{-1} x$$

From section 3.25, x at the highest frequency of operation is 2.19, and for the lowest frequency of operation it is 1.015. L_1 and C_3 are, from sections 3.2.4. and 3.2.5., 123 μH and 20.3 μF.

Substituting these values in the above equation the total commutation time for the highest voltage and frequency was found as 51.3 μsec, whereas that for the minimum voltage and frequency was 39.7 μsec.

The total commutation time is lower for low voltage and low frequency operation, as compared to that for high voltage and high frequency operation, if the auxiliary supply voltage and the current to be commutated remains constant.

3.2.8. Bridge thyristor reverse bias time

Itwas advisable at this stage to check that the reverse bias times t_o for both highest frequency-highest voltage, and lowest frequency-lowest voltage operation were acceptable.

The reverse bias time t_o from equations 2.28 and 2.5 is

$$t_o = (L_1 C_3)^{\frac{1}{2}} f_1(x, k)$$

In section 3.2.6.it has been shown that $f_1(x, k)$ is 0.6 at the highest voltage and frequency, and that at the lowest voltage and frequency it is 0.715.

For highest frequency of operation, t_o is therefore 30 μsec, and for the lowest frequency of operation is 35.8 μsec.

Unlike the total commutation time t_c, the reverse bias time t_o increases as the voltage and frequency decreases, if all other conditions remained the same.

3.2.9. Choice of commutating thyristors

The commutating thyristors, Th_7 and Th_8, undergo the "worst case" condition when the invertor is operating with full main supply voltage at the highest operating frequency.

The r.m.s., and average current of these thyristors can be determined from equation 2.37 and equation 2.39. The i^2t value of the thyristors can be also determined from equation 2.36.

Substituting the values of x, k, I_o, f and t_o given in section 3.2.2. in the above equations, the various ratings pertaining to current flow were calculated and are listed below :-

R.M.S. current = 7.08 Ampere

Average current = 0.942 Ampere

i^2t value = 0.302 A^2-sec

Peak current I_p = 126 Ampere

Conduction time t_c = 57.3 μsec.

The voltage rating of the commutating thyristors was determined as follows. Referring to figure 2.1, immediately prior to the end of commutation period, with thyristor Th_7 in conduction, the potential of the point X becomes $\frac{1}{2}V_1$ volt, causing the potential of the point m to be $\frac{1}{2}(V_1+V_2)$ volt.

During this period the diodes D_1 and D_3, along with thyristor Th_2, are in conduction, causing the voltage across the R & B, and Y & B terminals of the load to appear across the choke L_2. Due to the highly inductive nature of the induction motor-load this voltage is very nearly equal to the main D.C. supply V_1 (a condition set during the period when Th_1, Th_2 and Th_3 are conducting).

The potential of the point U is then at 1.5 V_1 volt. The forward voltage which the thyristor Th_8 has to block is $(2V_1+V_2)$ volt.

Taking a safety factor of 20% to allow for unpredictable transient over-voltage, the forward blocking voltage rating of the commutation thyristors Th_7 and Th_8 should be 530 volt.

From figure 2.1 it can be seen that no significant reverse voltage is applied to the commutation thyristors.

3.2.10 Choice of D.C. line diodes

The reverse voltage rating of the D.C. line diodes D_7 and D_8 was determined from the consideration that at the instant, say, of positive line commutation the point X drops to a potential of $-(\frac{1}{2}V_1+V_2)$ volt. The cathode of D_7 being held at $\frac{1}{2}V_1$ volt, the diode D_7 is reversed biased by (V_1+V_2) volt.

Substituting numerical values of V_1 and V_2 the D.C. line diodes D_7 and D_8 are reverse biased by 280 volt at the instant of commutation. Using a 20% factor of safety against any unpredictable transient over voltage, the reverse voltage rating of the D.C. line diodes D_7 and D_8 should therefore be equal or exceed 336 volt.

The average current through the diodes D_7 and D_8 can be calculated from equation 2.42. Substituting the value of the design variable x(=2.19) chosen in section 3.2.2. in the equation 2.42 the ratio of average value of the diode current $^{D}I_{AV}$ to the current at the instant of commutation I_o(= 52 Ampere, section 3.2.2.) was calculated to be 0.71. From this average current rating of the diodes D_7 and D_8 was determined as 37 Ampere. The peak current through the diodes is the difference between the peak current reached in

the D.C. line chokes at the end of commutation I_p(= 126 Ampere) and I_o. This yielded the peak diode current as 74 Ampere.

3.3. Design of Thyristor Bridge

The design of the thyristor bridge involves the determination of the voltage ratings and current ratings of the bridge thyristors Th_1 to Th_6.

3.3.1. Voltage ratings of bridge thyristors

The reverse voltage rating of the thyristors must be determined for the instant of commutation as explained below. Supposing thyristors 1, 2, and 3 are conducting (Figure 2.1) then triggering of thyristor Th_7 would cause the potential of the point X to fall to $-(\frac{1}{2}V_1+V_2)$ volt as shown in figure 2.5. The complementary diodes D_1 and D_3 would start conducting to maintain current continuity in the R and Y lines of the output. This would cause the cathodes of thyristors Th_1 and Th_3 to be clamped at $-\frac{1}{2}V_1$ volt, thereby causing the above thyristors to be reversed biased by $-(\frac{1}{2}V_1+V_2) - (-\frac{1}{2}V_1) = -V_2$ volt.

The forward blocking voltage rating of the bridge thyristors is determined by considering the interval during which the thyristors Th_1, Th_2, and Th_3 are conducting. Thyristors Th_4, Th_6 and Th_5 would then block the forward voltage of V_1 volt.

Since the main supply voltage V_1 is 160 volt, the bridge thyristors would need to block a forward voltage of 160 volt. Allowing a factor of safety of 20% the forward voltage blocking capability of the bridge thyristors should therefore equal or exceed 192 volt.

3.3.2. Current ratings of bridge thyristors

The calculation of the current ratings of the bridge thyristors is rather involved. Time domain analysis given in chapter 7 shows that although the sum of the conduction angles of the bridge thyristor and their complementary diode is always 180°, the conduction angles of the thyristors and that for the complementary diodes vary individually in accordance with the loading of the motor. With higher motor slip the angle of conduction of the bridge thyristor is also greater.

The worst case, from a current conduction point of view, occurs when the machine is at standstill with the supply voltage and frequency adjusted to maintain the fundamental component of air-gap flux at its rated value. Digital computer analysis under these conditions give the following results.

Machine terminal condition :-

Invertor-fed stator line to line peak voltage

$$L\hat{V}_{INV} = 15.3 \text{ volt}$$

Invertor-fed stator line to line time fundamental r.m.s. voltage

$$L V_{1\ INV}^{RMS} = 11.9 \text{ volt}$$

Invertor-fed supply frequency = 4 Hz

Invertor-fed r.m.s. value of stator line current

= 33.8 Ampere

Bridge thyristor condition :-

Average bridge thyristor current = 14.9 Ampere

R.M.S. bridge thyristor current = 24.0 Ampere

Peak bridge thyristor current = 52.0 Ampere

Bridge thyristor conduction angle = 167.45^{o}

Bridge thyristor i^2t = 143.45 A^2- sec.

Complementary diode conditions :-

Bridge diode average current = 0.486 Ampere

Bridge diode r.m.s. current = 3.3 Ampere

Bridge diode peak current = 31.9 Ampere

Bridge diode i^2t = 2.8 A^2-sec

Bridge diode conduction angle = 12.55^o

The wave-form of the stator R-phase line current under these conditions was calculated and shown in figure 3.1(a). The thyristors used in the bridge were chosen to be of higher current rating than required as the invertor was experimental.

3.4 Design of Diode Bridge

In a similar manner to the design of thyristor bridge, the design of the complementary diode bridge consists of determination of voltage rating and current rating of the diodes.

3.4.1 Voltage rating of bridge diodes

The reverse voltage rating of the complementary diodes was established in the following manner.

Considering that the bridge thyristors Th_1, Th_2 and Th_3 are conducting, and the instant when thyristor Th_7 is gated in order to switch off the thyristors Th_1 and Th_3, the potential of point X falls to $-(\frac{1}{2}V_1+V_2)$ volt. The thyristor Th_7 then diverts the current from flowing through thyristors Th_1 and Th_3.

This current starvation does not cause these bridge thyristors to be switched off at once. Only when the charge stored in these thyristors is removed (accelerated by reverse biasing) will the off condition be attained. Hence, as soon as thyristor Th_7 is gated the potential of the cathodes of thyristors Th_1 and Th_3, and hence anodes of the diodes D_4 and D_6 becomes $-(\frac{1}{2}V_1+V_2)$ volt. The continuity of current in the R and Y leads of the load demands an immediate flow of current through the diodes D_1 and D_3. This demand of current is initially met by the flow of charge in the diodes D_1, D_3. Since the cathodes of the diodes D_4 and D_6 are at a potential of $\frac{1}{2}V_1$ and the anodes of the diodes D_1 and D_3 are at a potential of $-\frac{1}{2}V_1$, the diodes D_4 and D_6 are reversed biased by (V_1+V_2) volt, whereas the diodes D_1 and D_3 are forward biased by V_2 volt. This forward biasing of diodes D_1 and D_3 causes accelerated injection of charge and rapidly switches them into the conduction mode, thereby making the currents through the R and Y terminals of the load to be of conduction type.

Once the diodes D_1 and D_3 are in conduction the cathodes of thyristors Th_1 and Th_3 are clamped at $-\frac{1}{2}V_1$ volt. Since the point X is at a potential of $-(\frac{1}{2}V_1+V_2)$ volt, these thyristors Th_1 and Th_2 are reversed biased by V_2 volt and switch off. Under this condition, neglecting the forward voltage drops in the diodes, D_1 and D_3 have no voltage across their terminals, whereas diodes D_4 and D_6 are reversed biased

by V_1 Volt.

Since the main supply voltage V_1 is 160 Volt and the auxiliary supply voltage V_2 is 120 Volt, the complementary bridge diodes are reversed -biased by 280 Volt. Using a safety factor of 20% the reverse voltage rating of these diodes should therefore be equal to or exceed 336 Volt.

3.4.2 Current ratings of bridge diodes

The worst case, for the bridge diodes, from current conduction point of view is considered to occur when the machine is running at super-synchronous speed with unity slip, the supply voltage and frequency adjusted to maintain the fundamental component of air-gap flux at its rated value.

Analysis on a digital computer based on the theory developed in chapter 7 yielded the following results.

Machine conditions :-

Invertor-fed stator line to line peak voltage

$$L\hat{V}_{INV} = 5.75 \text{ Volt}$$

Invertor-fed stator line to line time fundamental r.m.s. voltage

$$L V_{1\ INV}^{RMS} = 4.47 \text{ Volt}$$

R.M.S. value of stator line current

$$= 33.3 \text{ Ampere}$$

Supply frequency = 4 Hertz

Bridge thyristor conditions :-

Average bridge thyristor current = 4.6 Ampere

R.M.S. bridge thyristor current = 23.6 Ampere

Peak bridge thyristor current = 49.3 Ampere

Bridge thyristor conduction angle = 69.068

Bridge thyristor i^2t = 139.287 A^2-sec.

Bridge diode conditions :-

Bridge diode average current = 10.3 Ampere

Bridge diode r.m.s. current = 20.20 Ampere

Bridge diode peak current = 49.3 Ampere

Bridge diode i^2t = 101.6 A^2-sec.

Bridge diode conduction angle = 110.932^{o}

The wave-form of the stator R-phase line current under these conditions was calculated and shown in figure 3.1(b).

3.5 Protection of Invertor [2.3.4]

Since the semi-conductor switches used in the invertor are very susceptible to over-voltage and over-current, even of very short duration, any protection scheme used should be extremely fast acting.

It is possible to make an invertor "fail safe" by monitering currents and voltages at various strategic points in the circuit and feeding the signal to an electronic controller which in turn controls the gating signals.

Since such "fail safe" systems are complex, time consuming to design, costly and not required for an experimental invertor, simple protective schemes were used.

3.5.1 Transient over-voltage protection

Transient over-voltage protection was achieved by shunting each thyristor with a series circuit consisting of a 2 μF capacitor and a 5 Ω resistor. The capacitor limits the short duration voltage transients at the thyristor and the 5 Ω resistor limits the capacitor discharge current when the thyristor turns on.

3.5.2 Over-current protection

High-speed fuses were used to protect the thyristor from over-current, the i^2t rating of fuse and thyristor being correctly matched.

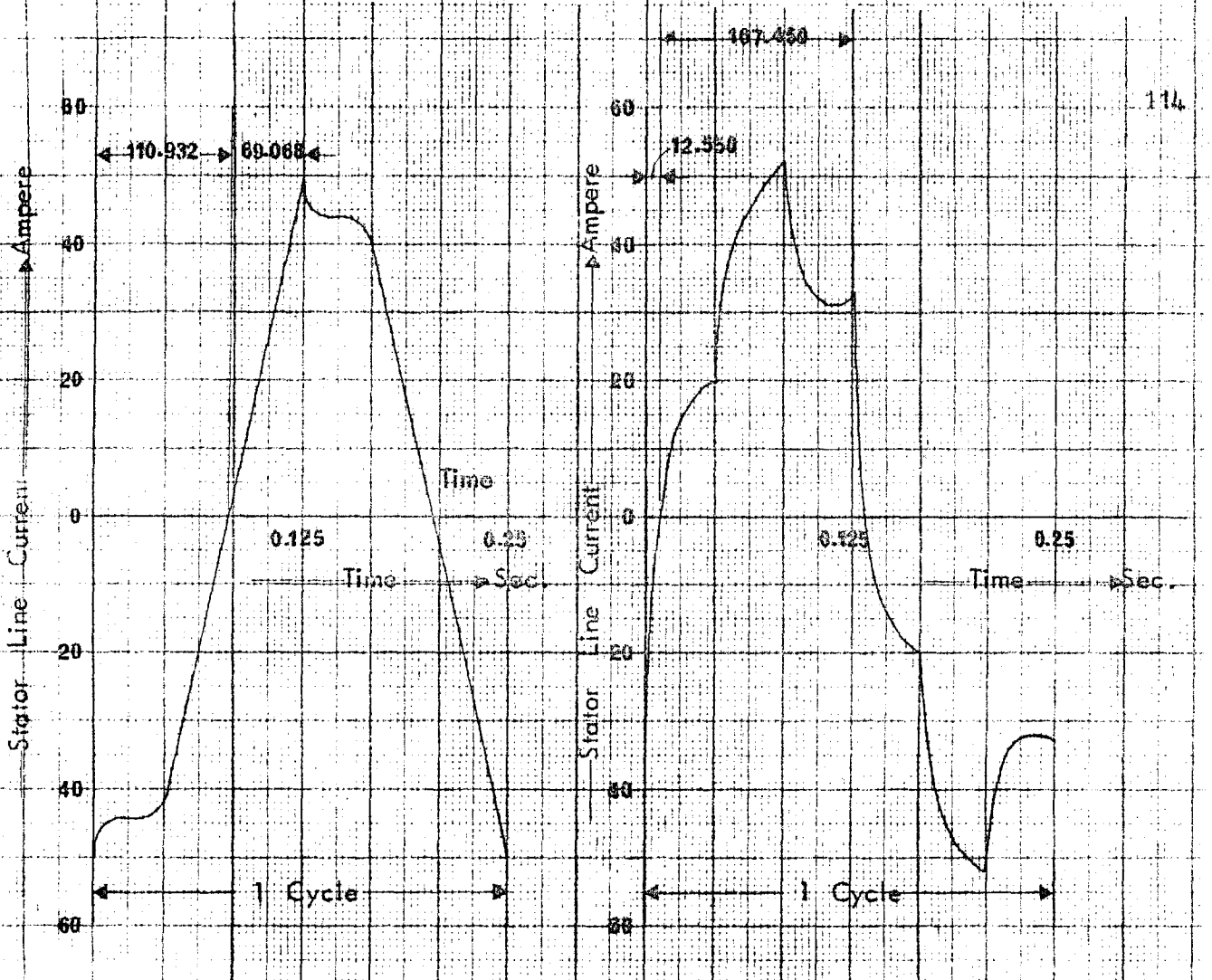

(a) 100% Rotor Slip (Generator)
$L_{V_{INV}} = 5.75$ V,
$f_{INV} = 4.0$ Hz.

(b) 100% Rotor Slip (Motor)
$L_{V_{INV}} = 15.3$ V,
$f_{INV} = 4.0$ Hz.

Items	Generating	Motoring
Bridge Diode Average Current	10.322 A	0.486 A
Bridge Diode R.M.S. Current	20.162 A	3.334 A
Bridge Diode Peak Current	49.257 A	31.901 A
Bridge Diode i^2t	101.627 A-Sec	2.779 A-Sec
Bridge Diode Conduction Angle	110.932 Deg	12.550 Deg
Bridge Thyristor Average Current	4.608 A	14.938 A
Bridge Thyristor R.M.S Current	23.604 A	23.962 A
Bridge Thyristor Peak Current	49.257 A	51.971 A
Bridge Thyristor i^2t	139.287 A^2-Sec	143.539 A^2-Sec
Bridge Diode Conduction Angle	69.068 Deg	167.450 Deg
Stator R.M.S. Line Current	33.326 A	33.800 A

FIGURE 3.1 STATOR CURRENT UNDER "WORST CASE" DESIGN CONDITION

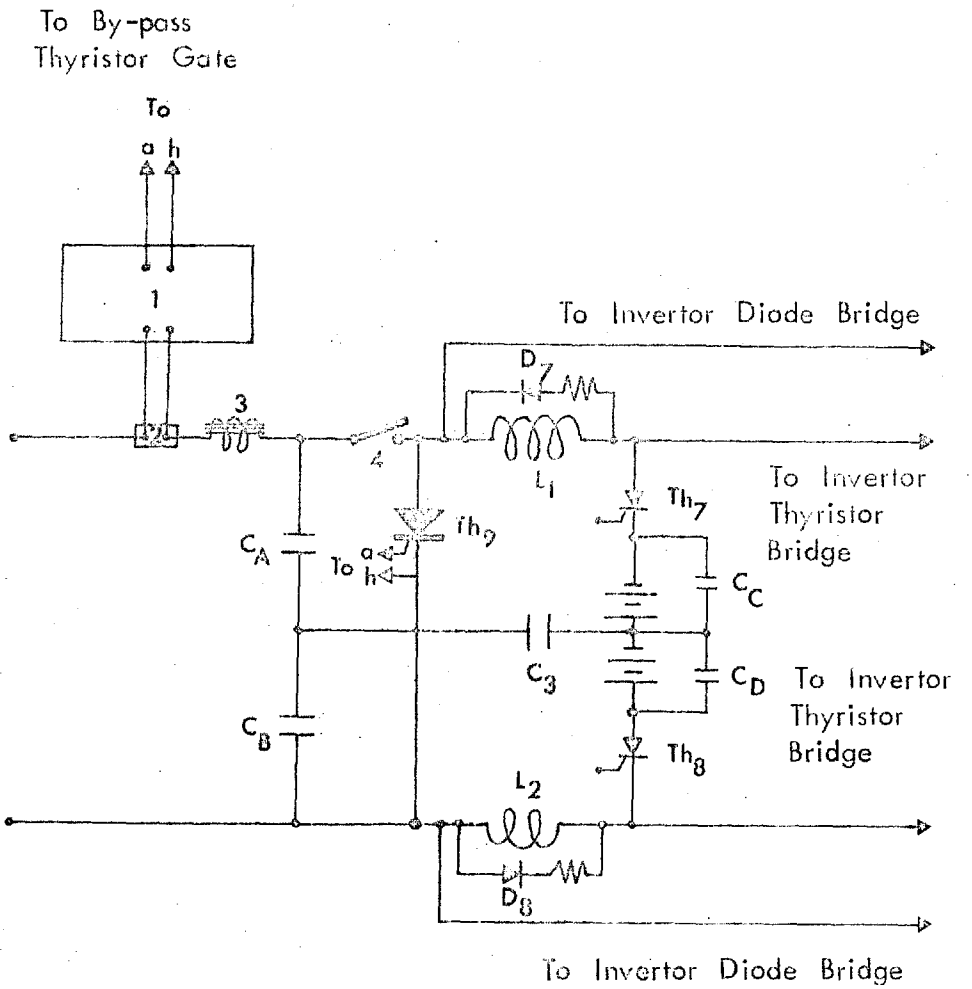

Legend:-

1. Over-current Detector Unit (Figure 3.3)
2. Shunt
3. Crow-bar Actuating Coil
4. Crow-bar

Figure 3.2 Inverior Overcurrent Protection By Electronic Crow-bar.

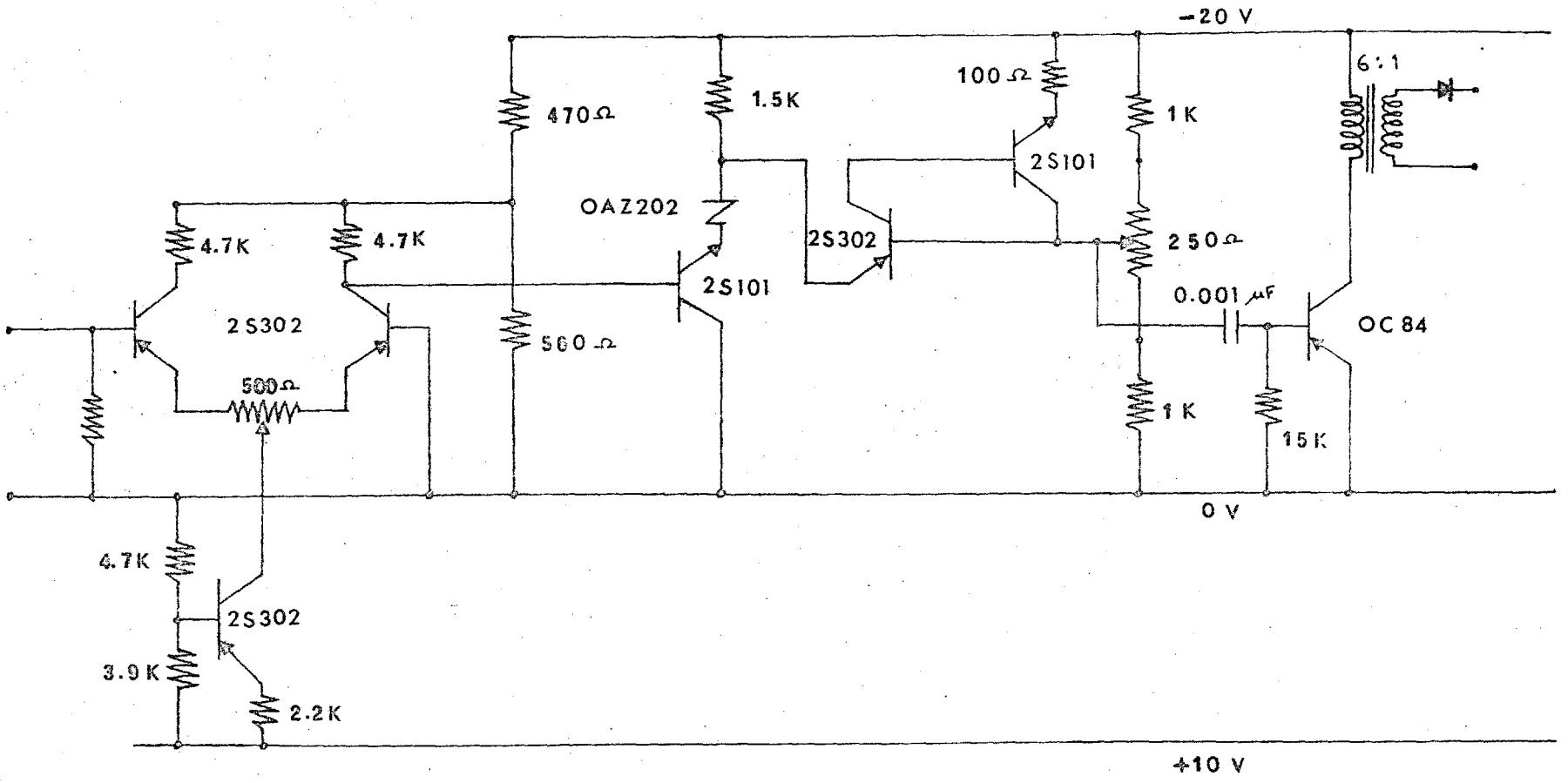

Figure 3.3 Electronic Circuit For Invertor Over-Current Protection.

No protection other than over-voltage protection was used for the diodes. Fuses were not used in series with the diodes. This is because, if due to any reason these diode fuses blow, excessive voltage would develop across the thyristors due to lack of feed-back path of energy stored in the load.

High-speed fuses were used in series with the D.C. supplies as well as at the three-phase output of the invertor to provide overall protection. These fuses were properly co-ordinated with the individual cell fuses.

Additional over-current protection by means of electronic "crow-bar" and by-pass thyristors was also used (Figure 3.2). The electronic circuit (Figure 3.3) monitors the invertor supply current and triggers the by-pass thyristor when a pre-set current level is exceeded. The by-pass thyristor places a short circuit across the invertor main supply terminals and diverts the short circuit current away from the invertor. Under such conditions the whole main supply voltage appears across the low impedance "crow-bar" actuating coil, causing a rapid build-up of current in it. This rapid current build-up causes fast opening of the switch. Since the by-pass thyristor is normally in the non-conducting state, when called upon it can handle a heavy surge current without damage.

CHAPTER 4

THE INDUCTION MOTOR AND EXPERIMENTAL DETERMINATION OF EQUIVALENT CIRCUIT PARAMETERS

4.1 Design Details of the Induction Motor

The induction motor used throughout the investigation had the following design details :-

B.T.H. motor M.Z. 3519

Serial Number 48929-H

5 H.P., 4 Pole, 110 Volt, 50 Hz, 3-Phase

	Stator	Rotor
Type of winding	Double layer lap	Double layer lap
Number of slots	36	24
Pitch of the windings %	77.8	66.7
Pitch of the windings slots	1 - 8	1 - 5
Number of coils	36	24
Turns per coil (Total)	33	26
Wires in parallel	1	2
Turns per coil (effective)	33	13
Wire diameter (bare)	0.048 inch	0.056 inch
" " " (covered)	0.051 inch	0.059 inch
" insulation	Lewmex	Lewmex

Mean length of turn	23 inch	18 inch
Circuits in parallel	1	1
Turns in series per phase	99	104
Connection of phases	Δ	Y
Insulation class	A	A
Resistance at 20° Centigrade per phase	0.215 Ω	0.260 Ω
Slot size	0.86 x 0.46 x 0.31"	1.2 x 0.19 x 0.44"

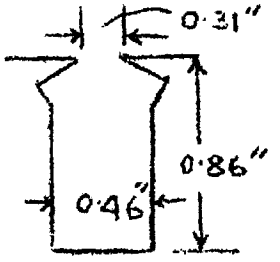

Stator slot

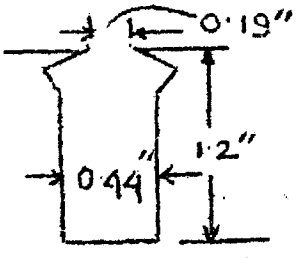

Rotor slot

4.2 Conventional Constant Frequency Equivalent Circuit

A conventional equivalent circuit representation of an asynchronous machine under fixed frequency sinusoidal excitation is shown in figure 4.1 This equivalent circuit refers to one phase of a star connected (or an equivalent star connected machine; the voltages shown are line to neutral voltages, and the currents are line current. The various parameters of the equivalent circuit are

R_1 = Stator resistance

R_2 = Rotor resistance referred to stator

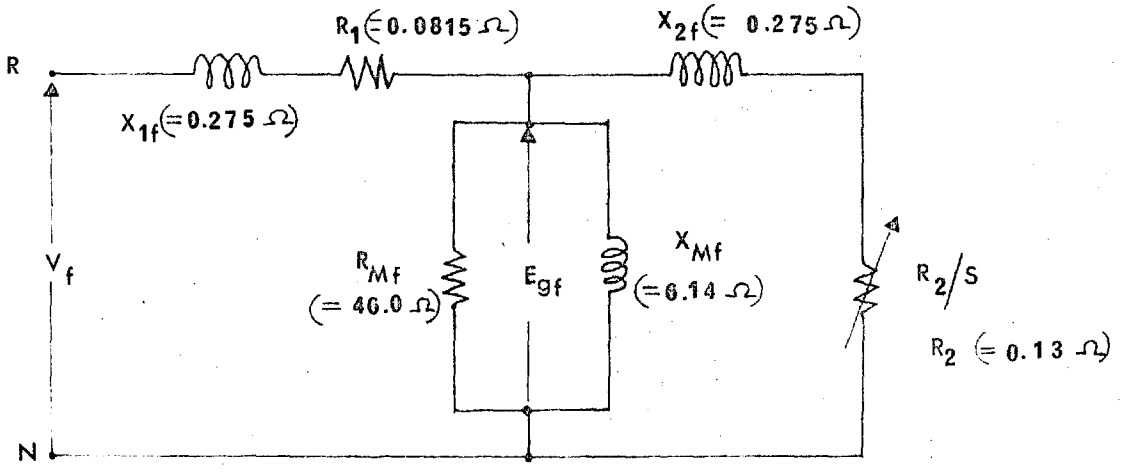

Figure 4.1 Simple Equivalent Circuit Of Induction Motor Supplied From Fixed Frequency Sinusoidal Source.
(Values In The Parenthesis Refer To Normal Voltage, Normal Frequency Operation)

X_{1f} = Stator leakage reactance at frequency f

X_{2f} = Rotor leakage reactance, referred to stator, at frequency f

X_{Mf} = Magnetizing reactance for space fundamental of air-gap mmf at frequency f

R_{Mf} = Iron loss, (in the main flux path) simulating resistance at frequency f

Except for R_1, the above parameters are not constant even over the full range of operation for a given supply voltage and frequency. The leakage reactances X_{1f} and X_{2f} depend on the leakage path saturation and are functions of load current. The magnetizing reactance X_{Mf} depends on main flux path saturation.

With varying supply voltages the magnitude of the main flux varies and also the stator leakage impedance drop, so that X_{Mf} depends on the stator current, but to a smaller degree than do X_{1f} and X_{2f}. The rotor resistance, R_2, may undergo skin effect changes with the frequency of induced rotor emf, and hence depends on rotor speed. Under normal operating conditions the rotor speed does not vary appreciably, so that the variation of R_2 is small. The core-loss simulating resistance R_{Mf} depends on the amount of core-loss and therefore on the air-gap voltage E_{gf}. The stator leakage impedance is small compared to the magnetizing

impedance so that the air-gap voltage does not vary appreciably with load and R_{Mf} may be considered constant over the range of normal operation.

Variable frequency (sinusoidal) no load test, with various supply voltages, and frequencies, were carried out in order to determine the variation of R_{Mf} and X_{Mf} with supply voltage and frequency.

Variable frequency (sinusoidal) locked rotor test were carried out for several values of stator line current and supply frequency. This yielded the variation of $(X_{1f} - X_{2f})$ and R_2 as a function of load current for different supply frequencies.

R_1 was determined by passing direct current through the stator winding and measuring the voltage drop across it (Figure 4.2).

4.3 Variable Frequency No-load Test

The experimental set-up was as shown in figure 4.3. For accurate determination of supply frequency a digital tachometer was used to moniter the alternator speed from which the supply frequency was computed from the formula $f = \frac{PN}{120}$ where f is the supply frequency, P the number of alternator poles, and N the speed of the alternator rotor in R.P.M. Since true no-load condition demanded that the slip of the induction motor rotor be zero, the induction motor rotor was driven by a D.C. machine which, under this condition, would

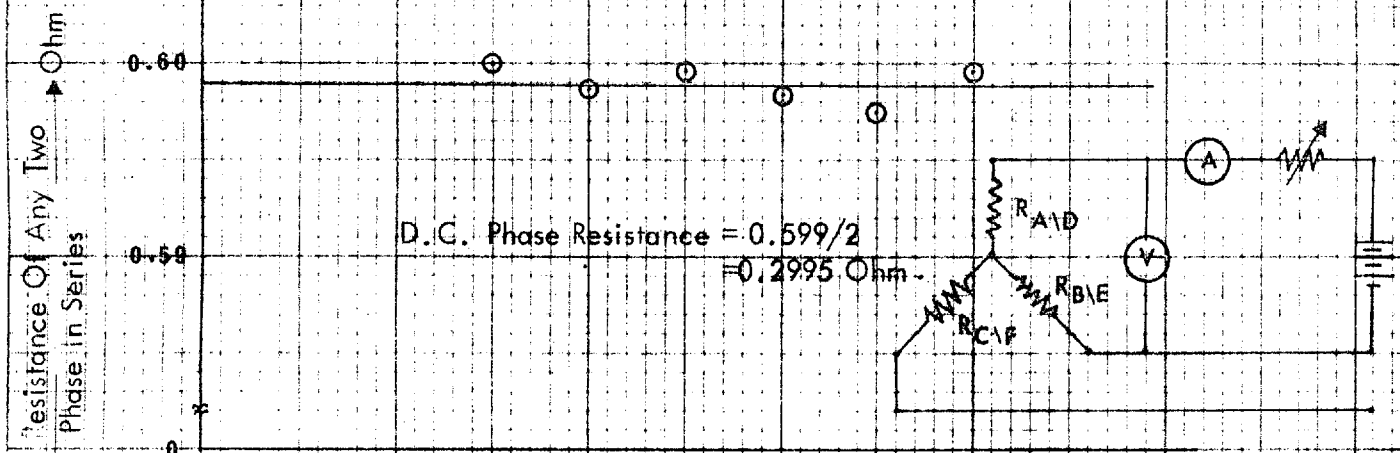

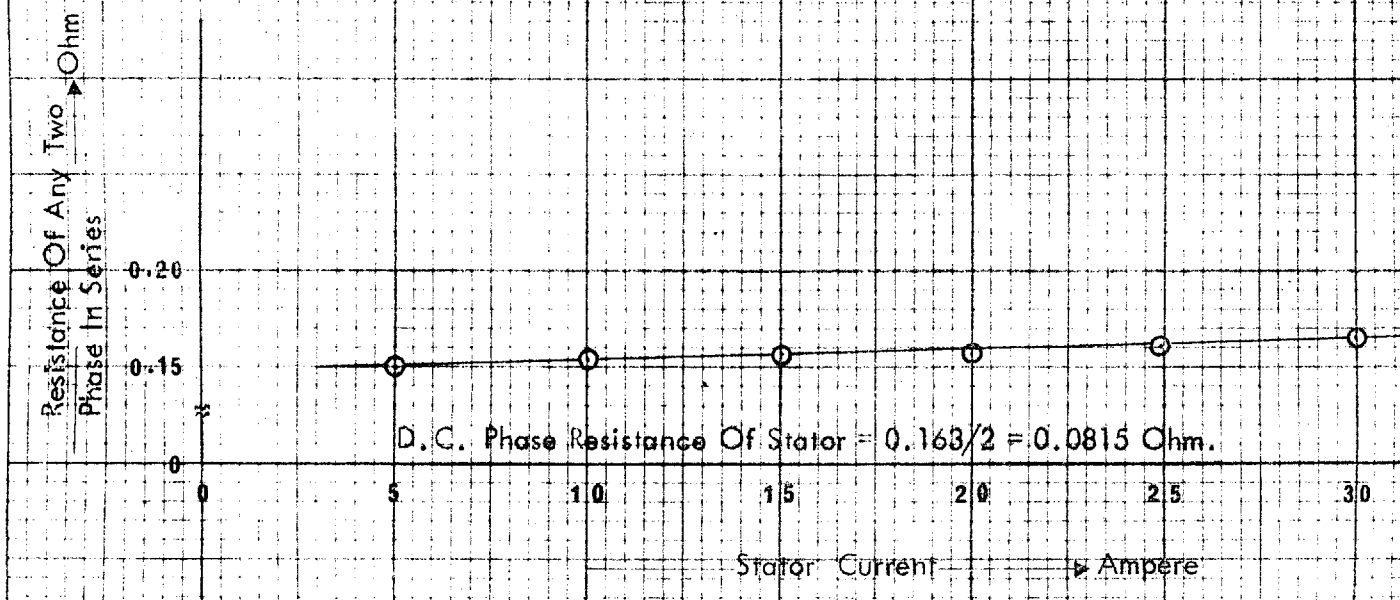

FIGURE 4.2 STATOR AND ROTOR RESISTANCE PER PHASE (D.C.) (EQUIVALENT STAR)

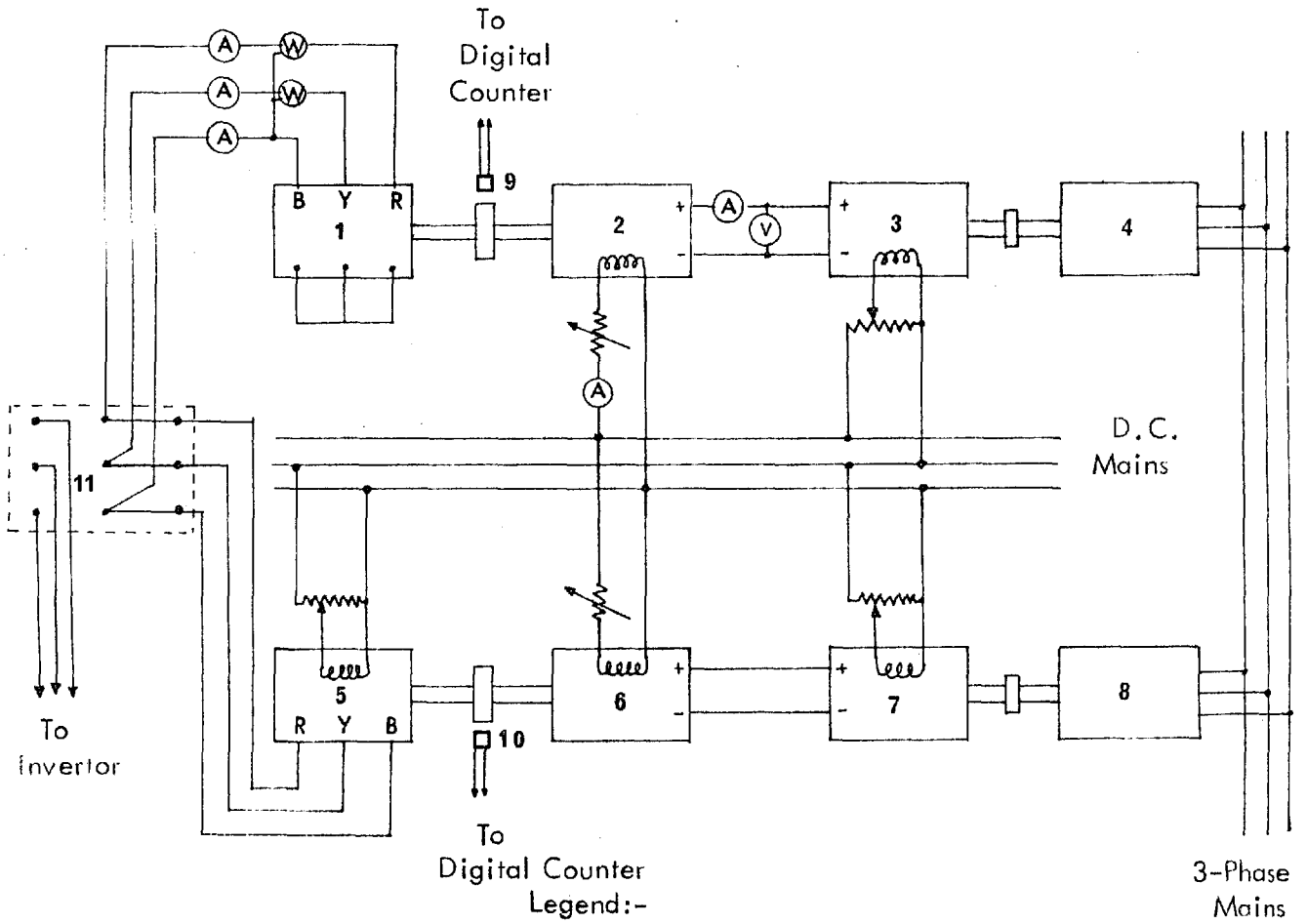

Legend:-

1. Induction Motor Under Test
2. D.C. Loading Motor
3. D.C. Generator
4. Induction Motor
5. Alternator
6. D.C. Driving Motor
7. D.C. Generator
8. Induction Motor
9. Photo-Electric Probe
10. Photo-Electric Probe
11. Change-Over Switch

Figure 4.3. Experimental Set-Up Used In The Investigation.

supply the windage and friction of the induction and D.C. motor combination including the rotational iron losses occurring in the teeth and on the surface of the stators and rotors. (Full details are given in Chapter 5.) In order to ascertain whether the induction motor was running at synchronous speed, the rotor speed was also monitored by another digital tachometer. These digital tachometers had an accuracy of $\pm$ 1 R.P.M. It was found that the D.C. machine was unable to maintain the synchronous speed within $\pm$ 1 R.P.M. continuously and so readings for the three stator-line currents and for the stator power input were taken just above synchronous speed and just below synchronous speed. The input current and the input power to the stator for the true no-load condition at synchronous speed were then interpolated from these sets of readings.

At synchronism, the slip S of the rotor is zero. From the simple equivalent circuit of figure 4.1 it can be seen that under this condition $\frac{R_2}{S} = \infty$, and the rotor may be considered to be open circuit. The power input to the stator winding consists of the main flux path iron loss and stator copper loss. The rotational iron loss is supplied by the D.C. machine and not by the alternating supply to the induction motor. The D.C. machine also supplied the windage and friction losses of the induction and D.C. motor combination.

Net power input P_{in} to the stator under no-load condition is given by

$$^{NL}P_{in} = 3\, I_{NL}^{2} R_1 + P_{h+e} \qquad (4.1)$$

where I_{NL} is the stator-line current at synchronous speed

P_{h+e} is the hysteresis and eddy current loss in the main flux path

The stator resistance R_1 being known, P_{h+e} were determined from the above equation 4.1.

The line to neutral air-gap voltage E_{gf} at frequency f induced in the stator winding by the main flux at no-load is given by

$$E_{gf} = V_{NL} - I_{NL}(R_1 + jX_{1f})$$

$$= V_{NL} - I_{NL}X_{1f} \qquad (4.2)$$

where V_{NL} is the no-load line to neutral voltage of the stator supply.

The stator leakage reactance X_{1f} was determined from the locked rotor test for a rotor current of I_{NL} Ampere.

Knowing E_{gf}, the magnetizing impedance elements, X_{Mf} and R_{Mf} of the equivalent circuit (Figure 4.1) were determined as follows

$$R_{Mf} = \frac{3E_{gf}^{2}}{P_{h+e}} \qquad (4.3)$$

and

$$X_{Mf} = \frac{E_{gf}}{I_{NL}\sin\phi_{NL}} \qquad (4.4)$$

where ϕ_{NL} is the angle by which the no-load current lags the air-gap voltage E_{gf}. This is very nearly equal to the angle by which the no-load current I_{NL} lags behind the stator supply voltage V_f because the stator leakage impedance is small compared with the magnetizing impedance.

A family of curves for R_{Mf} and X_{Mf} as functions of the supply voltage V_f for various constant supply frequencies are shown in figures 4.4 and 4.5. In order to examine the behaviour of R_{Mf} and X_{Mf} as functions of supply frequency another two graphs were drawn to the base of frequency for various constant values of V_f/f (Figures 4.6 and 4.7). For the frequency range considered and for any fixed air-gap flux, both X_{Mf} and R_{Mf} are linear functions of frequency. The linear variation of R_{Mf} with frequency, indicates that the iron loss in the main flux-path was mainly due to hysteresis. For an air-gap flux corresponding to 2 volt/Hz (taken to be the working air-gap flux in this investigation), the value of R_{Mf} and X_{Mf} at 50 Hz were 46 Ω and 6.14 Ω respectively. These values were taken for the equivalent circuit "constants". The variation of magnetizing reactance at 50 Hz with main flux-path saturation is shown in figure 4.8.

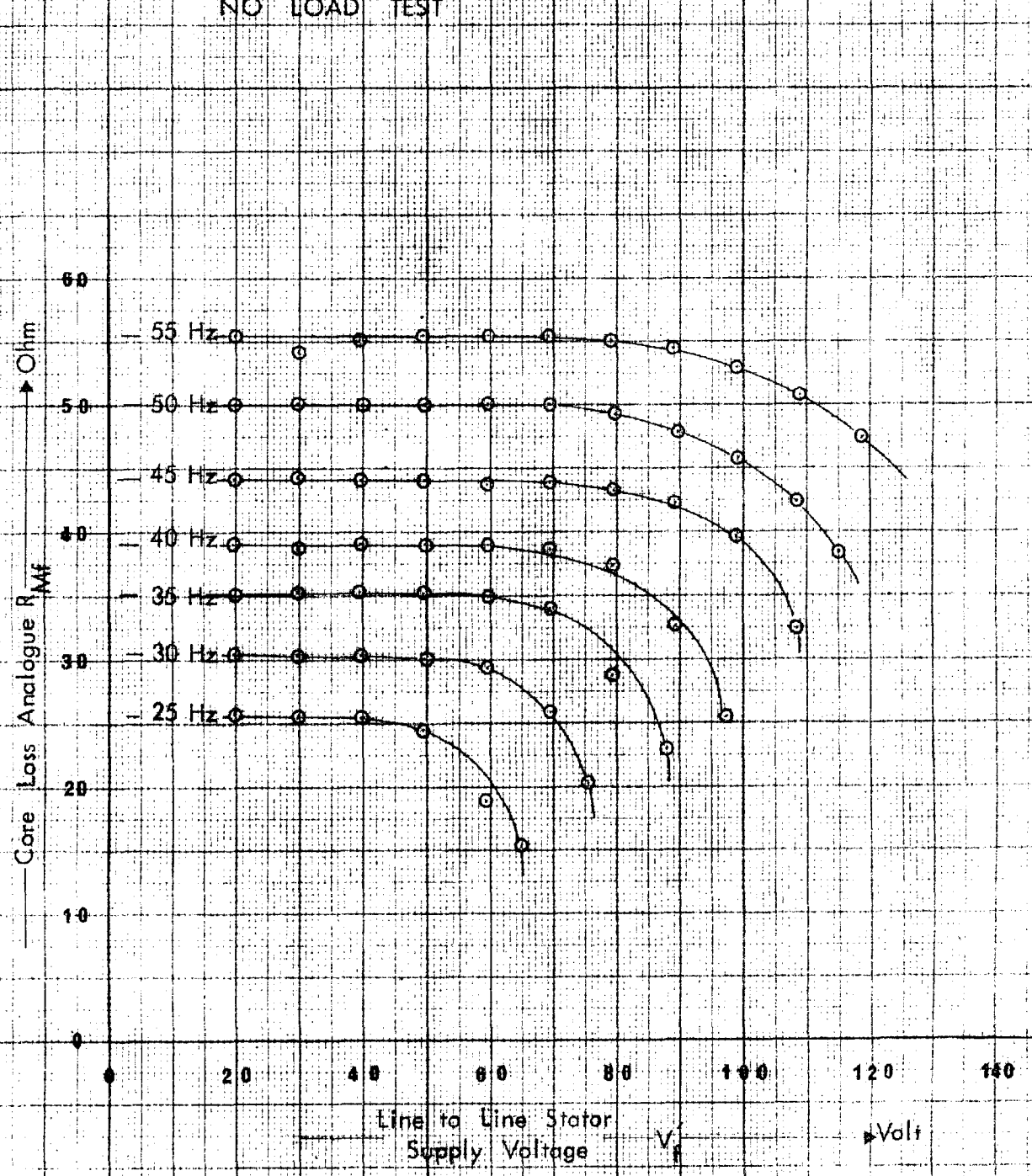

FIGURE 4.4 CORE LOSS R_{Mf} VS LINE TO LINE STATOR SUPPLY VOLTAGE V_f' FOR VARIOUS FIXED VALUES OF FREQUENCY.

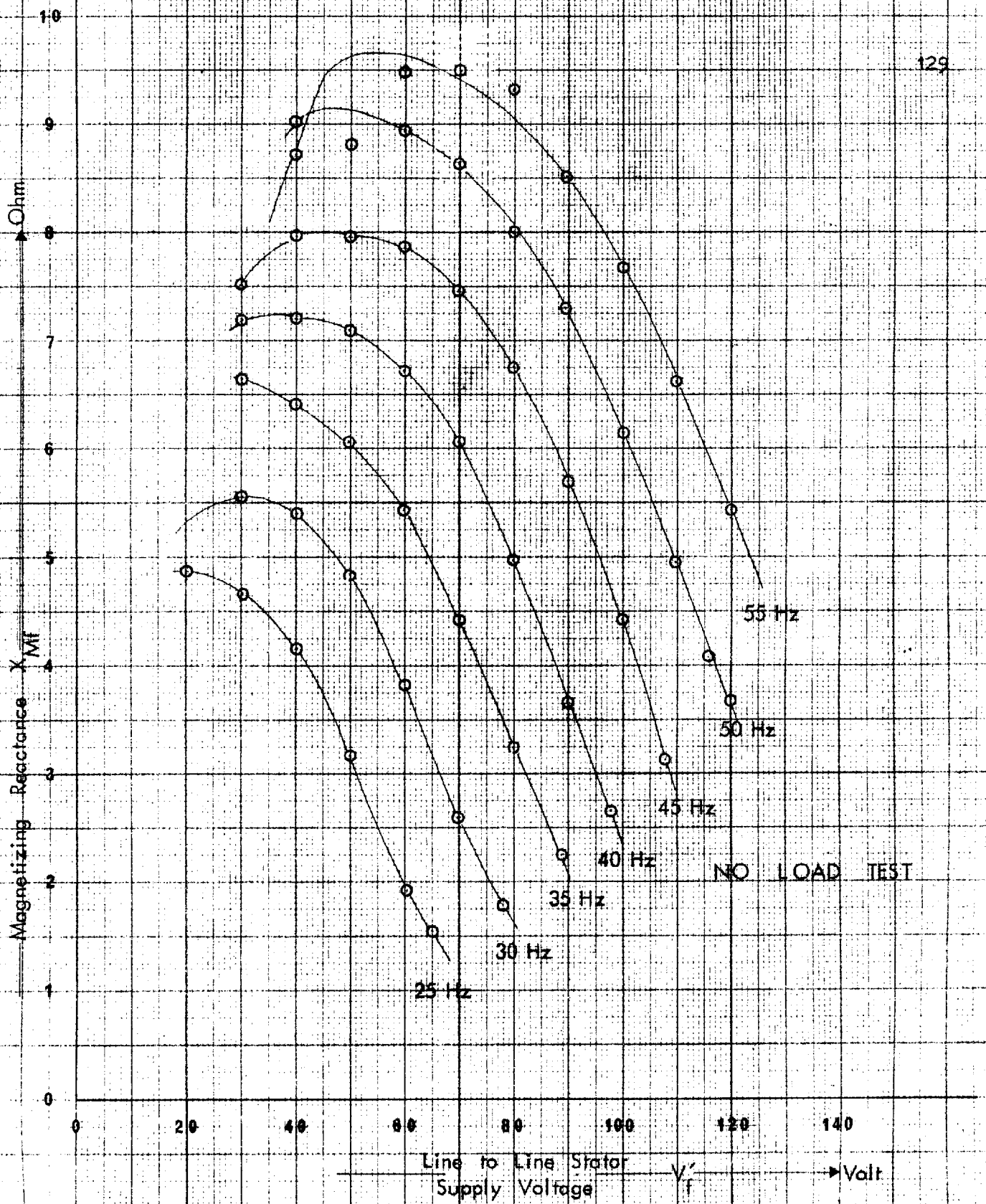

FIGURE 4.5 MAGNETIZING REACTANCE X_{Mf} VS LINE TO LINE STATOR SUPPLY VOLTAGE V'_f FOR VARIOUS FIXED VALUES OF FREQUENCY.

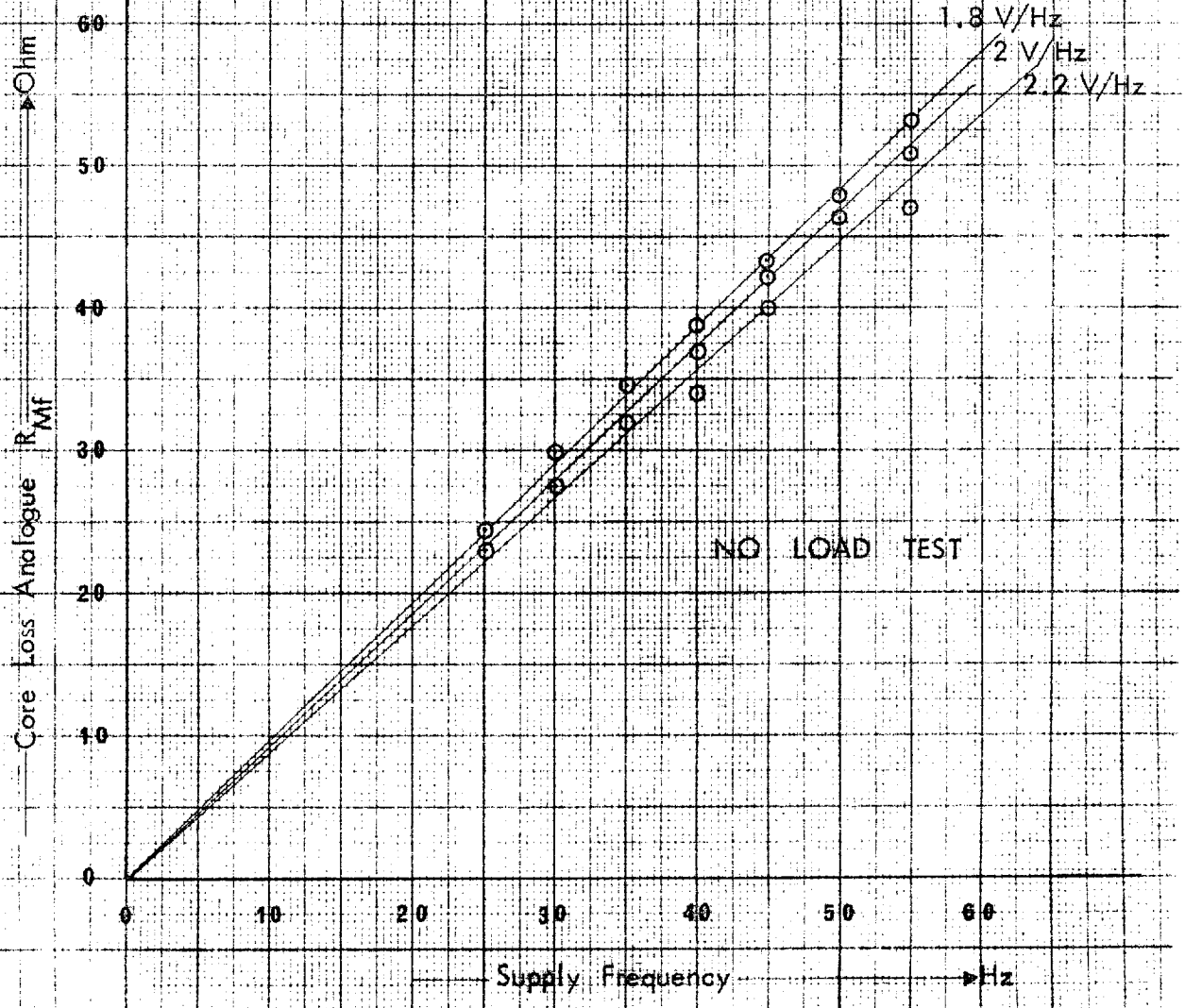

FIGURE 4.6 CORE LOSS ANALOUGE R_{Mf} VS SUPPLY FREQUENCY f FOR VARIOUS CONSTANT VALUES OF V'_f / f RATIO.

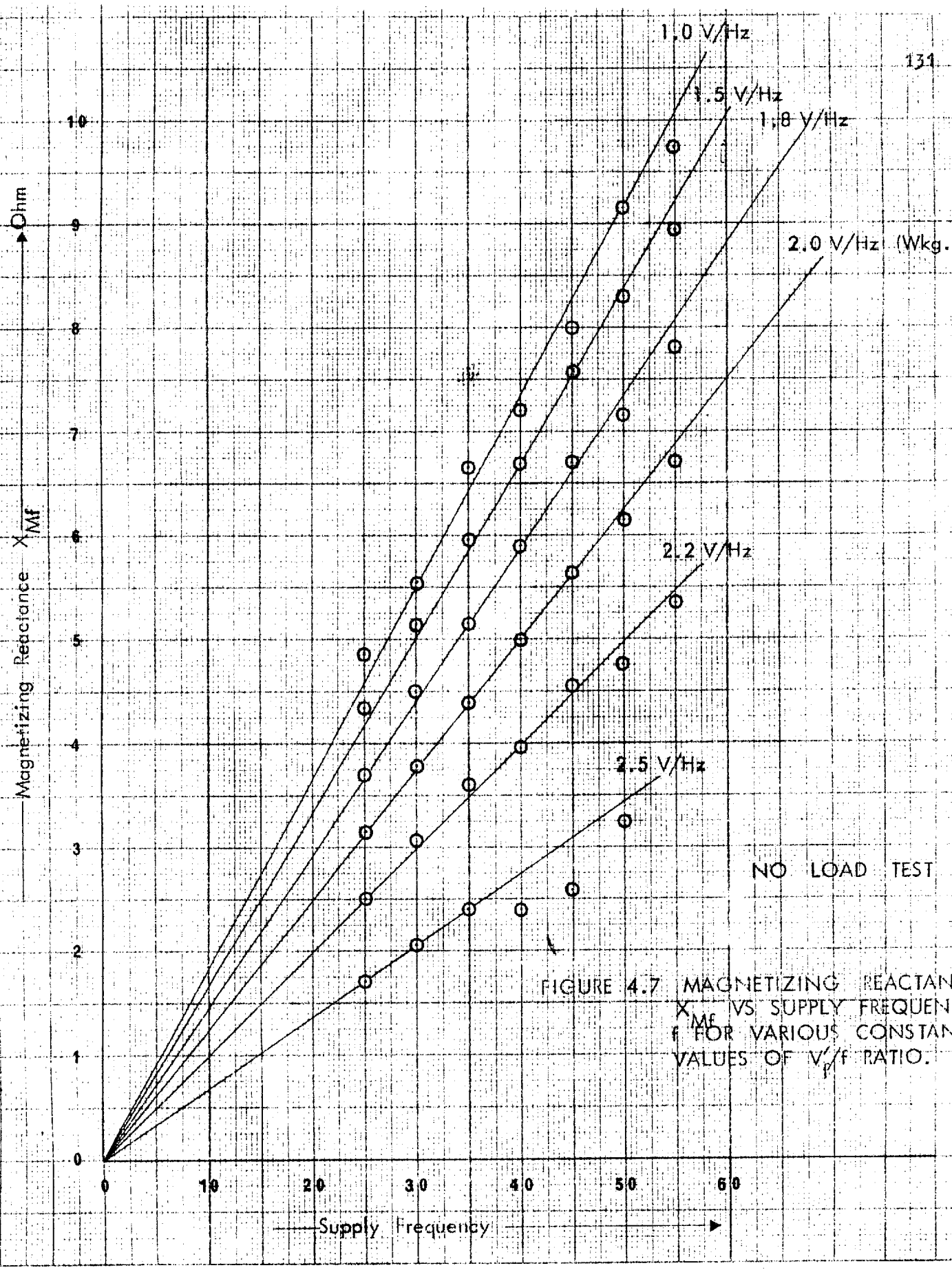

FIGURE 4.7 MAGNETIZING REACTANCE X_{Mf} VS SUPPLY FREQUENCY f FOR VARIOUS CONSTANT VALUES OF V_p/f RATIO.

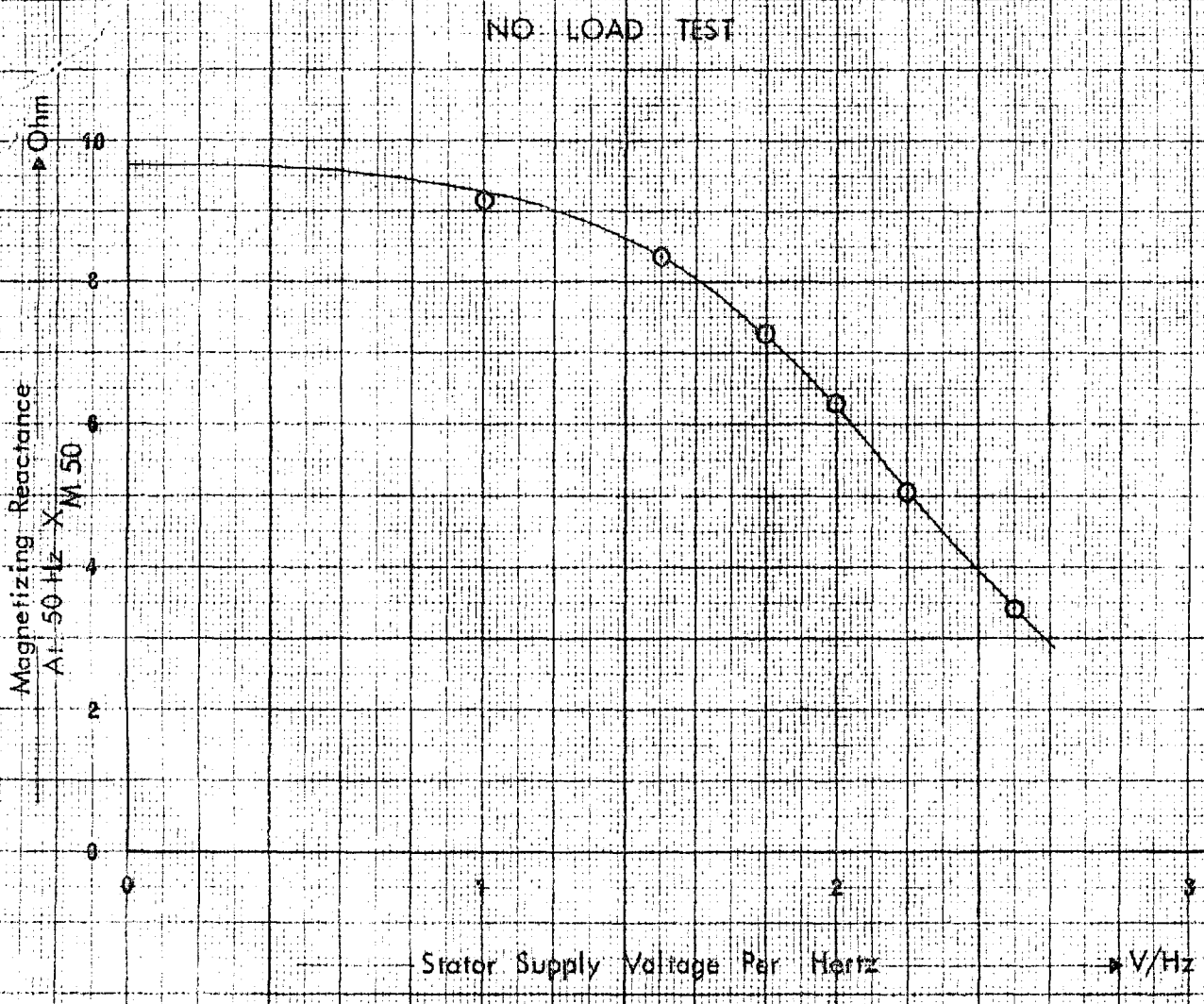

FIGURE 4.8 MAGNETIZING REACTANCE AT 50 Hz. $X_{M\,50}$ Vs. STATOR SUPPLY VOLTAGE PER HERTZ.

4.4 Variable Frequency Locked Rotor Test

The same experimental set-up as used for no-load test (Figure 4.3) was used in this test. The rotor was locked in such a position that the three stator-line currents were almost equal. Reduced voltages were applied to the stator at various constant frequencies in order to circulate currents in the stator from an almost negligible value up to 10% in excess of rated full load current. Simultaneous recordings of stator line to line voltages, stator-line currents and power input were made.

At standstill the slip S of the rotor is unity and hence the input impedance (line to neutral) of the motor consisted of a parallel combination of the stator-reflected rotor leakage impedance (R_2+jX_{2f}) and the shunt magnetizing impedance $1/(\frac{1}{R_{Mf}} + j\frac{1}{X_{Mf}})$ in series with the stator leakage impedance (R_1+jX_{1f}). Since the shunt magnetizing impedance is very high compared to the rotor leakage impedance (R_2+jX_{2f}), the input impedance of the motor may be considered to be approximately equal to $(R_1+R_2) + j(X_{1f}+X_{2f})$. Further, since the air-gap voltage E_{gf} is very small, about half of the locked rotor supply voltage to the stator (for wound rotor machine) the air-gap flux is correspondingly small, and hence the losses in the main flux-path are also small. Moreover, since the rotor is stationary the losses

associated with the rotor rotation, viz friction and windage, teeth and surface losses of the rotor and stator are zero. Therefore, with the assumption of negligible iron loss in the main flux-path the equivalent circuit under such condition is as given in figure 4.1 with R_{Mf} omitted. The input impedance for locked rotor condition is obtained from the equivalent circuit as

$$\frac{V_{bl}}{I_{bl}} = Z_{bl} = \left\{R_1 + \frac{X_{Mf}R_2(X_{Mf}+R_2) - R_2X_{2f}X_{Mf}}{R_2^2 + (X_{Mf}+X_{2f})^2}\right\} + j\left\{X_{1f} + \frac{X_{Mf}X_{2f}(X_{Mf}+X_{2f}) - X_{Mf}R_2^2}{R_2^2 + (X_{Mf}+X_{2f})^2}\right\}$$

$$= R_{blf} + jX_{blf} \qquad (4.5)$$

For motors of normal design X_{2f} and R_2 are very small compared to X_{Mf} numerically. Under the locked rotor condition X_{Mf} has the unsaturated value.

Therefore

$$R_{blf} = R_1 + R_2\frac{X_{Mf}^2}{(X_{Mf}+X_{2f})^2} \qquad (4.6)$$

and

$$X_{blf} = X_{1f} + X_{2f}\frac{X_{Mf}^2}{(X_{Mf}+X_{2f})^2} \qquad (4.7)$$

From test data of the locked rotor stator line current I_{bl}, the locked rotor stator power input P_{bl} and the locked

rotor line to neutral supply voltage V_{bl}, R_{blf} and X_{blf} were calculated as follows :-

$$R_{blf} = \frac{P_{bl}}{3I_{bl}^2} \tag{4.8}$$

and

$$Z_{blf} = \frac{V_{bl}}{I_{bl}} \tag{4.9}$$

$$X_{blf} = (Z_{blf}^2 - R_{blf}^2)^{\frac{1}{2}} \tag{4.10}$$

Although it is legitimate to neglect the core-loss under locked rotor conditions, it is not quite so for locked rotor magnetizing current due to the presence of a finite air-gap in the flux path. Therefore a suitable correction factor should be applied to R_{blf} and X_{blf} in order to determine the precise value of R_2 and X_{2f}. Since the leakage reactances of stator and rotor could not be determined individually from these tests, the stator and rotor leakage reactances were empirically taken to be equal to each other following the usual text-book procedure[10]. Further, from equation 4.7 it can be seen that if X_{Mf} is very high $X_{blf} = X_{1f} + X_{2f}$. No attempt was made to apply a correction to X_{blf} for the non-infinite value of X_{Mf} because of two reasons. The first was that an empirical distribution of leakage reactances had been assumed and second was the fact that

under normal operating conditions $R_2/S > X_{2f}$ and as such it is R_2 which primarily determines the rotor current and hence the stator current and the torque developed under normal operating conditions. Therefore R_2 required more accurate determination than X_{2f}. Hence it was assumed that

$$X_{1f} = X_{2f} = \frac{X_{blf}}{2} \qquad (4.11)$$

The value of X_{1f} at the no-load value of the stator current was used in the no-load test to determine X_{Mf} and R_{Mf}. The unsaturated value of X_{Mf} obtained from figure 4.8 was used to calculate the actual value of R_2 from equation 4.6.

$$R_2 = (R_{blf}-R_1)\left(\frac{X_{Mf}+X_{2f}}{X_{Mf}}\right)^2 \qquad (4.12)$$

It was noticed that the rotor frequency had a negligible effect on R_2 as should the case be for wound rotor construction. The variation of R_2 with stator current is shown in figure 4.9, and is perhaps due to the effective resistance of the carbon brushes on the slip-rings. As the equivalent circuit was required to simulate the behaviour of the induction motor from no-load to full-load (30 Ampere), the value of R_2 at 30 Ampere (0.13 Ω) was taken.

The value of the locked rotor reactance $X_{blf} = (X_{1f}+X_{2f})$ was plotted as a function of stator current for various constant values of supply frequency as shown in

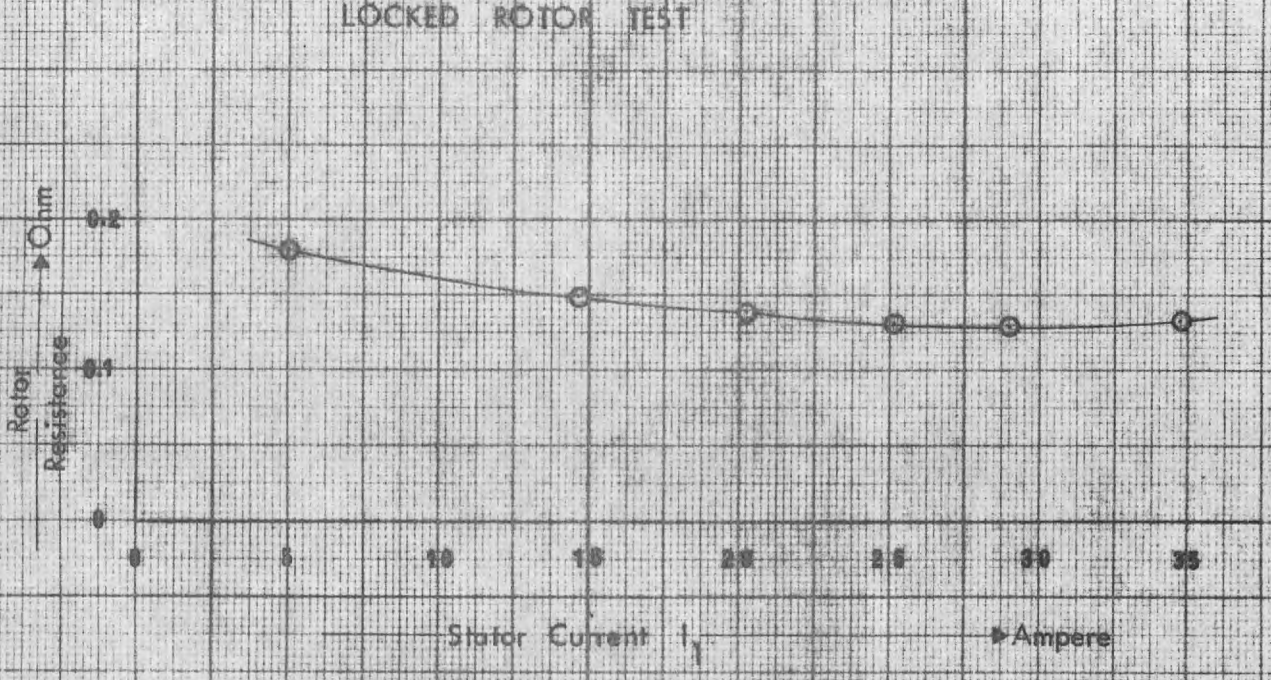

FIGURE 4.9 STATOR REFLECTED ROTOR RESISTANCE R_2 VS STATOR CURRENT

figure 4.10. From this another graph, figure 4.11, was plotted to depict the variation of X_{blf} as a function of supply frequency for various constant values of stator current. Variation of locked rotor inductance (l_1+l_2) with stator current was determined from this graph and plotted in figure 4.12. The leakage inductance was found to have a rather wide variation with stator current due to saturation of the iron in the leakage flux-path, which is usually more pronounced in a wound rotor machine than in an equivalent cage machine. The value of $X_{blf} = (X_{1f}+X_{2f})$ was taken as 0.55 Ω at 50 Hz for a stator current of 32 Ampere, because at these higher values of stator current X_{2f} tends to have an effect on the rotor circuit. At low values of slip, X_{2f} is swamped out by a much higher value of the effective rotor resistance R_2/S.

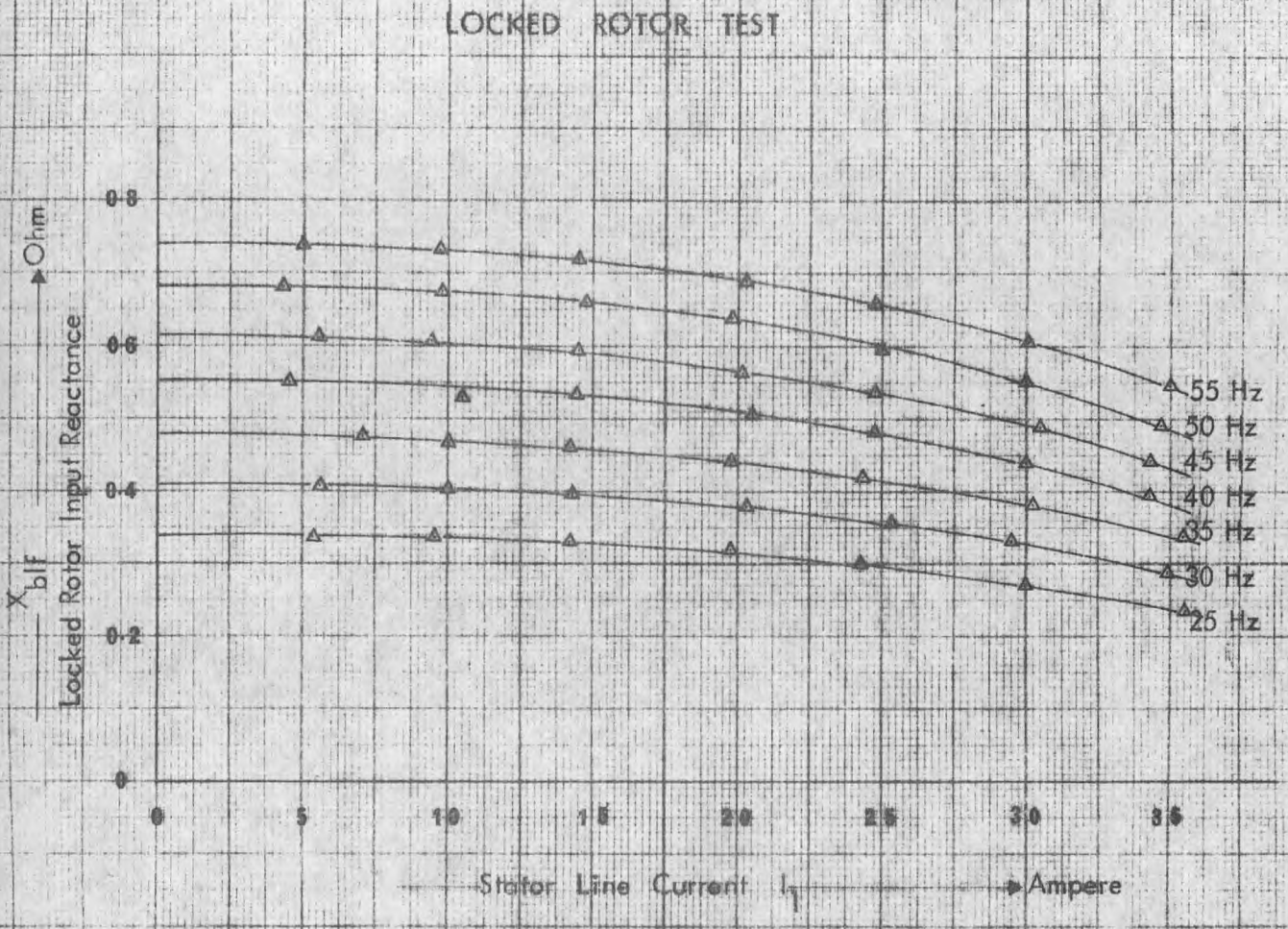

FIGURE 4.10 LOCKED ROTOR INPUT REACTANCE X_{blf} VS STATOR LINE CURRENT FOR VARIOUS CONSTANT VALUES OF STATOR SUPPLY FREQUENCY f.

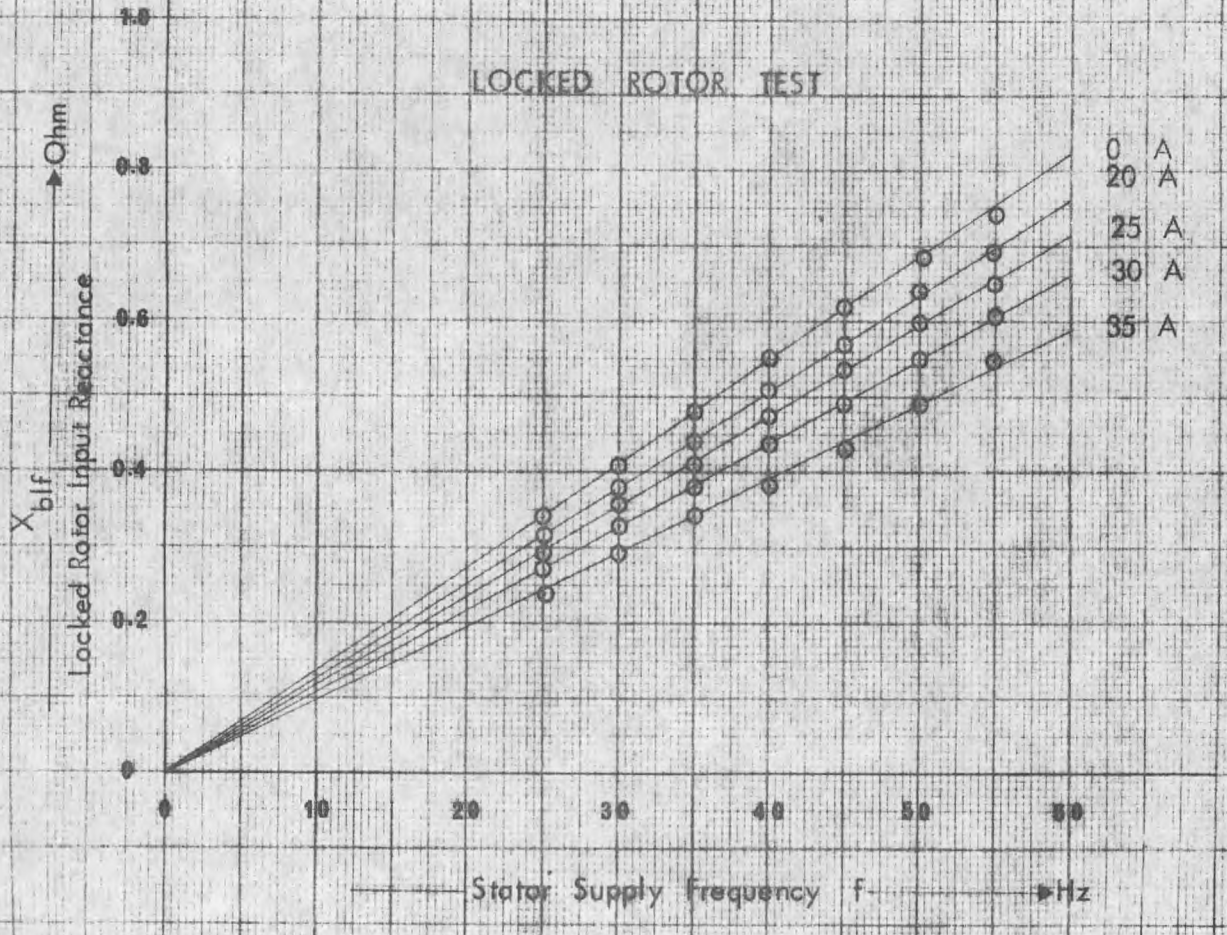

FIGURE 4.11 LOCKED ROTOR INPUT REACTANCE X_{blf} VS STATOR SUPPLY FREQUENCY f FOR VARIOUS CONSTANT VALUES OF STATOR CURRENT I_1.

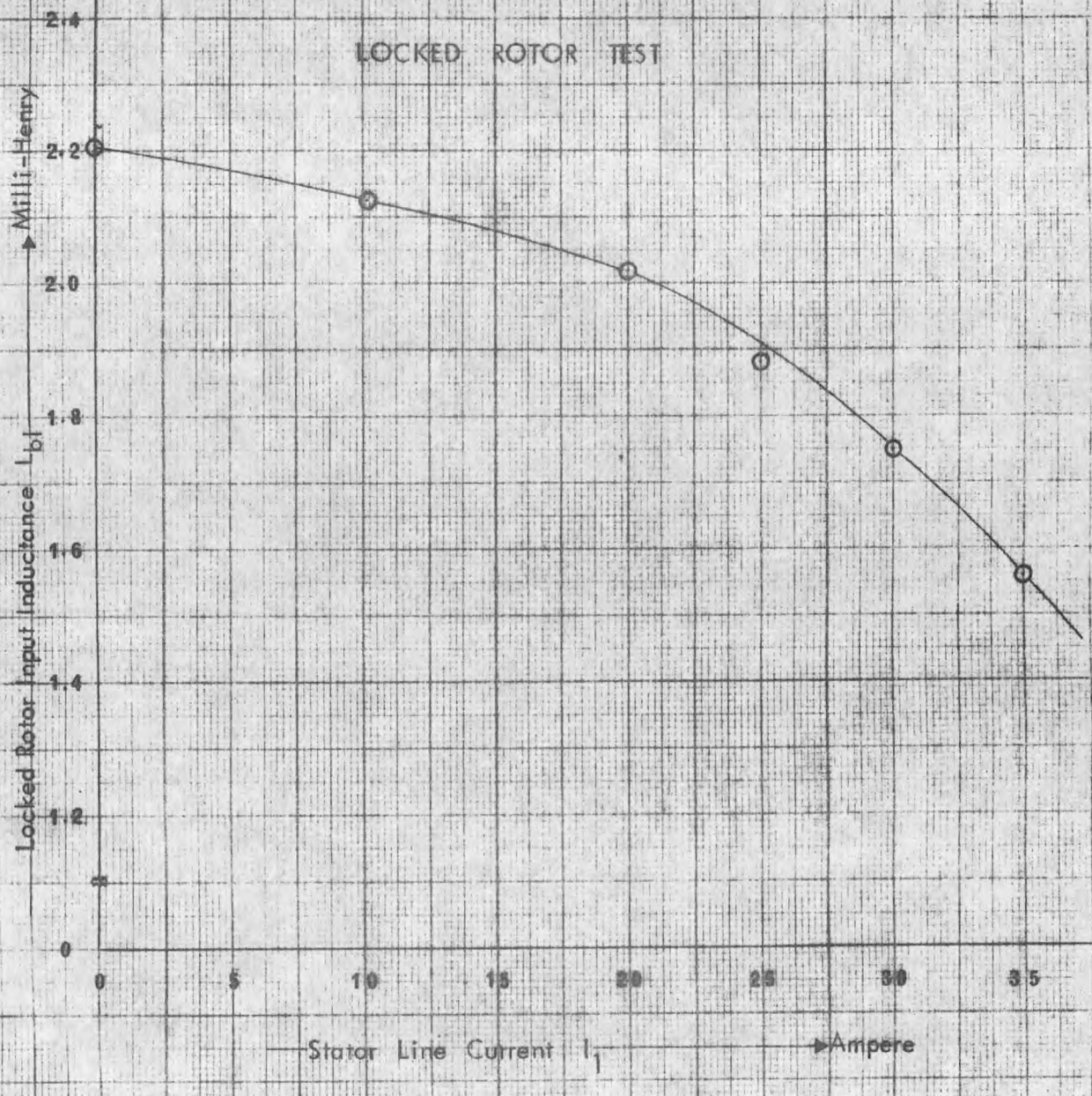

FIGURE 4.12 LOCKED ROTOR INPUT INDUCTANCE L_{bl} VS STATOR LINE CURRENT

CHAPTER 5

INDUCTION MOTOR LOSSES UNDER FIXED AND VARIABLE FREQUENCY SINUSOIDAL SUPPLY

In the process of energy conversion, from electrical to mechanical form in an induction motor five different kinds of loss occur. These are :-

i) stator copper loss due to load current flowing through the stator winding;

ii) iron loss due to the main flux. This iron loss is mainly confined to the stator iron, as under normal operation the rotor is subjected to a very low slip-frequency flux reversal;

iii) rotor copper loss due to current flowing through the rotor winding. The rotor current consists of a slip-frequency current induced by the fundamental component of stepped space distribution of air-gap flux and various other currents of higher slip-frequency contributed by the higher order space harmonics of the air-gap mmf;

iv) losses associated with the rotation of rotor which includes, apart from the friction and windage, the losses due to slot openings and stator and rotor surface losses.

The above-mentioned losses occur in any induction motor, i.e. either wound or cage rotor machine, but in the

latter type a further loss of energy occurs due to :-

v) cross-currents flowing between the uninsulated rotor bars via rotor iron.

Losses of types (i) and (ii) and a major part of (iii) contributed by the space fundamental of air-gap mmf can be taken into account by the conventional simple equivalent circuit of figure 4.1. The rest of the losses under type (iii) created by the harmonics of the air-gap mmf can also be taken into account by extending the simple equivalent circuit into a chain network shown in figure 5.1, the details of which will be presented in section 5.3.2. The parameters of these space harmonic branches could be calculated by assuming that the iron is unsaturated. Even if the main flux-path is unsaturated the tooth tips of the stator and the rotor are heavily saturated and as such the calculated values assuming unsaturated iron are, of doubtful value. Various authors[7,11] have suggested the use of various reduction factors empirically to counteract the effect of such heavy saturation. Losses of type (iv) are the most difficult to account for. Christofides[11] has shown how these losses could be accounted, but no attempt is made here to account for these losses. The losses due to interbar currents (v) are peculiar to squirrel-cage induction motor with cast aluminium rotors. Since the machine used throughout the investigation was of the wound rotor type, no attempt was

made to investigate these types of losses.

5.1 Losses Due to Main Flux

The main flux (space fundamental) of the air-gap rotates at synchronous speed with respect to the stator and at slip-speed, given by SN_s, with respect to the rotor. As the slip of the rotor S under normal operating conditions is very small (about 0.07 per unit) losses occur mainly in the stator core, and very little loss occurs in the rotor core. These stator losses are hysteresis and eddy current losses, the former being an inherent property of the ferro-magnetic core, and the latter due to emf induced in the core due to the changing magnetic field.

5.1.1 Hysteresis loss

Since the main flux moves with respect to the stator core at synchronous speed the iron is subjected to an alternating magnetization. This leads to hysteresis loss in the iron which depends on the area of the hysteresis loop, the number of flux alternation per second and the quality and quantity of iron.

According to Steinmetz the hysteresis loss per unit weight is given by

$$W_h = \eta_h f B_m^{\,n} \qquad (5.1)$$

where

B_m = the maximum value of flux density

f = frequency of flux alternation

η_h = a constant depending on the quality of iron

n = an exponent which varies from 1.5 to 2.0. Steinmetz used 1.6.

Richter[10] proposed a more accurate equation as follows

$$W_h = afB_m + bfB_m^2 \qquad (5.2)$$

where a and b are constants independent of the nature of flux variation as the hysteresis loss depends on the area of the B-H loop, and the area being indepedent of the way in which the flux varies with time. The area depends only on the maximum value of the flux density encountered.

Equation 5.2 as proposed by Richter is essentially a polynomial fit of the hysteresis loss versus flux density curve. For flux density greater than 1.2 Wb/m^2 Litchwiz[9] showed that the term $afB_m \ll bfB_m^2$ and as such proposed the following equation

$$W_h = bfB_m^2 \qquad (5.3)$$

Litchwiz's equation 5.3 and Steinmetz equation 5.1 are similar. Litchwiz takes the exponent n of the Steinmetz equation as 2. No value will be assigned to exponent n at this stage.

If the hysteresis loss is represented by the loss occurring in a resistor shunting the air-gap voltage in the stator, such that the power absorbed by this resistor equals the hysteresis loss then,

$$R_h = \frac{E_{gf}^2}{W_h} = \frac{E_{gf}^2}{\eta_h f B_m^n} \qquad (5.4)$$

where E_{gf} is the r.m.s. value of the line to neutral voltage induced in the stator winding at frequency f.

And W_h is one-third of the total hysteresis loss for a 3-phase machine.

Now the peak value of the main flux ϕ_m is given by

$$\phi_m = \frac{E_{gf}}{4K_f f N_1 Kw_1} \qquad (5.5)$$

where K_f is the form factor of the induced voltage $N_1 Kw_1$ is the effective number of stator turns per phase.

Kw_1 is the stator winding factor for space fundamental of air-gap mmf.

Therefore flux density B_m is given by

$$B_m = \frac{\phi_m}{A} = \frac{E_{gf}}{4K_f N_1 Kw_1 fA} \qquad (5.6)$$

By substituting equation 5.6 in equation 5.4 we can obtain the value of the hysteresis loss simulating resistor as

$$R_h = \frac{(4K_f N_1 Kw_1 A)^n}{\eta_h} \left(\frac{E_{gf}}{f}\right)^{(2-n)} f$$

$$= \frac{(4N_1 Kw_1 A)^n}{\eta_h} (K_f)^n \left(\frac{E_{gf}}{f}\right)^{(2-n)} f \qquad (5.7)$$

In the above equation 5.7, N_1, Kw_1 and A are constants for a given motor, η_h is almost constant (Equation 5.1), the form factor K_f depends on the wave-form of the line to neutral induced voltage of the stator. Neglecting the leakage impedance drop of the stator, the voltage applied is very nearly equal to the induced stator voltage. Further, under sinusoidal operation, the wave-form of the induced voltage remains the same and as such K_f equals 1.11. Therefore, under the above-mentioned constraints the iron loss due to hysteresis for a given (E_{gf}/f) ratio can be represented by a variable resistance R_h which is a linear function of frequency. The validity of equation 5.7 can be seen from figure 4.6. (Figure 4.6 gives the variation of R_{Mf}, the resistance simulating both the hysteresis and eddy current losses. It will be shown in section 5.1.2 that eddy current losses are negligible, and R_{Mf} equals R_h).

If the hysteresis loss simulating resistance R_h under sinusoidal 50 Hz operating condition R_{h50} is known for a given E_{gf}/f ratio, then the value of R_h for a different value of frequency but the same (E_{gf}/f) (under sinusoidal supply) can be determined from

$$R_h = R_{h50} \frac{f}{50} \tag{5.8}$$

The effect of frequency f and (E_{gf}/f) ratio on hysteresis loss can be found by substituting equation 5.6 into equation 5.1 yielding

$$W_h = \frac{\eta_h}{(4N_1 Kw_1 A)^n} K_f^{-n} \left(\frac{E_{gf}}{f}\right)^{n_f} \tag{5.9}$$

The hysteresis loss at 50 Hz sinusoidal operation is given by

$$W_{h50} = \frac{\eta_h}{(4N_1 Kw_1 A)^n} K_f^{-n} \left(\frac{E_{g50}}{50}\right)^n 50 \tag{5.10}$$

The ratio of hysteresis loss at any frequency to that at 50 Hz sinusoidal operating condition is given by

$$\frac{W_h}{W_{h50}} = \left(\frac{E_{gf}/f}{E_{g50}/50}\right)^n \frac{f}{50} \tag{5.11}$$

Induction motor running under "fixed maximum torque" operating condition requires that $E_{gf}/f = E_{g50}/50 =$ a constant. Hence, under such a condition

$$\frac{W_h}{W_{h50}} = \frac{f}{50} \qquad (5.12)$$

Having described the nature of hysteresis loss the value of the exponent n will be determined. Throughout the investigation the E_{gf}/f ratio was maintained at 2 Volt/Hertz. Referring to figure 4.6, R_{h50} has two values at 50 Hertz depending on E_g/f ratio.

$$R_{h50} \text{ (at 1.8 Volt/Hertz)} = 48\ \Omega$$

$$R_{h50} \text{ (at 2.2 Volt/Hertz)} = 45\ \Omega$$

Therefore from equation 5.7

$$48 \propto (1.8)^{(2-n)}$$

$$45 \propto (2.2)^{(2-n)}$$

Solving the above two proportionalities we obtain $n = 1.674$, so that R_h for this particular motor is given by

$$R_h = \frac{(4N_1 Kw_1 A)^{1.674}}{\eta_h} (K_f)^{1.674} \left(\frac{E_{gf}}{f}\right)^{0.326} f \qquad (5.13)$$

5.1.2 Eddy current loss

The eddy current loss W_c in a given plate of thickness δ and resistivity ρ_c is given by

$$W_e = \rho_e \delta^2 (K_f f B_m)^2 \qquad (5.14)$$

If the eddy current loss is represented by a resistor shunting the stator induced voltage E_{gf} such that the power absorbed by this resistance equals the eddy current loss, then

$$R_e = \frac{E_{gf}^2}{W_e} = \frac{E_{gf}^2}{\rho_e \delta^2 K_f^2 f^2 B_m^2} \qquad (5.15)$$

Substituting the value of B_m from equation 5.6 in equation 5.15 gives the eddy current loss as

$$R_e = \frac{16(N_1 K w_1 A)^2}{\rho_e \delta^2} \qquad (5.16)$$

For a given machine the value of the resistor simulating the eddy current loss is independent of the frequency and the wave-form of the line to neutral voltage induced in the stator winding.

Substituting equation 5.6 in equation 5.14 gives the eddy current loss as

$$W_e = \rho_e \delta^2 (K_f f)^2 \frac{E_{gf}^2}{4^2 K_f^2 f^2 (N_1 K w_1 A)^2}$$

$$= \frac{\rho_e \delta^2}{16(N_1 K w_1 A)^2} E_{gf}^2 \qquad (5.17)$$

The eddy current loss at 50 Hertz and under normal sinusoidal operating condition is given by

$$W_{e50} = \frac{\rho_e \delta^2}{16(N_1 K w_1 A)^2} E_{g50}^2 \qquad (5.18)$$

Then the ratio of eddy current loss at any frequency to that at 50 Hertz is given by

$$\frac{W_e}{W_{e50}} = \frac{E_{gf}^2}{(E_{g50})^2}$$

and since for fixed maximum torque operation $E_g/f = E_{g50}/50 =$ constant

$$\frac{W_e}{W_{e50}} = \left\{\frac{E_{gf}/f}{E_{g50}/50}\right\}^2 \frac{f^2}{50^2}$$

$$= \frac{f^2}{50^2} \qquad (5.19)$$

The eddy current loss is proportional to the square of frequency.

From the no-load and locked rotor tests described in chapter 4 and figure 4.6 it can be seen that the resistance simulating the combined iron loss for a constant air-gap flux density is a linear function of frequency. The iron loss caused by the variation of main flux in the stator consists mainly hysteresis loss.

5.2 Stator Copper Loss

The stator phase current flowing through the stator winding produces an I^2R loss in each phase. These losses are the simplest to evaluate and are given by the product of the square of the r.m.s. stator current and the stator phase resistance. Cross-fluxes in the slot may produce additional copper loss due to skin effect. Skin effect is proportional to the square root of frequency and has little effect (5% - 15%) on copper loss.

5.3 Rotor Copper Loss

It is well known that due to the concentration of stator windings in slots the mmf distribution of air-gap in space produced by the flow of current in a balanced three-phase winding is stepped. Such stepped space distribution of m.m.f can be resolved into a Fourier series giving a space fundamental and an infinite series of space harmonics. With the assumption of linearity of the magnetic circuit, the space fundamental mmf is considered to produce the main space fundamental flux, the space harmonic mmfs producing parasitic fluxes which travel with different speeds (some in the opposite direction) to the main flux. The strengths of these fluxes are proportional to the current in the winding and inversely proportional to the air-gap length.

For a given rotor speed the space fundamental and space harmonic fluxes pass the rotor at definite speeds and currents of various frequencies flow in the rotor winding. The space fundamental component of flux produces a rotor current of frequency Sf, the slip frequency, which comprises the major part of the total rotor current and develops the useful torque, but produces rotor winding copper loss. Since the space harmonic fluxes rotate at lower speeds, they give rise to extra copper loss. At no-load the stator current is small (and hence the strength of the harmonic components of mmf) and so the harmonic fluxes are small. As the motor is loaded the strength of these harmonic fluxes increase and so does the extra rotor copper loss. These extra losses in a well designed motor are about 0.03% to 0.05% of the output and more pronounced in a cage motor than in a wound rotor machine because all the space harmonics are slot harmonics which have the same winding factor as the fundamental.

The conventional text-book equivalent circuit (Figure 4.1) takes into account only the space fundamental of air-gap flux and as such the equivalent circuit fails to account for the extra copper loss in the rotor winding, as well as to predict the parasitic torques arising due to the space harmonic fluxes.

The same system used for the realization of the simple equivalent circuit can be extended to derive a more complete equivalent circuit taking into account the space harmonics and is shown in figure 5.1. The quantitative analysis of field harmonics and harmonic equivalent circuit parameters are given in the next section.

5.3.1 Field harmonics in the air-gap of induction motors [5, 6]

The space fundamental mmf rotates at a speed depending on the frequency of supply f and the number of poles of the machine P and is given by $N_s = \frac{2f}{P}$ r.p.s.

The amplitude of this space fundamental mmf is given by, for three-phase stator,

$$F_1 = \frac{3(2)^{\frac{1}{2}}}{\pi P} N_1 K_{w_1} I_1 \qquad (5.20)$$

Where N_1 is the number of stator turns per phase, $K_{w_1} = K_{d1}K_{y1}$ is the winding coefficient for the space fundamental and is equal to the product of coefficients for the distribution and the shortening of winding pitch.

The winding distribution coefficient for space fundamental is given by

$$K_{d1} = \frac{\sin \pi/6}{q_1 \sin \frac{\pi}{6q_1}} \qquad (5.21)$$

where q_1 = number of slots per pole per phase of the stator.

The pitch factor for space fundamental is given by

$$K_{y1} = \sin\frac{\pi}{2} y \qquad (5.22)$$

where y is the winding pitch expressed as a fraction of the full pitch.

The general expression for harmonics of the m.m.f for integral number of slots per pole per phase due to sinusoidal excitation is given by

$$F(x, t) = F \sin(2\pi ft - \frac{\pi}{\tau} - x) + F_5 \sin(2\pi ft - \frac{5\pi}{\tau} - x) + \ldots$$

$$= \sum_{\nu=1}^{\nu} F_\nu \sin(2\pi ft - \frac{\nu\pi}{\tau} - x) \qquad (5.23)$$

where ν is the order of space harmonic

τ space fundamental pole pitch

x distance along the centre line of the air-gap

The number of poles of the ν^{th} space harmonic is a ν^{th} multiple of the space fundamental, but its speed of rotation is less by the same proportion. Therefore the e.m.f. induced by the ν^{th} space harmonic of m.m.f. is equal to

the frequency of supply.

For balanced windings with q_1 as an integer, the orders of harmonics present are given by, for three-phase stator,

$$\nu = 1 \pm 6K_1 \tag{5.24}$$

where $K_1 = 0, 1, 2, 3, \ldots$ etc.

For $K_1 = 0$, we obtain the space fundamental $\nu = 1$. Positive values of ν indicate forward rotation whereas negative values of ν indicate backward rotation of the ν^{th} harmonic.

For $K_1 = K_{1z}q_1$

where $K_{1z} = 1, 2, 3, 4$ etc. slot harmonic orders are obtained.

$$\begin{aligned} \nu_z &= 1 \pm 6K_{1z}q_1 \\ &= 1 \pm 2K_{1z}\frac{S_1}{P} \end{aligned} \tag{5.25}$$

where S_1 is the total number of stator slots

All other harmonics are called belt harmonics, ν_b, because they are due to definite phase spreads.

$$\nu_b = 1 \pm 6K_1 \tag{5.26}$$

where $K_1 = 0, 1, 2, 3$ etc.

$$\neq K_{1z} q_1$$

The distinction is drawn between slot and belt harmonics for the following reasons :

i) The secondary voltages induced by the slot harmonics are effectively open-circuited by the rotor, whereas that due to the belt harmonics are substantially short-circuited.

ii) The slot harmonic magnetizing reactances are independent of winding pitch, but vary with the number of slots, whereas those due to the belt harmonics are nearly independent of the number of slots, but vary with the pitch and distribution of the windings.

The magnitude of the ν_b^{th} space harmonic m.m.f. can be found from the relation

$$F_{\nu_b} = \frac{3}{\pi} \frac{2(2)^{\frac{1}{2}}}{P} N_1 \frac{K_{w\nu_b}}{\nu_b} I_1$$

$$= \frac{1}{\nu_b} \frac{K_{w\nu_b}}{Kw_1} F_1 \qquad (5.27)$$

where $K_{w\nu_b}$ is the winding factor for ν_b^{th} belt harmonic and is given by

$$K_{w\nu_b} = K_{d\nu_b} K_{y\nu_b} \qquad (5.28)$$

where the ν_b^{th} harmonic distribution factor

$$K_{d\nu_b} = \frac{\sin(\nu_b \pi/6)}{q_1 \sin(\nu_b \pi/6q_1)}$$

$$= \frac{\sin \pi/6}{q_1 \sin \frac{\pi \nu_b}{6q_1}} \qquad (5.29)$$

and the ν_b^{th} harmonic pitch factor

$$K_{y\nu_b} = \sin \nu_b \frac{\pi}{2} y \qquad (5.30)$$

For slot harmonics

$$K_{d\nu_z} = K_{d1} \qquad (5.31)$$

and $$K_{y\nu_z} = K_{y1} \qquad (5.32)$$

The rotor currents create their own harmonics. The orders of the rotor space harmonics can be determined as follows. The space-fundamental stator field harmonic induces a slip frequency current in the rotor which produces a series of harmonics given by, for three-phase rotor

$$\mu = 1 \pm 6K_2$$

where $K_2 = 0, 1, 2, 3$ etc.

which may again be split up into belt and slot harmonics

$$\mu_b = 1 \pm 6K_2$$

where $K_2 = 0, 1, 2, 3$ etc.

$$\neq K_{2z}q_2 \qquad (5.33)$$

where $K_{2z} = 1, 2, 3$ etc.

$$\mu_z = 1 \pm 2K_{2z}\frac{S_2}{P} \qquad (5.34)$$

where S_2 is the total number of rotor slots.

For a cage motor μ_b is absent. Substituting $K_2 = 0$ in equation 5.33 we obtain $\mu = 1$, the first m.m.f. harmonic in the rotor.

The equations 5.33 and 5.34 give the order of rotor harmonics produced by the stator fundamental m.m.f. only. Also, every other stator harmonic induces its own harmonics in the rotor. Hence, in general, for three-phase machine

$$\mu = \nu \pm 6K_2 \qquad (5.35)$$

The pole number of μ^{th} harmonic of the rotor is a μ multiple of the poles of the stator space fundamental. Now the speed of the ν^{th} stator field harmonic with respect to the stator is N_s/ν. The speed of the μ^{th} rotor harmonic, produced by the ν^{th} stator harmonic with respect to the rotor, is $\frac{S_\nu N_s}{\mu}$. Since the rotor speed is $(1-S)N_s$, the speed of the μ^{th} rotor harmonic with respect to the stator is given by

$$\frac{1}{\mu}\left\{S_\nu N_s + (1-S)N_s\mu\right\}$$

$$= \frac{N_s}{\mu}\left\{S_\nu + (1-S)\mu\right\} \qquad (5.36)$$

Since the slip of the rotor with respect to ν^{π} stator field harmonic

$$S_\nu = 1 + \nu(S-1)$$

equation 5.36 can be written as

$$\frac{N_s}{\mu}\left\{1 - \nu(1-S) + \mu(1-S)\right\}$$

$$= \frac{N_s}{\mu}\left\{1 + (1-S)(\mu-\nu)\right\} \qquad (5.37)$$

From the above equation 5.37 it can be seen that when $\mu = \nu$, the speed of the μ^{th} rotor harmonic with respect to the stator is $\frac{N_s}{\mu} = \frac{N_s}{\nu}$ for all rotor speeds. The stator harmonic is rotating with respect to the stator at a speed of $\frac{N_s}{\nu}$, hence the relative speed between μ^{th} and ν^{th} harmonic is zero when $\nu = \mu$.

Under this condition an asynchronous torque is produced in the machine. When $\nu = \mu = 1$, the asynchronous torque produced is a useful one and for all other higher harmonics $\nu = \mu > 1$, the torques, are of no use as their speeds are very different from that of the space fundamental. These torques are therefore called the

asynchronous parasitic torques.

Quite apart from the asynchronous torques which are produced in an induction motor, synchronous torques can exist as a result of rotor sub-harmonics. A synchronous torque is produced when a stator harmonic ν_a produces a rotor harmonic μ_a which has the same order as another stator harmonic ν_b (i.e. $\mu_a = \pm \nu_b$) which at a single rotor speed is at standstill with respect to this second harmonic ν_b. In such a case ν_a is the source of excitation for the rotor and ν_b is the source of power of the stator.

5.3.2 Extension of conventional fixed frequency equivalent circuit to include the effects of space harmonics

Currents induced in the rotor by the space harmonic fields produce parasitic torques which modify the ideal machine (a machine whose air-gap flux contains the space fundamental component only) output torque. The effect may be considered to equal that produced by an ideal machine and a set of small machines with a common shaft and with series-connected stators. Each small machine produces the effect of one space harmonic and has ν times the number of poles of the ideal space fundamental machine.

At speeds above their respective synchronous values the forward harmonics produce braking torque, as do the

backward rotating harmonics at all forward speeds. These space harmonic fields give rise to stray load losses and parasitic torques.

In order to depict the behaviour of these field harmonics on the performance of the induction motor, the simple equivalent circuit of figure 4.1 has to be expanded to a chain network as shown in figure 5.1, where each section depicts the contribution of a particular space harmonic. The equivalent circuit now consists of

R_1 = pure resistance of stator

X_1 = pure reactance equal to the leakage reactance of the stator due to all the fluxes that do not link the rotor winding

$X_{2.1}$ = pure reactance equal to the leakage reactance of the rotor due to all the fluxes that do not link the stator winding

R_M = pure resistance analogue of main flux path iron loss at normal frequency and normal flux conditions

$X_{M.1}'$ & $X_{2.1}'$ & $R_{2.1}$ = a transformer whose magnetizing reactance is equal to the reactance corresponding to the fundamental air-gap flux density wave and whose secondary impedance is the

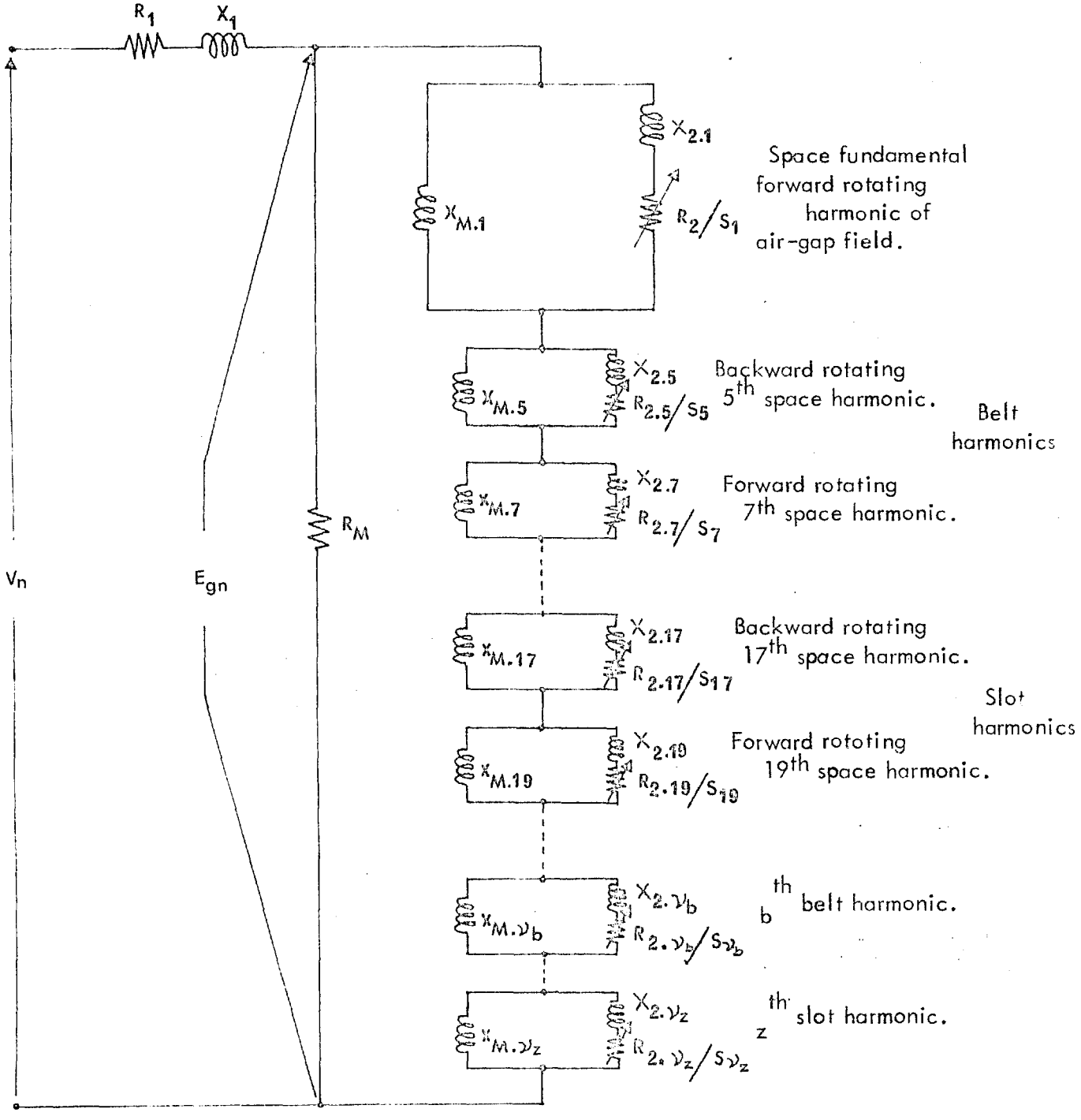

Figure 5.1 Normal Frequency Sinusoidally Excited Induction Motor Equivalent Circuit Taking Space Fundamental And Space Harmonics In Account.

impedance of the rotor winding for currents of slip-frequency Sf.

$X_{M.\nu}'$ & $X_{2.\nu}'$ & $R_{2.\nu}$ = a series of smaller transformers each having a magnetizing reactance corresponding to the air-gap flux density wave of a particular space harmonic with a stator-referred secondary impedance of the rotor winding of the same number of harmonic poles.

The space harmonic equivalent circuit parameters are calculated according to the methods given by various authors[8, 9, 10, 11].

The values of $X_{M\nu}$ for belt and slot harmonics are given by Liwschitz[10] as

For belt harmonics $$X_{M.\nu_b} = \left(\frac{S_{K_w\nu_b}}{S_{Kw_1}}\right)^2 \frac{X_{M.1}}{\nu_b^2} \qquad (5.38)$$

For slot harmonics $$X_{M.\nu_z} = \frac{X_{M.1}}{\nu_z^2} \qquad (5.39)$$

(As mentioned earlier for ν_z, $K_{w\nu_z} = Kw_1$)

Since the order of slot harmonics are such that their magnitudes are increased by the stator slot permeance variations the value of $X_{M.\nu_z}$ (Equation 5.38) would be low. Alger[7] showed that the effect of the air-gap

permeance variations can be taken into account by multiplying equation 5.38 by a factor $(1 + \frac{p_s}{2p_o})$ where p_o is the average value of the air-gap permeance and p_s half the amplitude of pulsation. The magnetizing reactance for the slot harmonic is therefore

$$X_{M.\nu_z} = \frac{X_{M.1}}{\nu_z^2}(1 + \frac{p_s}{2p_o}) \qquad (5.40)$$

Since the teeth are usually saturated under normal operating conditions it was considered that in the above equation 5.40 the terms $(1 + \frac{p_s}{2p_o})$ can be eliminated and the unsaturated value of $X_{M.1}$ be used (Figure 4.8) to compute $X_{M.\nu_z}$.

The rotor leakage reactance for the ν^{th} harmonic $X_{2\nu}$ comprises differential harmonic leakage, skew leakage and the rotor slot leakage.

The differential harmonic leakage as given by Richter[11] is

$$X_{2d\nu} = K_{M\nu} X_{M\nu} \qquad (5.41)$$

where $$K_{M\nu} = \left\{ \frac{\nu\pi P}{2S_2} / \sin\frac{\nu\pi P}{2S_2} \right\}^2 - 1 \qquad (5.42)$$

The value of differential leakage calculated from equation 5.41 yields too high a value and hence parasitic torques and losses computed are correspondingly low.

Agarwal[12] suggested that a value of 2/3 of that given by equation 5.41 should be used on the ground that eddy currents induced in the rotor iron help to damp the differential harmonic flux, and hence reduce the leakage reactance. Therefore, with Agarwal's empirical correction the differential harmonic leakage becomes

$$X_{2d\nu} = \frac{2}{3} X_{M\nu} K_{M\nu} \tag{5.43}$$

The damping action of the eddy currents induced in the rotor iron would depend on the frequency of the eddy currents induced in the rotor laminations and hence on the rotor speed. Since the stator and rotor tooth tips are heavily saturated due to the combined effects of the differential and slot leakage fluxes, this reduces the value of $X_{2d\nu}$ below that calculated from equation 5.43. Alger and Agarwal[8] takes into account the effect of saturation by introducing a correction factor K_{sdl} and the expression for $X_{2d\nu}$ now becomes

$$X_{2d\nu} = \frac{2}{3} K_{sdl} K_{M\nu} X_{M\nu} \tag{5.44}$$

K_{sdl} was not calculated because of the complexity involved with doubtful accuracy of $X_{2d\nu}$, but an attempt was made in a rather crude way to take into account saturation by computing $X_{M\nu}$ from the saturated value of

$X_{M.1}$ (Figure 4.8).

The skew leakage reactance for the ν^{th} harmonic is given by Alger[7] as

$$X_{sk\nu} = \left(\frac{1}{K_{sk\nu}^2} - 1\right)X_{M\nu} \tag{5.45}$$

where $K_{sk\nu}$ is the skew factor calculated from the geometrical skew of the rotor slots. This is given by

$$K_{sk\nu} = \sin\left(\frac{\nu c'}{\tau'}\,\pi/2\right)/\left(\frac{\nu c'}{\tau'}\,\frac{\pi}{2}\right) \tag{5.46}$$

where τ' = pitch of the fundamental poles in terms of rotor slots

c' = pitch of the rotor slot skew with respect to stator slots.

Lumping the differential and skew leakage reactance together, we get

$$X_{2d\nu} + X_{sk\nu} = \frac{2}{3}K_{M\nu}X_{M\nu} + \left(\frac{1}{K_{sk\nu}^2} - 1\right)X_{M\nu}$$

$$= X_{M\nu}\left\{\frac{2}{3}K_{M\nu} + \frac{1}{K_{sk\nu}^2} - 1\right\} \tag{5.47}$$

For space harmonics, rotor slot leakages are usually smaller than $(X_{2d\nu} + X_{sk\nu})$ by a factor of 10 and the calculation of $(X_{2d\nu} + X_{sk\nu})$ using the equation 5.47 yields a high value since saturation is not taken completely into

account. Neglecting rotor slot leakage reactance, $X_{2\nu}$ is given by

$$X_{2\nu} = X_{2d} + X_{sk}$$

$$= X_{M\nu}\left\{\frac{2}{3}K_{M\nu} + \frac{1}{K_{sk\nu}^{2}} - 1\right\} \qquad (5.48)$$

The stator referred rotor resistance for space harmonics can be calculated as follows. The rotor resistance for belt harmonics is given by[9]

$$R_{2\nu_b} = \left\{\frac{S_{Kw\nu_b}}{R_{Kw\nu_b}} \frac{R_{Kw_1}}{S_{Kw_1}} \frac{K_{skl}}{K_{sk\nu_b}}\right\}^2 R_{2.1} \qquad (5.49)$$

as the wound rotor resistance referred to stator depends on the effective turns-ratio of stator and rotor windings.

Since for slot harmonics $Kw_1 = Kw\nu_z$

$$R_{2\nu_z} = \left\{\frac{K_{skl}}{K_{sk\nu_z}}\right\}^2 R_{2.1} \qquad (5.50)$$

The final term required for evaluation is S_ν, which is the slip of the rotor for ν^{th} harmonic of field m.m.f. For the ν^{th} forward rotating space harmonic, the per unit synchronous speed is $1/\nu$. If the slip of the rotor with respect to the fundamental poles is S, then per unit rotor speed is (1-S).

$$\therefore \quad S_\nu = \frac{1/\nu - (1-S)}{1/\nu}$$

$$= 1 - \nu(1-S) \qquad (5.51)$$

From the above equation 5.51 it can be seen that $S_\nu = 0$ when $S = \frac{\nu-1}{\nu}$ and S_ν is a negative quantity for $S < \frac{\nu-1}{\nu}$. Therefore the torque produced by the forward rotating space harmonic adds to the fundamental torque for slip S between the values 1 and $\frac{\nu-1}{\nu}$ and subtracts from it for all smaller values of slip. The backward rotating harmonics do so at all forward speeds.

For backward rotating space harmonics ν has a negative value, and hence

$$S_\nu = 1 + \nu(1-S) \qquad (5.52)$$

5.4 Losses Due to Slot Openings[7, 12, 13, 14]

Considering the iron to be unsaturated and the air-gap m.m.f. to have a sinusoidal space distribution, the slotting of the stator and the rotor makes the space distribution of the resultant flux density wave depart from the sinusoidal. The distribution of flux density under such conditions can be considered to consist of three components :-

i) fundamental sinusoidal flux distribution having an amplitude determined by the effective air-gap length

(Carter's Coefficient);

ii) flux density ripple having a wave-length equal to that of a stator slot pitch caused by a stator slot, the rotor being considered smooth;

iii) flux density ripple having a wave-length equal to that of a rotor slot pitch, the stator being considered smooth.

These harmonics of air-gap flux density distribution are due to the variation of air-gap permeance and are not slot harmonics.

If the stator and the rotor surfaces were smooth, and the air-gap m.m.f. was sinusoidally distributed, saturation would cause the flux density distribution around the machine air-gap to be non-sinusoidal (flattened top) so that a fourth source of flux density space harmonics is present.

These space harmonic components give rise to two different kinds of loss :-

i) stator and rotor surface loss;

ii) stator and rotor tooth pulsation loss.

Rotor surface losses arise from the movement of stator slot ripple with respect to the rotor. The rotor slot ripple moves with respect to the stator and causes stator surface loss. Surface losses are larger in

machines with open slots.

The stator and the rotor tooth pulsation losses arise due to the flux penetration of the teeth themselves, and pulsation due to the relative motion between the stator and the rotor which results in eddy currents and hysteresis losses in the teeth. The frequency of these pulsations is the same as that for the tooth surface losses, i.e. for stator $S_2N_s/50$ (for this motor 720 Hertz) and for the rotor $S_1N_s/50$ (for this motor 1,080 Hertz). The magnitude of the variation of the flux density in the teeth depends upon the saturation of the teeth, the greater the saturation the greater is the hysteresis and eddy current losses in the teeth. Hence it can be seen that the teeth losses are related in a rather complex way to the speed of the rotor, and to the load current.

The permeance variation gave rise to these ripples of flux density distribution due to the sinusoidal space distribution of m.m.f. The situation becomes further complicated when there are higher order m.m.f. space harmonics present. The flux density distribution produced by these higher m.m.f. space harmonics are also effected by the non-uniformity of the air-gap and by saturation. Each space harmonic m.m.f. component (neglecting saturation) gives rise to two more ripples of flux density apart from

that which would be produced by the harmonic m.m.f. itself if the air-gap surfaces were smooth. The total losses due to slot openings are larger in induction machines than in D.C. machines and synchronous machines because of the relatively smaller air-gap. These losses, as a percentage of iron losses due to main flux, are approximately 80% to 120% in squirrel cage motors with semi-open slots in stator and rotor, 150% to 200% in squirrel cage motor with open slots in stator and semi-open slots in rotor, and 180% to 220% in wound rotor machines.

The flux density ripples produced by slot openings induce parasitic currents not only in the iron but also in the bars of a squirrel cage rotor. The currents induced in these bars may become considerable and give rise to extra copper losses, which may be high, if the slot pitch of the cage is very different from the stator slot pitch. A difference of up to 30% between the slot pitches keeps the losses at a low level. Equal stator and rotor slot pitches cannot be used because this would produce locking torques which may prevent starting of the motor.

5.5 Variable Frequency Equivalent Circuit. Operation Accounting For Space Fundamental M.M.F. Only[15]

The performance of an induction motor when supplied from a variable frequency source of frequency f can be

predicted from the simple equivalent circuit shown in figure 4.1, if the equivalent circuit reactances applicable to that frequency are used. This meant in this experiment that for each different supply frequency the equivalent circuit parameters had to be recalculated and the performance predicted. Unfortunately, the salient effects of the variable frequency on the motor performance cannot be visualized from such a method. Therefore it was desired to find an equivalent circuit with constant parameters which would be applicable to any frequency.

The sequence of development of the variable frequency equivalent circuit is as follows. Referring to figure 5.2 a supply of normal frequency f_n, for which the motor has been designed to operate, is frequency translated to a frequency f. A voltage V_f of this frequency is applied to the stator of the induction motor, the stator circuit of which is represented by the stator leakage impedance $(R_1 + jX_{1f})$ in series with the magnetizing impedance $1/(1/R_{Mf} - j1/X_{Mf})$. The rotor translates this frequency f to Sf, the slip frequency, and a rotor voltage E_{2Sf} of this frequency is applied across the rotor leakage impedance $(R_2 + jX_{2Sf})$.

For the maximum torque to remain fixed, V_f should be so adjusted that the air-gap mutual flux ϕ_m (space

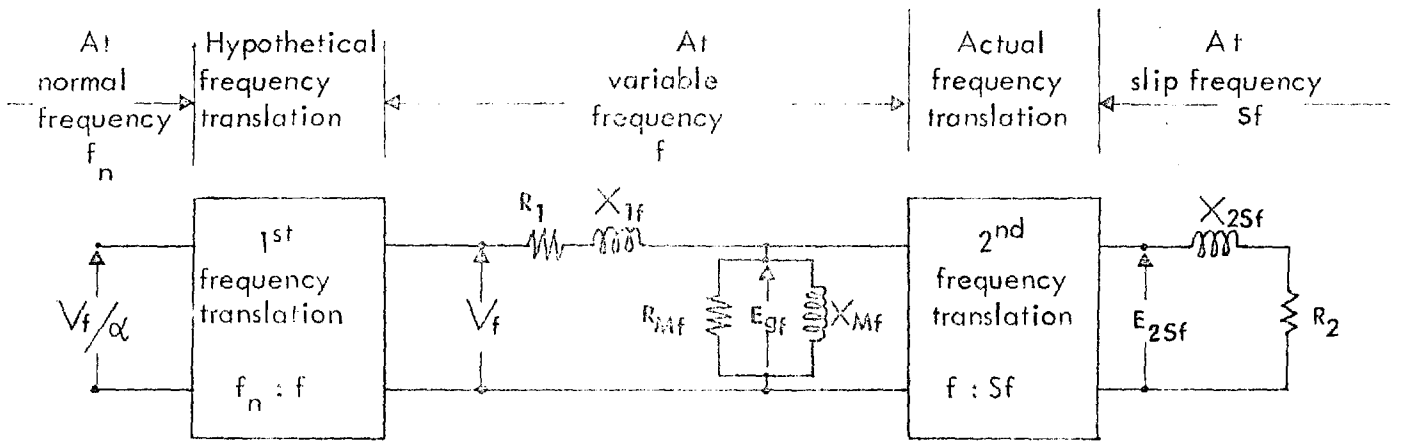

Figure 5.2 Stages of frequency translation in the development of variable frequency simple equivalent circuit of an induction motor under sinusoidal excitation.

fundamental) remains constant for any particular value of the stator current, i.e.

$$\phi_m = K \frac{E_{gf}}{f} = K \frac{E_{gn}}{f_n} = \text{constant} \qquad (5.53)$$

where E_{gf} is the air-gap voltage at any frequency f

and E_{gf_n} is the air-gap voltage at normal frequency f_n.

The rotor current as viewed from the output terminals of the "black box 2", termed the "frequency translation device 2", is

$$I_2 = \frac{E_{2sf}}{R_2 + jX_{2sf}} \qquad (5.54)$$

It has been shown in chapter 4 and figure 4.11 that the leakage reactances, for a given stator current, are directly proportional to the frequency. Therefore the slip-frequency stator reflected rotor leakage reactance X_{2Sf} can be written as

$$X_{2Sf} = SX_{2f} \qquad (5.55)$$

where X_{2f} is the stator reflected rotor leakage reactance at supply frequency f.

The term E_{2Sf} is the stator reflected rotor induced voltage (with a rotor slip of S) and is of

frequency Sf. If E_{2f} is the value of E_{2Sf} when the rotor is at standstill then

$$E_{2Sf} = SE_{2f} \qquad (5.56)$$

$$= SE_{gf} \quad (\text{since } E_{2f} = E_{gf})$$

Substituting equations 5.55 and 5.56 in equation 5.54, the stator-reflected rotor current becomes

$$I_2 = \frac{SE_{gf}}{R_2 + jSX_{2f}} \qquad (5.57)$$

The rotor current I_2 given by equation 5.57 is of the slip-frequency Sf.

Dividing the numerator and denominator of equation 5.57 by the slip S, the rotor current as viewed from the input end of the frequency translation device 2 (figure 5.2) which is at the variable frequency f, is obtained.

$$I_2 = \frac{E_{gf}}{\frac{R_2}{S} + jX_{2f}} \qquad (5.58)$$

Therefore the rotor circuit as viewed by the air-gap voltage E_{gf} looks as if its resistance has increased from R_2 to $\frac{R_2}{S}$ and the reactance has also increased from the slip-frequency value X_{2Sf} to the value X_{2f} at the variable frequency f.

The no-load current of frequency f is given by

$$I_{nl} = E_{gf}(1/R_{Mf} - j1/X_{Mf}) = I_M \qquad (5.59)$$

where R_{Mf} is the core loss simulating resistor

and X_{Mf} is the magnetizing reactance at frequency f

both for the magnetizing air-gap flux which is proportional to E_{gf}/f.

The stator current of variable frequency f as viewed from the output terminals of the "frequency translation device 1" is given by

$$I_1 = (V_f - E_{gf})/(R_1 + jX_{1f}) \qquad (5.60)$$

In order to transfer the three currents I_2, I_M and I_1 as given by equations 5.58, 5.59 and 5.60 respectively to the input terminals of the "frequency translation device 1" so that they are of normal frequency f_n a term $\alpha = f/f_n$ is introduced. Dividing the numerators and denominators of equations 5.58, 5.59 and 5.60 by α we obtain

$$I_2 = (E_{gf}/\alpha)/\{R_2/(S\alpha) + jX_{2f}/\alpha\}$$

$$= E_{gn}/\{R_2/(S\alpha) + jX_2\} \qquad (5.61)$$

$$I_M = (E_{gf}/\alpha)\{(\alpha/R_{Mf} - j\alpha/X_{Mf})\}$$

$$= E_{gn}(1/R_M - j1/X_M) \qquad (5.62)$$

$$I_1 = (V_f/\alpha - (E_{gf}/\alpha)/(R_1/\alpha - jX_{1f}/\alpha)$$

$$= (V_f/\alpha - E_{gn})/(R_1/\alpha - jX_1) \qquad (5.63)$$

The following equalities in the above equations 5.61, 5.62 and 5.63 should be observed :

i) $E_{gn} = E_{gf}/\alpha$. This means that the air-gap voltage at the variable frequency f when frequency translated by the ratio α to the normal frequency f_n has its magnitude changed from E_{gf} to E_{gn}, related by the above equality;

ii) $X_2 = X_{2f}/\alpha$. This means that since for a given stator current the rotor leakage reactance is proportional to the frequency (Figure 4.11), the reactance X_2 at the normal frequency f_n (50 c/s) is equal to the product of f_n/f and the reactance at the variable frequency f, X_{2f};

iii) $X_1 = X_{1f}/\alpha$. The reason for this equality is exactly the same as that for $X_2 = X_{2f}/\alpha$ given in ii).

iv) $\alpha/R_{Mf} = 1/R_M$. This means that since for a given air-gap flux defined by E_{gf}/f, the core loss analogue resistance is proportional to frequency (Figure 4.6), the resistance R_M at normal frequency f_n(50 c/s) is equal to the product of f_n/f and R_{Mf}, the resistance at the variable frequency f.

v) $\alpha/X_{Mf} = 1/X_M$. With the same reasoning as in iv) and with reference to figure 4.7, the given equality holds good.

Now the stator current is also given by

$$I_1 = I_2 + I_m$$

This current when viewed from the terminals of the normal frequency source is

$$I_1 = E_{gn}\left[(1/R_M - j1/X_M) + 1/\left\{R_2/(S\alpha) + jX_2\right\}\right]$$

$$E_{gn} = I_1/\left[(1/R_M - j1/X_M) + 1/\left\{R_2/(S\alpha) + jX_2\right\}\right] \quad (5.64)$$

Equation 5.63 can be re-written as

$$V_f/\alpha = E_{gn} + I_1(R_1/\alpha + jX_1)$$

Substituting the value of E_{gn} from equation 5.64 in the above equation

$$V_f/\alpha = I_1\left[(R_1/\alpha + jX_1) + \frac{1}{(1/R_M - j1/X_M) + 1/\left\{R_2/(S\alpha) + jX_2\right\}}\right] \quad (5.65)$$

The Volt/ampere relation given by equation 5.65 is identical to that of a passive bilateral network shown in

figure 5.3, and hence it could be treated as the equivalent circuit of the induction motor with variable frequency supply.

However, it must be emphasised that this equivalent circuit holds true only when the supply voltage V_f and the frequency is so adjusted that the equality $E_{gf}/f = E_{gn}/f_n$ is maintained for a given stator current, so that the air-gap flux remains constant. Otherwise equations 5.61, 5.62 and 5.63 will not be valid.

5.6 Modification of the Variable Frequency Equivalent Circuit for Constant Maximum Torque Operation

The equivalent circuit of the induction motor, figure 5.3, depicts performance under variable frequency supply, but it yet remains to be slightly modified for constant maximum torque operation to ensure that the equality $E_{gf}/f = E_{gn}/f_n$ is always maintained.

The air-gap voltage from figure 5.3 is

$$E_{gn} = V_f/\alpha - I_1(R_1/\alpha + jX_1)$$

$$= V_f/\alpha - I_1(R_1 + jX_1) - I_1R_1(1/\alpha - 1) \qquad (5.66)$$

When the induction motor is operated at normal frequency, $f = f_n$, $V_f = V_n$ and $\alpha = 1$, then from equation

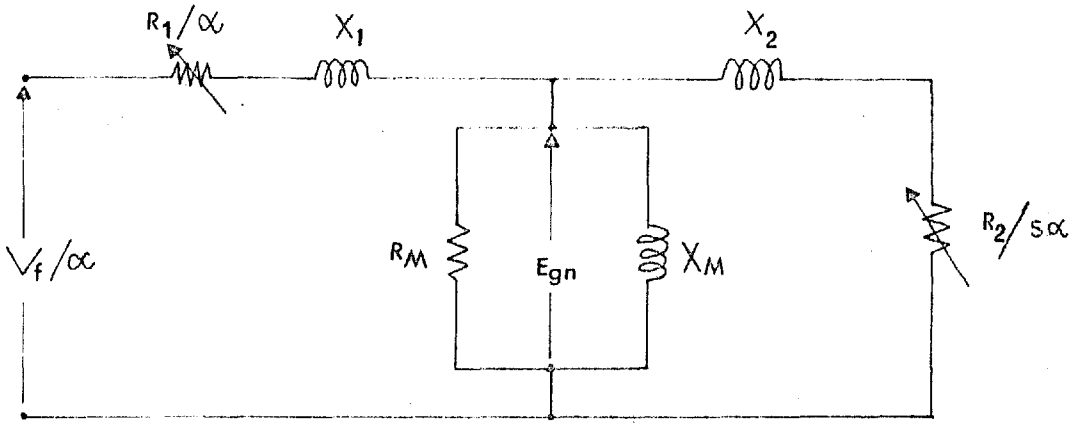

Figure 5.3 Variable Frequency Simple Equivalent Circuit Of An Induction Motor Under Sinusoidal Excitation And Fixed Maximum Torque Operation.

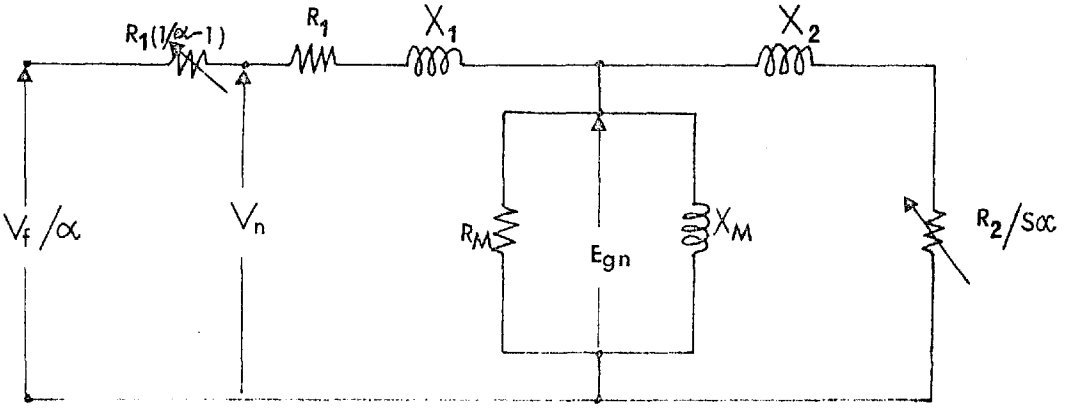

Figure 5.4 Variable Frequency Simple Equivalent Circuit Of An Induction Motor Under Sinusoidal Excitation Modified For Determination Of Supply Voltage Regulation.

5.66

$$E_{gn} = V_n - I_1(R_1 + jX_1) \qquad (5.67)$$

Substituting equation 5.67 in equation 5.66 gives

$$V_f/\alpha = V_n + I_1R_1(1/\alpha - 1) \qquad (5.68)$$

If the variable frequency equivalent circuit figure 5.3 is modified to figure 5.4 such that the condition given by equation 5.68 is satisfied, then for a given stator current the equality $E_{gf}/f = E_{gn}/f_n$ for constant air-gap flux, and hence constant maximum torque operating condition will always be ensured.

The equivalent circuit of figure 5.4 shows that under variable frequency constant maximum torque operation, the stator resistance, if viewed from the output terminals of the normal frequency source (Figure 5.2), would appear as if it was increased by a value $R_1(1/\alpha - 1)$. Further, to keep the air-gap flux constant at its normal operating value (for a given stator current) the variable frequency stator voltage V_f should be boosted by $R_1\alpha(1/\alpha - 1)I_1$ Volt above αV_n Volt. It may be noted that if R_1 was negligibly small, then the variable frequency voltage V_f required would have been simply αV_n Volt.

The voltages in the stator circuit are α times the analogue voltages for that part of the circuit, and those for the rotor circuit are $S\alpha$ times the analogue voltages of the equivalent unity effective turns-ratio rotor, whereas the actual machine currents and the analogue currents are invariant.

5.7 Variable Frequency Supply Voltage Regulation

It has been shown in section 5.6 that variable frequency constant maximum torque operation is obtainable if the analogue stator supply voltage V_f/α is so adjusted that equation 5.66 is satisfied.

The phasor diagram of the equation 5.66 is shown in figure 5.5. From the diagram it can be seen that V_f/α is the phasor sum of V_n and $I_1R_1(1/\alpha - 1)$, and the latter must be compensated by raising the analogue supply voltage V_f/α by the same amount, so as to maintain E_{gn} constant for a particular value of stator current I_1 and for any supply frequency f.

If the power factor is known then V_f/α could be calculated for various loads at any given variable frequency f from equation 5.68 or from figure 5.5. The power factor angle θ is given by the following equation

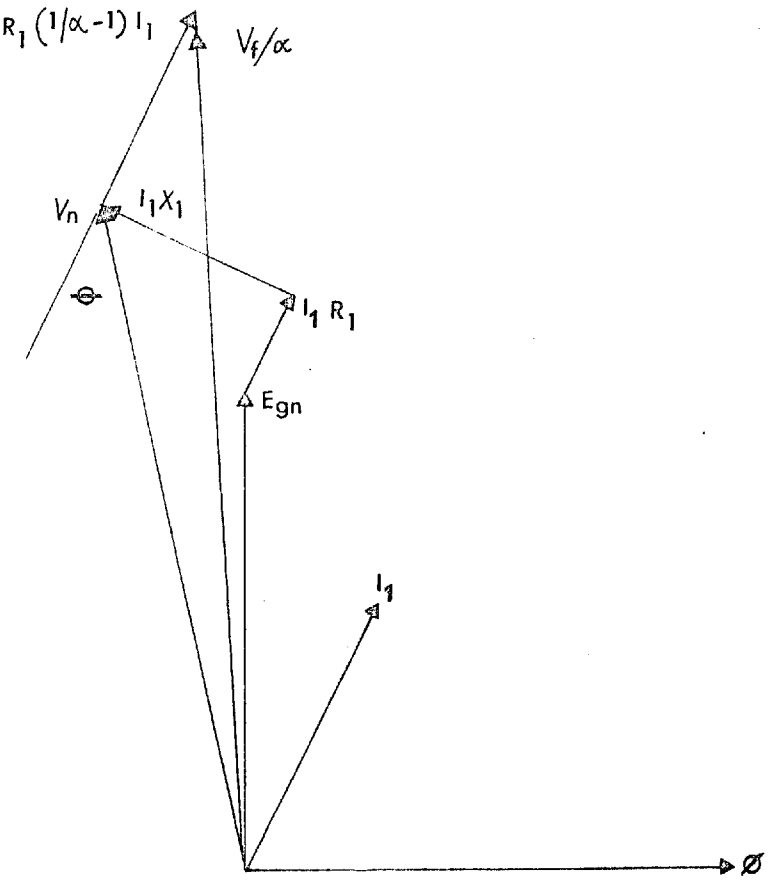

Figure 5.5 Stator Voltage Phasor Diagram Of Simple Variable Frequency Equivalent Circuit Of An Induction Motor Under Sinusoidal Excitation And Fixed Maximum Torque Operation.

$$\theta = \tan^{-1}\left[\left(\frac{X_2}{R_M} - \frac{R_2}{S\alpha X_M}\right)/\left(1 + \frac{R_2}{S\alpha R_M} + \frac{R_2}{X_M}\right)\right]$$
$$-\tan^{-1}\left[\left\{(X_1 + X_2) + \frac{1}{R_M}\left(R_1X_2 - \frac{R_2}{S\alpha}X_1\right)\right.\right.$$
$$\left.\frac{1}{X_M}\left(\frac{R_1R_2}{S\alpha} - X_1X_2\right)\right\}/\left\{\left(\frac{R_2}{S\alpha} + R_1\right)\right.$$
$$\left.\left. + \frac{1}{R_M}\left(\frac{R_1R_2}{S\alpha} - X_1X_2\right) + \frac{1}{X_M}\left(R_1X_2 - \frac{R_2}{S\alpha}X_1\right)\right\}\right] \quad (5.69)$$

From figure 5.5. the variable frequency analogue voltage required is

$$V_f/\alpha = \left\{V_n^2 + I_1^2R_1(1/\alpha - 1)^2 + 2V_nI_1R_1(1/\alpha - 1)\cos\theta\right\}^{\frac{1}{2}} \quad (5.70)$$

θ changes with slip (Equation 5.69) so that this method of finding V_f/α is tedious and a simple graphical method is therefore used. Equation 5.66 in terms of magnitudes can be rewritten as

$$|E_{gn}| = \left\{(V_f/\alpha - I_1R_1/\alpha)^2 + (I_1X_1)^2\right\}^{\frac{1}{2}} \quad (5.71)$$

If the variable frequency analogue voltage V_f/α is kept constant at V_n, then the air-gap analogue voltage E_{gn} would vary according to

$$|E_{gn}| = \left\{(V_n - I_1R_1/\alpha)^2 + (I_1X_1)^2\right\}^{\frac{1}{2}} \quad (5.72)$$

Plotting the value of $|E_{gn}|$, for various constant values of α, against stator current I_1 gives a family of curves AB, AC, AD, AE, etc. as shown in figure 5.6. At normal frequency $\alpha = 1$, the air-gap voltage $|E_{gn}|$ varies according to the curve AB. For other frequencies $\alpha_2 f_n$, $\alpha_3 f_n$, $\alpha_4 f_n$, etc. the variation of $|E_{gn}|$ is represented by AC, AD, AE, etc., when the analogue stator is impressed with a constant voltage of V_n. In order to ensure that constant air-gap flux for a given stator current is maintained irrespective of variation of frequency, the variable frequency analogue supply voltages V_{f2}/α_2, V_{f3}/α_3, V_{f4}/α_4 are boosted above the value V_n, such that the variable frequency air-gap analogue voltages represented by AB, AC, AD, AE, etc. coincide. The boost required, above V_n, say for a frequency $\alpha_5 f_n$ in terms of analogue voltage, is the difference between the ordinates of the curve AB and AF. When this analogue voltage boost is added to V_n we obtain the analogue supply voltage V_{f5}/α_5 shown by the curve AG. This voltage, when multiplied by α_5, results in the actual stator supply voltage V_{f5} required when the machine is operating at a frequency $f = \alpha_5 f_n$ (Figure 5.6).

Calculation was carried out using an I.B.M. 7090 digital computer from which the variable frequency supply voltage V_f was obtained and plotted in figure 5.6.

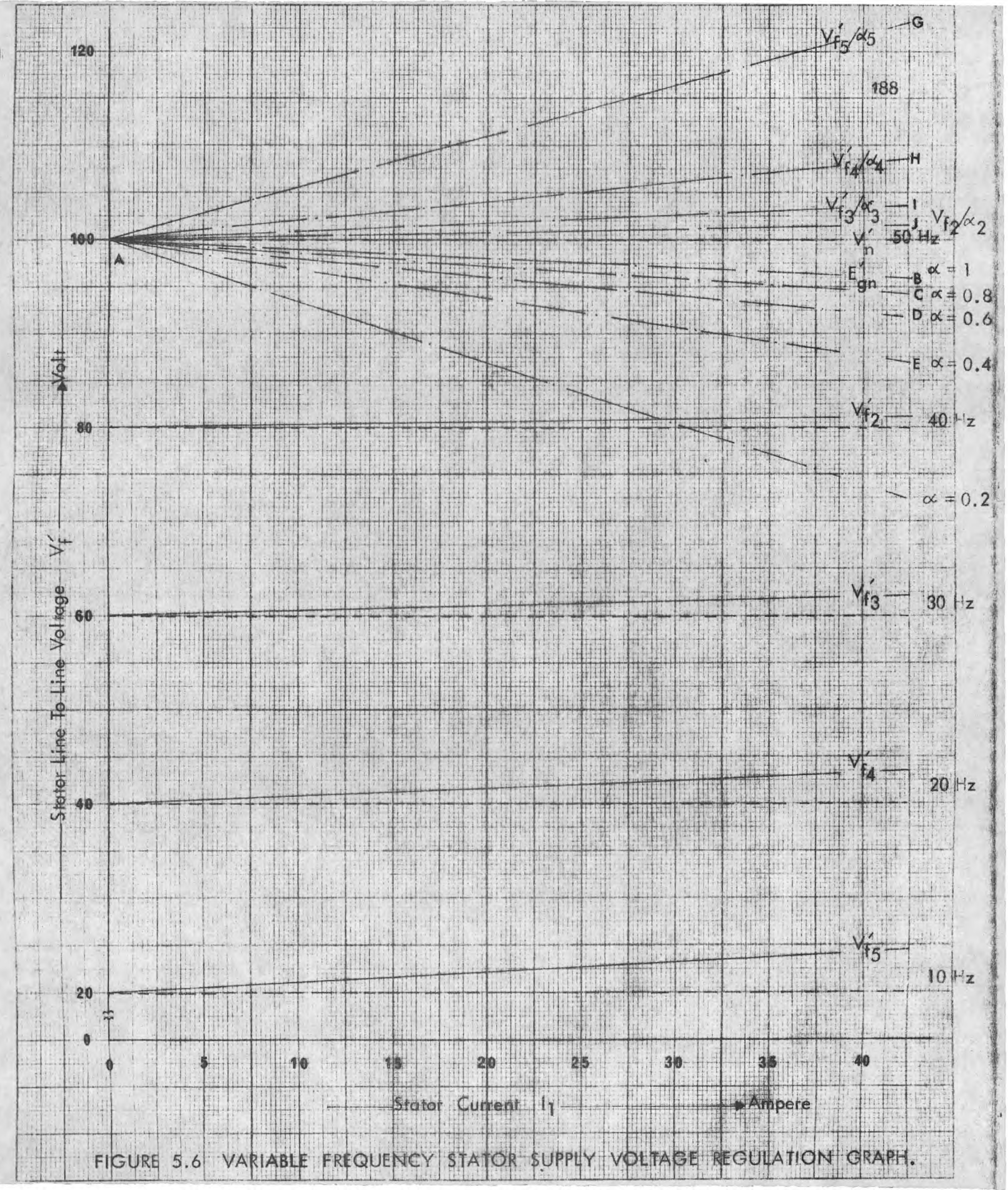

FIGURE 5.6 VARIABLE FREQUENCY STATOR SUPPLY VOLTAGE REGULATION GRAPH.

5.8 Performance Calculations from Variable Frequency Simple Equivalent Circuit

The impedances viewed by the analogue voltage V_n are given by (Figure 5.4)

Analogue stator impedance $Z_1 = R_1 + jX_1$ (5.73)

" " rotor " " $Z_2 = R_2/(Sc) + jX_2$ (5.74)

" " magnetizing admittance $Y_M = 1/R_M + j1/X_M$ (5.75)

$$\therefore \quad V_n = E_{gn} + I_1 Z_1$$

$$= E_{gn} + (I_2 + I_M)Z_1$$

$$= E_{gn} + Z_1 E_{gn}(1/Z_2 + Y_M)$$

$$= E_{gn}(Z_1 + Z_2 + Z_1 Z_2 Y_M)/Z_2$$

$$\therefore \quad E_{gn} = Z_2 V_n/(Z_1 + Z_2 + Z_1 Z_2 Y_M) \qquad (5.76)$$

(Equation 5.77 is given in table 5.2)

$$I_2 = E_{gn}/Z_2 = V_n/(Z_1 + Z_2 + Z_1 Z_2 Y_M) \qquad (5.78)$$

$$I_M = E_{gn} Y_M = V_n Y_M Z_2/(Z_1 + Z_2 + Z_1 Z_2 Y_M) \qquad (5.79)$$

$$I_1 = I_2 + I_M \qquad (5.80)$$

Table 5.2 VARIABLE FREQUENCY PERFORMANCE EQUATIONS FOR SPACE FUNDAMENTAL AND SINUSOIDAL EXCITATION

Items	Analogue	Actual
Air-gap voltage E_{gn}	$Z_2V_n/(Z_1+Z_2+Z_1Z_2Y_M)$ - (5.76)	$\alpha Z_2V_n/(Z_1+Z_2+Z_1Z_2Y_M)$ - (5.77)
Rotor current I_2	$V_n/(Z_1+Z_2+Z_1Z_2Y_M)$ - (5.78)	$V_n/(Z_1+Z_2+Z_1Z_2Y_M)$ - (5.78)
Magnetizing current I_M	$V_nY_MZ_2/(Z_1+Z_2+Z_1Z_2Y_M)$ - (5.79)	$V_nY_MZ_2/(Z_1+Z_2+Z_1Z_2Y_M)$ - (5.79)
Stator current I_1	$I_2 + I_M$ - (5.80)	$I_2 + I_M$ - (5.80)
Rotor input power P_{2in}	$m_2I_2^2R_2/(S\alpha)$ - (5.81)	$m_2I_2^2R_2/S$ - (5.82)
Rotor copper loss P_{cu2}	$m_2I_2^2R_2/\alpha$ - (5.83)	$m_2I_2^2R_2$ - (5.84)
Rotor power output P_{2o}	$m_2I_2^2R_2(1-S)/(S\alpha)$ - (5.85)	$m_2I_2^2R_2(1-S)/S$ - (5.86)
Core loss P_{FE}	$m_1E_{gn}^2/R_M$ - (5.87)	$\alpha m_1E_{gn}^2/R_M$ - (5.88)
Stator copper loss P_{cu1}	$m_1I_1^2R_1/\alpha$ - (5.89)	$m_1I_1^2R_1$ - (5.90)
Line to neutral stator supply voltage	$V_f/\alpha = V_n+I_1R_1(1/\alpha-1)$ - (5.68)	$V_f = \alpha V_n+I_1R_1(1-\alpha)$ - (5.91)

Items	Analogue	Actual
Input Volt-Ampere	$m_1\{V_n+I_1R_1(1/\alpha-1)\}$ x conj.(I_1) - (5.92)	$m_1\{\alpha V_n+I_1R_1(1-\alpha)\}$ x conj.(I_1) - (5.93)
Normal frequency synchronous speed	$N_{ns} = 120f_n/P$ - (5.94)	$N_s = 120\alpha f_n/P$ - (5.95)
Torque, electro-magnetic in lb-ft. T.	$\frac{33,000}{(2\pi x746)} \frac{m_2}{N_{ns}} I_2^2 \frac{R_2}{S\alpha}$ - (5.96)	$\frac{33,000}{2\pi x746} \frac{m_2}{N_{ns}} I_2^2 \frac{R_2}{S\alpha}$ - (5.96)

The various performance equations are given in table 5.2. The power and voltages are not invariant in the variable frequency simple analogue figure 5.4 and the actual machine, because of the frequency translation from variable frequency f to normal frequency f_n. The actual power and voltages (referred to the stator) are obtained by multiplying those from the analogue by α.

By introducing equivalent circuit parameters in the various performance equations, various interesting conclusions can be derived. The rotor current given by equation 5.78 rewritten for convenience

$$I_2 = \frac{V_n}{Z_2+Z_1+Z_2Z_1Y_M}$$

$$= V_n \Big/ \Big[\Big\{ \Big(\frac{R_2}{S\alpha} + R_1 \Big) + \frac{1}{R_M} \Big(\frac{R_1R_2}{S\alpha} - X_1X_2 \Big) + \frac{1}{X_M} \Big(R_1X_2 + \frac{R_2X_1}{S\alpha} \Big) \Big\} + j \Big\{ (X_1 + X_2) + \frac{1}{R_M} \Big(R_1X_2 + \frac{R_2X_1}{S\alpha} \Big) + \frac{1}{X_M} \Big(\frac{R_1R_2}{S\alpha} - X_1X_2 \Big) \Big\} \Big] \tag{5.97}$$

The scalar value of the rotor current is given by

$$|I_2| = V_n \Big/ \Big[\Big\{ \Big(\frac{R_2}{S\alpha} + R_1 \Big) + \frac{1}{R_M} \Big(\frac{R_1R_2}{S\alpha} - X_1X_2 \Big) + \frac{1}{X_M} \Big(X_2R_1 + \frac{R_2X_1}{S\alpha} \Big) \Big\}^2 + \Big\{ (X_1 + X_2) + \frac{1}{R_M} \Big(R_1X_2 - \frac{R_2X_1}{S\alpha} \Big) + \frac{1}{X_M} \Big(\frac{R_1R_2}{S\alpha} - X_1X_2 \Big) \Big\}^2 \Big]^{\frac{1}{2}} \tag{5.98}$$

so that

$$I_2 = V_n/(A)^{\frac{1}{2}} \tag{5.99}$$

where

$$A = \left[\left\{\left(\frac{R_2}{S\alpha} + R_1\right) + \frac{1}{R_M}\left(\frac{R_1R_2}{S\alpha} - X_1X_2\right) + \frac{1}{X_M}\left(X_2R_1 + \frac{R_2X_1}{S\alpha}\right)\right\}^2 + \left\{(X_1 + X_2) + \frac{1}{R_M}\left(R_1X_2 + \frac{R_2X_1}{S\alpha}\right) + \frac{1}{X_M}\left(\frac{R_1R_2}{\alpha S} - X_1X_2\right)\right\}^2\right] \tag{5.100}$$

The electromagnetic torque given by equation 5.96 (Table 5.2) is

$$T = \left\{33,000/(2\pi 746)\right\}\left\{m_2/(N_{ns})\right\}|I_2|^2 R_2/(S\alpha) \tag{5.96}$$

where N_{ns} = normal frequency synchronous speed

Substituting equation 5.99 in equation 5.96 gives

$$T = \left\{33,000/(2\pi 746)\right\}\left\{m_2/(N_{ns})\right\} V_n^2 \left\{R_2/(S\alpha)\right\}/A \tag{5.101}$$

The equation 5.101 is large and requires simplification. The terms containing R_M and X_M are small compared

with the others and may be neglected, so that

$$T = \left\{33,000/(2\pi 746)\right\} (m_2/N_{ns}) \frac{V_n^2 R_2/(S\alpha)}{\left\{R_2/(S\alpha)+R_1\right\}^2+(X_1+X_2)^2}$$

$$= \left\{33,000/(2\pi 746)\right\} (m_2/N_{ns})(V_n^2/R_2)$$

$$S\alpha/\left\{(1 + K_1 S\alpha)^2 + K_2^2 (S\alpha)^2\right\} \qquad (5.102)$$

where $K_1 = R_1/R_2$ (5.103)

and $K_2 = (X_1 + X_2)/R_2$ (5.104)

For small slips $S \rightarrow 0$

$$(1 + K_1 S\alpha)^2 \rightarrow 1$$

and

$$K_2^2 S^2 \alpha^2 \rightarrow 0$$

$\therefore$ From equation 5.100

$$\underset{S \rightarrow 0}{T} = \left\{33,000/(2\pi 746)\right\} (m_2/N_{ns})(V_n^2/R_2) S\alpha \qquad (5.105)$$

Equation 5.105 shows that the torque is a linear function of frequency for a fixed value of slip, when the slip is low.

At standstill S = 1. The starting torque is therefore

$$T_{S=1} = \left\{33{,}000/(2\pi 746)\right\}(m_2/N_{ns})(V_n^2/R_2)\left[\alpha/\left\{(1+K_1\alpha)^2+(K_2\alpha)^2\right\}\right] \quad (5.106)$$

The frequency at which maximum torque occurs during starting can be obtained from $\frac{dT}{d\alpha} = 0$ where T is given by equation 5.106.

This yields

$$\alpha = \pm\ 1/\left\{2(K_1+K_2)\right\}^{\frac{1}{2}}$$

or

$$f = f_n\left[R_2/\left\{2(R_1+X_1+X_2)\right\}\right]^{\frac{1}{2}} \quad (5.107)$$

Equation 5.107 shows that if a machine has to be designed to start at low frequency against full-load torque, the stator resistance and reactance should be high. A compromise with the normal running performance and stator copper loss is necessary.

For large slips $S \rightarrow \infty$

$$(1+K_1S\alpha)^2 \longrightarrow (K_1S\alpha)^2$$

Therefore torque at large slips from equation 5.102 is given by

$$T_{S\rightarrow\infty} = \left\{33{,}000/(2\pi 746)\right\}(m_2/N_{ns})(V_n^2/R_2)/\{$$

$$S \propto (K_1^2 + K_2^2)\} \qquad (5.108)$$

The torque for the same value of slip is less at high frequency than at low frequency and the relationship between torque and slip (constant $\propto$), and between torque and frequency (constant S) are both rectangular hyberbolae.

The slip at which maximum torque occurs can be determined by differentiating the expression for torque given by equation 5.101 with respect to slip and equating it to zero, and then eliminating the terms containing R_M.

This yields the slip for maximum torque as

$$S = \pm (R_2/\propto)/\left\{\frac{(1+X_1/X_M)^2 + (R_1/X_M)^2}{R_1^2(1+X_2/X_M)^2 + (X_1+X_2+X_1X_2/X_M)^2}\right\}^{\frac{1}{2}} \qquad (5.109)$$

The positive sign indicates motor action, and the negative sign indicates generator action. The maximum torque is obtained by substituting equation 5.109 in equation 5.101 giving

$$T = \left\{(33{,}000/(2\pi 746)\right\} (m_2/N_{ns})(V_n^2/K_3)/K_4 \qquad (5.110)$$

where

$$K_3 = \left\{\frac{(1+X_1/X_M)^2 + (R_1/X_M)^2}{R_1^2(1+X_2/X_M)^2 + (X_1+X_2+X_1X_2/X_M)^2}\right\}^{\frac{1}{2}} \qquad (5.111)$$

and

$$K_4 = \left[\left\{(1/K_3 + R_1) + (R_1/K_3 - X_1X_2)/R_M + (R_1X_2 + X_1/K_3)/X_M\right\}^2 + \left\{(X_1 + X_2) + (R_1X_2 + X_1/K_3)/R_M - (R_3/K_3 - X_1X_2)/X_M\right\}^2\right]^{\frac{1}{2}} \quad (5.112)$$

The maximum torque is independent of frequency but the slip at which it occurs is inversely proportional to frequency (Equation 5.109).

Equations 5.105, 5.108 and 5.109 contain the term $S\alpha$.

Now $S = (N_s - N)/N_s = (N_s - N)/(120f/P)$

and

$$\alpha = f/f_n$$

Therefore $S\alpha = \left\{P/(120f_n)\right\}(N_s - N)$, or in other words the term $S\alpha$ is proportional to the decrement ΔN of the rotor speed from the synchronous speed. Hence equations 5.105 and 5.108 indicate that at low and high slips, the torque developed is respectively, directly and inversely proportional to this decrement ΔN of rotor speed, irrespective of rotor

slip S and supply frequency f. Similarly equation 5.109 indicates that maximum torque occurs at a definite decrement ΔN irrespective of rotor slip and supply frequency.

5.9 Variable Frequency Equivalent Circuit for Constant Maximum Torque Operation Accounting for Space Fundamental and Space Harmonic M.M.Fs

The method by which the variable frequency simple analogue shown in figure 5.4 for the induction motor (Section 5.5) was derived, may be applied to figure 5.1. This results in figure 5.7 which is a passive circuit analogue of an induction motor under variable frequency operation, taking into account the space fundamental air-gap m.m.f. as well as space harmonics. The space fundamental part of figure 5.7 is identical to figure 5.4, and figure 5.7 is an extension of figure 5.4 to include the harmonic rotor branches.

5.10 Performance Calculations from a Variable Frequency Extended Equivalent Circuit

Referring to figure 5.7

The rotor ν^{th} space harmonic analogue impedance

$$Z_{2\nu} = R_{2\nu}/(S_\nu \alpha_1) + jX_2 \qquad (5.113)$$

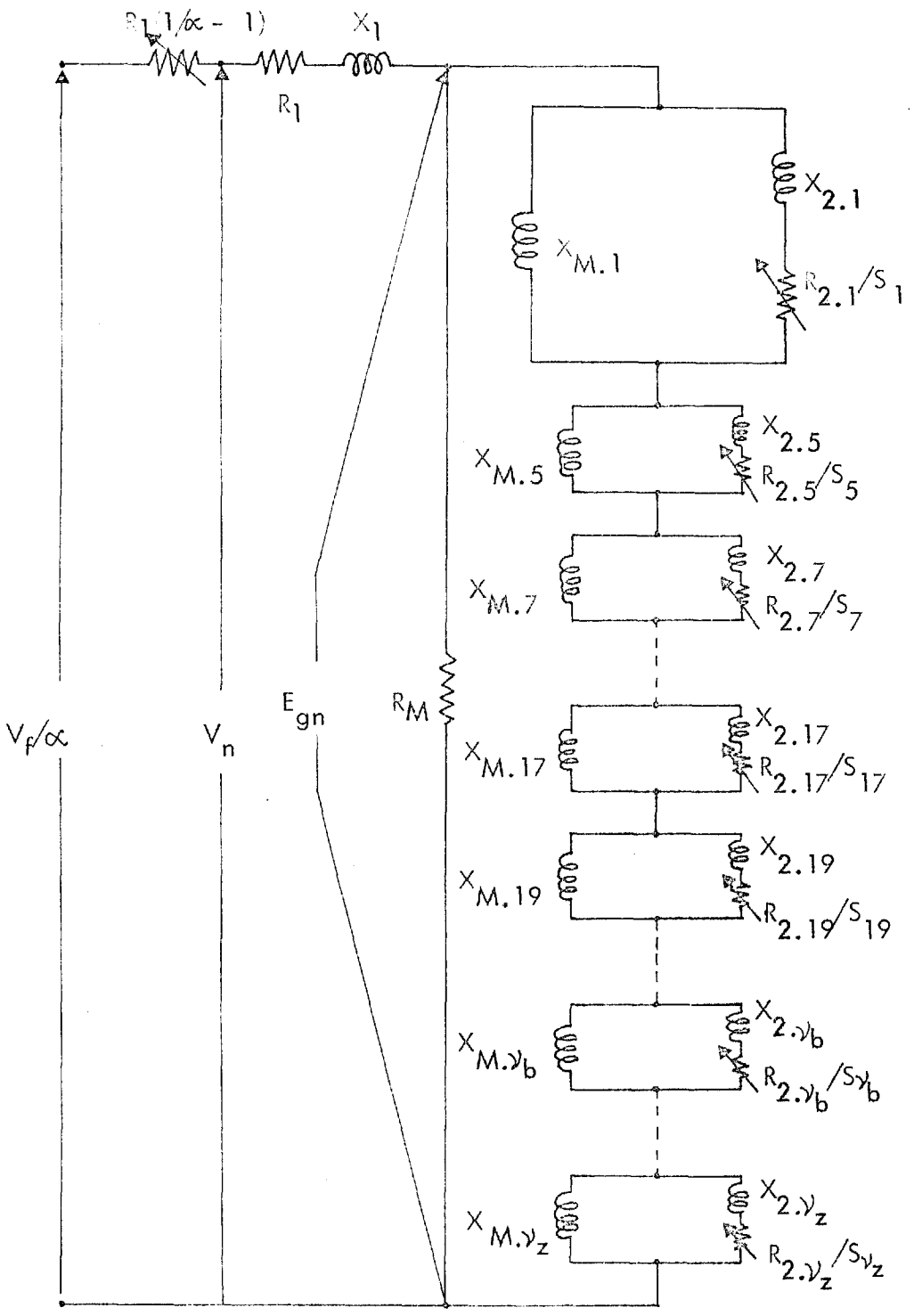

Figure 5.7 Variable Frequency Sinusoidally Excited Induction Motor Equivqlent Circuit Taking Space Fundamental And Space Harmonics In Account. Supply Voltage Regulated For Fixed Maximum Torque Operation.

where $R_{2\nu}$, $X_{2\nu}$ and S_ν are given by equations (5.49, 5.50), (5.48) and (5.51 and 5.52) respectively.

The analogue impedance of the ν^{th} space harmonic link is

$$Z_{A\nu} = \left\{-X_{2\nu}X_{M\nu} + jX_{M\nu}R_{2\nu}/(S_\nu\alpha)\right\}/\left\{R_2/(S_\nu\alpha) + j(X_{2\nu} + X_{M\nu})\right\} \qquad (5.114)$$

where $X_{M\nu}$ is given by equations 5.38 and 5.39.

Total impedance of the harmonic chain is

$$Z_A = \sum_\nu Z_{A\nu} \qquad (5.115)$$

Impedance including the core loss analogue R_M is

$$Z_B = R_M Z_A/(R_M + Z_A) \qquad (5.116)$$

The analogue impedance viewed by V_n is

$$Z_C = (R_1 + jX_1) + Z_B \qquad (5.117)$$

The analogue input impedance referred to the variable frequency analogue voltage V_f/α is

$$Z_D = R_1(1/\alpha - 1) + Z_C \qquad (5.118)$$

The various performance equations are given in table 5.3. The performance as predicted by these means and as measured is compared in chapter 8.

Table 5.3 VARIABLE FREQUENCY SINUSOIDALLY EXCITED INDUCTION MOTOR PERFORMANCE EQUATIONS ACCOUNTING FOR SPACE FUNDAMENTAL AND SPACE HARMONICS

Items	Analogue	Actual
Stator current I_1	V_n/Z_c - (5.119)	V_n/Z_c - (5.119)
Air-gap voltage E_{gn}	$V_n Z_B/Z_C$ - (5.120)	$\propto V_n Z_B/Z_C$ - (5.121)
Chain current I_A	E_{gn}/Z_A - (5.122)	E_{gn}/Z_A - (5.122)
Rotor current due to ν^{th} space harmonic $I_{2\nu}$	$I_A \dfrac{jX_{M\nu}}{\frac{R_{2\nu}}{S_{\nu\alpha}} + j(X_{2\nu}+X_{M\nu})}$ - (5.123)	$I_A \dfrac{jX_{M\nu}}{\frac{R_{2\nu}}{S_{\nu\alpha}} + j(X_{2\nu}+X_{M\nu})}$ - (5.123)
ν^{th} space harmonic rotor power input $P_{2in\nu}$	$m_2 I_{2\nu}^2 R_{2\nu}/(S_\nu \alpha)$ - (5.124)	$m_2 I_2^2 R_{2\nu}/S_\nu$ - (5.125)
ν^{th} space harmonic rotor copper loss $P_{cu2\nu}$	$m_2 I_{2\nu}^2 R_{2\nu}/\alpha$ - (5.126)	$m_2 I_{2\nu}^2 R_{2\nu}$ - (5.127)
ν^{th} space harmonic rotor power output $P_{2o\nu}$	$m_2 I_{2\nu}^2 \dfrac{R_{2\nu}}{S_{\nu\alpha}}(1-S_\nu)$ - (5.128)	$m_2 I_{2\nu}^2 \dfrac{R_{2\nu}}{S_\nu}(1-S_\nu)$ - (5.129)
Net rotor power input P_{2in}	$\sum_\nu P_{2in\nu}$ - (5.130)	$\sum_\nu P_{2in\nu}$ - (5.131)

Items	Analogue	Actual
Net rotor copper loss P_{cu2}	$\sum_{\nu} P_{cu2}$ - (5.132)	$\sum_{\nu} P_{cu2}$ - (5.133)
Net rotor power output P_{2o}	$\sum_{\nu} P_{2o\nu}$ - (5.134)	$\sum_{\nu} P_{2o\nu}$ - (5.135)
Core loss P_{FE}	$m_1 E_{gn}^2 / R_M$ - (5.136)	$\alpha m_1 E_{gn}^2 / R_M$ - (5.137)
Stator copper loss P_{cu1}	$m_1 I_1^2 R_1 / \alpha$ - (5.138)	$m_1 I_1^2 R_1$ - (5.139)
Line to neutral supply voltage	$\frac{V_f}{\alpha} = V_n + I_1 R_1 (\frac{1}{\alpha} - 1)$ - (5.140)	$V_f = \alpha V_n + I_1 R_1 (1-\alpha)$ - (5.141)
Volt-ampere input	$(V_f/\alpha)\,\text{conj.}(I_1)$ - (5.142)	$(V_f)\,\text{conj.}(I_1)$ - (5.143)
Electromagnetic torque in lb-ft produced by ν^{th} space harmonic T_ν	$\frac{33,000}{2\pi 746} \frac{m_2}{N_{ns}} \nu I_{2\nu}^2 \frac{R_{2\nu}}{S_{\nu\alpha}}$ - (5.144)	$\frac{33,000}{2\pi 746} \frac{m_2}{N_{ns}} \nu I_{2\nu}^2 \frac{R_{2\nu}}{S_{\nu\alpha}}$ - (5.144)
Net electro-magnetic torque T	$\sum_{\nu} T_\nu$ - (5.145)	$\sum_{\nu} T_\nu$ - (5.145)

CHAPTER 6

TIME HARMONIC ANALYSIS OF THE INVERTOR-FED INDUCTION MOTOR

Machine torques and losses are dependent upon supply wave-form. Iron losses increase if the wave-form of the air-gap voltage is flat topped and decrease if it is peaky. Copper losses increase whenever time harmonics are present. Analysis of the idealized voltage wave-form at the output of the thyristor invertor shows (Appendix II) the presence of time harmonics of the order

$$\gamma = (1 \pm 6K) \qquad (6.1)$$

where

$$K = 0, 1, 2, 3 \ldots \text{etc.}$$

Those harmonics which have positive values of γ viz 7^{th}, 13^{th}, 19^{th}, etc, have the same phase sequence as that of the time fundamental, and as such they produce forward torques by reacting with the space fundamental flux produced by them.

On the contrary, those harmonics which have negative values of γ, viz -5^{th}, -11^{th}, -17^{th}, have an opposite phase sequence to that of the time fundamental and as such they produce backward torques by reacting with the space

fundamental flux produced by them. Since the amplitudes of the harmonics of negative phase sequence are in general greater than that of the positive phase sequence, slight decrement of torque produced by the motor, as compared to equivalent sinusoidal operation, is expected. Those time harmonics γ which have the same numerical value as that of the space harmonic ν, always produce forward torques irrespective of their phase sequence. Moreover, this combination produces fluxes which have the same speed as that produced by the time fundamental voltage and space fundamental m.m.f. The relative synchronous speeds and the direction of rotation of the various combinations of γ and ν are shown in table 6.1.

6.1 Iron Loss in the Main Flux Path

The increase of iron loss occuring when the induction motor is fed from the invertor is due to the increase of the magnitude of the air-gap flux ϕ_m in the machine. This increase of the air-gap flux ϕ_m is due to two reasons:

i) since the air-gap flux $\phi_m = E_{gf(non\sim)}/(4K_f f N_1 K_{w1})$ (Equation 5.5), for a given frequency f and air-gap r.m.s. voltage $E_{gf_{(non\sim)}}$, the flux ϕ_m depends inversely on the form factor K_f of the air-gap voltage. For sinusoidal operation

Table 6.1 SYNCHRONOUS SPEEDS (IN PER UNIT) OF MACHINE AIR-GAP FIELD HARMONICS FOR VARIOUS TIME HARMONICS OF INVERTOR SUPPLY

ν \ δ	1	-5	7	-11	13	-17	19	-23	25	-29	31	-35	37
1	1	-5	7	-11	13	-17	19	-23	25	-29	31	-35	37
-5	$\frac{-1}{5}$	1	$\frac{-7}{5}$	$\frac{11}{5}$	$\frac{-13}{5}$	$\frac{17}{5}$	$\frac{-19}{5}$	$\frac{23}{5}$	$\frac{-25}{5}$	$\frac{29}{5}$	$\frac{-31}{5}$	$\frac{35}{5}$	$\frac{-37}{5}$
7	$\frac{1}{7}$	$\frac{-5}{7}$	1	$\frac{-11}{7}$	$\frac{13}{7}$	$\frac{-17}{7}$	$\frac{19}{7}$	$\frac{-23}{7}$	$\frac{25}{7}$	$\frac{-29}{7}$	$\frac{31}{7}$	$\frac{-35}{7}$	$\frac{37}{7}$
-11	$\frac{-1}{11}$	$\frac{5}{11}$	$\frac{-7}{11}$	1	$\frac{-13}{11}$	$\frac{17}{11}$	$\frac{-19}{11}$	$\frac{23}{11}$	$\frac{-25}{11}$	$\frac{29}{11}$	$\frac{-31}{11}$	$\frac{35}{11}$	$\frac{-37}{11}$
13	$\frac{1}{13}$	$\frac{-5}{13}$	$\frac{7}{13}$	$\frac{-11}{13}$	1	$\frac{-17}{13}$	$\frac{19}{13}$	$\frac{-23}{13}$	$\frac{25}{13}$	$\frac{-29}{13}$	$\frac{31}{13}$	$\frac{-35}{13}$	$\frac{37}{13}$
-17	$\frac{-1}{17}$	$\frac{5}{17}$	$\frac{-7}{17}$	$\frac{11}{17}$	$\frac{-13}{17}$	1	$\frac{-19}{17}$	$\frac{23}{17}$	$\frac{-25}{17}$	$\frac{29}{17}$	$\frac{-31}{17}$	$\frac{35}{17}$	$\frac{-37}{17}$
19	$\frac{1}{19}$	$\frac{-5}{19}$	$\frac{7}{19}$	$\frac{-11}{19}$	$\frac{13}{19}$	$\frac{-17}{19}$	1	$\frac{-23}{19}$	$\frac{25}{19}$	$\frac{-29}{19}$	$\frac{31}{19}$	$\frac{-35}{19}$	$\frac{37}{19}$
-23	$\frac{-1}{23}$	$\frac{5}{23}$	$\frac{-7}{23}$	$\frac{11}{23}$	$\frac{-13}{23}$	$\frac{17}{23}$	$\frac{-19}{23}$	1	$\frac{-25}{23}$	$\frac{29}{23}$	$\frac{-31}{23}$	$\frac{35}{23}$	$\frac{-37}{23}$
25	$\frac{1}{25}$	$\frac{-1}{25}$	$\frac{7}{25}$	$\frac{-11}{25}$	$\frac{13}{25}$	$\frac{-17}{25}$	$\frac{19}{25}$	$\frac{-23}{25}$	1	$\frac{-29}{25}$	$\frac{31}{25}$	$\frac{-35}{25}$	$\frac{37}{25}$
-29	$\frac{-1}{29}$	$\frac{5}{29}$	$\frac{-7}{29}$	$\frac{11}{29}$	$\frac{-13}{29}$	$\frac{17}{29}$	$\frac{-19}{29}$	$\frac{23}{29}$	$\frac{-25}{29}$	1	$\frac{-31}{29}$	$\frac{35}{29}$	$\frac{-37}{29}$
31	$\frac{1}{31}$	$\frac{-5}{31}$	$\frac{7}{31}$	$\frac{-11}{31}$	$\frac{13}{31}$	$\frac{-17}{31}$	$\frac{19}{31}$	$\frac{-23}{31}$	$\frac{25}{31}$	$\frac{-29}{31}$	1	$\frac{-35}{31}$	$\frac{37}{31}$
-35	$\frac{-1}{35}$	$\frac{1}{7}$	$\frac{-7}{35}$	$\frac{11}{35}$	$\frac{-13}{35}$	$\frac{17}{35}$	$\frac{-19}{35}$	$\frac{23}{35}$	$\frac{-5}{7}$	$\frac{29}{35}$	$\frac{-31}{35}$	1	$\frac{-37}{35}$
37	$\frac{1}{37}$	$\frac{-5}{37}$	$\frac{7}{37}$	$\frac{-11}{37}$	$\frac{13}{37}$	$\frac{-17}{37}$	$\frac{19}{37}$	$\frac{-23}{37}$	$\frac{25}{37}$	$\frac{-29}{37}$	$\frac{31}{37}$	$\frac{-35}{37}$	1

K_f = 1.11. As the air-gap voltage becomes more flat-topped K_f decreases and hence ϕ_m increases. Since the stator leakage impedance is very much smaller than the magnetizing impedance (Figure 4.1) it can be assumed that the wave-form of the line to neutral air-gap voltage is almost identical to that of the idealized line to neutral voltage supplied by the invertor. It can be seen from appendix II that K_f for such a wave-form is 1.06. Therefore for a given frequency and r.m.s. air-gap voltage, the invertor supply would cause 100(1-1.11/1.06) = 4.8% increase of the main flux;

ii) in order to produce identical torque at a given slip the r.m.s. value of the fundamental component of the air-gap voltage should be equal to its r.m.s. value with sinusoidal supply. This requires an increase in the r.m.s. value of the non-sinusoidal air-gap voltage by a factor $\pi/3$ = 1.048 or 104.8%, thereby causing a further increase of the air-gap flux by the same factor.

For equivalent operation the invertor supply causes the air-gap flux to increase to a total of (1.048 x 1.048) x 100 = 109.9%. This increase of flux ϕ_m causes an increase in iron loss.

6.1.1 Hysteresis loss

It has been shown, in equation 5.6, that for a

given r.m.s. line to neutral voltage E_{gf}, of form factor K_f, and frequency f, the air-gap flux density in a given machine is

$$B_m = E_{gf(non\sim)}/(4K_fN_1Kw_1fA) \qquad \text{(Equation 5.6)}$$

Writing the r.m.s. value of the non-sinusoidal air-gap voltage as $E_{g(non\sim)}$ and expressing it as a constant C times the r.m.s. value of its time fundamental E_{g1}

$$E_{g(non\sim)} = CE_{g1} \qquad (6.2)$$

Substituting equation 6.2 in equation 5.6 gives

$$B_m = CE_{g1}/(4K_fN_1Kw_1fA) \qquad (6.3)$$

Substituting equation 6.3 in the Steinmetz's hysteresis loss equation 5.1 we obtain the hysteresis loss due to non-sinusoidal wave-form

$$\begin{aligned} W_{h(non\sim)} &= \eta_h fC^n E_{g1}{}^n/\{(4N_1Kw_1A)^n K_f{}^n f^n\} \\ &= \eta_h C^n E_{g1}{}^n K_f{}^{-n_f(1-n)}/(4N_1Kw_1A)^n \\ &= \eta_h C^n K_f{}^{-n}(E_{g1}/f)^n f/(4N_1Kw_1A)^n \end{aligned} \qquad (6.4)$$

Hysteresis loss simulating resistance under non-sinusoidal supply condition is given by

$$R_{h(non\sim)} = E_{g(non\sim)}^{2} / W_{h(non\sim)}$$

$$= E_{gl}^{2} C^{2} / W_{h(non\sim)}$$

$$= E_{gl}^{2} C^{2} (4N_1 Kw_1 A)^{n} (E_{gl}/f)^{-n} / (\eta_h C^{n} K_f^{-n} f)$$

$$= (4N_1 Kw_1 A)^{n} / \eta_h \} K_f^{n} \{ C E_{gl}/f \}^{(2-n)} f \qquad (6.5)$$

It can be seen from appendix II that the factor C for the idealized line to neutral voltage wave-form of the invertor output is 1.048 and that K_f is 1.06. In section 5.1.1 Steinmetz exponent n has been shown to be 1.674.

Since the leakage impedance of the stator is very small compared to the magnetizing impedance (Figure 4.1), it may be assumed that the wave-form of the induced stator voltage is almost the same as that impressed on it. A further assumption will be made at this stage that the output voltage of the invertor has always the wave-form of the idealized voltage. With these assumptions the hysteresis loss when the motor is fed from the invertor is

$$W_{h(INV)} = \{ \eta_h / (4N_1 Kw_1 A)^{1.674} \} (1.048/1.06)^{1.674} (E_{gl}/f)^{1.674} f \qquad (6.6)$$

Now hysteresis loss under sinusoidal supply is, from equation 5.9,

$$W_{h(\sim)} = \{\eta_h/(4N_1 Kw_1 A)^{1.674}\}(1/1.11)^{1.674} (E_{gf}/f)^{1.674} f \qquad (6.7)$$

Dividing equation 6.6 by equation 6.7 gives

$$W_{h(INV)}/W_{h(\sim)} = (1.11 \times 1.048/1.06)^{1.674} \left\{\frac{E_{g1}/f}{E_{gf}/f}\right\}^{1.674} \qquad (6.8)$$

When an induction motor is running from a non-sinusoidal supply "constant maximum torque" operation demands that the ratio of the fundamental component of the air-gap voltage to the operating frequency should remain constant. Therefore $E_{g1}/f = E_{gf}/f$. Hence

$$W_{h(INV)}/W_{h(\sim)} = (1.11 \times 1.048/1.06)^{1.674} = 1.191$$

It could, therefore, be concluded that for "constant maximum torque" operation, supply from the thyristor invertor causes hysteresis loss to increase by 19.1% over similar operation from a sinusoidal source.

In order to determine the hysteresis loss simulating resistance for invertor operation $R_{h(INV)}$ the following procedure is adopted. It will be assumed that the value of this resistance under 50 Hertz sinusoidal operation $R_{h50(\sim)}$ is known. From equation 5.7

$$R_{h50(\sim)} = \{(4N_1Kw_1A)^{1.674}/\eta_h\}(1.11)^{1.674} (E_{g50(\sim)}/50)^{0.326} \times 50 \quad (6.9)$$

$R_{h(INV)}$ for invertor operation is, from equation 6.5,

$$R_{h(INV)} = \{(4N_1Kw_1A)^{1.674}/\eta_h\}(1.06)^{1.674} (1.048)^{1.674}(E_{g1}/f)^{0.326}f \quad (6.10)$$

Therefore

$$R_{h(INV)}/R_{h50(\sim)} = (1.06/1.11)^{1.674}(1.048)^{0.326} \left(\frac{E_{g1}/f}{E_{g50(\sim)}/50}\right)$$

$$= 0.954(f/50) \quad (6.11)$$

since $(E_{g1}/f = E_{g50(\sim)}/50)$

$R_{h(INV)}$ at 50 Hertz will be taken as 95.4% of its equivalent value at 50 Hertz sinusoidal operation (Equation 6.11). Under sinusoidal 50 Hertz operation with E_{gf}/f ratio of 2 Volt/Hertz, the value of $R_{h50(\sim)} = 46\Omega$

$R_{h(INV)}$ at 50 ~~c/s~~ Hz should be $46 \times 0.954 = 43.8\Omega$.

6.1.2 Eddy current loss

From equation 5.16 it can be seen that for a given machine the resistance simulating the eddy current loss is

independent of frequency and wave-form of line to neutral voltage induced in the stator winding.

From equation 5.17 eddy current losses do not depend on the wave-form of the stator induced line to neutral voltage. Rewriting equation 5.17 for a non-sinusoidal wave-form gives

$$W_{e(non\sim)} = \rho_e \delta^2 E_{g(non\sim)}^2 / \{16(N_1 K_{w_1} A)^2\} \quad (6.12)$$

Replacing the r.m.s. value of the non-sinusoidal air-gap voltage $E_{g(non\sim)}$ in terms of the r.m.s. value of the time fundamental E_{g1} gives

$$W_{e(non\sim)} = \rho_e \delta^2 C^2 E_{g1}^2 / \{16(N_1 K_{w_1} A)^2\} \quad (6.13)$$

The eddy current loss at 50 Hertz sinusoidal operation is given by

$$W_{e50(\sim)} = \rho_e \delta^2 E_{g50(\sim)}^2 / \{16(N_1 K_{w_1} A)^2\}$$

(Equation 5.17)

$$\therefore \quad W_{e(non\sim)} / W_{e50(\sim)} = C^2 (E_{g1} / E_{g50(\sim)})^2$$

$$= C^2 \left(\frac{E_{g1}/f}{E_{g50(\sim)}/50}\right)^2 (f^2/50^2)$$

(6.14)

Hence, at "constant maximum torque" we get

$$W_{e(non\sim)}/W_{e50(\sim)} = C^2 f^2/50^2 \qquad (6.15)$$

For invertor operation C = 1.048 for the idealized output voltage of the invertor, and hence the ratio of eddy current loss under invertor operation to similar operation under sinusoidal condition is given by

$$W_{e50(INV)}/W_{e50(\sim)} = (1.048)^2 = 1.099$$

The invertor operation causes 9.9% increase in eddy current loss.

Since in section 5.1.2 it has been shown that in the particular machine used the eddy current loss under sinusoidal operation is negligibly small, and hence the total loss is simulated by that in R_h, no attempt is made to determine the resistance simulating the eddy current loss under invertor operation.

6.2 Effect of Stator Connection on Iron Losses

Until now it has been assumed that the stator windings are star connected and the iron losses are calculated on the basis of line to neutral voltage. With sinusoidal excitation the line to line and line to neutral voltage wave-forms are sinusoidal and connection of stator windings (star or delta) do not make any difference in loss calculation. On the contrary, the line to line and

the line to neutral voltage wave-form of the invertor output are very different producing in general a completely different value for the form factor K_f and the constant C which relates the r.m.s. value of the non-sinusoidal wave-form to the r.m.s. value of the time fundamental. If the machine was delta-connected it seems logical to base the iron loss computation on the line to line voltage wave-form. From appendix II for line to line voltage wave-form, $K_f = (1.5)^{\frac{1}{2}}$ and C remains unchanged at $\pi/3$. From equation 6.8, basing calculations on line to line voltage wave-form for a delta-connected machine results in

$$W_{h(INV)}/W_{h(\sim)} = 1.11 \times 1.048/(1.5)^{\frac{1}{2}}\ 1.674$$

$$= 0.9095$$

which implies that a delta-connected machine under invertor operation results in about 9% less hysteresis loss compared to equivalent sinusoidal operation.

Since C is the same for line to line and line to neutral voltage wave-forms, it can be seen from equation 6.15 that there is no apparent change in eddy current loss due to delta connection of the stator winding.

Measurements (Figure 8.51) indicate that in practice the above statements regarding hysteresis and eddy current loss are not true. The anomalies occurring are

due to the fact that when calculations are based on line to tc line voltage wave-form, the reference axes which are automatically chosen thereby are non-existent as far as the machine magnetic circuit is concerned. The concept of reference axes is dealt with in chapter 7.

The difference not only arises when the machine magnetic circuit is connected in star or in delta, but also when series or parallel connections are made in machines with assymetric magnetic circuit[19].

6.3 Variable Frequency Equivalent Circuit Representing the Contribution of Arbitrary Time Harmonics on Motor Performance taking into account the Space Fundamental M.M.F. only

The effect of γ^{th} time harmonic of the fundamental variable frequency f on the performance of an induction motor can be determined as follows. Referring to figure 5.2, the stator of the induction motor is at a frequency of γf Hertz considering the γ^{th} time harmonic only. Since the input of the "frequency translation device 1" is at the normal frequency f_n, the net frequency translated by this hypothetical device is reduced by the factor $\alpha\gamma$. The process of reasoning which led to the development of figure 5.3 from figure 5.2 can now be applied for this case. If the r.m.s. value of the γ^{th} time harmonic voltage is

$V_{f\gamma}$ then the analogue input should be $V_{f\gamma}/(\alpha\gamma)$ Volt. The stator resistance would then be $R_1/(\alpha\alpha)$ whereas the rotor resistance would be $R_2/(S_\gamma \alpha\gamma)$ (S_γ is the slip for the rotor for the γ^{th} time harmonic). All other parameters would be unchanged. This analogue taking into account the γ^{th} time harmonic is shown in figure 6.1. Since there is a hypothetical frequency translation factor of $\alpha\gamma$, the analogue voltage, impedance and power as viewed from the stator side should be multiplied by $\alpha\gamma$ to derive the actual values. Currents and power-factor remain unchanged. This treatment demands that the leakage reactances for a particular value of stator and rotor current be directly proportional to the harmonic frequency considered. For a particular value of air-gap flux density the magnetizing reactance should also be directly proportional to the harmonic frequency. In performing experiments it was found that time harmonic voltages higher than 19^{th} were very small and as such all harmonic voltages of orders higher than 19^{th} were neglected.

At a fundamental frequency of 50 Hertz (top frequency of test) the 19^{th} harmonic has a frequency of 950 Hertz. It is doubtful whether the parameters X_1, X_2 and X_M vary linearly with frequency up to 950 Hertz. Determination of these parameters involves no-load and

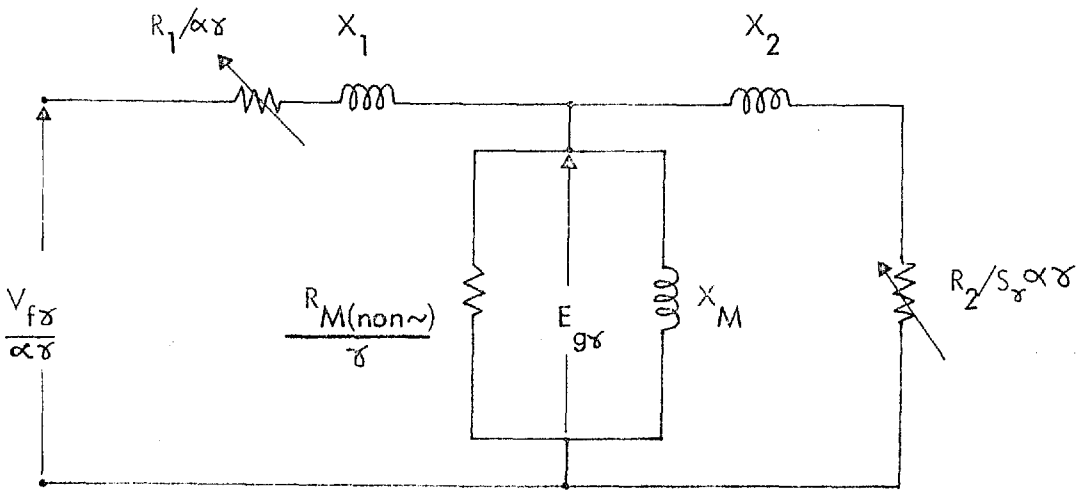

Figure 6.1 Variable Frequency Simple Equivalent Circuit Of Induction Motor For Arbitrary Time Harmonics Under Non-Sinusoidal Excitation.

locked rotor tests and no attempt was made to conduct these tests at such high frequencies. The value of actual core loss simulating resistance $R_{Mf(non\sim)}$ at a fundamental frequency f, however, unaffected by the time harmonics because it is determined from equation 6.11 which already takes into account the contribution to iron loss by the time harmonics. The iron loss in terms of actual air-gap line to neutral r.m.s. voltage $E_{gf(non\sim)}$ at fundamental frequency f, is

$$W_{hf(non\sim)} = E^2_{gf(non\sim)} / R_{Mf(non\sim)} \qquad (6.16)$$

In terms of the r.m.s. value of γ^{th} time harmonic air-gap line to neutral voltages $E_{gf\gamma}$ of fundamental frequency f, the iron loss is

$$W_{hf(non\sim)} = \sum_{\gamma=1}^{\infty} \{E^2_{gf\gamma} / R_{Mf(non\sim)}\} \qquad (6.17)$$

Since the actual iron loss is $\propto \gamma$ times the analogue iron loss, and also the actual voltage is $\propto \gamma$ times the analogue voltage, then for the γ^{th} time harmonic

$$\propto \gamma \frac{\{\gamma^{th} \text{ time harmonic analogue (air-gap line to neutral voltage)}\}^2}{\gamma^{th} \text{ time harmonic analogue core loss simulating resistance}}$$

= Actual contribution to core loss by γ^{th} time harmonic air-gap line to

to neutral voltage.

or

$$\alpha_\gamma \frac{\{E_{gf\gamma}/(\alpha\gamma)\}^2}{R_{M\gamma}} = E_{gf\gamma}^2 / R_{Mf(non\sim)} \quad (6.18)$$

where $R_{M\gamma}$ is the analogue iron loss simulating resistance for γ^{th} time harmonic.

Therefore

$$\alpha\gamma R_{M\gamma} = R_{Mf(non\sim)}$$

or

$$R_{M\gamma} = R_{Mf(non\sim)}/(\alpha\gamma) = R_{M(non\sim)}/\gamma \quad (6.19)$$

where $R_{M(non\sim)}$ is the analogue iron loss simulating resistance at normal frequency and non-sinusoidal excitation. For invertor operation at normal frequency $R_{M(non\sim)}$ is denoted by $R_{M(INV)}$ and is given by equation 6.11. It must be emphasized at this point that all the iron loss is wholly due to hysteresis and has no contribution from eddy currents as was shown in section 5.1.2.

6.4 Performance Calculation for γ^{th} Time Harmonic and Space Fundamental M.M.F.

Referring to the passive circuit analogue of figure 6.1:-

The analogue stator impedance $Z_{1\gamma} = R_1/(\alpha\gamma) + jX_1$

(Equation 6.21 is given in table 6.2)

The analogue rotor impedance

$$Z_2 = R_2/(S_\gamma \alpha\gamma) + jX_2 \qquad (6.22)$$

(Equation 6.23 is given in table 6.2)

The slip of the rotor with respect to the space fundamental m.m.f. produced by the γ^{th} time harmonic is

$$S_\gamma = 1 - (1 - S)/\gamma \qquad (6.24)$$

where S is the slip of the rotor with respect to the space fundamental m.m.f. produced by the time fundamental of the invertor supply.

The analogue admittance of the magnetizing branch

$$Y_{M\gamma} = \gamma/R_{M(INV)} - j1/X_M \qquad (6.25)$$

(Equation 6.26 is given in table 6.2)

If the r.m.s. value of γ^{th} time harmonic (fundamental frequency f Hertz) of invertor supply to the machine is $V_{f\gamma}$, then when referred to the analogue (figure 6.2) it is

$$V_{f\gamma}/(\alpha\gamma) = E_{g\gamma} + I_{1\gamma} Z_{1\gamma}$$

$$= E_{g\gamma}(Z_{1\gamma} + Z_{2\gamma} + Z_{1\gamma} Z_{2\gamma} Y_{M\gamma})/Z_{2\gamma}$$

The γ^{th} time harmonic r.m.s. value of air-gap line to neutral analogue voltage is

$$E_{g\gamma} = \{V_{f\gamma}/(\alpha\gamma)\}\{Z_{2\gamma}/(Z_{1\gamma} + Z_{2\gamma} + Z_{1\gamma} Z_{2\gamma} Y_{M\gamma})} \quad (6.27)$$

The rest of the performance equations are given in table 6.2.

The electro-magnetic torque developed by the γ^{th} time harmonic is given by equation 6.44 as

$$T_\gamma = \{33,000/(2\pi 746)\}(m_2/N_{ns})\, I_{2\gamma}^2\, R_2/(S_\gamma \alpha\gamma)$$

(Equation 6.44)

$I_{2\gamma}$ is given by equation 6.29 and is

$$I_{2\gamma} = \frac{V_{f\gamma}}{\alpha\gamma}\,\frac{1}{Z_{1\gamma} + Z_{2\gamma} + Z_{1\gamma} Z_{2\gamma} Y_{M\gamma}}$$

$$= \frac{V_{f\gamma}}{\alpha\gamma}/\left\{\left(\frac{R_1}{\alpha\gamma} + jX_1\right) + \left(\frac{R_2}{S_\gamma \alpha\gamma} + jX_2\right) + \left(\frac{R_1}{\alpha\gamma} + jX_1\right)\left(\frac{R_2}{S_\gamma \alpha\gamma} + jX_2\right)\left(\frac{\gamma}{R_{M(INV)}} - j\frac{1}{X_M}\right)\right\}$$

$$= \frac{V_f}{\alpha\gamma}/\left[\left\{\left(\frac{R_1}{\alpha\gamma} + \frac{R_2}{S_\gamma \alpha\gamma}\right) + \frac{\gamma}{R_{M(INV)}}\right.\right.$$

$$\times\left(\frac{R_1R_2}{S_\gamma\alpha^2\gamma^2} - X_1X_2\right) + \frac{1}{X_M}\left(\frac{R_1X_2}{\alpha\gamma} + \frac{R_2X_1}{S_\gamma\alpha\gamma}\right)\Bigg\}$$
$$+ j\Bigg\{(X_1 + X_2) + \frac{\gamma}{R_{M(INV)}}\left(\frac{R_1X_2}{\alpha\gamma} + \frac{R_2X_1}{S_\gamma\alpha\gamma}\right)$$
$$- \frac{1}{X_M}\left(\frac{R_1R_2}{S_\gamma\alpha^2\gamma^2} - X_1X_2\right)\Bigg\}\Bigg] \qquad (6.49)$$

The scalar value of $I_{2\gamma}$ is

$$\left|I_{2\gamma}\right| = \left\{V_{f\gamma}(\alpha\gamma)\right\}/(D)^{\frac{1}{2}} \qquad (6.63)$$

where

$$D = \Bigg[\Bigg\{\left(\frac{R_1}{\alpha\gamma} + \frac{R_2}{S_\gamma\alpha\gamma}\right) + \frac{\gamma}{R_{M(INV)}}\left(\frac{R_1R_2}{S_\gamma\alpha^2\gamma^2}\right.$$
$$\left. - X_1X_2\right) + \frac{1}{X_M}\left(\frac{R_1X_2}{\alpha\gamma} + \frac{R_2X_1}{S_\gamma\alpha\gamma}\right)\Bigg\}^2$$
$$+ \Bigg\{(X_1 + X_2) + \frac{\gamma}{R_{M(INV)}}\left(\frac{R_1X_2}{\alpha\gamma} + \frac{R_2X_1}{\alpha\gamma S_\gamma}\right)$$
$$- \frac{1}{X_M}\left(\frac{R_1R_2}{S_\gamma\alpha^2\gamma^2} - X_1X_2\right)\Bigg\}^2\Bigg] \qquad (6.64)$$

The electro-magnetic torque can now be determined by substituting equation 6.63 in equation 6.44

$$T = \left\{33{,}000/(2\pi 746)\right\}(m_2/N_{ns})\left\{V_{f\gamma}^2 R_2/(S_\gamma\alpha^3\gamma^3)\right\}/D$$

where D is given by equation 6.64.

The terms containing $R_{M(INV)}$ and X_M may be neglected as they are small compared to the others (implying infinite magnetizing impedance), then

$$T_\gamma = \frac{33,000}{2\pi 746}\frac{m_2}{N_{ns}}\frac{V_{f\gamma}^2 R_2/(S_\gamma \alpha^3 \gamma^3)}{\left(\frac{R_1}{\alpha\gamma} + \frac{R_2}{S_\gamma \alpha \gamma}\right)^2 + (X_1 + X_2)^2}$$

$$= \frac{33,000}{2\pi 746}\frac{m_2}{N_{ns}}\frac{V_{f\gamma}^2 R_2/(S_\gamma \alpha^3 \gamma^3)}{\left(\frac{R_2}{S_\gamma \alpha \gamma}\right)^2\left\{\left(1 + S_\gamma \frac{R_1}{R_2}\right)^2 + \left(\frac{X_1 + X_2}{R_2} \times S_\gamma \alpha \gamma\right)^2\right\}}$$

Substituting

$$K_1 = R_1/R_2$$

and

$$K_2 = (X_1 + X_2)/R_2$$

$$T_\gamma = \left\{33,000/(2\pi 746)\right\}(m_2/N_{ns})\left\{V_{f\gamma}^2 S_\gamma/(R_2 \alpha \gamma)\right\} 1/\left\{(1 + S_\gamma K_1)^2 + (K_2 S_\gamma \alpha \gamma)^2\right\} \quad (6.65)$$

For high values of time harmonics (5^{th}, 7^{th}, 11^{th}, 13^{th}, etc.)

$$S_{\substack{\gamma \\ \gamma \to \infty}} = 1 - \left[1/\gamma\right](1 - S) \qquad \text{(Equation 6.22)}$$

$$\to 1$$

$$\therefore T_{\substack{\gamma \\ \gamma \to \infty}} = \left\{33,000/(2\pi 746)\right\}(m_2/N_{ns})\,(V_{f\gamma}^2/R_2)\left\{1/(K_2^2 \alpha^3 \gamma^3)\right\} \quad (6.66)$$

From the above discussion it may be concluded that the higher time harmonics reacting with the space fundamental air-gap flux produce a small torque which is independent of slip S and is inversely proportional to the cube of the order of the time harmonics. This could be either a motoring or braking torque depending on the phase sequence of the time harmonics.

6.5 Equivalent Circuit Representing the Contribution of Time Harmonics on Motor Performance taking into account the Fundamental and Higher Space Harmonics

In order to take into account space harmonics, the equivalent circuit of figure 6.1 has to be expanded to that shown in figure 6.2. It may be noted that figure 6.2 is identical to figure 6.1 except for the addition of the $X_{M\nu}$ and $Z_{2\nu}$ representing the space harmonics in the air-gap of the machine.

6.6 Performance Calculations taking into account the Time Fundamental and Time Harmonics of Supply, and Space Fundamental and Space Harmonics of Machine Air-Gap M.M.F.

Referring to figure 6.2:-

The analogue rotor ν^{th} space harmonic to γ^{th} time harmonic is

$$Z_{2\gamma\nu} = R_{2\nu}/S_{\nu\gamma} + jX_{2\nu} \qquad (6.67)$$

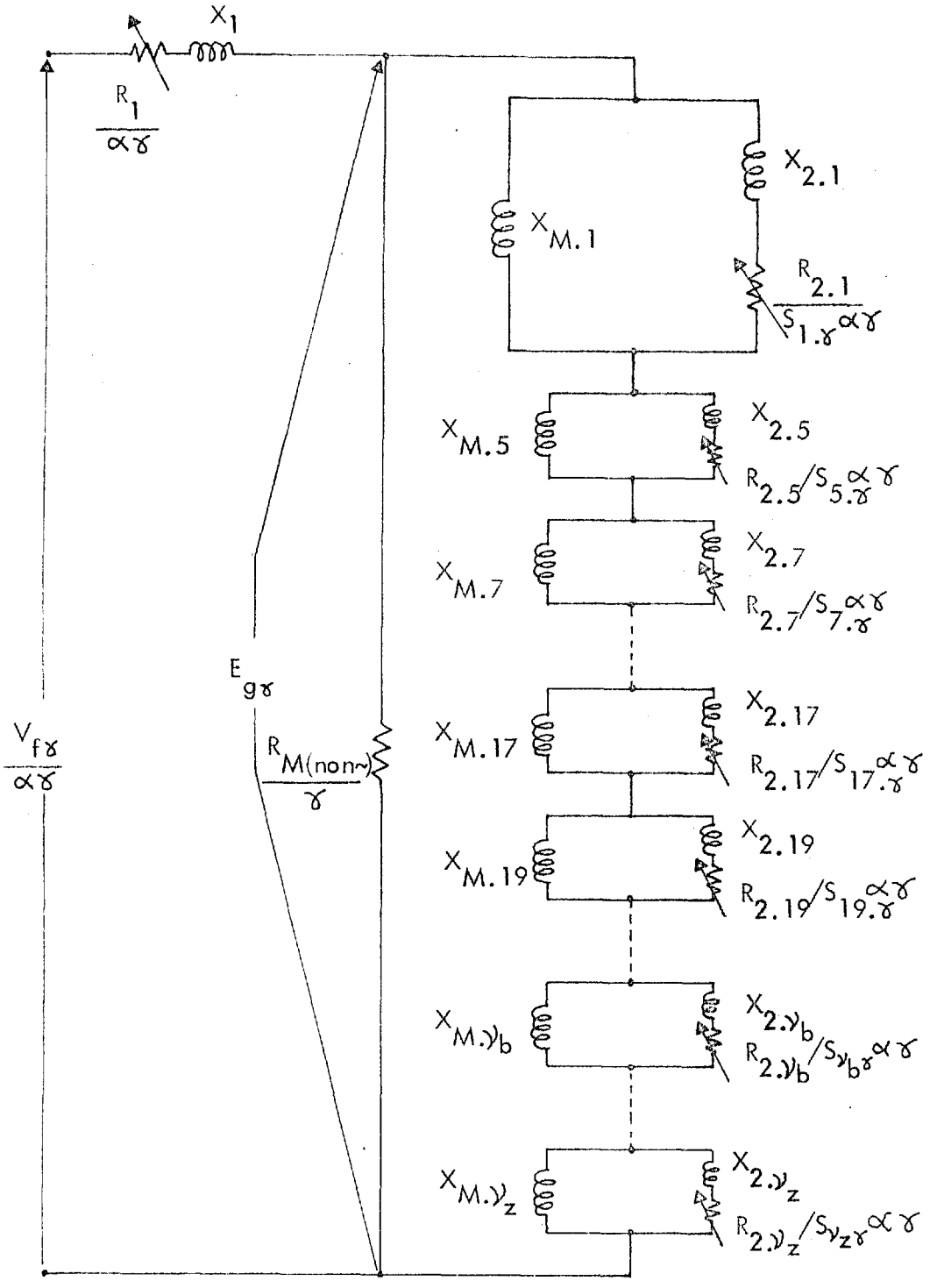

Figure 6.2 Variable Frequency Equivalent Circuit Of An Induction Motor For Arbitrary Time Harmonics Under Non-Sinusoidal Excitation Taking Space Fundamental And Space Harmonics In Account.

(Equation 6.68 is given in table 6.3)

The analogue impedance of the ν^{th} space harmonic link to γ^{th} time harmonic is

$$Z_{A\gamma\nu} = \left\{-X_{M\nu}X_{2\nu} + jX_{M\nu}R_{2\nu}/(S_{\gamma\nu}\propto\gamma)\right\}/\left\{R_{2\nu}/(S_{\gamma\nu}\propto\gamma) + j(X_{M\nu} + X_{2\nu})\right\} \quad (6.69)$$

(Equation 6.70 is given in table 6.3)

Total analogue impedance of the space harmonic chain to γ^{th} time harmonic is

$$Z_{A\gamma} = \sum_{\nu} Z_{A\gamma\nu} \quad (6.71)$$

(Equation 6.72 is given in table 6.3)

Analogue impedance including the core loss resistance to γ^{th} time harmonic is

$$Z_{B\gamma} = \left\{R_{M(INV)}Z_{A\gamma}/\gamma\right\}/\left\{R_{M(INV)}/\gamma + Z_{A\gamma}\right\} \quad (6.73)$$

(Equation 6.74 is given in table 6.3)

Input impedance of the analogue to γ^{th} time harmonic is

$$Z_{D\gamma} = \left\{R_1/(\propto\gamma) + jX_1\right\} + Z_{B\gamma} \quad (6.75)$$

(Equation 6.76 is given in table 6.3)

Slip of the rotor to ν^{th} space harmonic produced by γ^{th} time harmonic is

$$S_{\gamma\nu} = 1 - \nu(1 - S)/\gamma \qquad (6.77)$$

The various other performance equations are given in table 6.3. A digital programme was written for an IBM 7090 computer to take into account up to 37^{th} space and 19^{th} time harmonic and was used to predict the performance of the induction motor when supplied by the thyristor invertor.

Table 6.2 VARIABLE FREQUENCY INVERTOR-FED INDUCTION MOTOR PERFORMANCE EQUATIONS ACCOUNTING FOR SPACE FUNDAMENTAL ONLY

Items	Analogue	Actual
Stator impedance for γ^{th} time harmonic $Z_{1\gamma}$	$R_1/(\alpha\gamma) + jX_1$ - (6.20)	$R_1 + j\alpha\gamma X_1$ - (6.21)
Rotor impedance for γ^{th} time harmonic $Z_{2\gamma}$	$R_2/(S_\gamma \alpha\gamma) + jX_1$ - (6.22)	$R_2 + jS_\gamma\alpha\gamma X_2$ - (6.23)
Slip of the rotor w.r.t. the space fundamental m.m.f. produced by γ^{th} time harmonic S	$1 - 1(1 - S)/\gamma$ - (6.24)	$1 - 1(1 - S)/\gamma$ - (6.24)
Admittance of magnetizing branch for γ^{th} time harmonic $Y_{M\gamma}$	$\gamma/R_{M(INV)} - j1/X_M$ - (6.25)	$1/(\alpha R_{M(INV)} - j1/(\alpha\gamma X_M)$ - (6.26)
γ^{th} time harmonic r.m.s. value of air-gap line to neutral voltage $E_{g\gamma}$	$\frac{V_{f\gamma}}{\alpha\gamma} \frac{Z_{2\gamma}}{Z_{1\gamma} + Z_{2\gamma} + Z_{1\gamma} Z_{2\gamma} Y_{M\gamma}}$ - (6.27)	$V_{f\gamma} \frac{Z_2}{Z_{1\gamma} + Z_{2\gamma} + Z_{1\gamma} Z_{2\gamma} Y_{M\gamma}}$ - (6.28)

Items	Analogue	Actual
γ^{th} time harmonic rotor current $I_{2\gamma}$	$\frac{V_{f\gamma}}{\alpha\gamma} \frac{1}{Z_{1\gamma}+Z_{2\gamma}+Z_{1\gamma}} \frac{}{Z_{2\gamma} Y_{M\gamma}}$ - (6.29)	$\frac{V_{f\gamma}}{\alpha\gamma} \frac{1}{Z_{1\gamma}+Z_{2\gamma}+Z_{1\gamma}} \frac{}{Z_{2\gamma} Y_{M\gamma}}$ - (6.29)
γ^{th} time harmonic magnetizing current $I_{M\gamma}$	$\frac{V_{f\gamma}}{\alpha\gamma} \frac{Z_{2\gamma} Y_{M\gamma}}{Z_{1\gamma}+Z_{2\gamma}+Z_{1\gamma} Z_{2\gamma} Y_{M\gamma}}$ - (6.30)	$\frac{V_{f\gamma}}{\alpha\gamma} \frac{Z_{2\gamma} Y_{M\gamma}}{Z_{1\gamma}+Z_{2\gamma}+Z_{1\gamma} Z_{2\gamma} Y_{M\gamma}}$ - (6.30)
γ^{th} time harmonic stator current $I_{1\gamma}$	$I_{2\gamma} + I_{M\gamma}$ - (6.31)	$I_{2\gamma} + I_{M\gamma}$ - (6.31)
γ^{th} time harmonic rotor power input $P_{2in\gamma}$	$m_2 I_{2\gamma}^2 R_2/(S_\gamma \alpha\gamma)$ - (6.32)	$m_2 I_{2\gamma}^2 R_2/(S_\gamma)$ - (6.33)
γ^{th} time harmonic rotor copper loss $P_{cu2\gamma}$	$m_2 I_{2\gamma}^2 R_2/(\alpha\gamma)$ - (6.34)	$m_2 I_{2\gamma}^2 R_2$ - (6.35)
γ^{th} time harmonic rotor power output $P_{2o\gamma}$	$m_2 I_{2\gamma}^2 \{R_2/(S_\gamma \alpha\gamma)\}(1 - S_\gamma)$ - (6.36)	$m_2 I_{2\gamma}^2 \{R_2/(S_\gamma)\}(1 - S_\gamma)$ - (6.37)
γ^{th} time harmonic iron loss $P_{FE\gamma}$	$m_1 E_{g\gamma}^2 \gamma/(R_{M(INV)})$ - (6.38)	$m_1 \alpha\gamma^2 E_{g\gamma}^2 / R_{M(INV)}$ - (6.39)
γ^{th} time harmonic stator copper loss $P_{cu1\gamma}$	$m_1 I_{1\gamma}^2 R_1/(\alpha\gamma)$ - (6.40)	$m_1 I_{1\gamma}^2 R_1$ - (6.41)

Items	Analogue	Actual
γ^{th} time harmonic Volt-ampere input VA_γ	$m_1 V_{f\gamma} \text{ xconj.}(I_{1\gamma})/(\alpha\gamma)$ - (6.42)	$m_1 V_{f\gamma} \text{ xconj.}(I_{1\gamma})$ - (6.43)
γ^{th} time harmonic electro-magnetic torque T_γ Lb.-ft.	$\frac{33,000}{2\pi 746} \frac{m_2}{N_{ns}} I_{2\gamma}^2 \frac{R_2}{S_\gamma \alpha\gamma}$ - (6.44)	$\frac{33,000}{2\pi 746} \frac{m_2}{N_{ns}} I_{2\gamma}^2 \frac{R_2}{S_\gamma \alpha\gamma}$ - (6.44)
R.m.s. value of air-gap line to neutral voltage $E_{g(non\sim)}$	$\left\{\sum_\gamma E_{g\gamma}^2\right\}^{\frac{1}{2}}$ - (6.45)	$\left\{(\alpha\gamma E_{g\gamma})^2\right\}^{\frac{1}{2}}$ - (6.46)
R.m.s. value of rotor current I_2	$\left\{\sum_\gamma I_{2\gamma}^2\right\}^{\frac{1}{2}}$ - (6.47)	$\left\{\sum I_{2\gamma}^2\right\}^{\frac{1}{2}}$ - (6.47)
R.m.s. value of magnetizing current I_M	$\left\{\sum_\gamma I_{M\gamma}^2\right\}^{\frac{1}{2}}$ - (6.48)	$\left\{\sum_\gamma I_{M\gamma}^2\right\}^{\frac{1}{2}}$ - (6.48)
R.m.s. value of stator current I_1	$\left\{\sum_\gamma I_{1\gamma}^2\right\}^{\frac{1}{2}}$ - (6.49)	$\left\{\sum_\gamma I_{1\gamma}^2\right\}^{\frac{1}{2}}$ - (6.49)
Nett rotor power input P_{2in}	$\sum_\gamma P_{2\gamma in}$ - (6.50)	$\sum_\gamma \alpha\gamma P_{2\gamma in}$ - (6.51)
Nett rotor copper loss P_{cu2}	$\sum_\gamma P_{cu2\gamma}$ - (6.52)	$\sum_\gamma \alpha\gamma P_{cu2\gamma}$ - (6.53)
Nett rotor power output P_{2o}	$\sum_\gamma P_{2o\gamma}$ - (6.54)	$\sum_\gamma \alpha\gamma P_{2o\gamma}$ - (6.55)

Items	Analogue	Actual
Nett iron loss P_{FE}	$\sum_{\gamma} P_{FE\gamma}$ - (6.56)	$\sum_{\gamma} \alpha_\gamma P_{FE\gamma}$ - (6.57)
Nett stator copper loss P_{cul}	$\sum_{\gamma} P_{cul\gamma}$ - (6.59)	$\sum_{\gamma} \alpha_\gamma P_{cul\gamma}$ - (6.59)
Nett Volt-ampere input VA	$\sum_{\gamma} VA_\gamma$ - (6.60)	$\sum_{\gamma} \alpha_\gamma VA_\gamma$ - (6.61)
Nett electro-magnetic torque T	$\sum_{\gamma} T_\gamma$ - (6.62)	$\sum_{\gamma} T_\gamma$ - (6.62)

Table 6.3 VARIABLE FREQUENCY INVERTOR FED INDUCTION MOTOR PERFORMANCE EQUATIONS TAKING TIME AND SPACE HARMONICS INTO ACCOUNT

Items	Analogue	Actual
Rotor ν^{th} space harmonic impedance to γ^{th} time harmonic $R_{2\gamma\nu}$	$\frac{R_2}{(S_{\gamma\nu}\alpha_\gamma)} + jX_{2\nu}$ - (6.67)	$R_{2\nu} + jS_{\gamma\nu}\alpha_\gamma X_{2\nu}$ - (6.68)
Impedance of ν^{th} space harmonic link to γ^{th} time harmonic $Z_{A\gamma\nu}$	$\frac{-X_{M\nu}X_{2\nu}+jX_{M\nu}\frac{R_{2\nu}}{S_{\gamma\nu}\alpha_\gamma}}{\frac{R_{2\nu}}{S_{\gamma\nu}\alpha_\gamma}+j(X_{M\nu}+X_{2\nu})}$ - (6.69)	$\frac{-X_{M\nu}X_{2\nu}\alpha_\gamma+jX_{M\nu}\frac{R_{2\nu}}{S_{\gamma\nu}}}{\frac{R_{2\nu}}{S_{\gamma\nu}\alpha_\gamma}+j(X_{M\nu}+X_{2\nu})}$ - (6.70)
Total impedance of the space harmonic chain to γ^{th} time harmonic $Z_{A\gamma}$	$\sum_\nu Z_{A\gamma\nu}$ - (6.71)	$\sum_\nu \alpha_\gamma Z_{A\gamma\nu}$ - (6.72)
Impedance to γ^{th} time harmonic air-gap voltage $Z_{B\gamma}$	$\frac{\frac{R_{M(INV)}}{\gamma}Z_{A\gamma}}{\frac{R_{M(INV)}}{\gamma}+Z_{A\gamma}}$ - (6.73)	$\frac{\alpha R_{M(INV)}Z_{A\gamma}}{\frac{R_{M(INV)}}{\gamma}+Z_{A\gamma}}$ - (6.74)
Input impedance to γ^{th} time harmonic $Z_{D\gamma}$	$(\frac{R_1}{\alpha_\gamma}+jX_1)+Z_{B\gamma}$ - (6.75)	$(R_1+j\alpha_\gamma X_1)+\frac{\alpha R_{M(INV)}Z_{A\gamma}}{\frac{R_{M(INV)}}{\gamma}+Z_{A\gamma}}$ - (6.76)

Items	Analogue	Actual
Slip of the rotor to ν^{th} space harmonic produced by γ^{th} time harmonic $S_{\gamma\nu}$	$1 - \nu(1 - S)/\gamma$ - (6.77)	$1 - \nu(1 - S)/\gamma$ - (6.77)
γ^{th} time harmonic current of stator $I_{1\gamma}$	$\{V_{f\gamma}/(\propto\gamma)\}/Z_{D\gamma}$ - (6.78)	$\{V_{f\gamma}/(\propto\gamma)\}/Z_{D\gamma}$ - (6.78)
γ^{th} time harmonic air-gap voltage r.m.s. $E_{g\gamma}$	$\{V_{f\gamma}/(\propto\gamma)\}(Z_{B\gamma}/Z_{D\gamma})$ - (6.79)	$V_{f\gamma}(Z_{B\gamma}/Z_{D\gamma})$ - (6.80)
γ^{th} time harmonic current through space harmonic chain $I_{A\gamma}$	$E_{g\gamma}/Z_{A\gamma}$ - (6.81)	$E_{g\gamma}/Z_{A\gamma}$ - (6.81)
Rotor ν^{th} space harmonic current due to γ^{th} time harmonic $I_{2\gamma\nu}$	$I_{A\gamma}\dfrac{jX_{M\nu}}{\dfrac{R_{2\nu}}{S_{\gamma\nu}\propto\gamma} + j(X_{2\nu}+X_{M\nu})}$ - (6.82)	$I_{A\gamma}\dfrac{jX_{M\nu}}{\dfrac{R_{2\nu}}{S_{\gamma\nu}\propto\gamma} + j(X_{2\nu}+X_{M\nu})}$ - (6.82)
ν^{th} space harmonic rotor power input due to γ^{th} time harmonic $P_{2in\gamma\nu}$	$m_2 I_{2\gamma\nu}^2 \dfrac{R_{2\nu}}{S_{\gamma\nu}\propto\gamma}$ - (6.83)	$m_2 I_{2\gamma\nu}^2 \dfrac{R_{2\nu}}{S_{\gamma\nu}}$ - (6.84)
Nett rotor power input due to γ^{th} time harmonic $P_{2in\gamma}$	$\sum_{\nu} m_2 I_{2\gamma\nu}^2 \dfrac{R_{2\nu}}{S_{\gamma\nu}\propto\gamma}$ - (6.85)	$\sum_{\nu} m_2 I_{2\gamma\nu}^2 \dfrac{R_{2\nu}}{S_{\gamma\nu}}$ - (6.86)

Items	Analogue	Actual
Gross rotor power input P_{2in}	$\sum_{\gamma}\sum_{\nu} m_2 I_{2\gamma\nu}^2 \frac{R_{2\nu}}{S_{\gamma\nu}\alpha_\gamma}$ - (6.87)	$\sum_{\gamma}\sum_{\nu} m_2 I_{2\gamma\nu}^2 \frac{R_{2\nu}}{S_{\gamma\nu}}$ - (6.88)
ν^{th} harmonic rotor copper loss due to γ^{th} time harmonic $P_{cu2\gamma\nu}$	$m_2 I_{2\gamma\nu}^2 \frac{R_{2\nu}}{\alpha_\gamma}$ - (6.89)	$m_2 I_{2\gamma\nu}^2 R_{2\nu}$ - (6.90)
Nett rotor copper loss due to γ^{th} time harmonic $P_{cu2\gamma}$	$\sum_{\nu} m_2 I_{2\gamma\nu}^2 \frac{R_2}{\alpha_\gamma}$ - (6.91)	$\sum_{\nu} m_2 I_{2\gamma\nu}^2 R_{2\nu}$ - (6.92)
Gross rotor copper loss P_{cu2}	$\sum_{\gamma}\sum_{\nu} m_2 I_{2\gamma\nu}^2 \frac{R_{2\nu}}{\alpha_\gamma}$ - (6.93)	$\sum_{\gamma}\sum_{\nu} m_2 I_{2\gamma\nu}^2 R_{2\nu}$ - (6.94)
ν^{th} harmonic rotor power output due to γ^{th} time harmonic $P_{2o\gamma\nu}$	$m_2 I_{2\gamma\nu}^2 \frac{R_{2\nu}}{S_{\nu\gamma}\alpha_\gamma}(1 - S_{\gamma\nu})$ - (6.95)	$m_2 I_{2\gamma\nu}^2 \frac{R_{2\nu}}{S_{\nu\gamma}}(1 - S_{\gamma\nu})$ - (6.96)
Nett rotor power output due to γ^{th} time harmonic $P_{2o\gamma}$	$\sum_{\nu} m_2 I_{2\gamma\nu}^2 \frac{R_{2\nu}}{S_{\nu\gamma}}(1 - S_{\nu\gamma})$ - (6.97)	$\sum_{\nu} m_2 I_{2\gamma\nu}^2 \frac{R_{2\nu}}{S_{\nu\gamma}}(1 - S_{\nu\gamma})$ - (6.98)
Gross rotor power output P_{2o}	$\sum_{\gamma}\sum_{\nu} m_2 I_{2\gamma\nu}^2 \frac{R_{2\nu}}{S_{\nu\gamma}}(1-S_{\nu\gamma})$ - (6.99)	$\sum_{\gamma}\sum_{\nu} m_2 I_{2\gamma\nu}^2 \frac{R_{2\nu}}{S_{\nu\gamma}}(1 - S_{\nu\gamma})$ - (6.100)
Iron loss due to γ^{th} time harmonic $P_{FE\gamma}$	$\alpha_\gamma (E_{g\gamma}^2)/R_{M(INV)}$ - (6.101)	$(\alpha_\gamma^2 E_{g\gamma}^2)/R_{M(INV)}$ - (6.102)

Items	Analogue	Actual
Gross iron loss P_{FE}	$\sum_{\gamma}(\gamma E_{g\gamma}^{2})/R_{M(INV)}$ - (6.103)	$\sum_{\gamma}(\alpha\gamma^{2}E_{g\gamma}^{2})/R_{M(INV)}$ - (6.104)
Stator copper loss due to γ^{th} time harmonic $P_{cul\gamma}$	$I_{1\gamma}^{2}\ R_{1}/(\alpha\gamma)$ - (6.105)	$I_{1\gamma}^{2}\ R_{1}$ - (6.106)
Gross stator copper loss P_{cul}	$\sum_{\gamma} I_{1\gamma}^{2}\ R_{1}/(\alpha\gamma)$ - (6.107)	$\sum_{\gamma} I_{1\gamma}^{2} R_{1}$ - (6.108)
R.M.S. value of stator current	$(\sum_{\gamma} I_{1\gamma}^{2})^{\frac{1}{2}}$ - (6.109)	$(\sum_{\gamma} I_{1\gamma}^{2})^{\frac{1}{2}}$ - (6.109)
Stator Volt-ampere input VA	$\sum_{\gamma} V_{f\gamma}\ \text{conj.}(I_{1\gamma})/(\alpha\gamma)$ - (6.110)	$\sum_{\gamma} V_{f\gamma}\ \text{conj.}(I_{1\gamma})$ - (6.111)
Electro-magnetic torque produced by γ^{th} time and ν^{th} space harmonic $T_{\gamma\nu}$	$\frac{33,000}{2\pi 746}\frac{m_2}{N_{ns}}\nu I_{2\gamma\nu}^{2}\frac{R_{2\nu}}{S_{\gamma\nu}\alpha\gamma}$ - (6.112)	$\frac{33,000}{2\pi 746}\frac{m_2}{N_{ns}}\nu I_{2\gamma\nu}^{2}\frac{R_{2\nu}}{S_{\gamma\nu}\alpha\gamma}$ - (6.112)
Nett electro-magnetic torque produced by γ^{th} time harmonic T_{γ}	$\sum_{\nu} T_{\gamma\nu}$ - (6.113)	$\sum_{\nu} T_{\gamma\nu}$ - (6.113)
Gross electro-magnetic torque developed T	$\sum_{\gamma}\sum_{\nu} T_{\gamma\nu}$ - (6.114)	$\sum_{\gamma}\sum_{\nu} T_{\gamma\nu}$ - (6.114)

CHAPTER 7

TIME DOMAIN ANALYSIS OF INVERTOR-FED INDUCTION MOTOR

The two methods of analysis are:-

i) Harmonic analysis (Chapter 6)

and ii) Time domain analysis (to be presented in this chapter.

The first method takes into account the extra losses and parasitic torques occurring due to the non-sinusoidal distribution of air-gap m.m.f., by taking large numbers of space harmonics into account. When the motor is fed from a non-sinusoidal source, effects on losses and torques of various time harmonics can also be calculated by taking into account a sufficient number of these time harmonics.

The harmonic analysis cannot directly predict the instantaneous variation of stator line current which is vital for invertor commutation circuit design and determination of the rating of the semi-conductors used in the invertor. Harmonic analysis can only predict the steady mean torque developed and gives no indication of the nature of torque fluctuations of the invertor-fed machine.

Analysis directly in the time domain with certain assumptions yields a fairly accurate prediction of instantantous stator line current and torque of the invertor-fed machine. It fails, however, in predicting the

parasitic torques and extra losses occurring due to the space harmonics of the air-gap m.m.f.

7.1 Assumptions

The analysis of the invertor-fed machine starts with certain basic assumptions, as otherwise the mathematics involved becomes too difficult. The assumptions are

i) The two iron surfaces of the air-gap are smooth. This eliminates the slot harmonics of the air-gap m.m.f. and also the permeance variation arising due to the relative motion between stator and rotor.

ii) Windings are sinusoidally distributed over the stator and rotor surfaces. This eliminates the belt harmonics of the air-gap m.m.f.

Assumptions i) and ii) make the mutual inductance between stator and rotor windings to be a purely sinusoidal function of rotor position with respect to the stator windings.

iii) The magnetic circuit of the machine is in an unsaturated condition. This assumption makes it possible to use linear transformation and super-position of voltages, currents, fluxes, impedances, etc.

iv) Main flux path iron loss simulating resistance is assumed to be shunting the supply voltage. This reduces the order of the differential equation involved.

v) The voltage fed to the motor is idealized to a rectangular wave-form. This is the most drastic approximation of all.

vi) The rotor is rotating at a constant angular velocity w_r.

7.2 Representation of Machine and Machine Equations [16, 17, 18]

With the above assumptions the machine can be represented by a group of linear coupled circuits. By tensor analysis the basic equations of the machine differ depending on the axes of reference. Starting with the physically existing spatially distributed three-phase reference axes on stator and rotor with relative motion between them, two other transformations are now introduced, based on two new hypothetical reference axes, both relatively stationary. This is done in order to simplify the basic machine equations.

7.2.1 Representation of machine along the three phase spatial rotor and stator holonomic reference frames. (∝ frames RYB and ryb)

Stator and rotor quantities are denoted by subscripts which give the particular phase. Upper case letters denote stator quantities and lower case letters denote rotor quantities.

The machine representation is shown in figure 7.1. The performance equations along the above-mentioned physically existing reference axes result in a set of six complicated simultaneous differential equations with time-varying co-efficients. These time-varying co-efficients are introduced by stator-rotor mutual inductances, which are sinusoidal functions of the angle between stator and rotor axes. These angles for contant rotor speed are linear functions of time.

7.2.2 Representation of machine along stator DQO and rotor dqo axes - frame

The above-mentioned set of six differential equations with time-varying co-efficients can be reduced to a set of six linear differential equations with constant co-efficients by splitting the air-gap m.m.f. into components along two perpendicular axes. Since there are no two axes of symmetry (i.e. no brushes or salient poles) to dictate any particular choice of position for the reference axes, the DQO axes of stator and dqo axes of rotor are orientated such that D and d axes coincide with the R axes of the stator. This makes the D axis to be the physically existing reference axis.

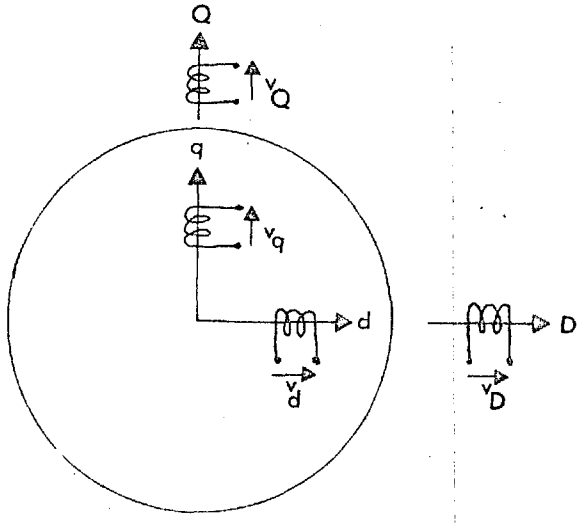

Figure 7.2 Hypothetical α' Reference Frame . Stator axes DQO And Rotor Axes dqo Stationary In Space With Axes D And d Coincident With R Axis.

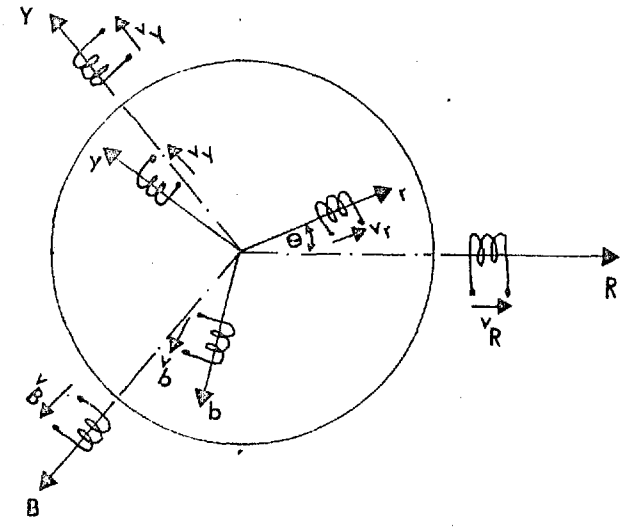

Figure 7.1 Physically Existing α Reference Frame. Stator Axes RYB Stationary In Space And Rotor Axes ryb Rotating With Rotor.

This transformation results in non-holonomic reference frame, rotor dqo coils carrying currents at supply frequency given by f and stator DQO coils carrying currents also at supply frequency f. It may be noted that the α' coils of stator and rotor are stationary in space. Such representation of the machine is shown in figure 7.2.

The transformation tensors which transform the holonomic three spatial axes RYB and ryb quantities to non-holonomic DQO and dqo axes quantities are given in figures 7.3 and 7.4 in terms of currents. If time is so measured that at time zero the rotor r axis is coincident with stator R axis then the stator and rotor transformation tensors given by figures 7.3 and 7.4 become identical at instant t = 0. The same transformation is applied to the stator voltages. Figure 7.5 shows the idealized line to line and line to neutral voltage wave-form at the stator terminals, whereas figure 7.6 shows the stator line to neutral voltage when transformed to DQ axes voltages. It may be noted that no voltage can exist along O axis for the line to line and line to neutral voltage wave-forms shown, and hence no current can exist along that axis. The stator D axis voltage wave-form is identical to stator R axis voltage wave-form because the D axis was taken to be coincident with R axis. Table 7.1 is a summary of line to neutral and DQ axes voltages.

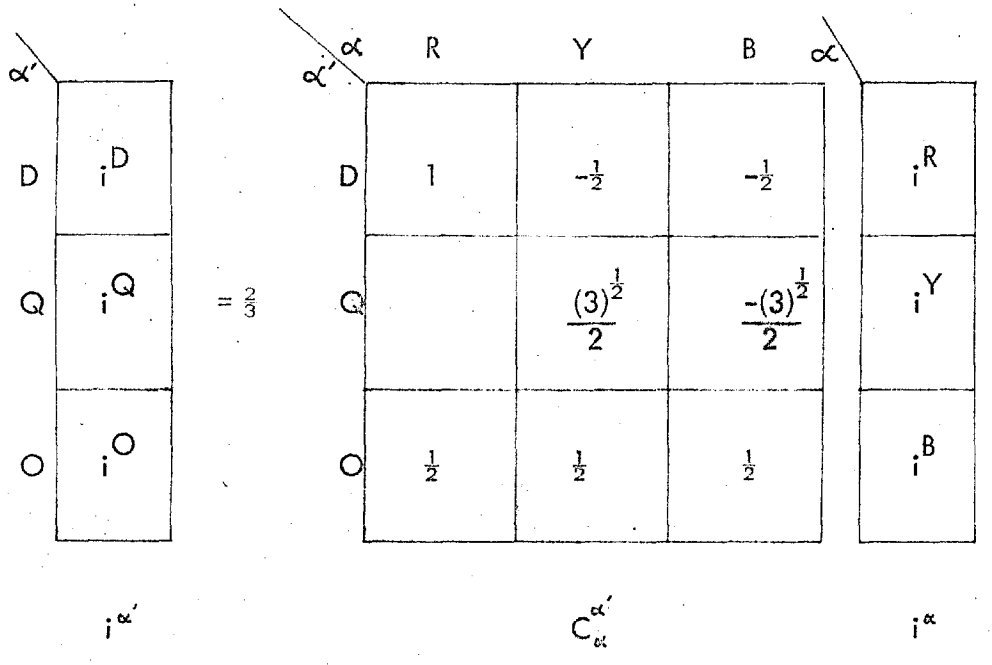

Figure 7.3 Stator DQO Quantities Expressed In Terms Of Stator RYB Quantities. D Axis Stationary In Space And Coincident With The Stationary R Axis.

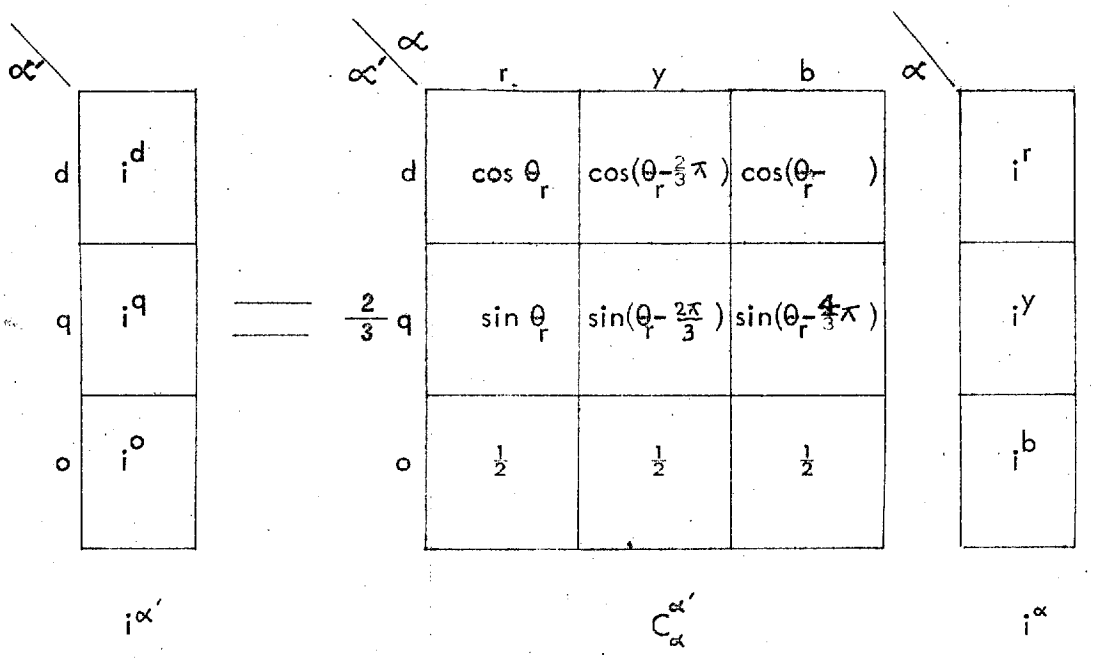

θ_r angle between r and d axes at any instant of time t.
$= w_r t$

Figure 7.4 Rotor dqo Quantities Expressed In Terms Of Rotor ryb Quantities. d Axis Stationary In Space And Coincident With Stator D Axis. Rotor r Axis Rotating With Respect To dqo Axes At A Speed w_r.

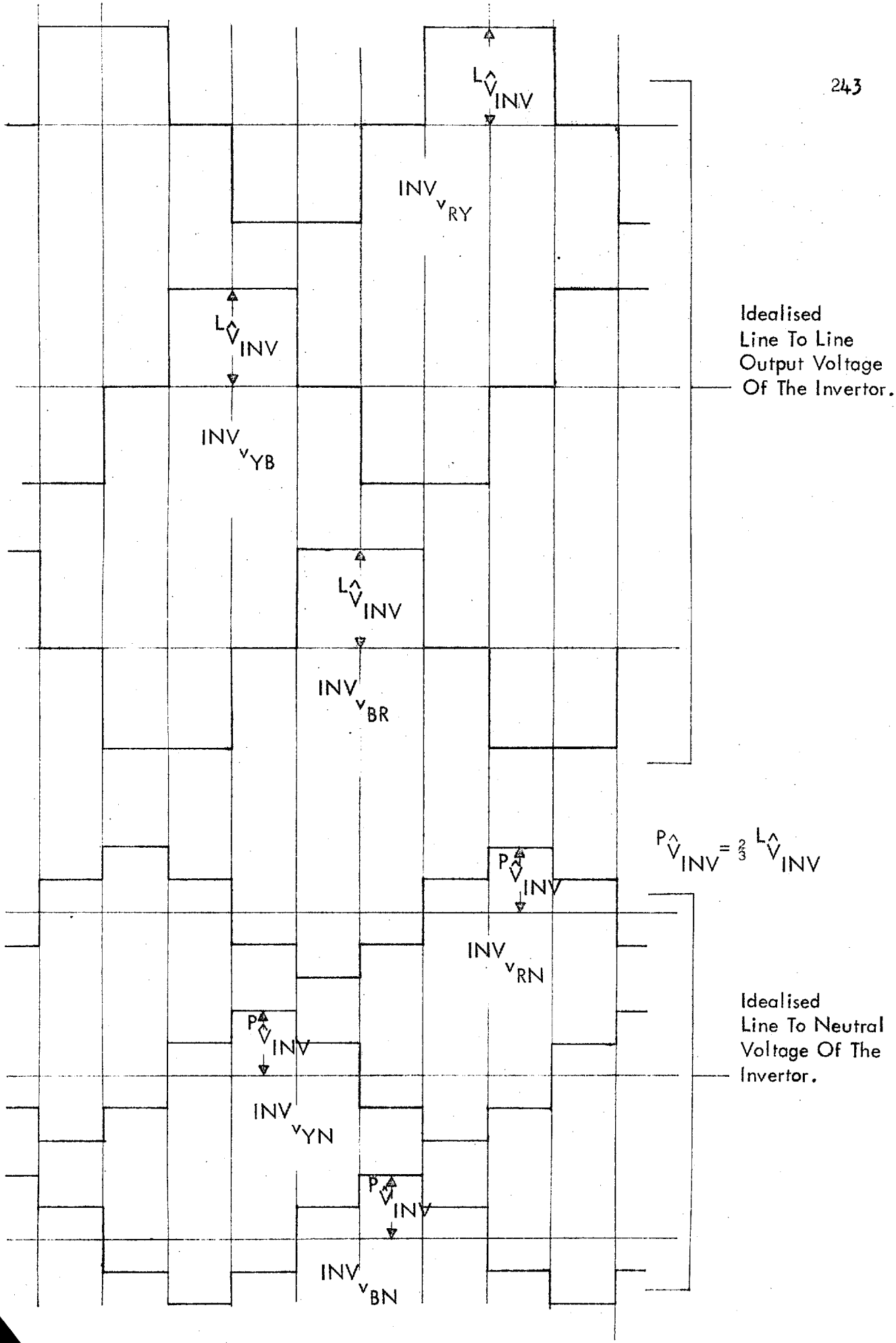

Figure 7.5 Idealised Instanteneous Line To Line And Line To Neutral Output Voltage Of The Invertor.

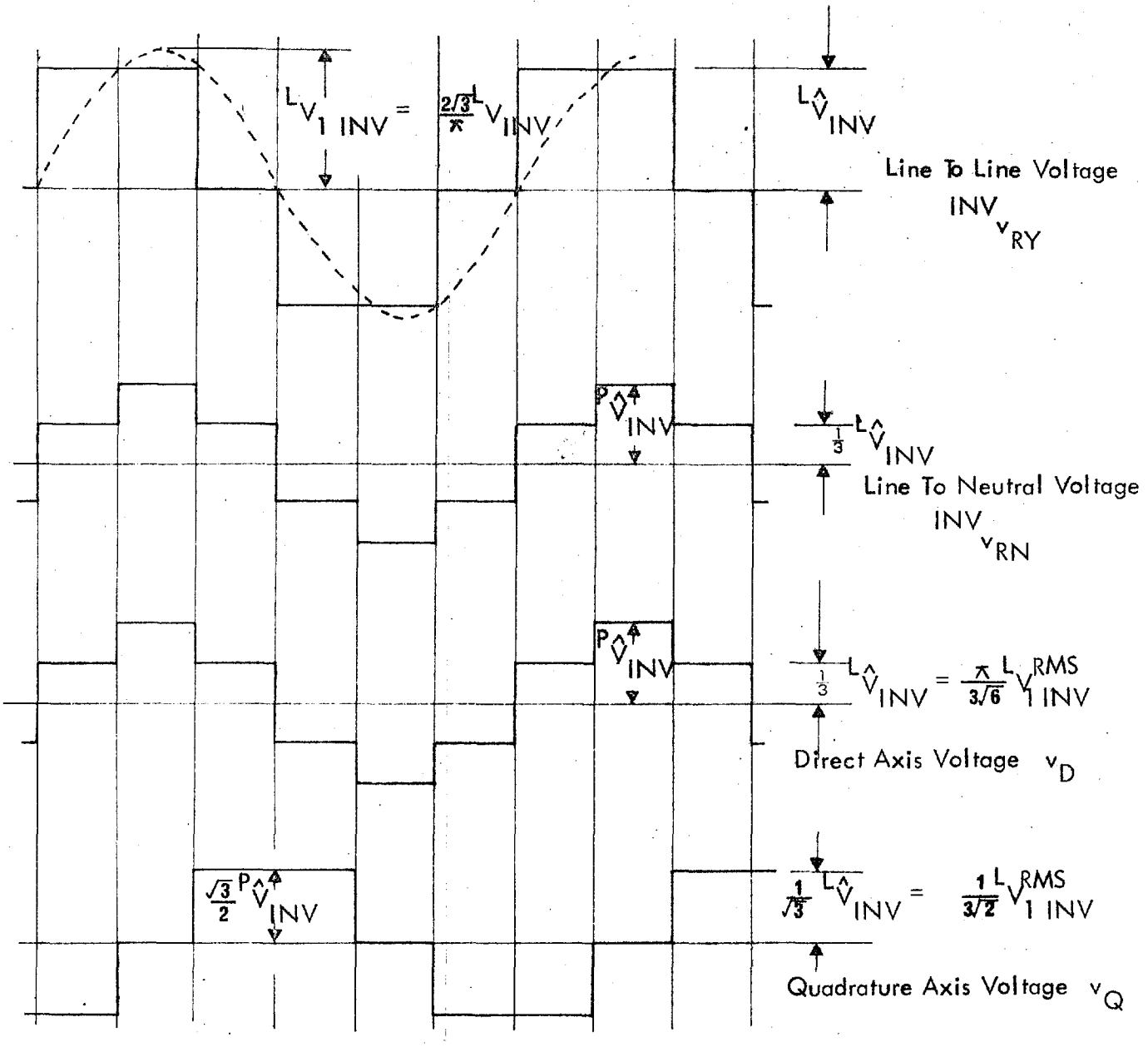

Figure 7.6 Idealised (Instanteneous) Stator Line To Neutral Voltages Transformed To Stator DQO Voltages.

Table 7.1 CONVERSION OF PHASE VOLTAGES INTO DIRECT AND QUADRATURE AXIS VOLTAGES

Time/Period in Degrees	$RN_{v_{INV}}$	$YN_{v_{INV}}$	$BN_{v_{INV}}$
0° - 60°	$\frac{1}{2}P\hat{V}_{INV}$	$-1P\hat{V}_{INV}$	$\frac{1}{2}P\hat{V}_{INV}$
60° - 120°	$1P\hat{V}_{INV}$	$-\frac{1}{2}P\hat{V}_{INV}$	$-\frac{1}{2}P\hat{V}_{INV}$
120° - 180°	$\frac{1}{2}P\hat{V}_{INV}$	$\frac{1}{2}P\hat{V}_{INV}$	$-1P\hat{V}_{INV}$
180° - 240°	$-\frac{1}{2}P\hat{V}_{INV}$	$1P\hat{V}_{INV}$	$-\frac{1}{2}P\hat{V}_{INV}$
240° - 300°	$-1P\hat{V}_{INV}$	$\frac{1}{2}P\hat{V}_{INV}$	$\frac{1}{2}P\hat{V}_{INV}$
300° - 360°	$-\frac{1}{2}P\hat{V}_{INV}$	$-\frac{1}{2}P\hat{V}_{INV}$	$1P\hat{V}_{INV}$

Table 7.1 CONVERSION OF PHAS. VOLTAGES INTO DIRECT AND QUADRATURE AXIS VOLTAGES

Time/Period in Degrees	In terms of peak phase voltage	
	V_D	V_Q
0^o - 60^o	$\frac{1}{2}P\hat{V}_{INV}$	$-\frac{(3)^{\frac{1}{2}}}{2}P\hat{V}_{INV}$
60^o - 120^o	$1P\hat{V}_{INV}$	0
120^o - 180^o	$\frac{1}{2}P\hat{V}_{INV}$	$+\frac{(3)^{\frac{1}{2}}}{2}P\hat{V}_{INV}$
180^o - 240^o	$-\frac{1}{2}P\hat{V}_{INV}$	$+\frac{(3)^{\frac{1}{2}}}{2}P\hat{V}_{INV}$
240^o - 300^o	$-1P\hat{V}_{INV}$	0
300^o - 360^o	$-\frac{1}{2}P\hat{V}_{INV}$	$-\frac{(3)^{\frac{1}{2}}}{2}P\hat{V}_{INV}$

Table 7.1 CONVERSION OF PHASE VOLTAGES INTO DIRECT AND QUADRATURE AXIS VOLTAGES

Time/Period in Degrees	In terms of crest line to line voltage		In terms of time fundamental r.m.s. line to line voltage	
	V_D	V_Q	V_D	V_Q
0° - 60°	$\frac{1}{3}L\hat{V}_{INV}$	$-\frac{1}{(3)^{\frac{1}{2}}}L\hat{V}_{INV}$	$\frac{\sqrt{2}}{3(6)^{\frac{1}{2}}}L_{V}RMS_{1\ INV}$	$-\frac{1}{3(2)^{\frac{1}{2}}}L_{V}RMS_{1\ INV}$
60° - 120°	$\frac{2}{3}L\hat{V}_{INV}$	0	$\frac{2\sqrt{2}}{3(6)^{\frac{1}{2}}}L_{V}RMS_{1\ INV}$	0
120° - 180°	$\frac{1}{3}L\hat{V}_{INV}$	$+\frac{1}{(3)^{\frac{1}{2}}}L\hat{V}_{INV}$	$\frac{\sqrt{2}}{3(6)^{\frac{1}{2}}}L_{V}RMS_{1\ INV}$	$+\frac{1}{3(2)^{\frac{1}{2}}}L_{V}RMS_{1\ INV}$
180° - 240°	$-\frac{1}{3}L\hat{V}_{INV}$	$+\frac{1}{(3)^{\frac{1}{2}}}L\hat{V}_{INV}$	$\frac{\sqrt{2}}{3(6)^{\frac{1}{2}}}L_{V}RMS_{1\ INV}$	$+\frac{1}{3(2)^{\frac{1}{2}}}L_{V}RMS_{1\ INV}$
240° - 300°	$-\frac{2}{3}L\hat{V}_{INV}$	0	$-\frac{2\sqrt{2}}{3(6)^{\frac{1}{2}}}L_{V}RMS_{1\ INV}$	0
300° - 360°	$-\frac{1}{3}L\hat{V}_{INV}$	$-\frac{1}{(3)^{\frac{1}{2}}}L\hat{V}_{INV}$	$-\frac{\sqrt{2}}{3(6)^{\frac{1}{2}}}L_{V}RMS_{1\ INV}$	$-\frac{1}{3(2)^{\frac{1}{2}}}L_{V}RMS_{1\ INV}$

The impedance tensor $Z_{\alpha'\beta'}$ along the stator DQO and rotor dqo axes can be obtained by inspection of figure 7.2 and is shown in figure 7.7. Since the rotor is short-circuited no external voltage can exist in the rotor dqo axes. The impressed voltage and the response current along α' reference frame is shown in figure 7.8.

7.2.3 Representation of machine along non-holonomic forward and backward revolving FBO and fbo axes - α'' frame

These are the Forstescue symmetrical components except that they are now applied directly in time domain in place of frequency domain. Transformation to this reference frame is introduced for three purposes viz:-

i) in order to reduce the number of terms of the impedance tensor $Z_{\alpha'\beta'}$;

ii) the relatively easier elimination of rotor axes (since no impressed voltages are present in the rotor), resulting in a matrix which is diagonal and hence evaluation of the admittance tensor $Y^{\beta''\alpha''}$ is greatly simplified;

iii) the resulting equations of response are similar, for the machine at standstill, to that of a short-circuited transformer. This makes possible the direct use of familiar equivalent circuit parameters.

The representation of the machine along these new

$Z_{\alpha'\beta'} =$

α' \ β'	D	d	q	Q	O	o
D	$R_s + pL_s$	pM				
d	pM	$R_r + pL_r$	$pL_r\theta_r$	$pM\theta_r$		
q	$-pM\theta_r$	$-pL_r\theta_r$	$R_r + pL_r$			
Q				$R_s + pL_s$		
O					$R_{Os} + pL_{Os}$	
o						$R_{or} + pL_{or}$

Figure 7.7 Induction Motor Impedance Tensors Along DQO And dqo Axes.

$v_{\alpha'} =$

α'	D	d	q	Q	O	o
	v_D			v_Q	v_O	

$i^{\alpha'} =$

α'	D	d	q	Q	O	o
	i^D	i^d	i^q	i^Q	i^O	i^o

Figure 7.8 Impressed DQO And dqo Voltages And Response Currents.

reference axes is shown in figure 7.9. The transformation tensors $C^{\alpha'}_{\cdot\alpha''}$ which relates α' quantities to α'' quantities is shown in figure 7.10. The FBO and fbo axes voltages can be derived from DQO and dqo axes voltages from the relation

$$v_{\alpha''} = C^{\cdot\alpha'}_{\alpha''} v_{\alpha'} \tag{7.1}$$

where the matrix representing $C^{\cdot\alpha'}_{\alpha''}$ is the conjugate of the transpose of the matrix representing $C^{\alpha'}_{\cdot\alpha''}$ and is shown in figure 7.11.

The impedance tensor $Z_{\alpha'\beta'}$ along the previous reference frame α' can be transformed to fit into the new reference frame α'' by

$$Z_{\alpha''\beta''} = Z_{\alpha'\beta'} C^{\cdot\alpha'}_{\alpha''} C^{\beta'}_{\cdot\beta''} \tag{7.2}$$

$Z_{\alpha''\beta''}$ is evaluated in steps shown in figures 7.12 and 7.13.

The performance equation for this reference frame is

$$v_{\alpha''} = Z_{\alpha''\beta''} i^{\beta''} \tag{7.3}$$

7.3 Elimination of Rotor Axes

Since there is no impressed voltage along the rotor axes, it is convenient to eliminate these axes. Let the

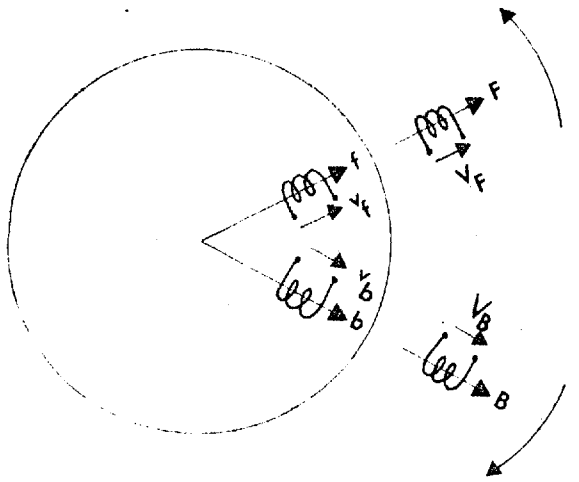

Figure 7.9 Hypothetical Forward And Backward Rotating α'' Reference Frame.

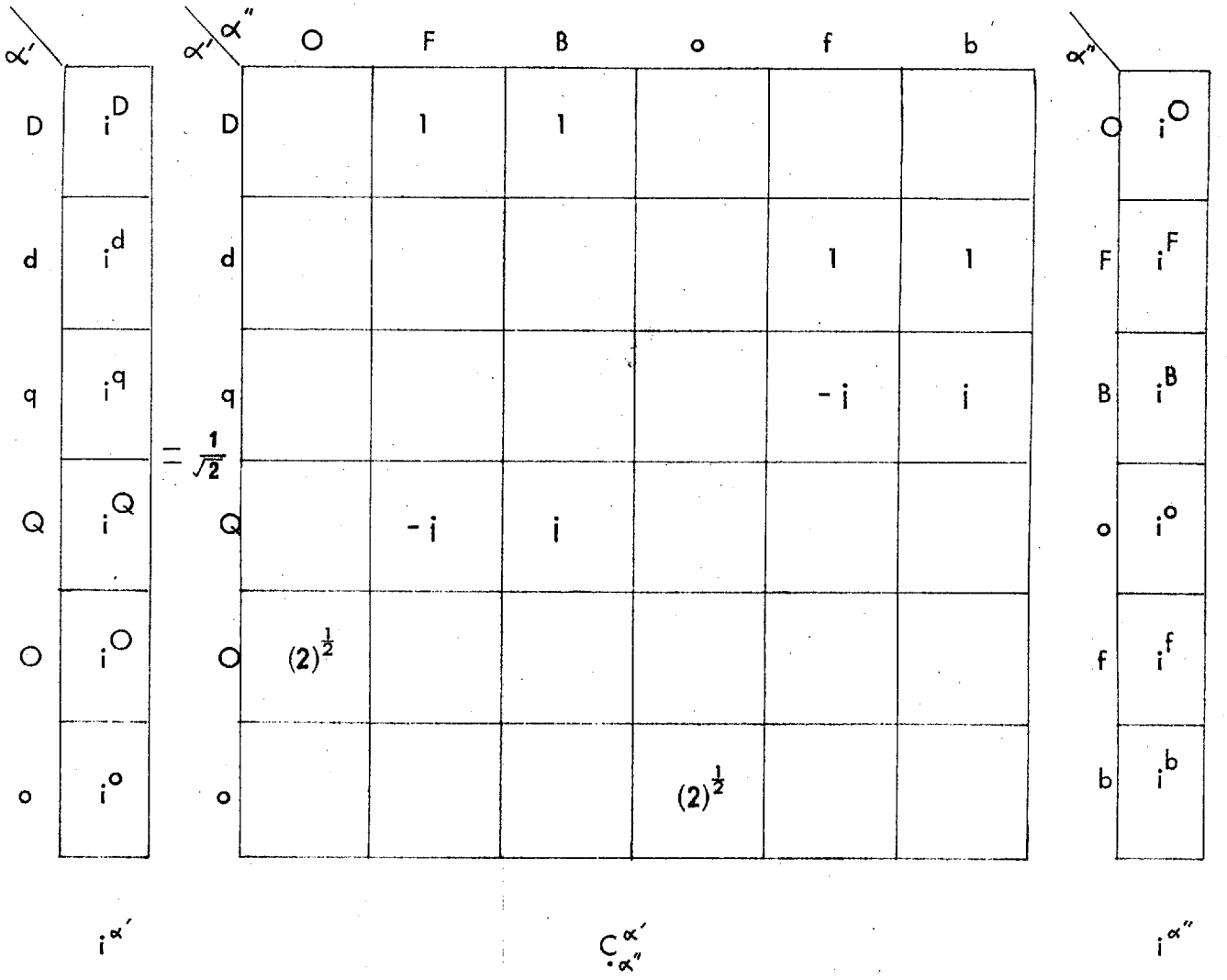

Figure 7.10 Currents Of α' Reference Frame Expressed In Terms Of Currents Of α'' Reference Frame.

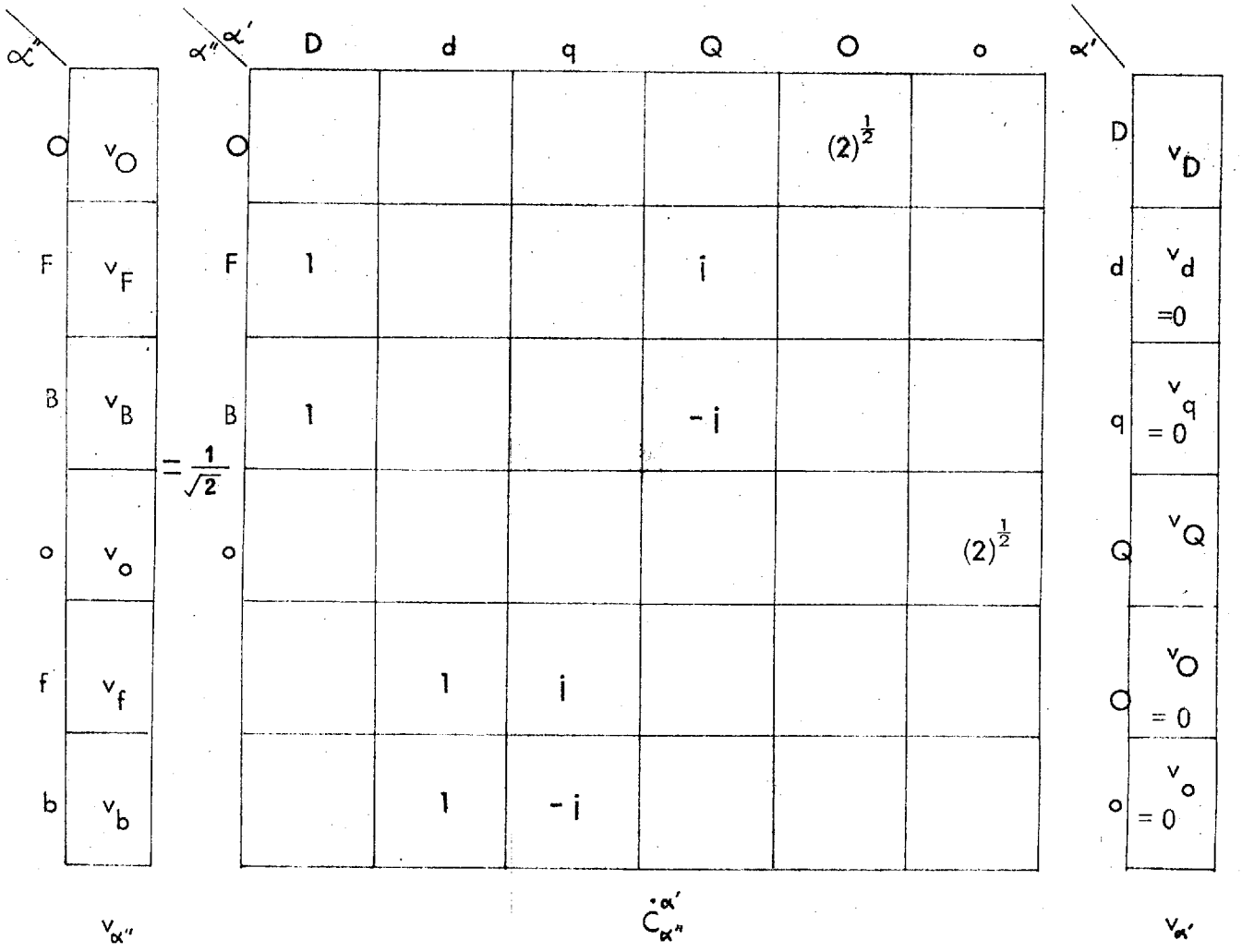

v_o, v_d and v_q are 0 because the rotor is short-circuited.

v_O is 0 because the phase voltages are such that no zero sequence voltage can exist.

Figure 7.11 Voltages Of α'' Reference Frame Expressed In Terms Of Voltages Of α' Reference Frame.

$\frac{1}{(2)^{\frac{1}{2}}}$ X

$\alpha'' \backslash \beta'$	D	d	q	Q	O	o
O					$2\,(R_{Os} + pL_{Os})$	
F	$R_s + pL_s$	pM	jpM	$j(R_s + pL_s)$		
B	$R_s + pL_s$	pM	$-jpM$	$-j(R_s + pL_s)$		
o					$2\,(R_{or} + pL_{or})$	
f	$pM - jpM\theta_r$	$-jL_r p\theta_r + (R_r + pL_r)$	$L_r p\theta_r + j(R_r + pL_r)$	$Mp\theta_r + jpM$		
b	$pM + jMp\theta_r$	$jL_r p\theta_r + (R_r + pL_r)$	$L_r p\theta_r - j(R_r + pL_r)$	$Mp\theta_r - jpM$		

$$C^{\alpha'}_{\alpha''}\, Z_{\alpha'\beta'} = Z_{\alpha''\beta'}$$

Figure 7.12 Steps In Converting $Z_{\alpha'\beta'}$ To $Z_{\alpha''\beta'}$ (Step 1)

α'' \ β''	O	F	B	o	f	b
O	$R_{Os} + pL_{Os}$					
F		$R_s + pL_s$			pM	
B			$R_s + pL_s$			pM
o				$R_{or} + pL_{or}$		
f		$pM - jMp\theta_r$			$R_r + jpL_r$ $- jL_r p\theta_r$	
b			$pM + jMp\theta_r$			$R_r + pL_r$ $+ jL_r p\theta_r$

$$Z_{\alpha''\beta''} = C^{\cdot\alpha'}_{\alpha''} Z_{\alpha'\beta'} C^{\beta'}_{\cdot\beta''} = Z_{\alpha''\beta'} C^{\beta'}_{\cdot\beta''} \qquad \text{(Step 2)}$$

Figure 7.13 Induction Motor Impedance Tensors Along α'' Reference Frame.

voltage, current and impedance of the motor along α'' reference axes be each split into two sets, one set representing the stator axes and the other set representing the rotor axes. Hence voltages, currents and impedances can be written as

$$v_{\alpha''} = v_{\alpha''_s} + v_{\alpha''_r} \tag{7.4}$$

$$i^{\alpha''} = i^{\alpha''_s} + i^{\alpha''_r} \tag{7.5}$$

$$Z_{\alpha''\beta''} = Z_{\alpha''_s \beta''_s} + Z_{\alpha''_r \beta''_r} \tag{7.6}$$

where the subscripts α''_s denote the stator reference axes (FBO) and α''_r the same for rotor (fbo).

Hence,

$$v_{\alpha''_s} = Z_{\alpha''_s \beta''_s} i^{\alpha''_s} + Z_{\alpha''_s \beta''_r} i^{\alpha''_r} \tag{7.7}$$

$$v_{\alpha''_r} = Z_{\alpha''_r \beta''_s} i^{\alpha''_s} + Z_{\alpha''_r \beta''_r} i^{\alpha''_r} \tag{7.8}$$

Equation 7.8 can be rewritten as

$$Z_{\alpha''_r \beta''_r} i^{\alpha''_r} = v_{\alpha''_r} - Z_{\alpha''_r \beta''_s} i^{\alpha''_s} \tag{7.9}$$

$$\therefore \quad i^{\alpha''_r} = Y^{\beta''_r \alpha''_r} (v_{\alpha''_r} - Z_{\alpha''_r \beta''_s} i^{\alpha''_s}) \tag{7.10}$$

Substituting equation 7.10 in equation 7.7 gives

$$v_{\alpha''_s} = Z_{\alpha''_s \beta''_s} i^{\alpha''_s} + Z_{\alpha''_s \beta''_r} Y^{\beta''_r \alpha''_r} (v_{\alpha''_r} - Z_{\alpha''_r \beta''_s} i^{\alpha''_s})$$

$$= Z_{\alpha''_s \beta''_s} i^{\alpha''_s} + Z_{\alpha''_s \beta''_r} Y^{\beta''_r \alpha''_r} v_{\alpha''_r}$$

$$- Z_{\alpha''_s \beta''_r} Y^{\beta''_r \alpha''_r} Z_{\alpha''_r \beta''_s} i^{\alpha''_s}$$

$$\therefore \quad v_{\alpha''_s} - Z_{\alpha''_s \beta''_r} Y^{\beta''_r \alpha''_r} v_{\alpha''_r} = Z_{\alpha''_s \beta''_r} Y^{\beta''_r \alpha''_r} v_{\alpha''_r}$$

$$+ (Z_{\alpha''_s \beta''_s}$$

$$- Z_{\alpha''_s \beta''_r} Y^{\beta''_r \alpha''_r} Z_{\alpha''_r \beta''_s})$$

$$\times i^{\alpha''_s} \qquad (7.11)$$

Since $v_{\alpha''_r} = 0$, equation 7.11 reduces to

$$v_{1\alpha''_s} = v_{\alpha''_s}$$

$$= (Z_{\alpha''_s \beta''_s} - Z_{\alpha''_s \beta''_r} Y^{\beta''_r \alpha''_r} Z_{\alpha''_r \beta''_s}) i^{\alpha''_s}$$

$$= Z_{1\alpha''_s \beta''_s} i^{\alpha''_s} \qquad (7.12)$$

where

$$Z_{1\alpha''_s \beta''_s} = Z_{\alpha''_s \beta''_s} - Z_{\alpha''_s \beta''_r} Y^{\beta''_r \alpha''_r} Z_{\alpha''_r \beta''_s} \qquad (7.13)$$

and

$$v_{1\alpha''_s} = v_{\alpha''_s} - Z_{\alpha''_s \beta''_r} Y^{\beta''_r \alpha''_r} v_{\alpha''_r} \qquad (7.14)$$

7.4 Evaluation of Stator and Rotor Currents along Frame

Equation 7.13 is evaluated by first determining $Y^{\beta''_r \alpha''_r}$ and then post-multiplying it with $Z_{\alpha''_r \beta''_s}$ shown in figure 7.14. The result is then pre-multiplied by $Z_{\alpha''_s \beta''_r}$ as shown in figure 7.15. Finally, this triple product is subtracted from $Z_{\alpha''_s \beta''_s}$ to yield $Z_{1\alpha''_s \beta''_s}$ as given in figure 7.16. It may be noted that the matrix representing $Z_{\alpha''_r \beta''_r}$ is diagonal and hence $Y^{\beta''_r \alpha''_r}$ is simply evaluated by allowing its elements to be the reciprocal of those in the matrix representing $Z_{\alpha''_r \beta''_r}$. Having evaluated $Z_{1\alpha''_s \beta''_s}$, $i^{\alpha''_s}$ can be evaluated from

$$i^{\alpha''_s} = Y^{1\beta''_s \alpha''_s} v_{\alpha''_s} \tag{7.15}$$

as shown in figure 7.17. Since the matrix representing the impedance tensor $Z_{1\alpha''_s \beta''_s}$ is diagonal, the admittance tensor $Y^{1\beta''_s \alpha''_s}$ is simple to evaluate. Since $v_{\alpha''_r} = 0$, the rotor current $i^{\alpha''_r}$ from equation 7.8 is

$$i^{\alpha''_r} = -Y^{\beta''_r \alpha''_r} Z_{\alpha''_r \beta''_s} i^{\alpha''_s} \tag{7.16}$$

Substituting $i^{\alpha''_s}$ from equation 7.15 to equation 7.16 the rotor currents are obtained

$$i^{\alpha''_r} = -Y^{\beta''_r \alpha''_r} Z_{\alpha''_r \beta''_s} Y^{1\alpha''_s \beta''_s} v_{\alpha''_s} \tag{7.17}$$

$Y^{\beta''_r \alpha''_r} Z_{\alpha''_r \beta''_s}$ =

$\beta''_r \backslash \alpha''_r$	o	f	b
o	$\frac{1}{R_{or} + pL_{or}}$		
f		$\frac{1}{R_r + L_r(p - j p\theta_r)}$	
b			$\frac{1}{R_r + L_r(p + j p\theta_r)}$

$\alpha''_r \backslash \beta''_s$	O	F	B
o			
f		$M(p - j p\theta_r)$	
b		$M(p + j p\theta_r)$	

=

$\beta''_r \backslash \beta''_s$	O	F	B
o			
f		$\frac{M(p - j p\theta_r)}{R_r + L_r(p - j p\theta_r)}$	
b			$\frac{M(p + j p\theta_r)}{R_r + L_r(p + j p\theta_r)}$

Figure 7.14 Steps In Eliminating Rotor Axes. (Step 1)

$$Z_{\alpha_s''\beta_r''}\, Y^{\beta_r''\alpha_r''}\, Z_{\alpha_r''\beta_s''} =$$

$\alpha_s'' \backslash \beta_r''$	o	f	b
O			
F		pM	
B			pM

$\beta_r'' \backslash \beta_s''$	O	F	B
o			
f		$\dfrac{M(p-j p\theta_r)}{R_r + L_r(p-j p\theta_r)}$	
b			$\dfrac{M(p+j p\theta_r)}{R_r + L_r(p+j p\theta_r)}$

$\alpha_s'' \backslash \beta_s''$	O	F	B
O			
F		$\dfrac{pM^2(p - j p\theta_r)}{R_r + L_r(p-j p\theta_r)}$	
B			$\dfrac{pM^2(p + j p\theta_r)}{R_r + L_r(p + j p\theta_r)}$

Figure 7.15 Steps In Eliminating Rotor Axes. (Step 2)

$$Z_{1\alpha_s''\beta_s''} = Z_{\alpha_s''\beta_s''} - Z_{\alpha_s''\beta_r''} Y^{\beta_r''\alpha_r''} Z_{\alpha_r''\beta_s''}$$

α_s'' \ β_s''	O	F	B
O	$R_{Os} + pL_{Os}$		
F		$R_s + pL_s$	
B			$R_s + pL_s$

$-$

α_s'' \ β_s''	O	F	B
O			
F		$\frac{pM^2(p - jp\theta_r)}{R_r + L_r(p - jp\theta_r)}$	
B			$\frac{pM^2(p + jp\theta_r)}{R_r + L_r(p + jp\theta_r)}$

$=$

α_s'' \ β_s''	O	F	B
O	$R_{Os} + pL_{Os}$		
F		$(R_s + pL_s) - \frac{pM^2(p - jp\theta_r)}{R_r + L_r(p - jp\theta_r)}$	
B			$(R_s + pL_s) - \frac{pM^2(p + jp\theta_r)}{R_r + L_r(p + jp\theta_r)}$

Figure 7.16 Induction Motor Impedance Along α_s'' Reference Frame. Short-Circuited Rotor Reference Frame α_r'' Eliminated. (Step 3)

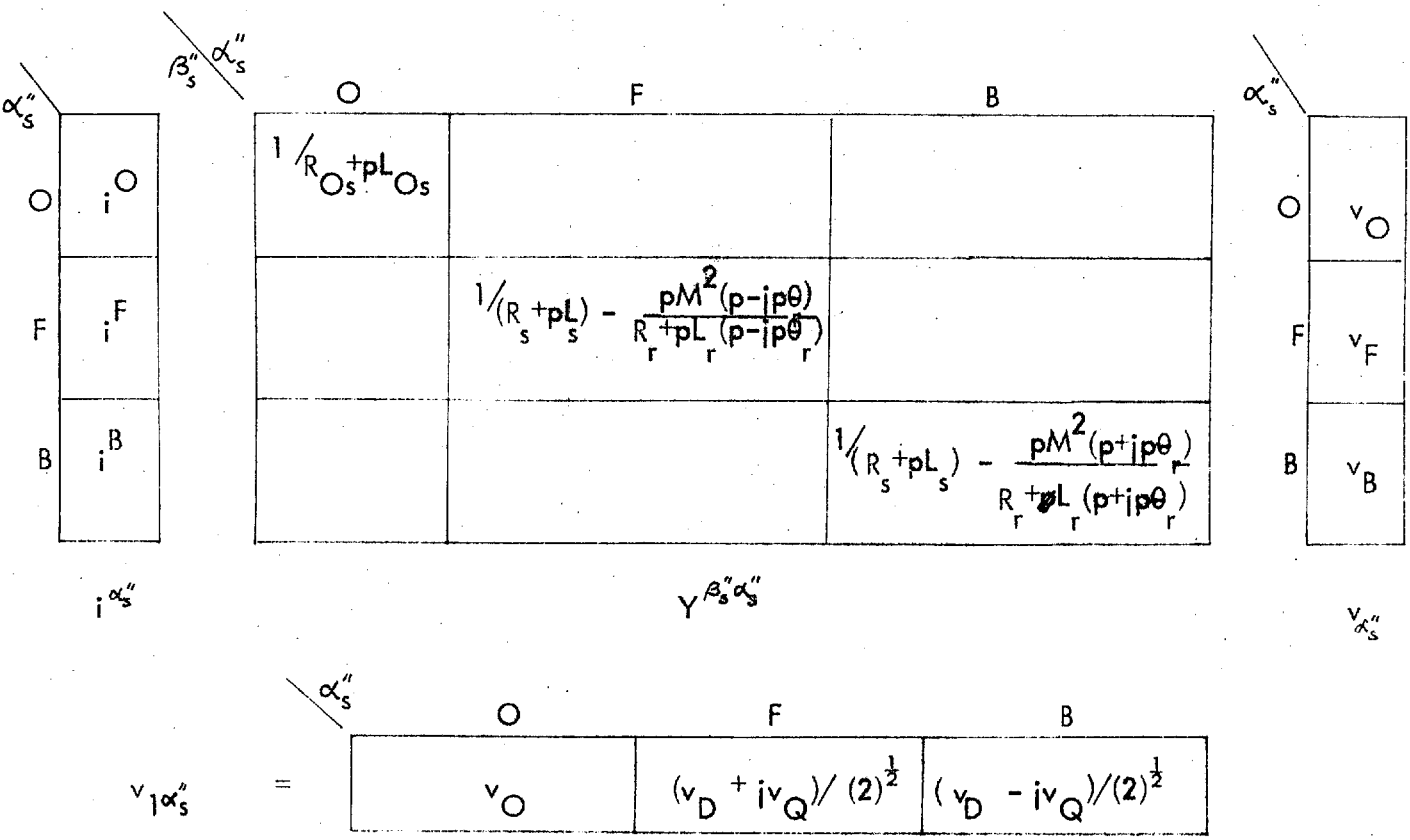

Figure 7.17 Induction Motor Stator Currents Along α_s'' Reference Frame. Short-Circuited Rotor Reference Frame Eliminated.

The quantity $Y^{\beta''_r \alpha''_r} Z_{\alpha''_r \beta''_s}$ has already evaluated and is shown in figure 7.14. The evaluation of $Y^{\beta''_r \alpha''_r} Z_{\alpha''_r \beta''_s} Y^{1\alpha''_s \beta''_s}$ and the equations for the rotor currents are shown in figures 7.18 and 7.19 respectively.

7.5 The Differential Equations for Currents

Equations 7.15 and 7.17 give the forward and backward rotating currents of the stator and the rotor. These currents are also given in matrix form in figures 7.17 and 7.19. Since there is no zero-sequence forcing function v_0 and v_o, no zero-sequence currents can exist in the stator and rotor. Rewriting the equations, the forward rotating stator current i^F is given by

$$i^F = v_F / \left[(R_s + pL_s) - pM^2 (p - jp\theta_r) / \left\{ R_r + L_r (p - jp\theta_r) \right\} \right]$$

$$= \left\{ (v_D + jv_Q)/(2)^{\frac{1}{2}} \right\} / \left[(R_s + pL_s) - pM^2 (p - jp\theta_r) / \left\{ R_r + L_r (p - jp\theta_r) \right\} \right] \qquad (7.18)$$

where

$$p = d/dt$$

$$y^{\beta_r''\alpha_r''} Z_{\alpha_r''\beta_s''} y^{1\alpha_s''\beta_s''}$$

β_r'' \ β_s''	O	F	B
o			
f		$\frac{M(p - j p\theta_r)}{R_r + L_r(p - j p\theta_r)}$	
b			$\frac{M(p+j p\theta_r)}{R_r + L_r(p+j p\theta_r)}$

β_s'' \ α_s''	O	F	B
O	$\frac{1}{R_{Os}+pL_{Os}}$		
F		$\frac{1}{(R_s+pL_s)-\frac{pM^2(p-j p\theta_r)}{R_r+pL_r(p-j p\theta_r)}}$	
B			$\frac{1}{(R_s+pL_s)-\frac{pM^2(p+j p\theta_r)}{R_r+pL_r(p+j p\theta_r)}}$

=

β_r'' \ α_s''	O	F	B
o			
f		$\frac{\frac{M(p - j p\theta_r)}{R_r + L_r(p - j p\theta_r)}}{(R_s + pL_s) - \frac{pM^2(p - j p\theta_r)}{R_r + pL_r(p - j p\theta_r)}}$	
b			$\frac{\frac{M(p + j p\theta_r)}{R_r + L_r(p + j p\theta_r)}}{(R_s + pL_s) - \frac{pM^2(p + j p\theta_r)}{R_r + pL_r(p + j p\theta_r)}}$

Figure 7.18 Short-Circuited Rotor Impedance Which Relates The Rotor Currents To The Stator Impressed Voltages Along α'' Reference Frame.

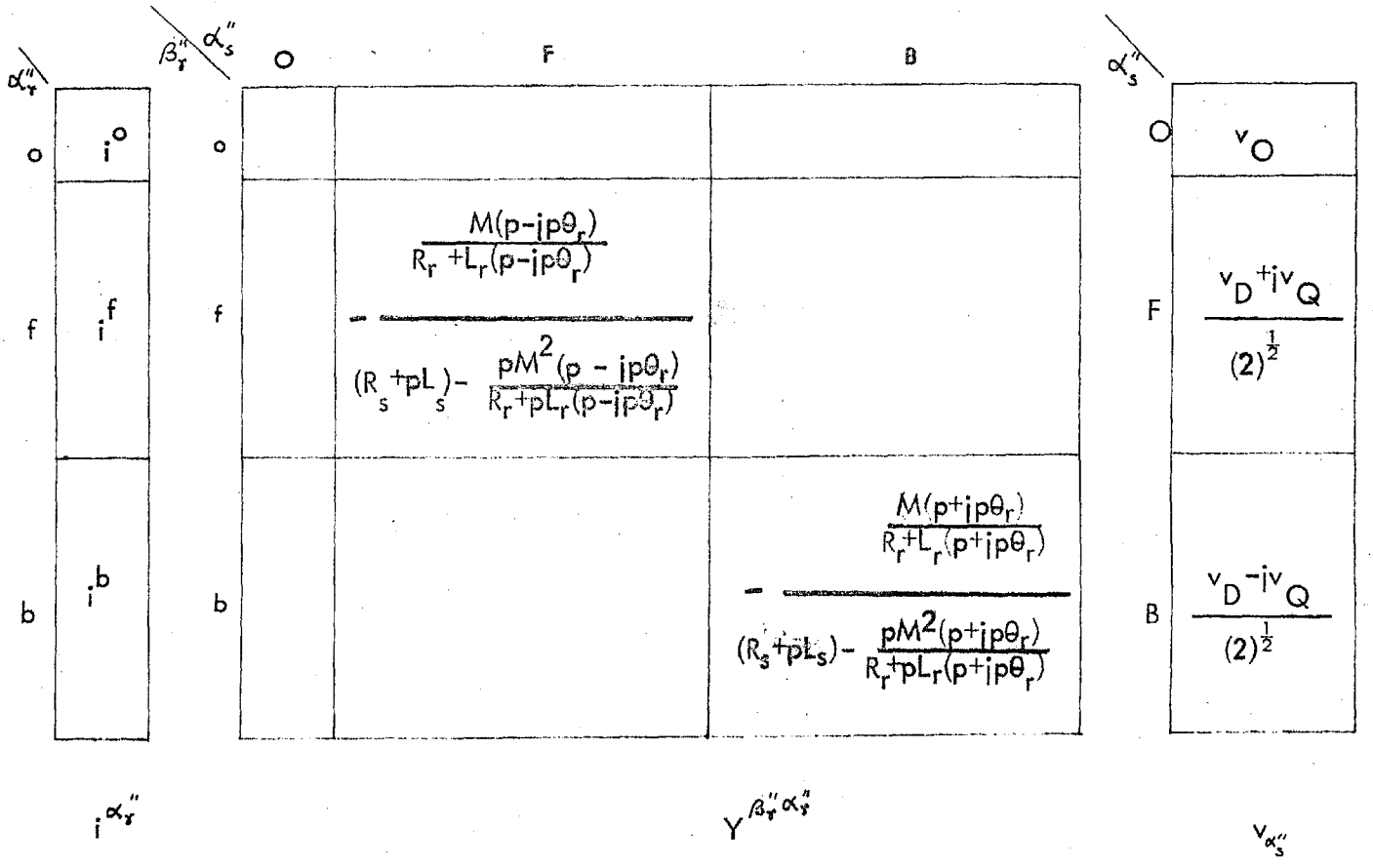

Figure 7.19 Rotor Current Along α'' Reference Frame.

The backward rotating stator current i^B is given by

$$i^B = v_B/\left[(R_s + pL_s) - pM^2(p + jp\theta_r)/\left\{R_r + L_r(p + jp\theta_r)\right\}\right]$$

$$= \left\{(v_D - jv_Q)/(2)^{\frac{1}{2}}\right\}/\left[(R_s + pL_s) - pM^2(p + jp\theta_r)/\left\{R_r + L_r(p + jp\theta_r)\right\}\right] \quad (7.19)$$

The forward rotating rotor current i^f is given by

$$i^f = -\left\{M(p - jp\theta_r)v_F\right\}/\left[(R_s + pL_s)\left\{R_r + L_r(p - jp\theta_r)\right\} - pM^2(p - jp\theta_r)\right]$$

$$= \left\{M(p - jp\theta_r)(v_D + jv_Q)/(2)^{\frac{1}{2}}\right\}/\left[pM^2(p - jp\theta_r) - (R_s + pL_s)\left\{R_r + L_r(p - jp\theta_r)\right\}\right] \quad (7.20)$$

The backward rotating rotor current i^b is given by

$$i^b = -\left\{M(p + jp\theta_r)v_B\right\}/\left[(R_s + pL_s)\left\{R_r + L_r(p + jp\theta_r)\right\} - pM^2(p + jp\theta_r)\right]$$

$$= \left\{M(p + jp\theta_r)(v_D - jv_Q)/(2)^{\frac{1}{2}}\right\}/\left[pM^2(p + jp\theta_r) - (R_s + pL_s)\left\{R_r + L_r(p + jp\theta_r)\right\}\right] \quad (7.21)$$

It may be noted that the above equations with rotor at standstill ($p\theta_r = 0$) are similar to that of a transformer with the secondary short-circuited, hence the parameters of the conventional equivalent circuit of figure 4.1 are directly applicable.

The direct axis stator and rotor currents can be easily evaluated by the connection tensors $C^{\alpha'}_{\alpha''}$ (Figure 7.10) which when attached to the quantities of α'' reference frame, transform them to quantities of α' reference frame.

The direct axis stator current i^D is therefore

$$i^D = (i^F + i^B)/(2)^{\frac{1}{2}} \tag{7.22}$$

Since the D axis of α' reference frame is made coincident on the physically existing R axis of α reference frame, then

$$i^D = i^R \tag{7.23}$$

Similarly the direct axis rotor current is given by

$$i^d = (i^f + i^b)/(2)^{\frac{1}{2}} \tag{7.24}$$

In this case the rotor r phase current is not the same as the rotor d axis current. This is because the r axis of the α reference frame is sweeping past the stationary d axis of α' reference frame with the speed

of that of the rotor. To determine the actual current of the rotor, another transformation, which involves rotor speed, has to be introduced in order to project i^d and i^q along the rotating r axis to derive i^r. Since the actual rotor current is not of importance in this investigation, no attempt is made to determine it. The rotor copper loss will, however, be calculated on the basis of the hypothetical d axis current.

7.6 Evaluation of Electromagnetic Torque

Torque is produced by the interaction of the currents $i^{\alpha''}$ and the air-gap flux density $B_{\alpha''}$. The flux density $B_{\alpha''}$ is given by the product of the torque tensors $G_{\alpha''\beta''}$ and the current $i^{\alpha''}$. The torque tensors $G_{\alpha''\beta''}$ contains only those terms of the impedance tensors $Z_{\alpha''\beta''}$ which involve rotor velocity $p\theta_r$ and hence can be establsihed by inspection of $Z_{\alpha''\beta''}$ (Figure 7.13).

Therefore

$$B_{\alpha''} = G_{\alpha''\beta''}\, i^{\beta''} \tag{7.25}$$

and

$$T = jw_r(i^{\alpha''})^{conj.} B_{\alpha''} \tag{7.26}$$

Equations 7.25 and 7.26 are shown in matrix form in figure 7.20. The above value of torque has to be multiplied by

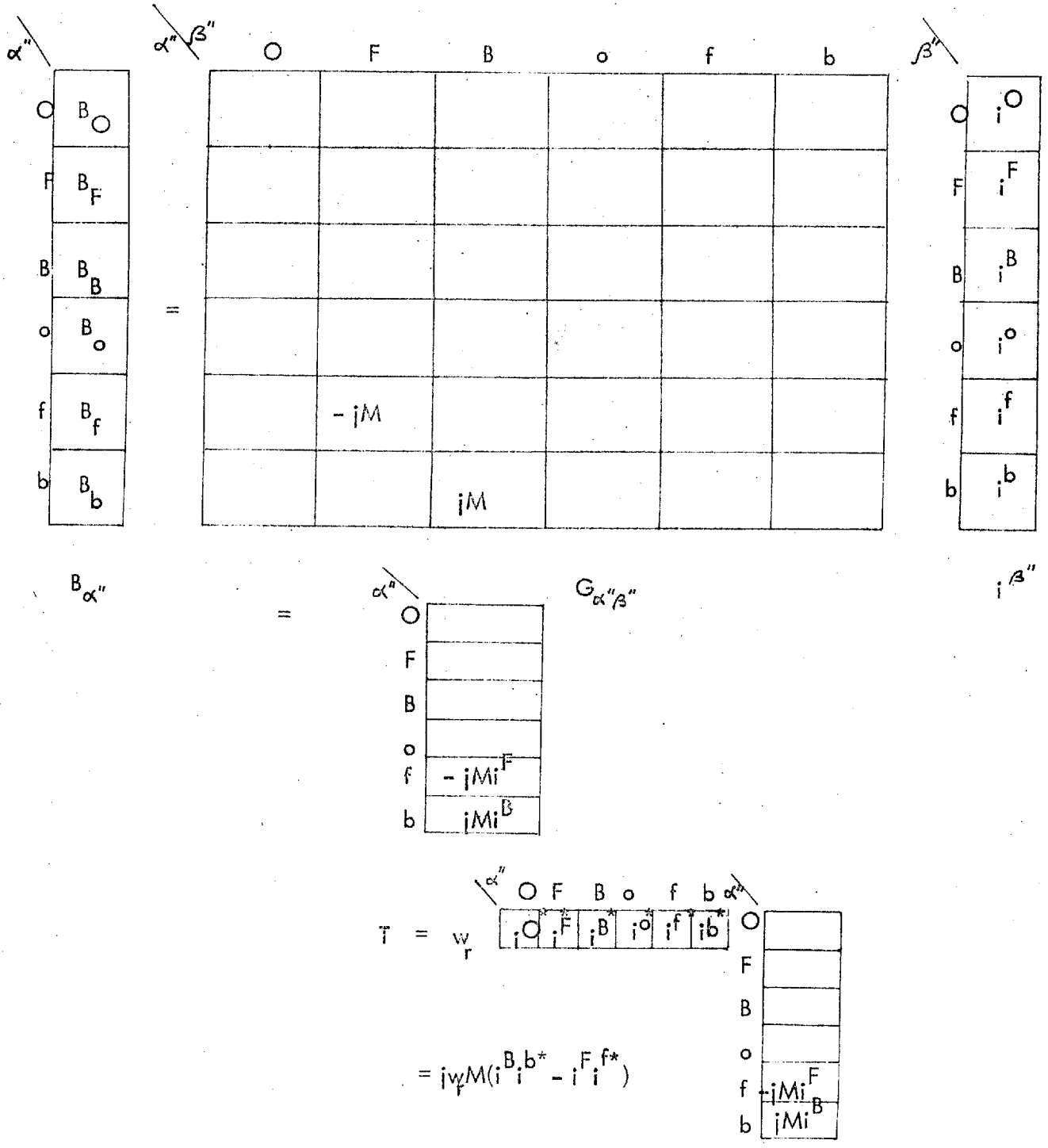

Figure 7.20 Evaluation Of Torque Per Phase In Terms Of The Currents Along α'' Reference Frame.

3 to obtain the total three-phase torque. Therefore

$$T = j3w_r M(i^B i^{b*} - i^F i^{f*}) \qquad (7.27)$$

where i^{b*} and i^{f*} are the conjugates of i^b and i^f

and w_r is the rotor speed.

7.7 Generalization of the Differential Equations giving Stator and Rotor Sequence Currents

The equations 7.18 to 7.21 are cumbersome, and are best written in a modified general form so that a general solution can be formulated. No approximations are made and two time constants are introduced

$$\text{For stator } \tau_s = L_s/R_s \qquad (7.28)$$

$$\text{For rotor } \tau_r = L_r/R_r \qquad (7.29)$$

Another constant, called the leakage factor, is also introduced as

$$\sigma = 1 - M^2/(L_s L_r) \qquad (7.30)$$

Considering rotor speed constant, the term $p\theta_r (= w_r)$ is constant (Equation 7.18).

The forward rotating stator current is therefore

$$i^F = \frac{(v_D + jv_Q)/(2)^{\frac{1}{2}}}{L_s(\frac{R_s}{L_s} + p) - \frac{pM^2(p - jw_r)}{R_r + L_r(p - jw_r)}}$$

$$= \frac{1}{(2)^{\frac{1}{2}}} \frac{(v_D+jv_Q)\{R_r+pL_r-jL_rw_r\}}{L_s(\frac{1}{\tau_s} + p)\{R_r+pL_r-jw_rL_r\} - (p^2M^2-jpM^2w_r)}$$

$$= \frac{1}{(2)^{\frac{1}{2}}L_s} \frac{(v_D+jv_Q)\{\frac{1}{\tau_r} + p - jw_r\}}{(\frac{1}{\tau_s}+ p)\{\frac{1}{\tau_r} + p - jw_r\} - \{\frac{p^2M^2}{L_sL_r} - j\frac{pM^2}{L_sL_r}w_r\}}$$

$$= \frac{1}{(2)^{\frac{1}{2}}L_s} \frac{(v_D+jv_Q)\{\frac{1}{\tau_r} + p - jw_r\}}{\frac{1}{\tau_s}(\frac{1}{\tau_r} + p - jw_r) + p(\frac{1}{\tau_r} - jw_r) + p^2(1 - \frac{M^2}{L_sL_r}) - jp\frac{M^2w_r}{L_sL_r}}$$

$$= \frac{1}{(2)^{\frac{1}{2}}L_s} \frac{(v_D + jv_Q)\{\frac{1}{\tau_r} + p - jw_r\}}{p^2\sigma + p(\frac{1}{\tau_s} + \frac{1}{\tau_r} - jw_r) + \frac{1}{\tau_s}(\frac{1}{\tau_r} - jw_r) + jp\frac{M^2w_r}{L_sL_r}}$$

$$= \frac{1}{(2)^{\frac{1}{2}}L_s} \frac{(v_D + jv_Q)\{\frac{1}{\tau_r} + p - jw_r\}}{p^2\sigma + p\{\frac{1}{\tau_s} + \frac{1}{\tau_r} - jw_r(1 - \frac{M^2}{L_sL_r})\} - \frac{1}{\tau_s}(\frac{1}{\tau_r} - jw_r)}$$

$$= \frac{1}{(2)^{\frac{1}{2}}L_s\sigma} \frac{(v_D + jv_Q)\{\frac{1}{\tau_r} + p - jw_r\}}{p^2 + p\{\frac{1}{\sigma\tau_s} + \frac{1}{\sigma\tau_r} - jw_r\} + \frac{1}{\sigma\tau_s}(\frac{1}{\tau_r} - jw_r)} \qquad (7.31)$$

Inspection of the original differential (Equations 7.18 and 7.19) for the stator sequence currents, shows that they are conjugates of each other. Therefore, the backward rotating stator current can be written down by inspection of equation 7.31 as

$$i^B = \frac{1}{(2)^{\frac{1}{2}} L_s \sigma} \frac{(v_D - jv_Q)\left\{\frac{1}{\tau_r} + p + jw_r\right\}}{p^2 + p\left\{\frac{1}{\sigma\tau_s} + \frac{1}{\sigma\tau_r} + jw_r\right\} + \frac{1}{\sigma\tau_s}\left(\frac{1}{\tau_r} + jw_r\right)} \tag{7.32}$$

These two equations (7.31 and 7.32) are given similar mathematical forms after defining certain constants as follows

$$B_F = \left\{1/(\sigma\tau_s) + 1/(\sigma\tau_r) - jw_r\right\} \tag{7.33}$$

$$B_B = \left\{1/(\sigma\tau_s) + 1/(\sigma\tau_r) + jw_r\right\}$$

$$= B_F^* \tag{7.34}$$

$$C_F = (1/\tau_r - jw_r)/(\sigma\tau_s) \tag{7.35}$$

$$C_B = (1/\tau_r + jw_r)/(\sigma\tau_s)$$

$$= C_F^* \tag{7.36}$$

$$D_F = (1/\tau_r - jw_r) \tag{7.37}$$

$$D_B = (1/\tau_r + jw_r)$$

$$= D_F^* \qquad (7.38)$$

$$K_S = 1/\{(2)^{\frac{1}{2}} L_s \sigma\} \qquad (7.39)$$

Substituting equation 7.33 to 7.39 in the equations 7.31 and 7.32 the stator sequence currents are obtained in identical mathematical form as

$$i^F = (v_D + jv_Q)K_s \frac{p + D_F}{p^2 + pB_F + C_F} \qquad (7.40)$$

$$i^B = (v_D - jv_Q)K_s \frac{p + D_B}{p^2 + pB_B + C_B} \qquad (7.41)$$

The forward rotating rotor current from equation 7.20 is

$$i^f = \{M(p - jw_r)(v_D + jv_Q)/(2)^{\frac{1}{2}}\} / [pM^2(p - jw_r) - (R_s + pL_s)\{R_r + L_r(p - jw_r)\}]$$

Dividing the numerator and denominator by $R_r + L_r(p - jw_r)$ the following expression is obtained

$$i^f = -M(p - jw_r)/\{R_r + L_r(p - jw_r)\} \cdot \frac{(v_D + jv_Q)/(2)^{\frac{1}{2}}}{(R_s + pL_s) - \frac{pM^2(p - jw_r)}{R_r + L_r(p - jw_r)}}$$

The term in [ ] is, by equation 7.18, equal to i^F.

Replacing this term by equation 7.40 gives

$$i^f = \left[\{-M(p - jw_r)\}/\{R_r + L_r(p - jw_r)\}\right](v_D + jv_Q)$$
$$K_s(p + D_F)/(p^2 + pB_F + C_F)$$
$$= \left[\{-M(p - jw_r)\}/\{L_r(1/\tau_r + p - jw_r)\}\right](v_D + jv_Q)$$
$$K_s(p + D_F)/(p^2 + pB_F + C_F)$$

Substituting equation 7.37 in the above equation gives

$$i^f = \left[\{-M(p - jw_r)\}/\{L_r(p + D_F)\}\right](v_D + jv_Q)$$
$$K_s(p + D_F)/(p^2 + pB_F + C_F)$$
$$= \left[\{-M(p - jw_r)\}/L_r\right](v_D + jv_Q)K_s/(p^2 + pB_F + C_F) \qquad (7.42)$$

Defining another two constants

$$D_f = -jw_r \qquad (7.43)$$

and

$$K_r = -(MK_s)/L_r$$
$$= -M/\{L_sL_r\sigma(2)^{\frac{1}{2}}\} \qquad (7.44)$$

gives

$$i^f = (v_D + jv_Q)K_r(p + D_f)/(p^2 + B_F p + C_F) \qquad (7.45)$$

Since the backward rotating rotor current is the conjugate of the forward rotating rotor current i^f then

$$i^b = (v_D - jv_Q)K_r(p + D_b)/(p^2 + B_B p + C_B) \qquad (7.46)$$

where

$$D_b = D_f^* = +jw_r \qquad (7.47)$$

From equations 7.40, 7.41, 7.45 and 7.46 the sequence currents of both stator and rotor have the same general form

$$i = (v_D \pm jv_Q)K(p + D)/(p^2 + pB + C) \qquad (7.18)$$

A general solution of the above equation is derived in appendix I. Particular currents could be obtained by giving appropriate values to the constants in equations 7.33 to 7.39, 7.43, 7.44 and 7.47. For backward rotating currents v_Q should be negative.

Knowing the sequence currents, the stator and rotor direct axis currents can be found from equations 7.22 and 7.24. The instantaneous torque can be

calculated from equation 7.27 after determining the instantaneous values of the stator and rotor sequence currents.

Stator and rotor copper loss can be determined after finding the r.m.s. value of i^D and i^d by numerical integration (Simpson's rule). Iron loss can be calculated by connecting the iron loss simulating resistor for invertor operation right at the stator input end.

Input power can be calculated by first determining the instantaneous power input, averaging it over one period, and then adding the iron loss. Output power can be calculated by first finding the average torque and then multiplying it with a constant and the speed of the rotor.

A digital computer programme was written to predict the invertor-fed induction motor performance.

7.8 Effect of Stator Connection (Star or Delta) on Iron Loss Due to Main Flux

The apparent decrease of hysteresis loss in the induction motor when the stator is connected in delta (Section 6.2) is due to basing calculations on a physically non-existing reference frame for the magnetic circuit of the machine.

Figure 7.21 shows the reference axes of line to line and line to neutral three-phase supply voltage.

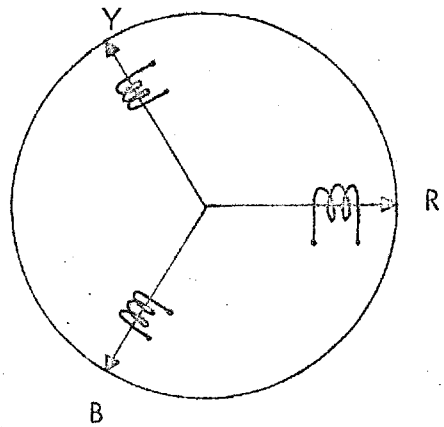

Figure 7.22 Spatial Configuration Of The Magnetic Circuit Axes Of The Machine.

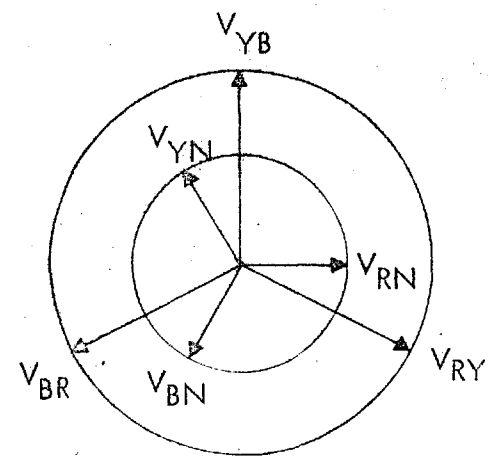

Figure 7.21 Axes Configuration Of Balanced Line To Line And Line To Neutral Voltages Fed To The Stator.

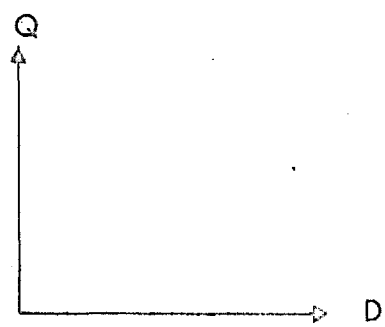

Figure 7.23 Machine Magnetic Circuit DQ Axes (Hypothetical).

(Could be orientated to coincide with either ^{P}D, ^{P}Q or ^{L}D, ^{L}Q axes shown in figure 7.24)

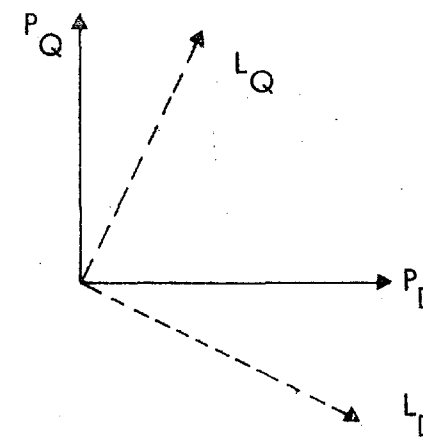

Figure 7.24 ^{P}D & ^{P}Q Axes (Hypothetical) Of Line To Neutral Supply Voltage And ^{L}D & ^{L}Q Axes (Hypothetical) Of Line To Line Supply Voltage.

Figure 7.22 shows the three-phase stator coils spatially distributed by 120^{o}. Excitation of these three coils, say by D.C. would create fluxes in the machine whose directions would be as shown by the arrows in figure 7.22. It may be noted that due to the very nature of flux-flow direction, it could be concluded that the magnetic circuit of the machine is star connected, although by the very nature of construction one can hardly visualize this fact. This is also true for D.C. and synchronous machines. Therefore it can be argued a star connected reference frame for the magnetic circuit of the machine is a physically existing reference frame. Whatever electro-magnetic cause and effects or phenomenon takes place along these axes are real and physically existing quantities.

On the contrary the physically existing reference axes for the stator electric circuit would depend on whether the coils are connected in star or delta. If the coils are connected in delta, and calculations, say, for currents are based on the equivalent star, this simply means that these currents are not the physically existing coil currents, but they are hypothetical currents as viewed along the hypothetical star connected reference axes. Calculations based on the hypothetical star currents would yield identical results to that which would be obtained

from the physically existing delta reference frame currents only if the wave-forms do not contain any third harmonics, otherwise the effects of third or triplen harmonic circulating current in the delta, which is absent in the hypothetical star reference frame (no neutral connection), would not be taken into account. This fact is further justified because the two reference frame r.m.s. currents are related by a factor of $(3)^{\frac{1}{2}}$ only when there are no triplen harmonics present, and as such star delta transformation is valid for the currents devoid of triplen harmonics.

Since the magnetic circuit of the machine is star connected, the physically existing fluxes along these axes (Figure 7.22) would be proportional to the time integral of the voltage wave-form along these axes. Therefore, for magnetic circuit calculations the reference frame for the voltage should always be star connected and orientated to be coincident to that of the magnetic circuit, irrespective of the nature of the stator coil connection. This is shown in figures 7.21 and 7.22. This means that if a search coil is placed in the magnetic circuit, the voltage induced in it would have the wave-form of the line to neutral air-gap voltage irrespective of stator coil connection.

In figure 7.23 the machine three-phase magnetic circuit axes are replaced by two mutually perpendicular axes D and Q for ease of calculation and also to eliminate the effect of any time varying component of Q axis on D axis. The D axis is arranged to coincide with the magnetic circuit R axis (denoted by ^{P}D axis), and D axis phenomena are therefore physically existing, whereas ^{P}Q, being a non-existing axis, the phenomena taking place along this axis have no physical existence. Whatever sequence of events take place in the R axis of the magnetic circuit also identically take place along the ^{P}D axis. The wave-form of voltage and flux along this axis, due to a star connected stator coil fed from the invertor, is shown in figures 7.26 and 7.27 along with the line to neutral stator voltages shown in figure 7.25. (This assumes negligible stator leakage impedance drop so that the stator-impressed voltage equals the air-gap voltage.) The ^{P}Q axis being a hypothetical axis the voltage and flux along this axis as shown in figures 7.28 and 7.29 are non-existing. Hence a search coil placed in the magnetic circuit would register the effect of the physically existing flux as shown in figure 7.27.

When the machine stator coils are connected in delta the coils or the electric circuit of the stator sees the

STATOR ELECTRIC CIRCUIT CONNECTED IN STAR.

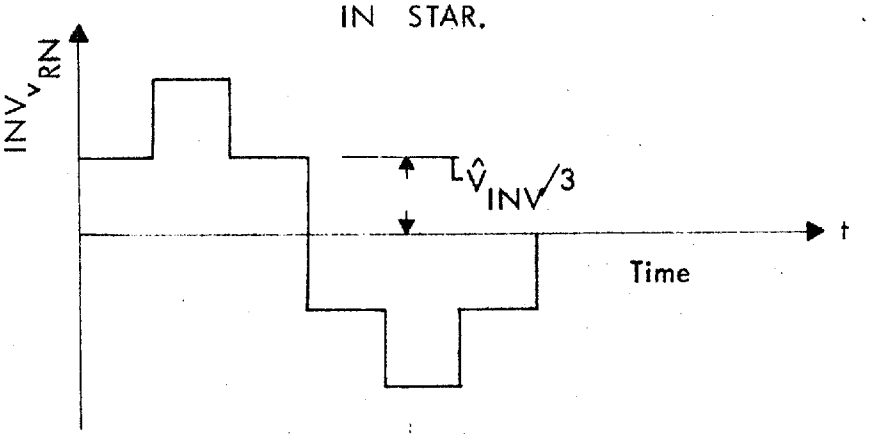

Figure 7.25 Line To Neutral Voltage Fed To The Stator

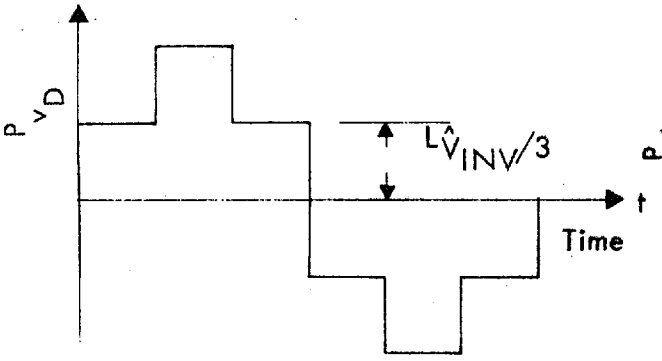

Figure 7.26 Voltage Along Physically Existing ^{P}D Axis Which Is Coincident With The Magnetic Circuit R Axis

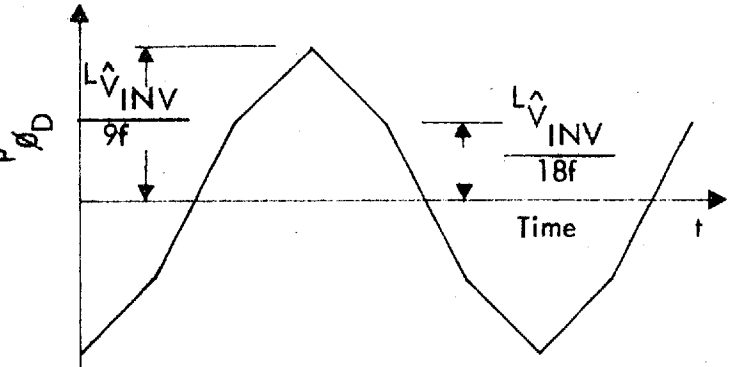

Figure 7.27 Flux Along Physically Existing Magnetic Circuit ^{P}D Axis.

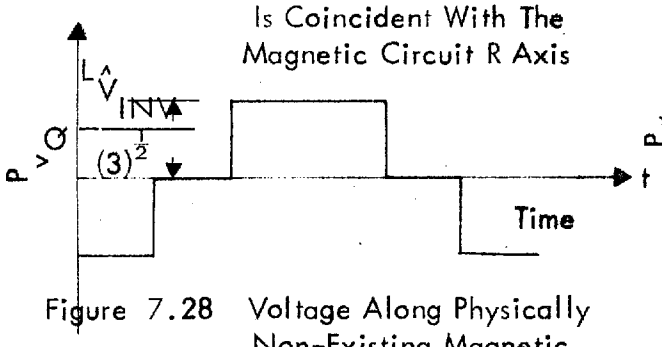

Figure 7.28 Voltage Along Physically Non-Existing Magnetic Circuit ^{P}Q Axis.

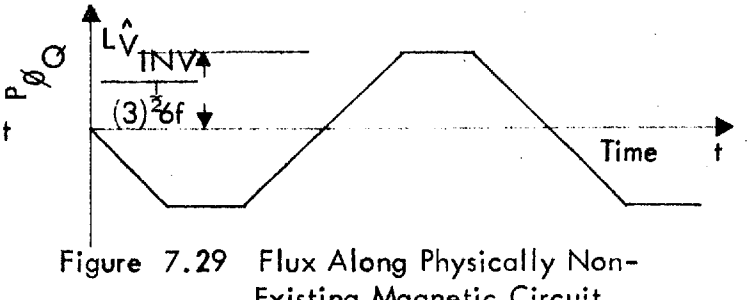

Figure 7.29 Flux Along Physically Non-Existing Magnetic Circuit ^{P}Q Axis.

line to line voltages, the axes of which are no longer coincident with the physically existing star connected magnetic circuit axes as shown in figures 7.21 and 7.22. Therefore the magnetic circuit does not react to these voltages directly but to their components along the physically existing axes of figure 7.22.

The line to line voltages shown in figure 7.30 are transformed to D, Q axes quantities as shown in figure 7.31. The D axis is made to coincide with that of the line to line voltage across RY terminals as shown in figures 7.21 and 7.24 (denoted by ^{L}D axis). In this case the ^{L}D axis is the physically non-existing one, whereas the ^{L}Q axis is coincident with the physically existing magnetic circuit B phase axis, but with 180° phase difference between them. Therefore the magnetic circuit sees a voltage variation as shown for the ^{L}Q axis (Figure 7.31).

The above fact can be further substantiated by transforming the line to line $^{L}D^{L}Q$ axes quantities to that of the magnetic circuit D,Q axes which are also coincident with the $^{P}D^{P}Q$ axes of line to neutral voltages. The transformed voltage is shown in figure 7.32. The magnetic circuit D axis being physically existing, the magnetic circuit sees the voltage along this axis which is exactly the same as that of the line to neutral voltage (Figure 7.5).

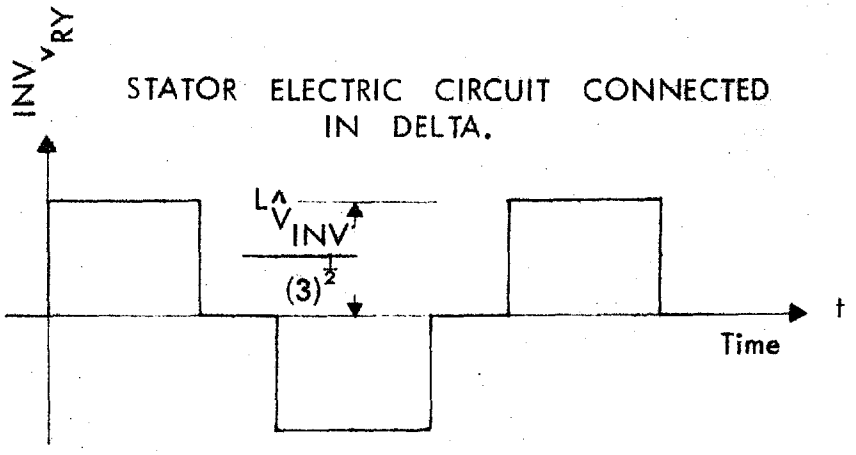

Figure 7.30 Line To Line Voltage Fed To The Stator.

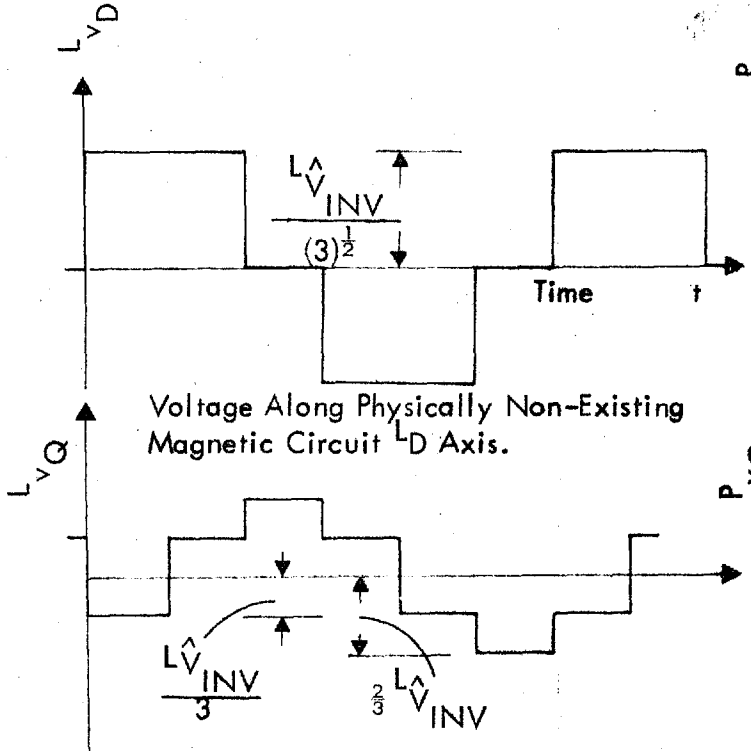

Figure 7.31 Voltage Along Physically Existing Magnetic Circuit ^{L}Q Axis Which Is Coincident With The Magnetic Circuit - B Axis.

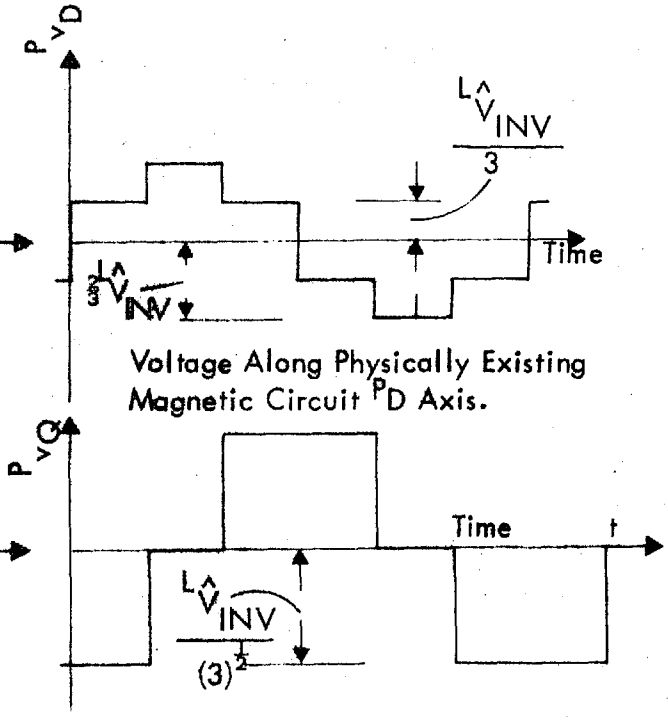

Figure 7.32 Voltage Along Physically Non-Existing Magnetic Circuit ^{P}Q Axis.

The general conclusion is, that since the magnetic circuit of the machine is star connected, the flux follows the variation of voltages projected along a star connected reference frame which is coincident with that of the magnetic circuit. Therefore the flux produced in the magnetic circuit follows the line to neutral voltage of supply (neglecting stator leakage impedance drop), irrespective of whether the stator coils are connected in star or delta, and hence the magnetic circuit losses do not depend on the windings being connected in star or delta.

If a machine could be so constructed that its magnetic circuit is delta connected, the iron loss, when fed from the invertor would be less than that for equivalent sinusoidal operation as shown in section 6.2.

CHAPTER 8

INDUCTION MOTOR LOAD TESTS

In order to verify the performance theory so far developed in chapters 5 to 7 load tests on the induction motor were carried out.

Load tests under sinusoidal excitation were carried out for two reasons.

i) To test the accuracy with which the simple equivalent circuit "constants" were determined experimentally.

AND ii) To compare this mode of operation with that of the invertor operation.

The experimental system was as shown in figure 4.3.

8.1 Windage and Friction Loss of the Induction and D.C. Loading Motor

In order to determine the electro-magnetic power output of the induction motor 1 from the D.C. power output of the loading motor 2 (Figure 4.3), measurements were made to determine the windage and friction losses of the induction D.C. loading motor combination.

The induction motor was unexcited and driven by the D.C. loading motor. Rated current was allowed to flow through the field of the D.C. loading motor and control of

speed was achieved by varying the armature supply voltage. The windage and friction losses of the combination were determined by calculating the power input to the armature and subtracting from it the armature copper loss and the brush volt-drop loss. The windage and friction loss of the combination was then

$$P_{W+F} = V_A I_A - I_A^2 R_A - I_A \times 4 \qquad (8.1)$$

where

V_A = D.C. voltage impressed across the armature.

I_A = D.C. current flowing through the armature.

The armature resistance R_A was determined from the D.C. Volt drop test on the locked armature (Figure 8.1). The windage and friction loss P_{W+F} as determined from equation 8.1 is as shown in figure 8.2. The speed of the combination was determined accurately by a digital tachometer.

8.2 Variable Frequency Load Test under Sinusoidal Excitation

This test was carried out to verify the theory developed in chapter 5, which predicts the induction motor performance under variable frequency sinusoidal operation.

Referring to figure 4.3, variable frequency and

FIGURE 8.1 ARMATURE RESISTANCE OF THE D.C. LOADING MOTOR.

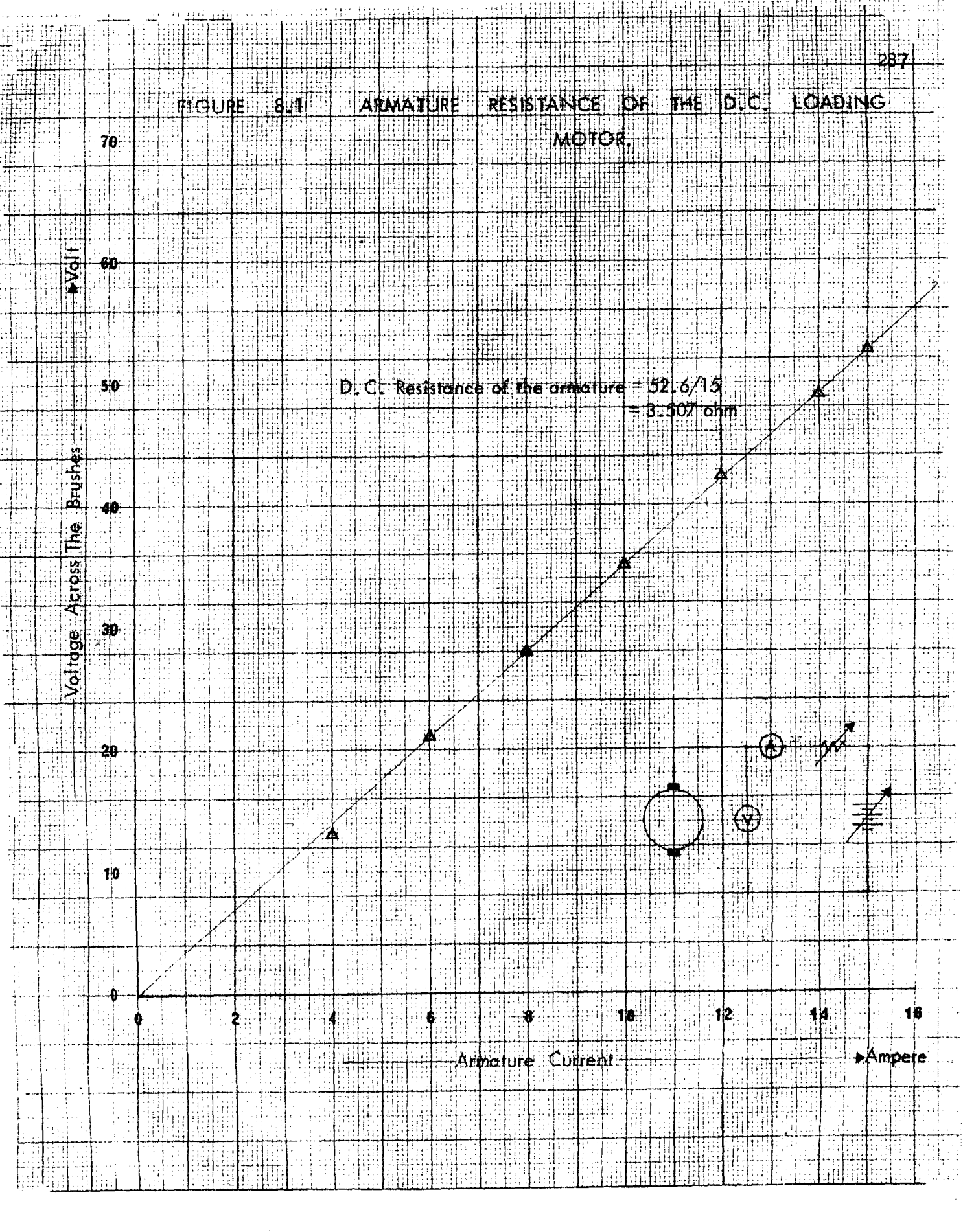

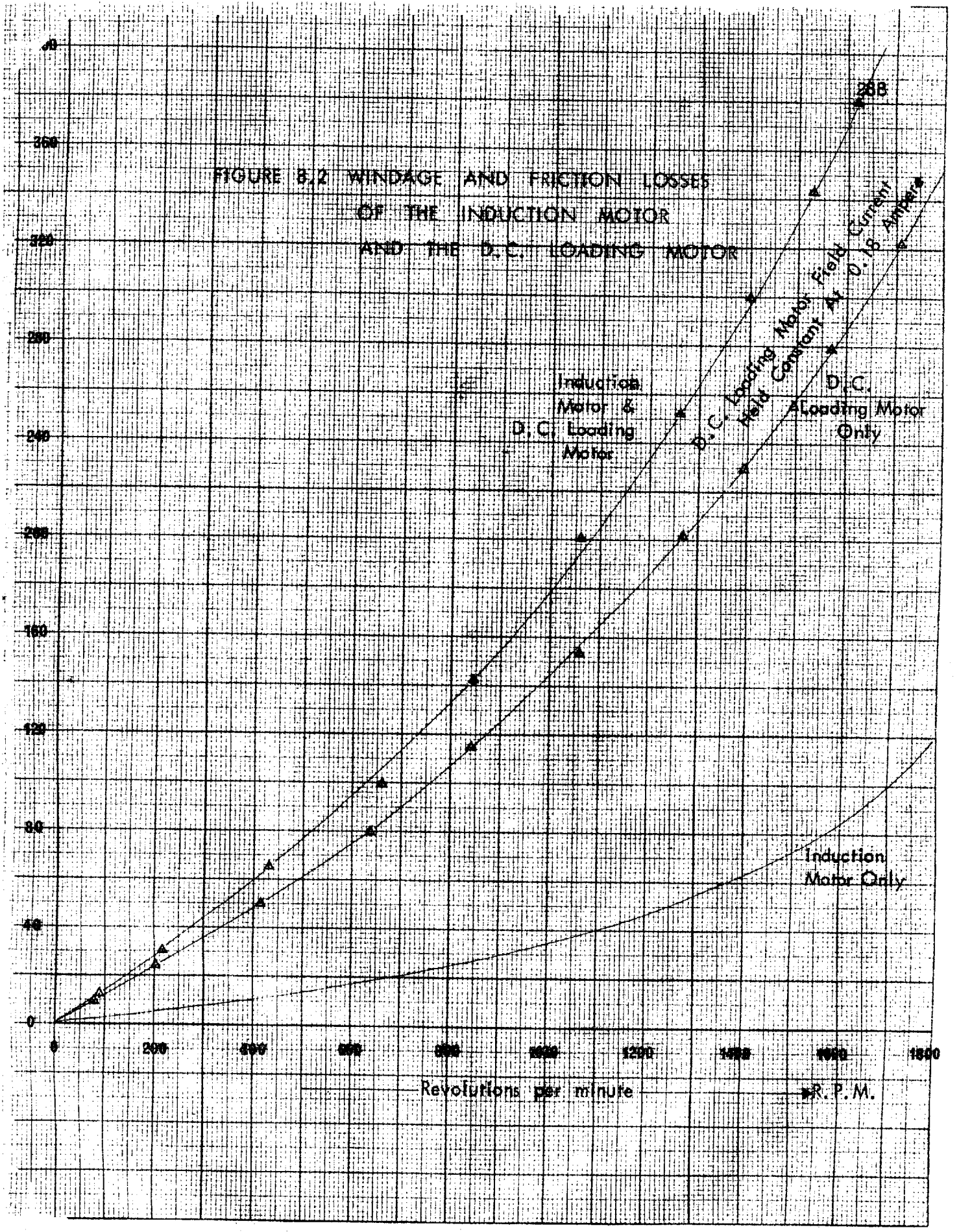
FIGURE 8.2 WINDAGE AND FRICTION LOSSES
OF THE INDUCTION MOTOR
AND THE D. C. LOADING MOTOR
Induction Motor & D. C. Loading Motor
D. C. Loading Motor Field Constant At 2.8 D. C. Amperes
D. C. Loading Motor Only
Induction Motor Only
Revolutions per minute
R. P. M.
0
200
1200
1500

variable voltage were obtained from an alternator, (5). Variable voltage was obtained by controlling the field current of the alternator. Alternator speed was controlled by variation of the armature supply voltage of the D.C. drive motor (6). Adjustment of the field current of this motor enabled fine control of speed. The variable D.C. armature supply voltage of motor (6) was obtained from the field controlled separately excited D.C. generator (7) driven by the induction motor (8) fed from the three-phase mains.

The variable voltage of variable frequency from alternator (5) was fed to the test induction motor (1) via a three-pole double throw switch. This switch was used to change over to invertor operation without disturbing or changing of any leads, so that the test conditions were identical for both sinusoidal and invertor-fed load tests.

Three moving iron ammeters were inserted in the stator leads of the test induction motor (1). The power input to the induction motor was measured by the two wattmeter method. A moving iron voltmeter was connected across the supply leads to measure the voltage input to the induction motor. The frequency of the supply was measured by monitoring the alternator rotor speed by the digital tachometer (2). The speed of the induction motor

was measured by a similar digital tachometer (1).

The test induction motor (1) was loaded by the D.C. machine (2) which was excited at a constant field current from +200, 0, - 200 Volt D.C. mains. Loading of the induction motor was achieved by running the D.C. machine (2) as a generator supplying the separately excited D.C. machine (3). This D.C. machine operated as a motor to drive the induction machine (4), as an asynchronous generator to feed power to the three-phase supply mains.

The amount of loading of the test induction motor (1) was controlled by varying the field excitation of the D.C. machine (3). A moving coil ammeter and a moving coil voltmeter was used to measure the power output of the D.C. loading machine (2).

8.2.1 Variation of stator current with slip for various constant values of supply frequency

Tests were performed for various constant operating frequencies from 10 Hertz to 50 Hertz in steps of 10 Hertz. No measurements were taken above 50 Hertz as at the next step of 60 Hertz , the alternator set (5) and (6) tended to scream and vibrate too much and it was felt to be unsafe to operate at that frequency.

Selecting a given frequency, the test induction motor (1) was loaded in steps. Simultaneous readings of

the three ammeters and the two wattmeters in the stator leads, as well as the ammeter and voltmeter at the armature leads of the D.C. loading machine (2) were taken. The supply frequency and the test induction motor speed was noted from the digital tachometers (2) and (1).

The stator input current was taken to be the average of the readings of the three ammeters inserted in the stator supply leads. The experimental results, together with the calculated values of stator currents from equation 5.119 are given in figure 8.3. The calculated and predicted values agree to within 2% at the rated (= 30A) stator current.

8.2.2 Electro-magnetic power output

Knowing the combined windage and friction losses P_{W+F} of the machines (1) and (2) (Section 8.1 and Figure 8.2), and the D.C. electrical power output of the loading machine (2), the power output of the induction motor (1) under test was determined from

$$P_{2o} = V_A I_A + I_A^2 R_A + 4I_A + P_{W+F} \qquad (8.2)$$

where

V_A and I_A are the output voltage and current of the D.C. loading machine (2).

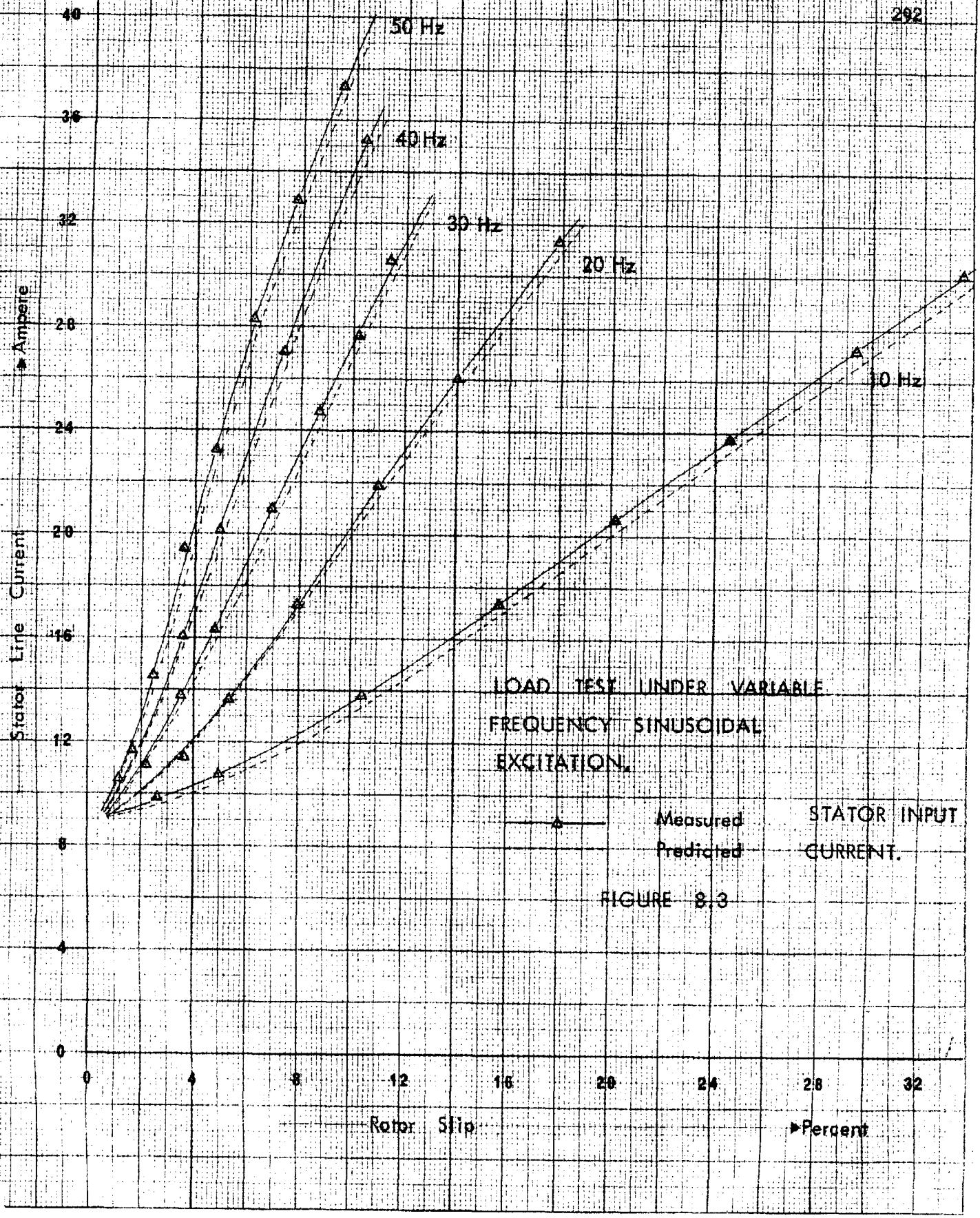

LOAD TEST UNDER VARIABLE FREQUENCY SINUSOIDAL EXCITATION.

—△— Measured
——— Predicted

STATOR INPUT CURRENT.

FIGURE 8.3

R_A is the armature resistance of the same machine.

$4I_A$ is the power lost in the brush voltage drop of the same machine. This voltage drop is empirically taken as 2 Volt per brush.

The measured induction motor electro-magnetic power output under sinusoidal excitation is calculated from equation 8.2. The output is also predicted from equation 5.135 (Table 5.3) and both are shown in figure 8.4 for comparison.

8.2.3 Electro-magnetic torque developed

The electro-magnetic torque developed by the rotor of the induction motor was determined from the rotor power output given by equation 8.2. The electro-magnetic torque in Lb.-ft.

$$T = \left\{33,000/(2\pi 746)\right\} (P_{2o}/N) \qquad (8.3)$$

where N is the actual speed of the rotor in R.P.M.

A graphical plot of the electro-magnetic torque T as a function of rotor percentage slip for various constant values of frequency is given in figure 8.5. The predicted torque given by equation 5.145 is also given in the same figure (Figure 8.5) for comparison. The measured and

LOAD TEST UNDER VARIABLE FREQUENCY SINUSOIDAL EXCITATION.

FIGURE 8.4 ROTOR POWER OUTPUT

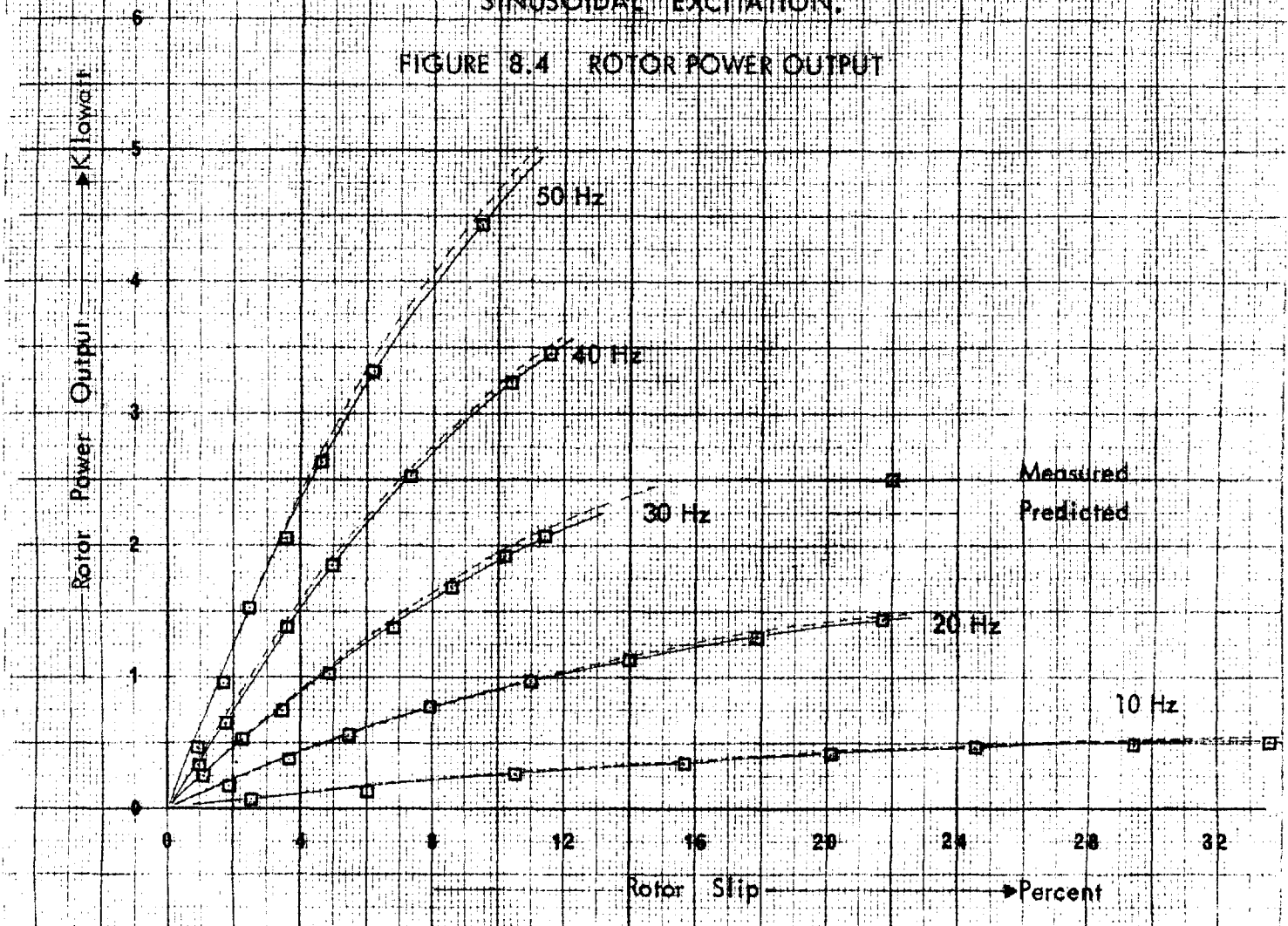

LOAD TEST UNDER VARIABLE FREQUENCY
SINUSOIDAL EXCITATION
FIGURE 8.5 ELECTRO-MAGNETIC TORQUE
DEVELOPED

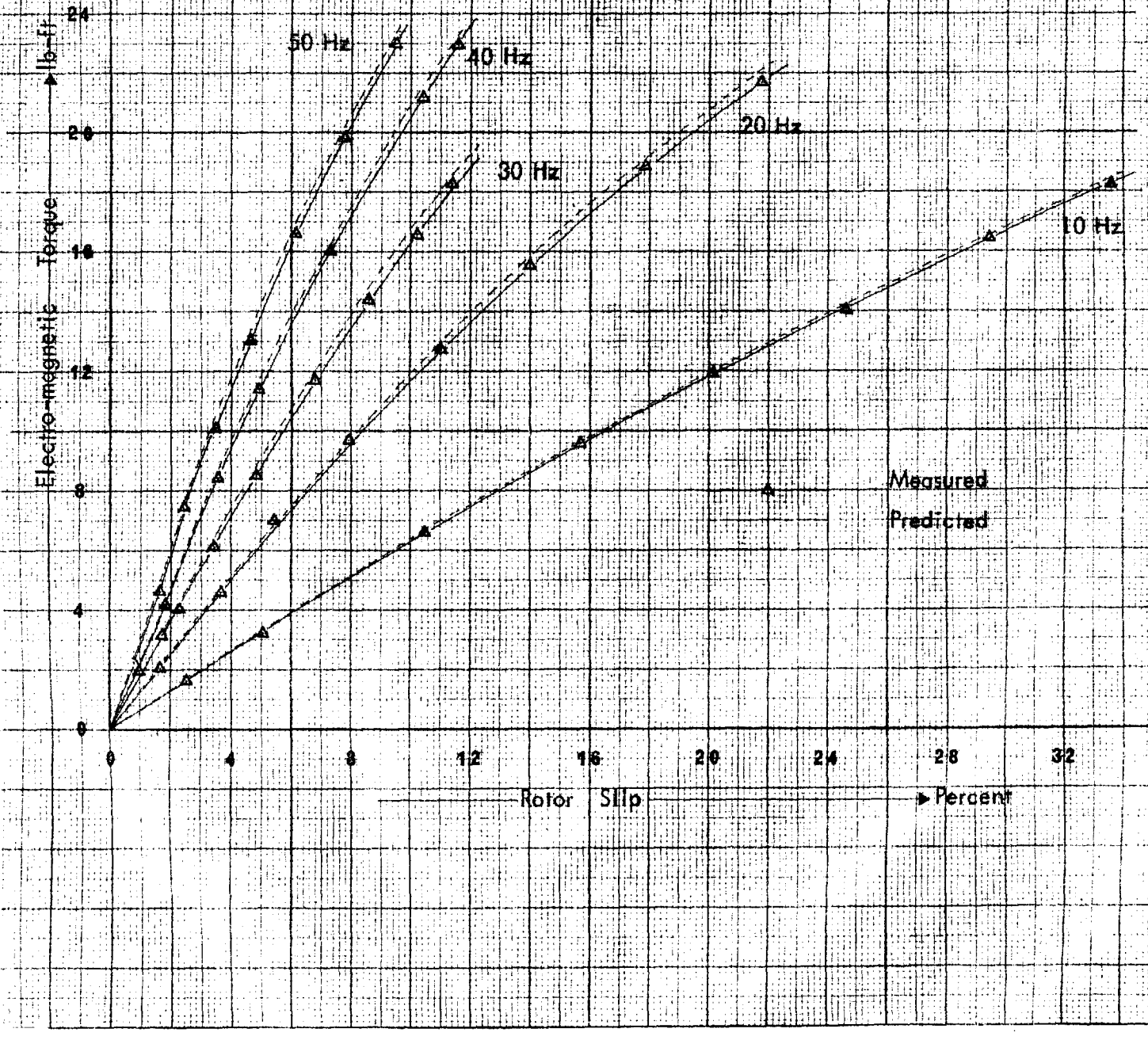

predicted torque, as functions of rotor speed for various constant values of frequency, are given in figure 8.6. It is seen that all other conditions remaining the same, torque developed by the motor is the same for a given decrement of speed from the synchronous speed, irrespective of frequency. This is in accordance to the theoretical inference drawn at the end of the section 5.8.

8.2.4 Electrical power input

The power input P_{lin} to the induction motor was measured using two wattmeters connected at the stator input. The measured and predicted input powers (Equation 5.143) as a function of percentage slip of the rotor, for various constant values of frequency, are given in figure 8.7.

8.2.5 Total electro-magnetic loss

The total loss occurring in the induction motor was measured by taking the difference between the measured power input (Section 8.2.4) and the electro-magnetic power output of the rotor (Section 8.2.2). This loss is the total electro-magnetic loss occurring and does not include the windage and friction loss of the machine. The variation of this loss, with slip for various constant values of frequency, is shown in figure 8.8. This loss is

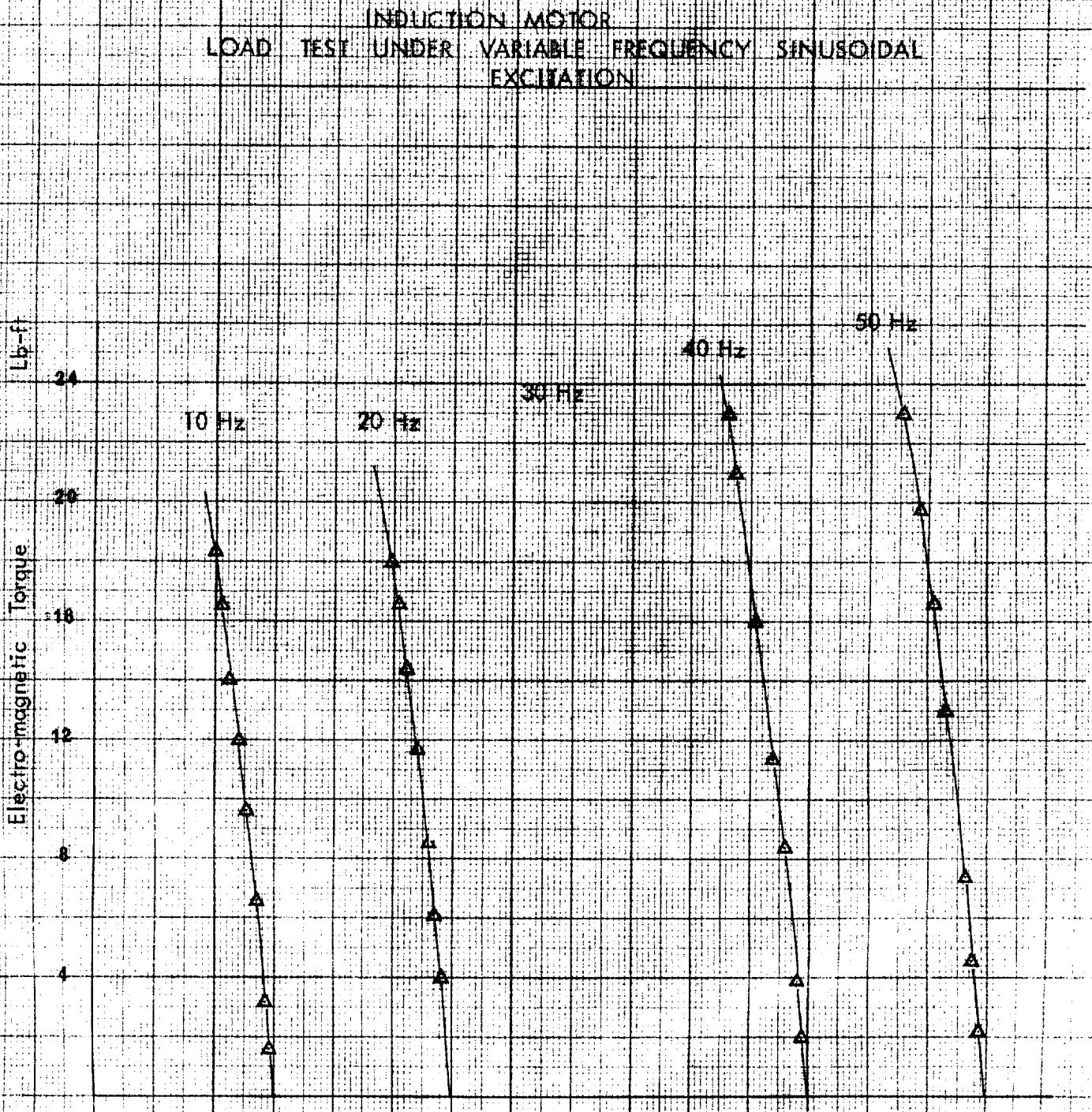

FIGURE 8.6 ELECTRO-MAGNETIC TORQUE VS ROTOR SPEED

LOAD TEST UNDER VARIABLE FREQUENCY
SINUSOIDAL EXCITATION

FIGURE 8.7 STATOR INPUT POWER

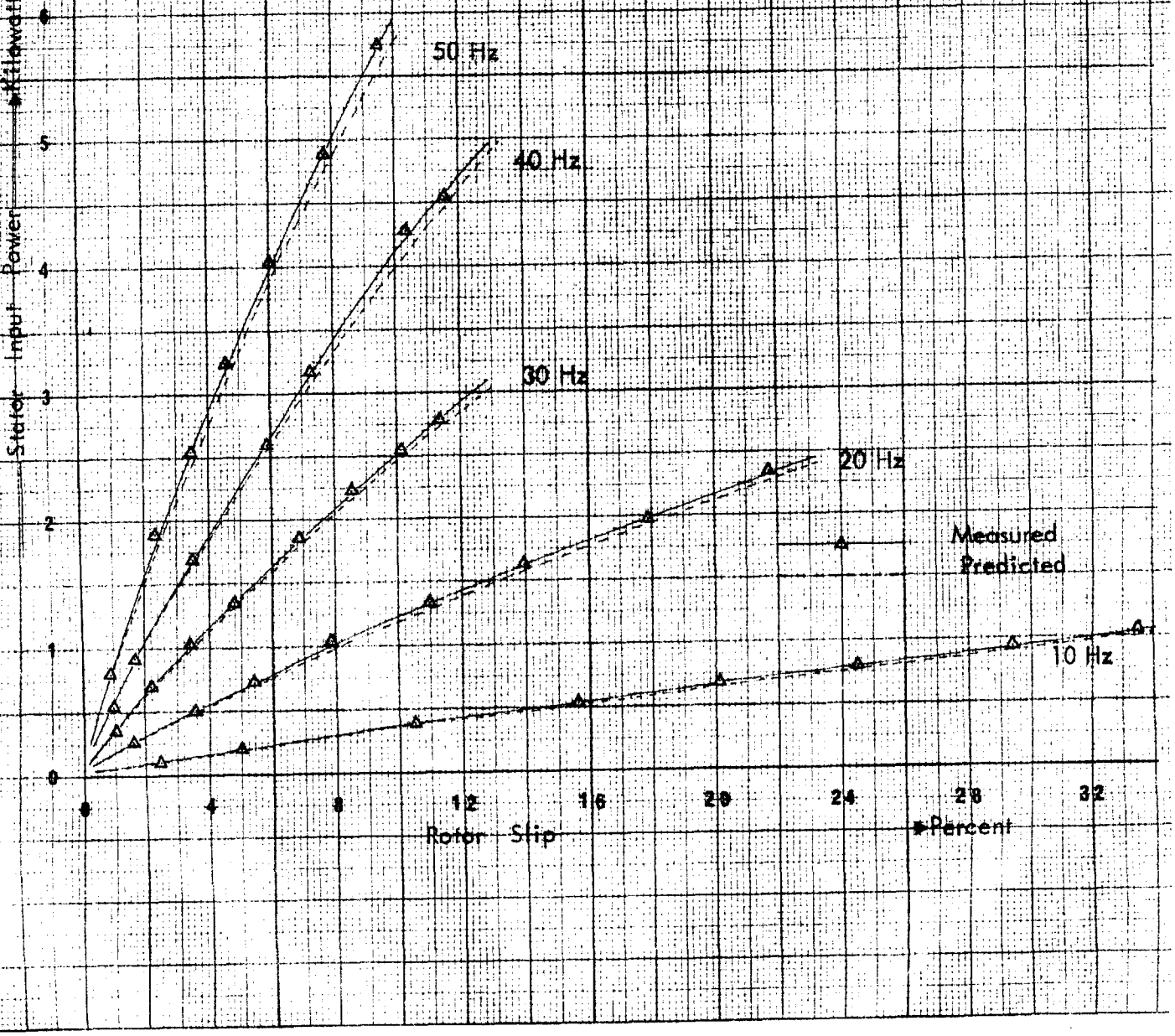

LOAD TEST UNDER VARIABLE FREQUENCY
SINUSOIDAL EXCITATION

FIGURE 8.8 ELECTRO-MAGNETIC LOSS

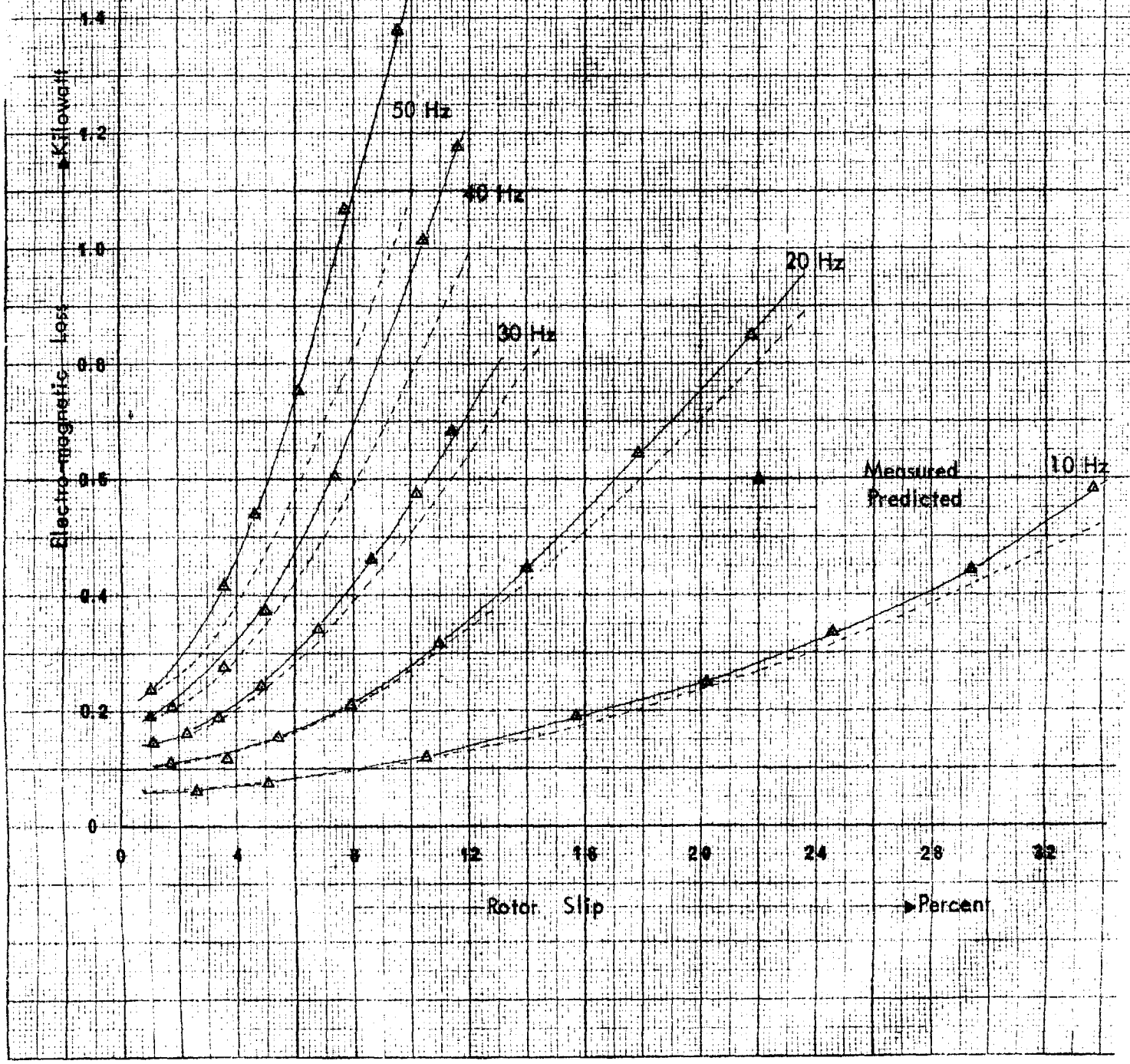

also predicted by summing the net rotor copper loss (Equation 5.133), iron loss (Equation 5.137) and stator copper loss (Equation 5.139). This predicted loss is also plotted in figure 8.8.

8.2.6 Electro-magnetic efficiency

Knowing the power input (Section 8.2.4) and the total electro-magnetic loss (Section 8.2.5), the efficiency was calculated from the usual formula

$$\eta_M = (1 - \text{Losses/Input}) \times 100 \qquad (8.4)$$

Measured and predicted values of efficiency are shown in figure 8.9.

8.3 Variable Frequency Load Test under Invertor Operation

To measure the performance of the invertor-fed induction motor the experimental set-up shown in figure 8.10 was used, together with the test circuit shown in figure 4.3. The shunts in the stator leads shown in figure 8.10 were ommitted in figure 4.3 for clarity. These shunts, although not required for the no-load, locked rotor and load tests under variable frequency sinusoidal excitation, were in the test circuit permanently. In this way all the above-mentioned tests, including the invertor-fed motor load tests, were carried out by simple

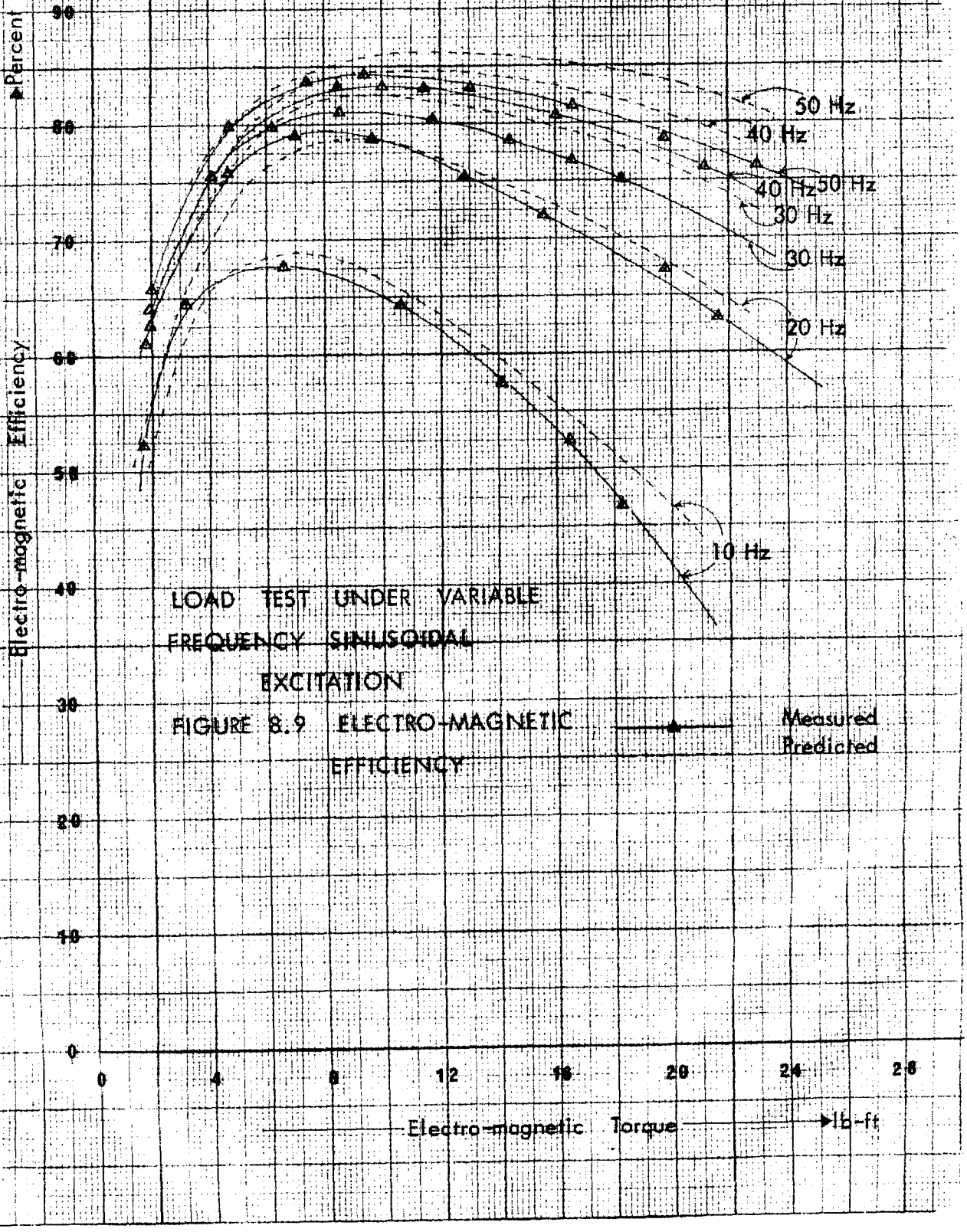

LOAD TEST UNDER VARIABLE FREQUENCY SINUSOIDAL EXCITATION

FIGURE 8.9 ELECTRO-MAGNETIC EFFICIENCY

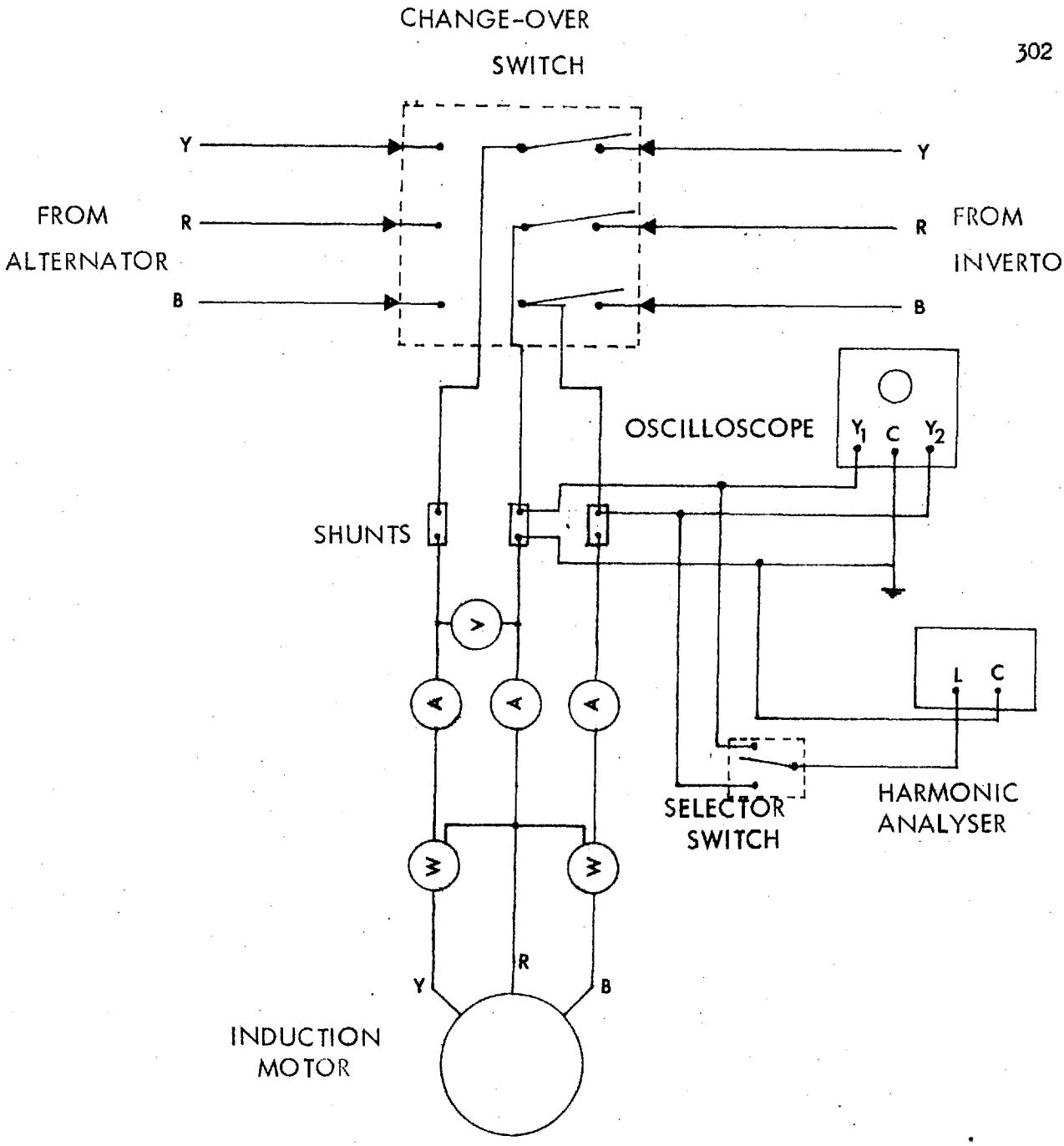

FIGURE 8.10 MEASUREMENT CIRCUIT FOR INVERTOR-FED INDUCTION MOTOR

switching. No change of circuit connections or change of leads were required, so that all the tests were carried out under the same experimental conditions.

The harmonic analyser was used to measure the harmonic content of the supply voltage and, in conjunction with the shunts, the harmonic content of the stator line current. A simple switching scheme shown in figure 8.10 was used so that a single harmonic analyser could be conveniently used to measure the harmonic contents of both line to line voltage and line current. The oscilloscope monitored the wave-form of line to line voltage and line current (in conjunction with the shunts). The supply frequency was measured by feeding the voltage across the invertor commutating capacitor C_3 (Figure 2.1) to a digital counter via a capacitor voltage dividing network.

8.3.1 Variation of stator current with slip for various constant values of supply frequency

The test induction motor (1) was fed from the invertor at various constant frequencies from 10 Hertz to 50 Hertz in steps of 10 Hertz.

A certain test frequency was selected and the induction motor was gradually loaded, taking due care that the time fundamental of the supply voltage was in accordance to the demand of the supply voltage regulation

(Figure 5.6).

The harmonic contents of stator line to line voltage are shown in figures 8.11 to 8.16. The measured and predicted (Equation 6.78) fundamental and harmonic content of stator line currents are shown in figures 8.17 to 8.21.

The wave-forms of stator line to line voltages and stator line currents were photographed and predicted (Equation 7.23) for various loading and frequencies of 50 Hertz, 40 Hertz and 10 Hertz. These are shown and compared in figures 8.22 to 8.35.

The measured and predicted peak currents of bridge thyristors and diodes are shown in figures 8.36 and 8.37.

The measured and predicted conduction angles of bridge thyristors and diodes are shown in figures 8.38 and 8.39.

The predicted values of average and r.m.s. values of bridge thyristors and diodes are given in figures 8.40 to 8.43.

8.3.2 Electro-magnetic torque developed

The average electro-magnetic torque was measured as in section 7.2.3. The average torque was predicted by harmonic analysis from equation 6.114. The instantaneous torque was predicted by time domain analysis from equation

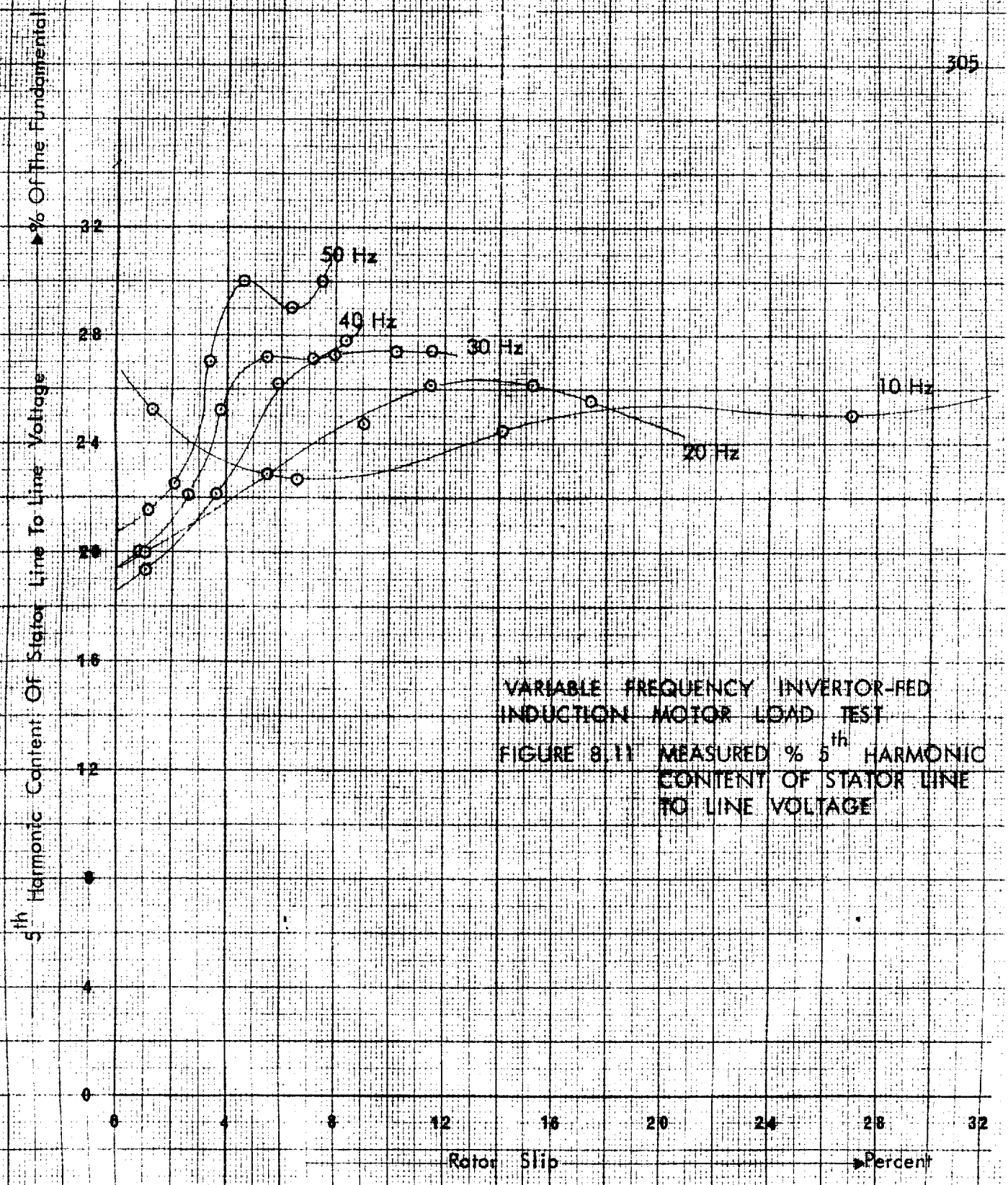

VARIABLE FREQUENCY INVERTOR-FED INDUCTION MOTOR LOAD TEST

FIGURE 8.11 MEASURED % 5th HARMONIC CONTENT OF STATOR LINE TO LINE VOLTAGE

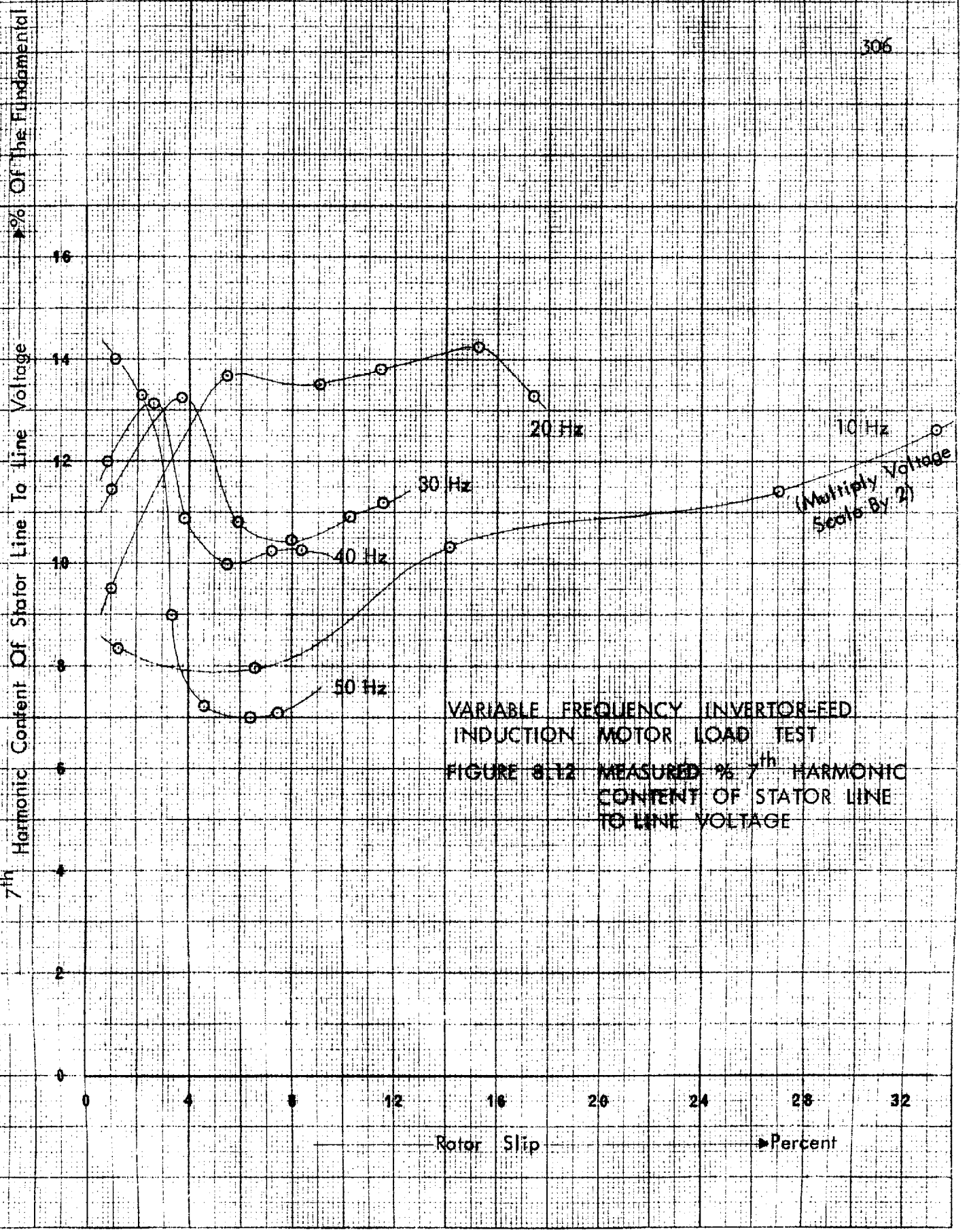

VARIABLE FREQUENCY INVERTOR-FED INDUCTION MOTOR LOAD TEST

FIGURE 8.12 MEASURED % 7th HARMONIC CONTENT OF STATOR LINE TO LINE VOLTAGE

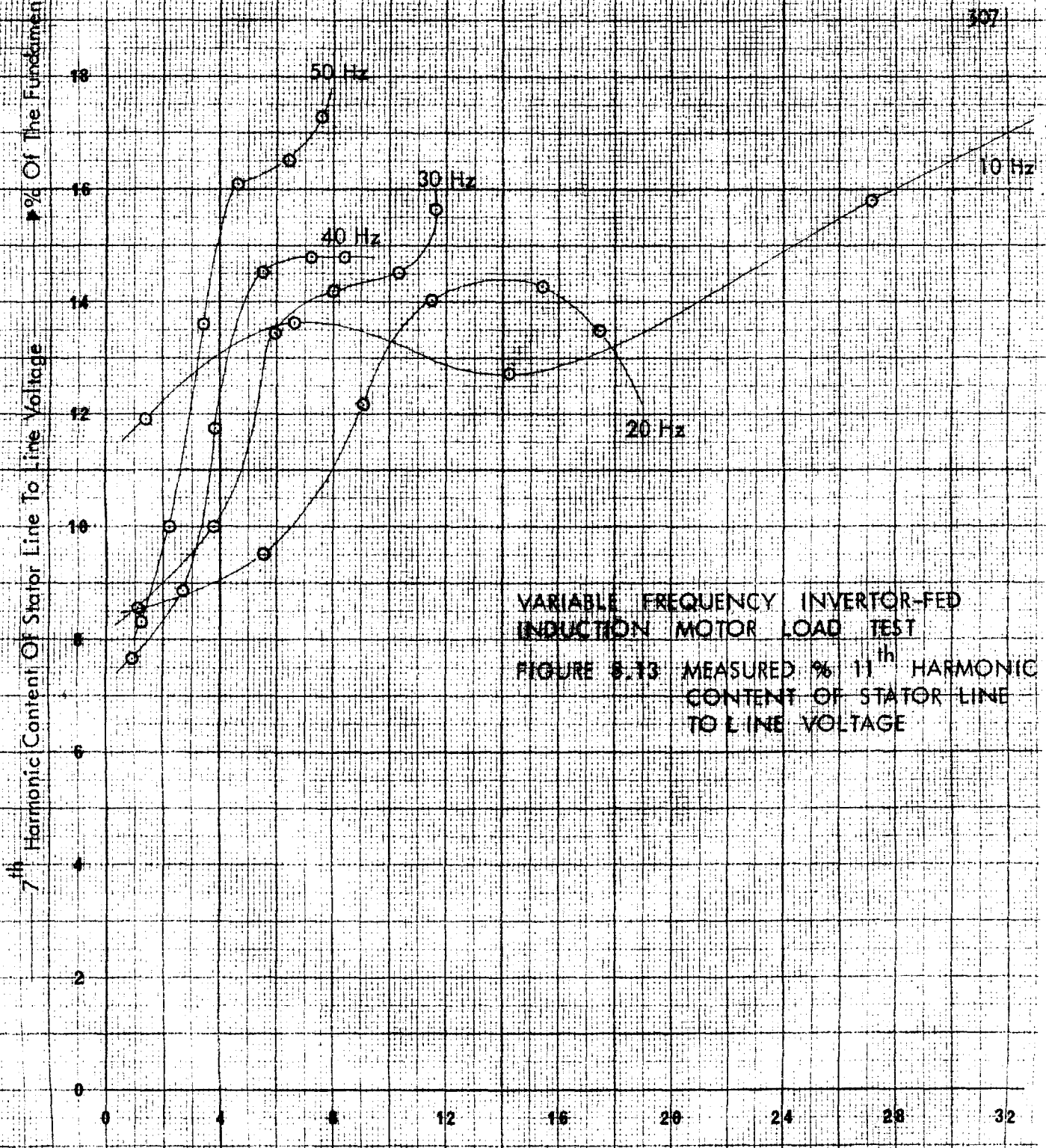

VARIABLE FREQUENCY INVERTOR-FED INDUCTION MOTOR LOAD TEST

FIGURE 5.13 MEASURED % 11th HARMONIC CONTENT OF STATOR LINE TO LINE VOLTAGE

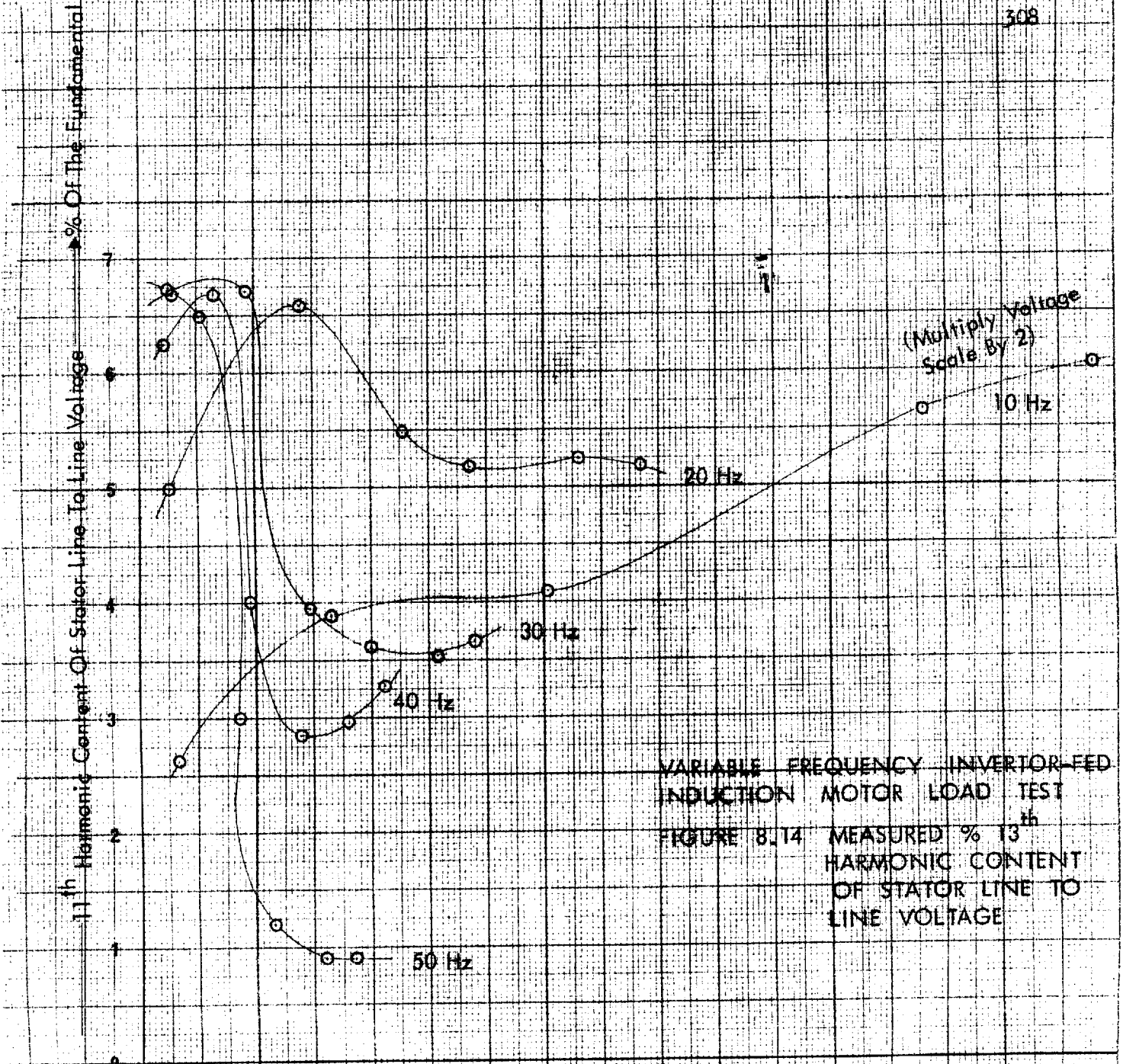

VARIABLE FREQUENCY INVERTOR-FED INDUCTION MOTOR LOAD TEST

FIGURE 8.14 MEASURED % 13^{th} HARMONIC CONTENT OF STATOR LINE TO LINE VOLTAGE

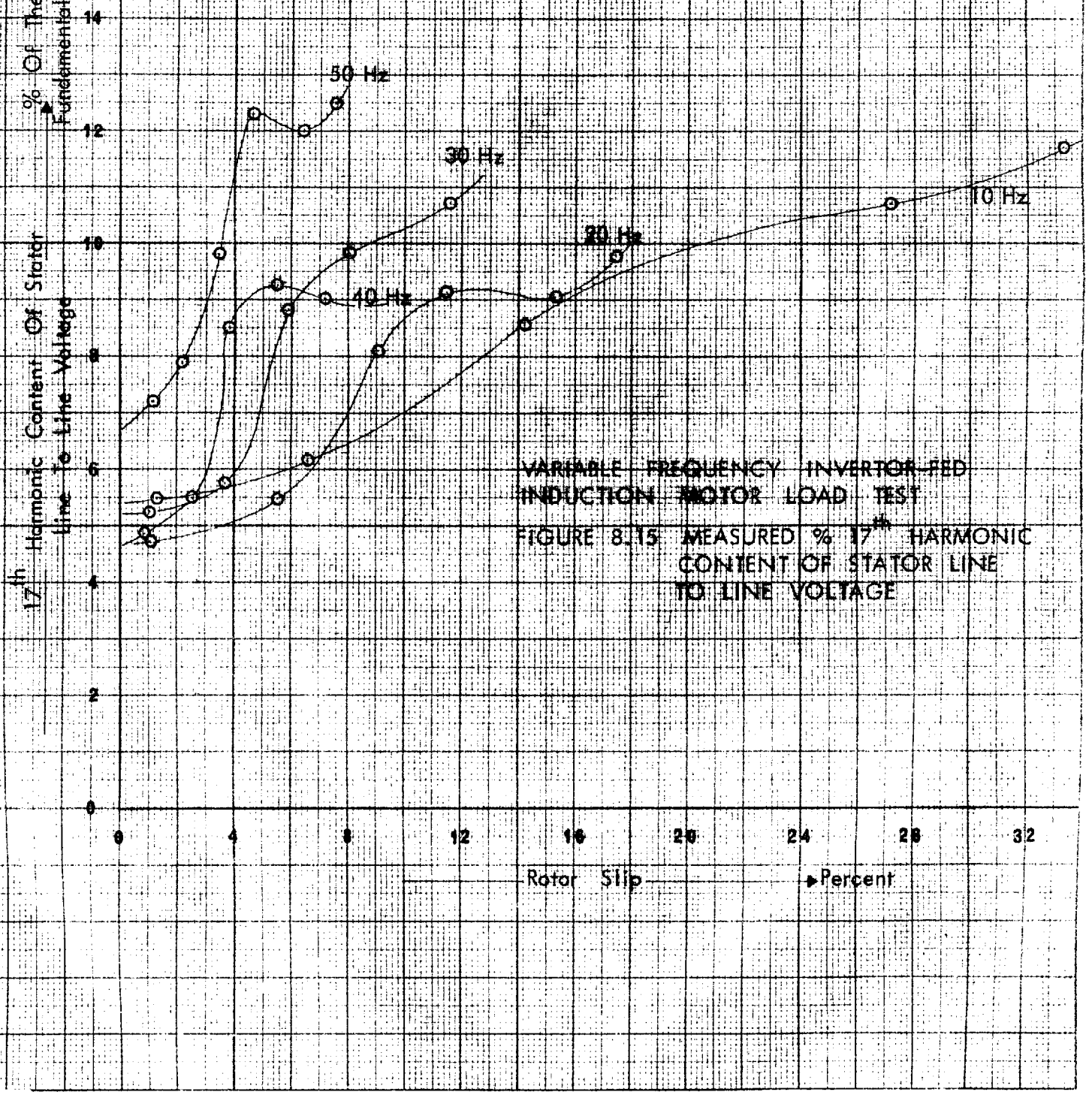

VARIABLE FREQUENCY INVERTOR-FED INDUCTION MOTOR LOAD TEST

FIGURE 8.15 MEASURED % 17th HARMONIC CONTENT OF STATOR LINE TO LINE VOLTAGE

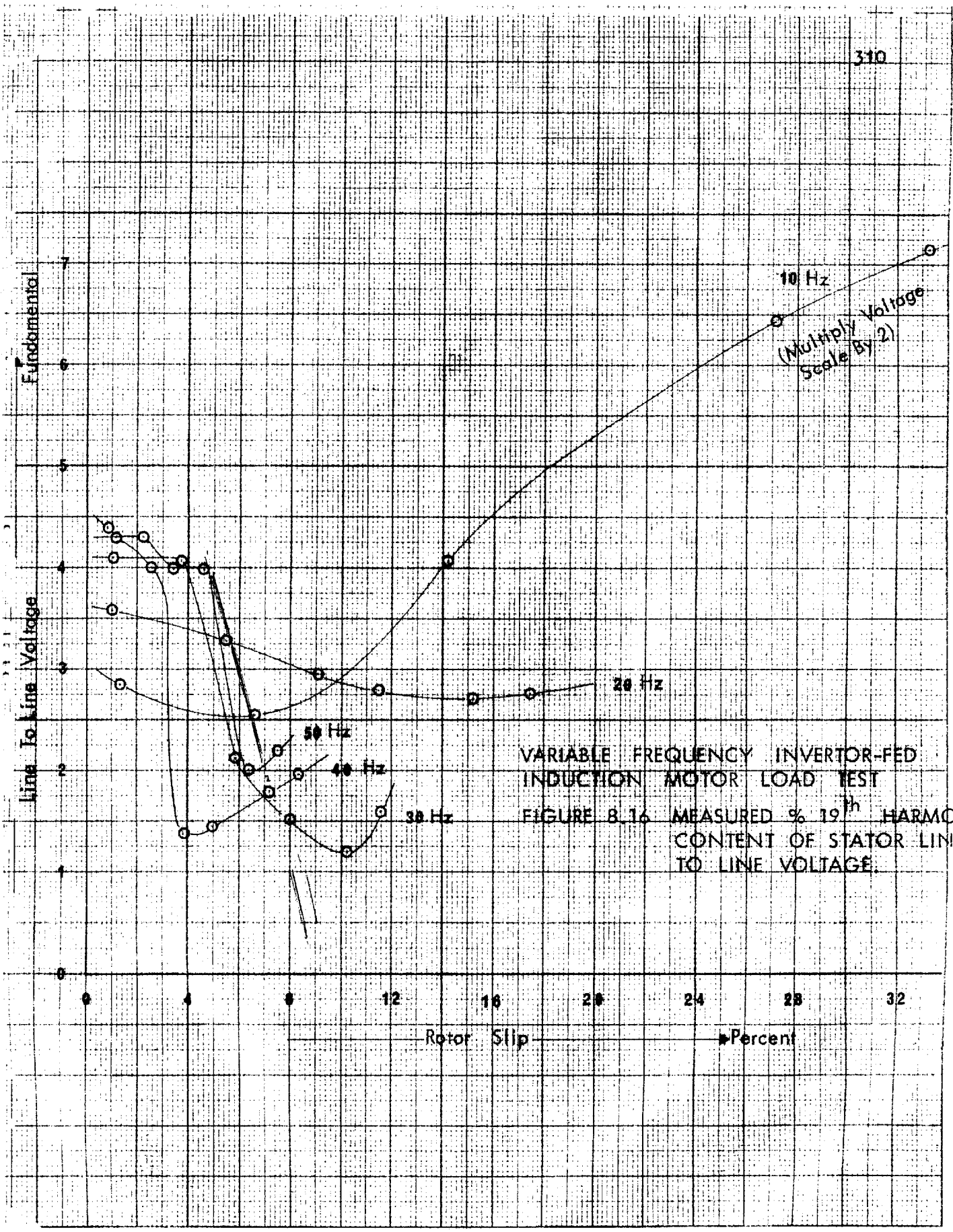

VARIABLE FREQUENCY INVERTOR-FED INDUCTION MOTOR LOAD TEST

FIGURE 8.16 MEASURED % 19th HARMONIC CONTENT OF STATOR LINE TO LINE VOLTAGE.

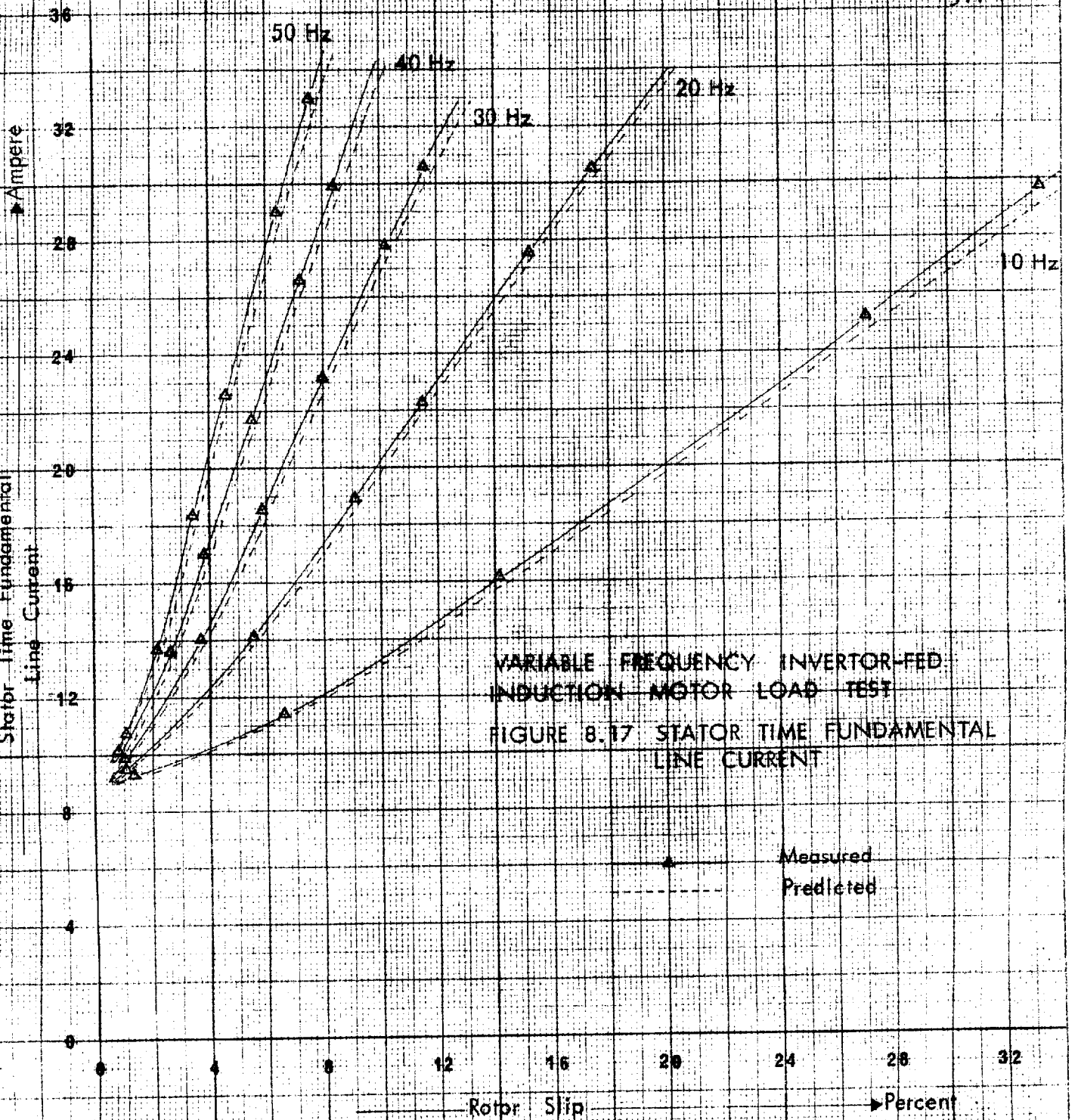

VARIABLE FREQUENCY INVERTOR-FED INDUCTION MOTOR LOAD TEST

FIGURE 8.17 STATOR TIME FUNDAMENTAL LINE CURRENT

VARIABLE FREQUENCY INVERTOR-FED
INDUCTION MOTOR LOAD TEST

FIGURE 8.18 % 5th HARMONIC CONTENT
OF STATOR LINE CURRENT

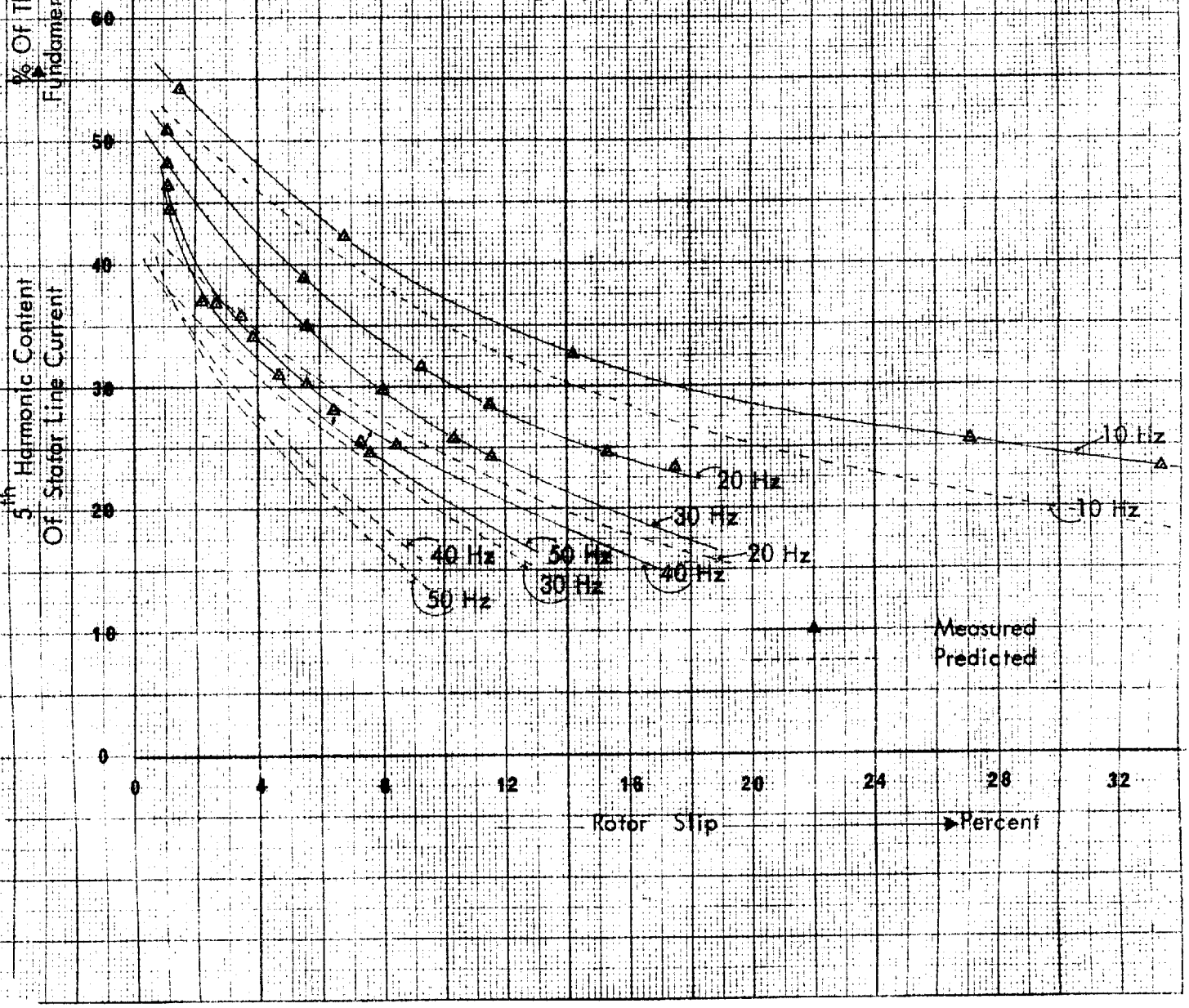

VARIABLE FREQUENCY INVERTOR-FED
INDUCTION MOTOR LOAD TEST

FIGURE 8.19 % 7^{th} HARMONIC CONTENT
OF STATOR LINE CURRENT

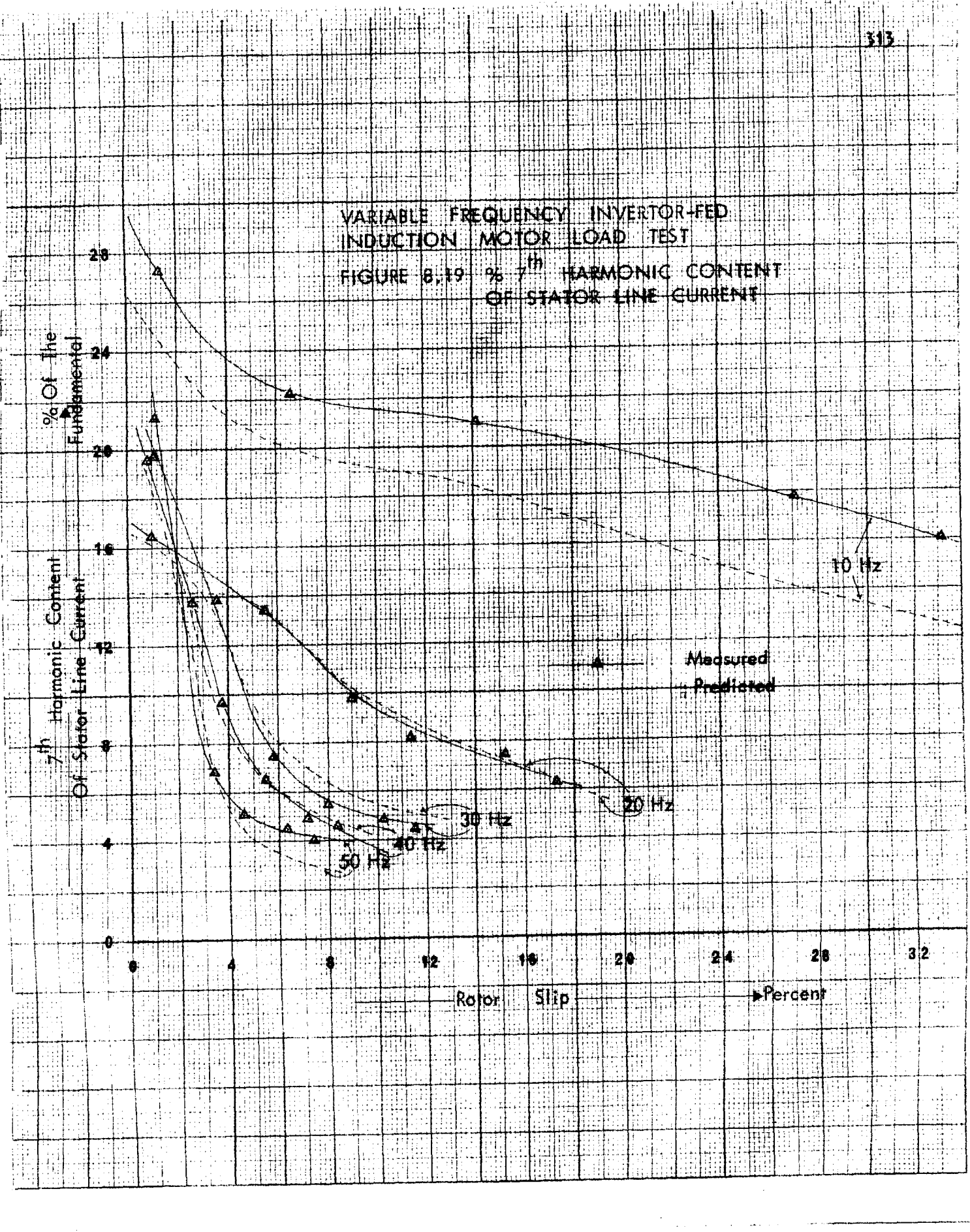

VARIABLE FREQUENCY INVERTOR-FED
INDUCTION MOTOR LOAD TEST

FIGURE 8.20 % 11th HARMONIC CONTENT
OF STATOR LINE CURRENT

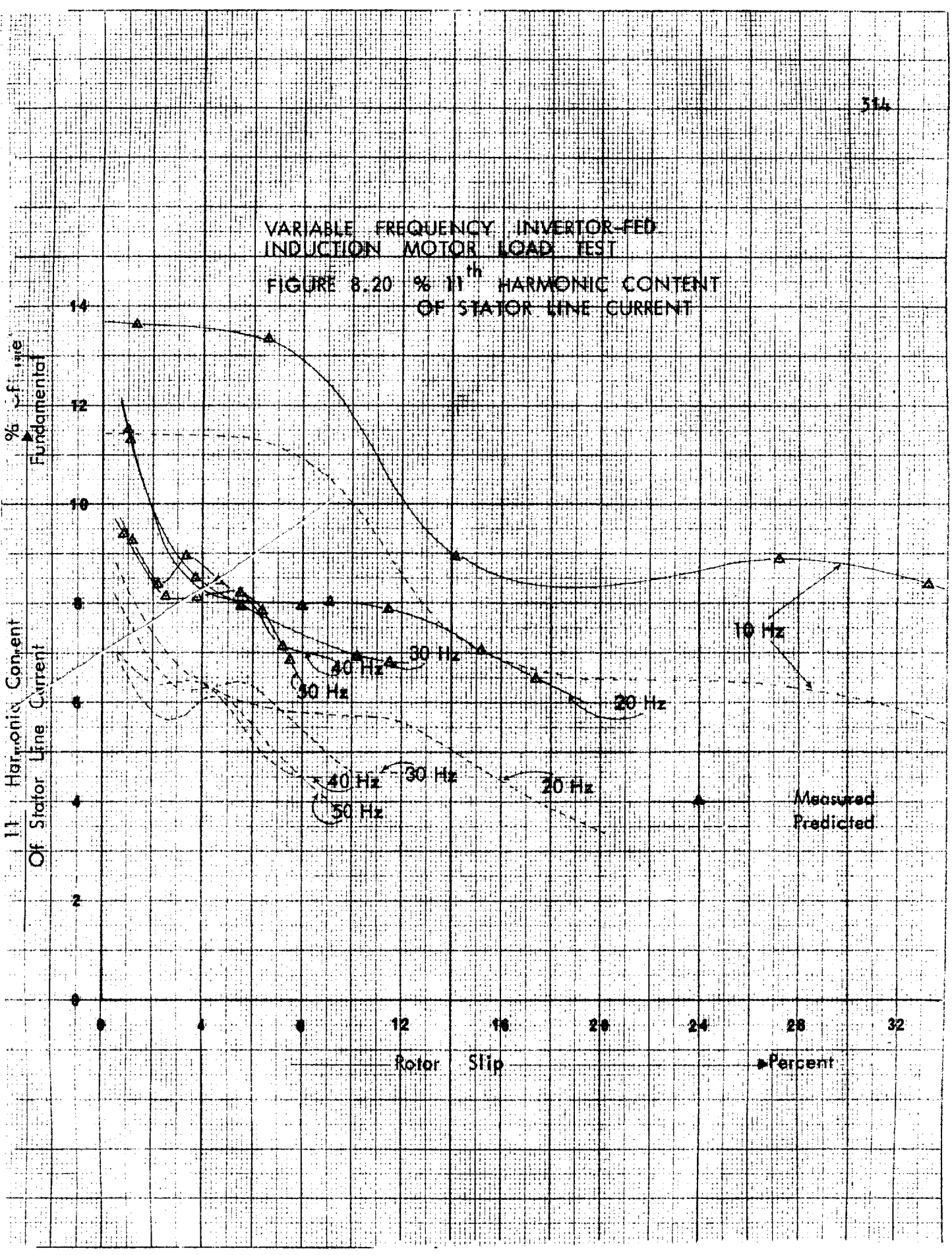

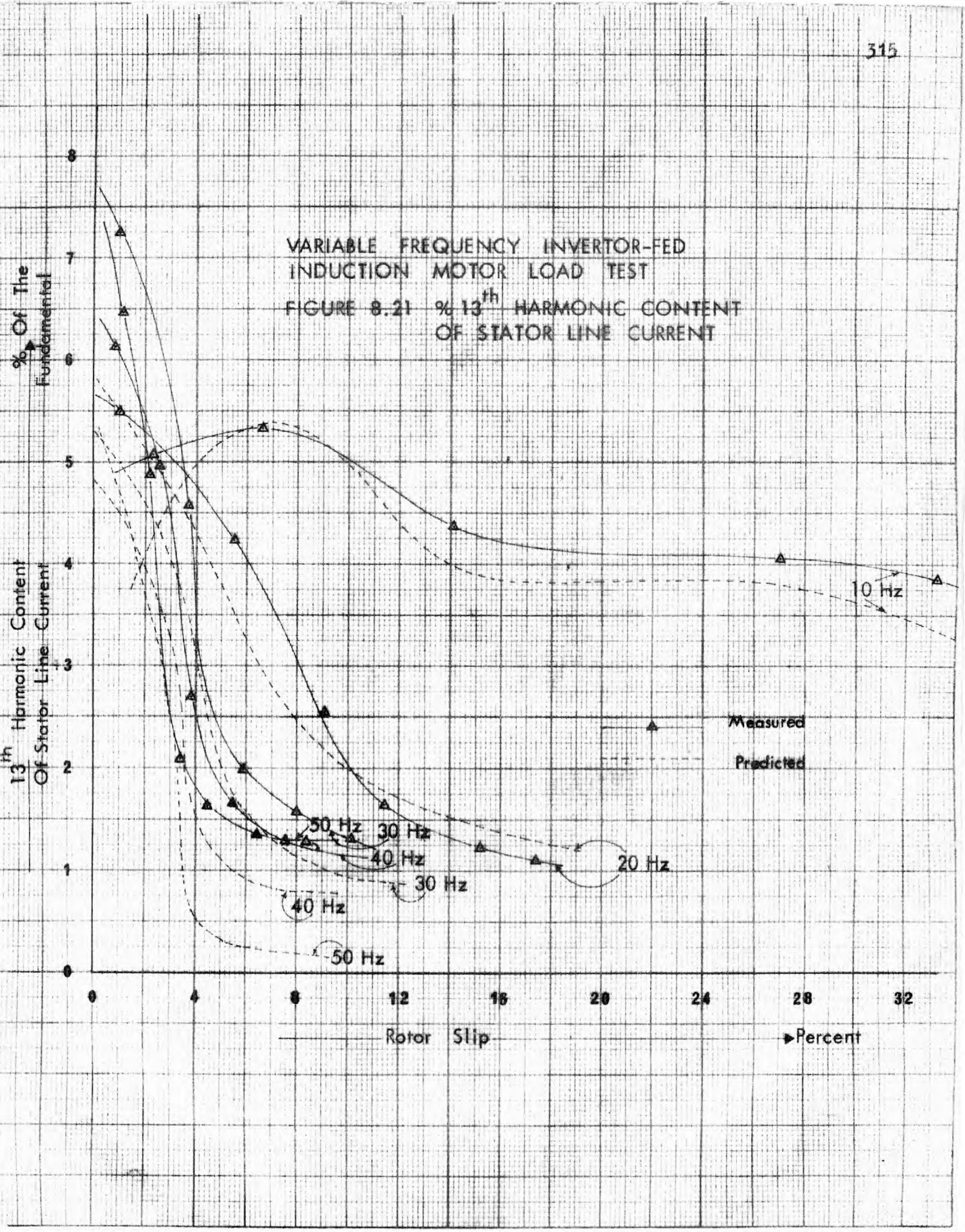
VARIABLE FREQUENCY INVERTOR-FED
INDUCTION MOTOR LOAD TEST
FIGURE 8.21 % 13th HARMONIC CONTENT
OF STATOR LINE CURRENT
% Of The Fundamental
13th Harmonic Content Of Stator Line Current
8
7
6
5
4
3
2
1
0
0
4
8
12
16
20
24
28
32
Rotor Slip
Percent
Measured
Predicted
10 Hz
20 Hz
30 Hz
40 Hz
50 Hz
50 Hz
30 Hz
40 Hz

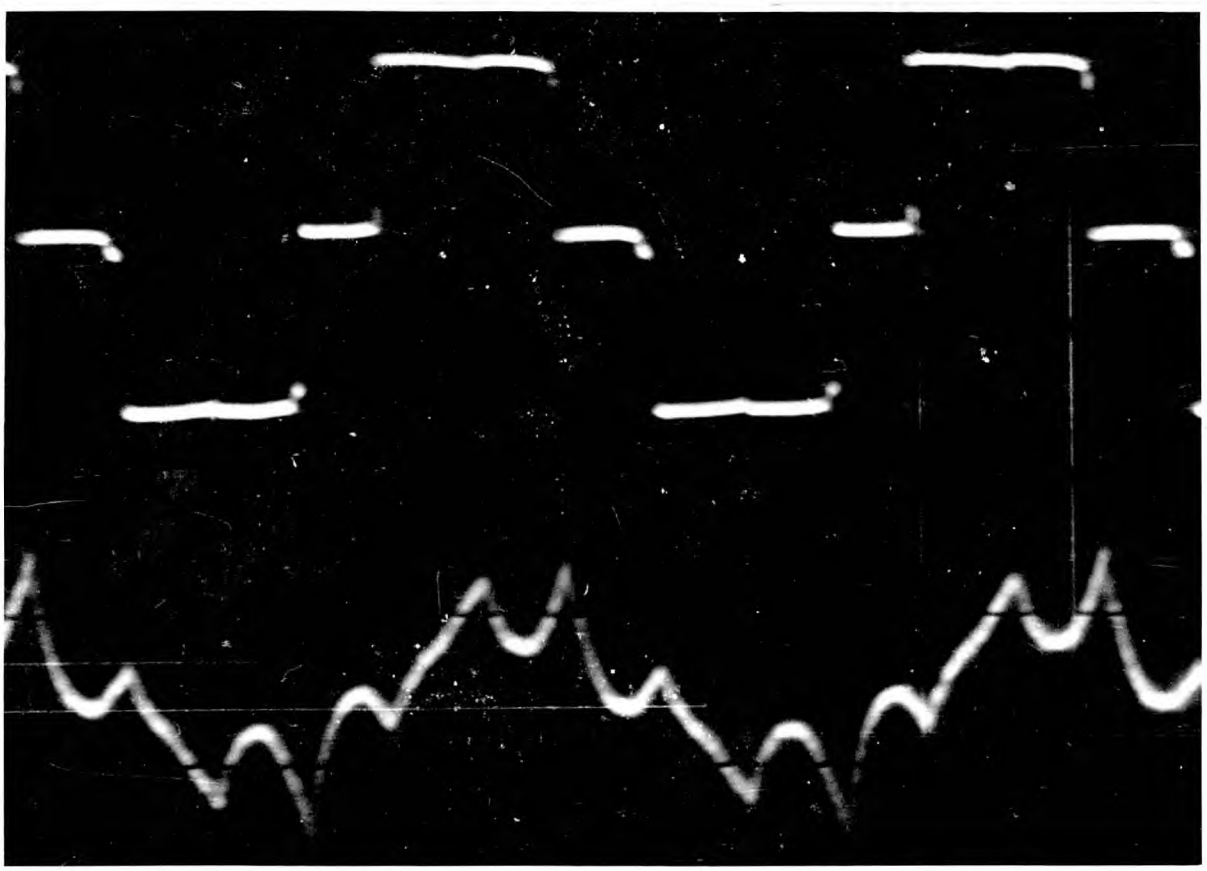

TOP TRACE: LINE TO LINE VOLTAGE : SCALE 54 V/cm

BOTTOM TRACE: LINE CURRENT : SCALE 14.2 A/cm

VARIABLE FREQUENCY INVERTOR-FED INDUCTION MOTOR LOAD TEST.

FIGURE 8.22 STATOR LINE CURRENT WAVE-FORM

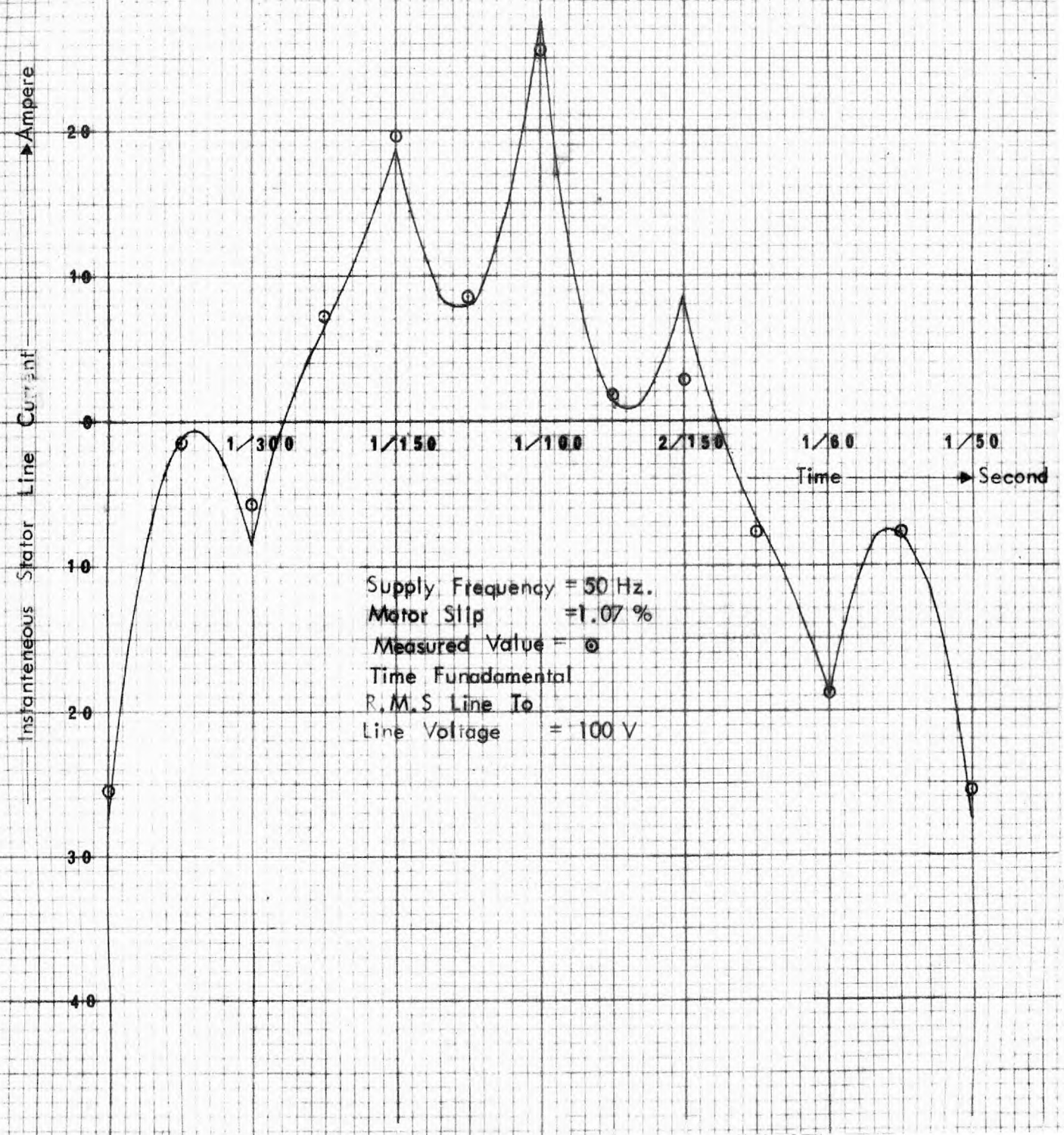

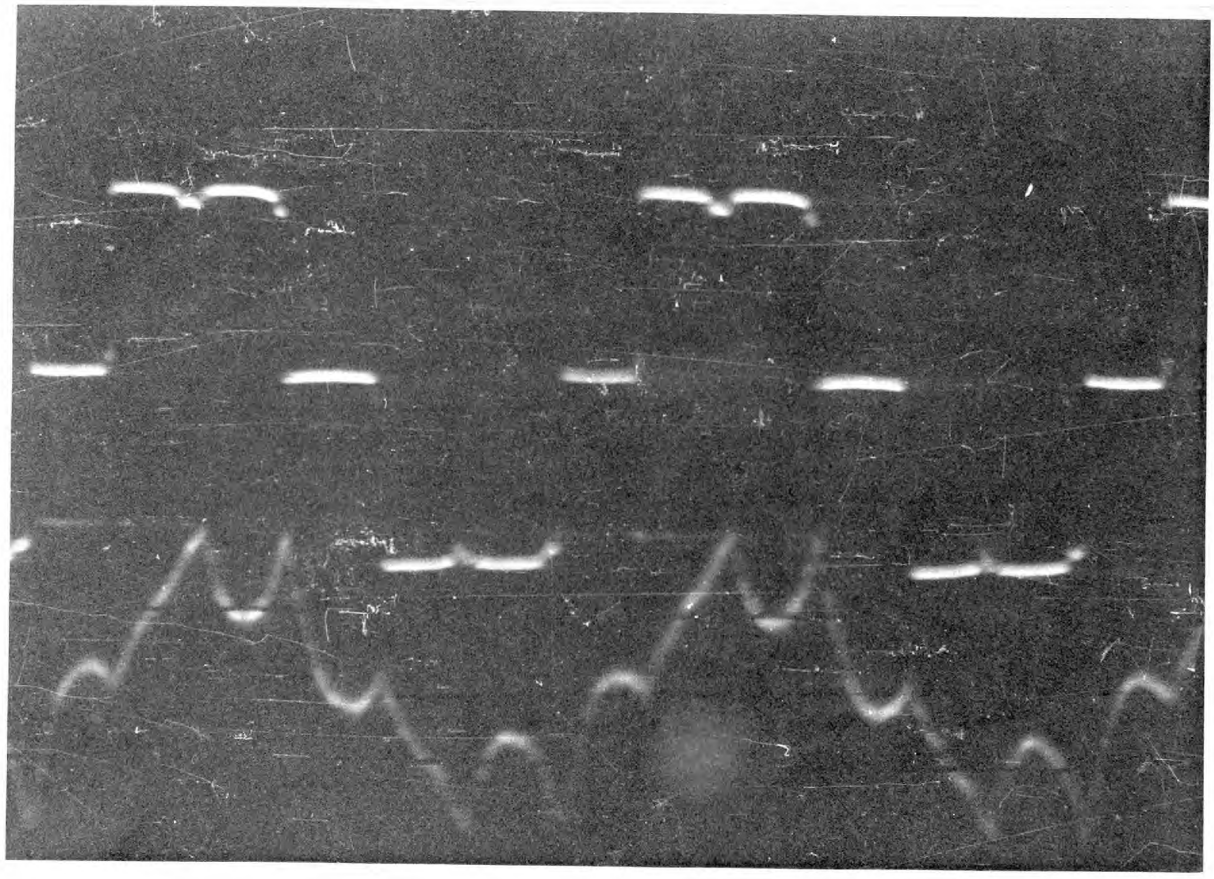

TOP TRACE: LINE TO LINE VOLTAGE : SCALE 54 V/cm

BOTTOM TRACE: LINE CURRENT : SCALE 14.2 A/cm

VARIABLE FREQUENCY INVERTOR-FED INDUCTION MOTOR LOAD TEST.

FIGURE 8.23 STATOR LINE CURRENT WAVE-FORM.

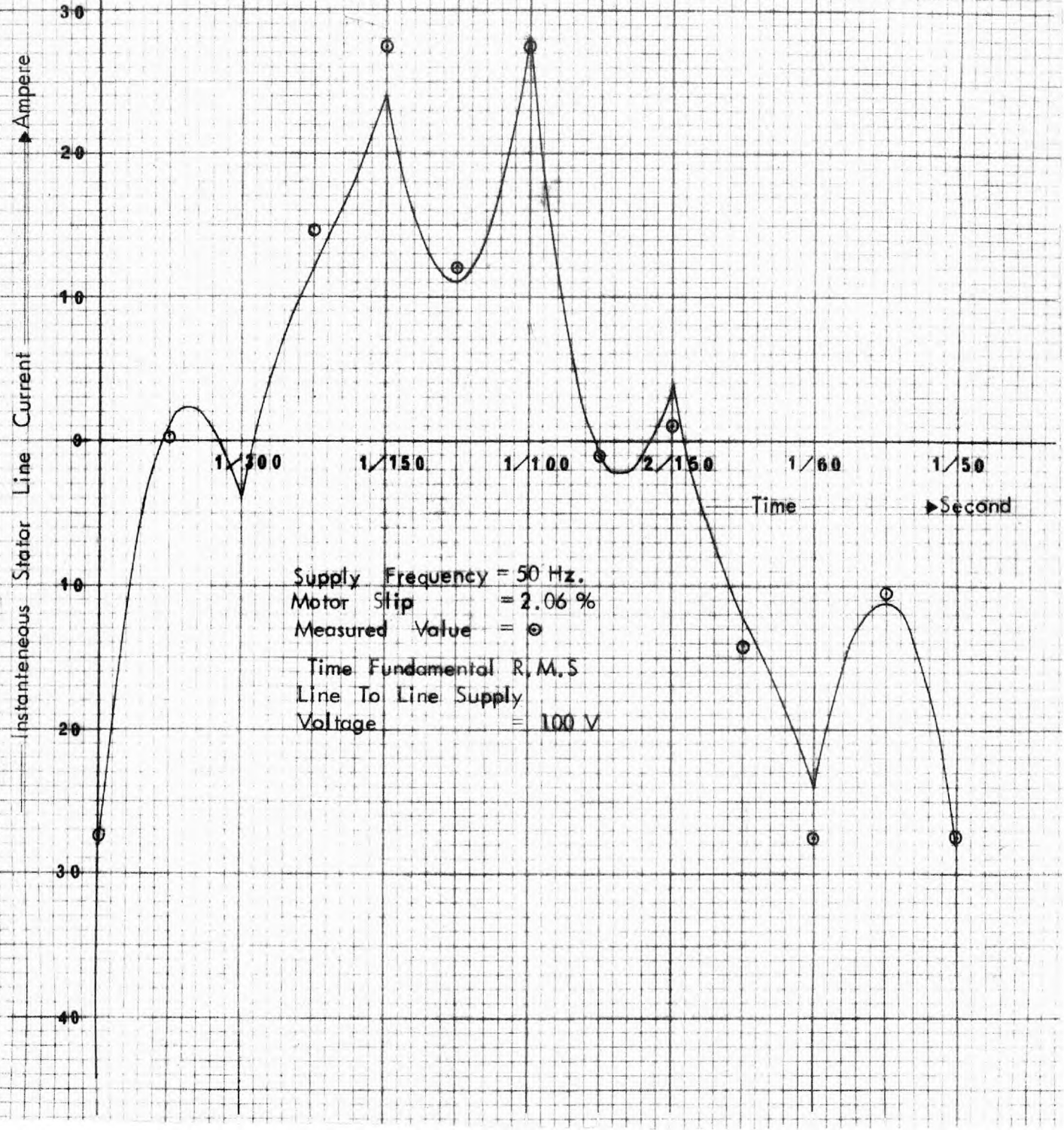

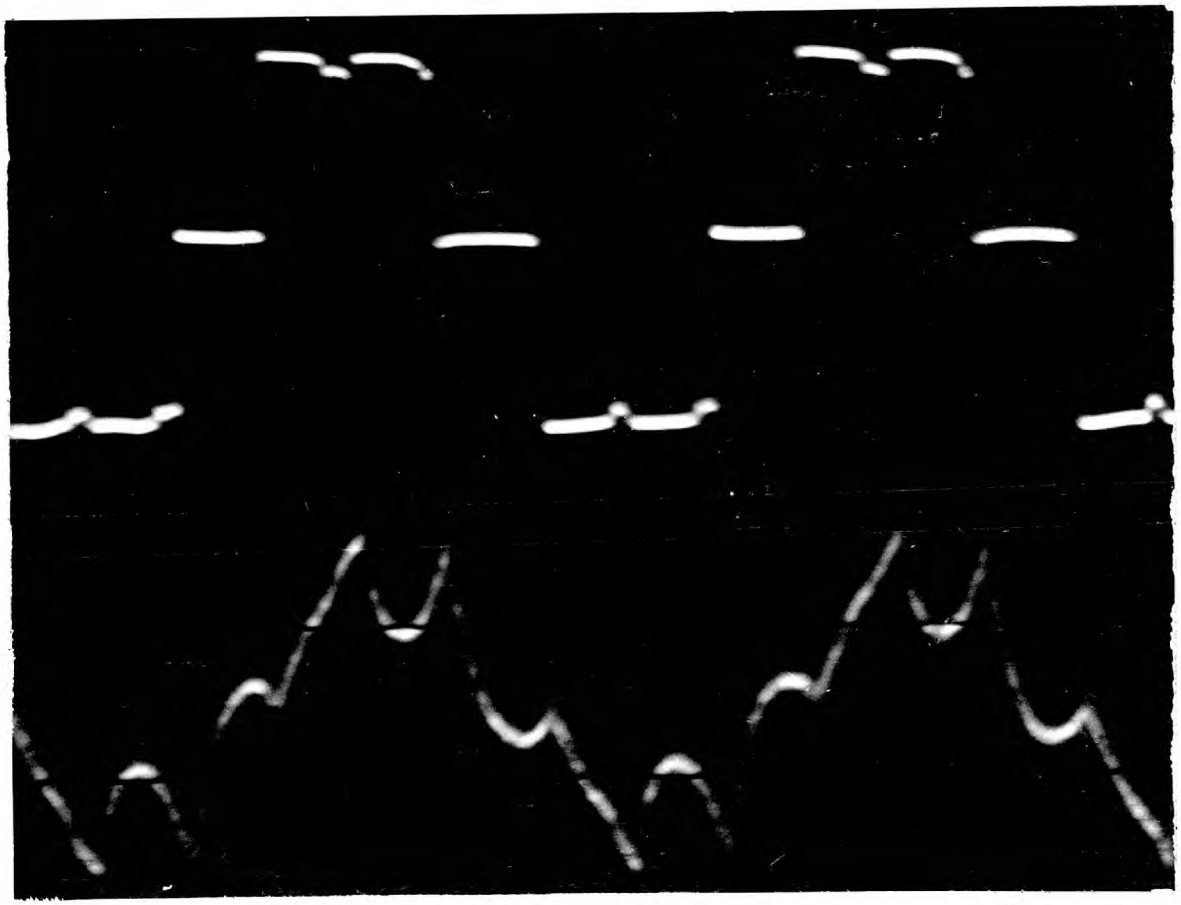

TOP TRACE : LINE TO LINE VOLTAGE : SCALE 54 V/cm

BOTTOM TRACE: LINE CURRENT : SCALE 14.2 A/cm

VARIABLE FREQUENCY INVERTOR-FED INDUCTION MOTOR
LOAD TEST

FIGURE 8.24 STATOR LINE CURRENT WAVE-FORM

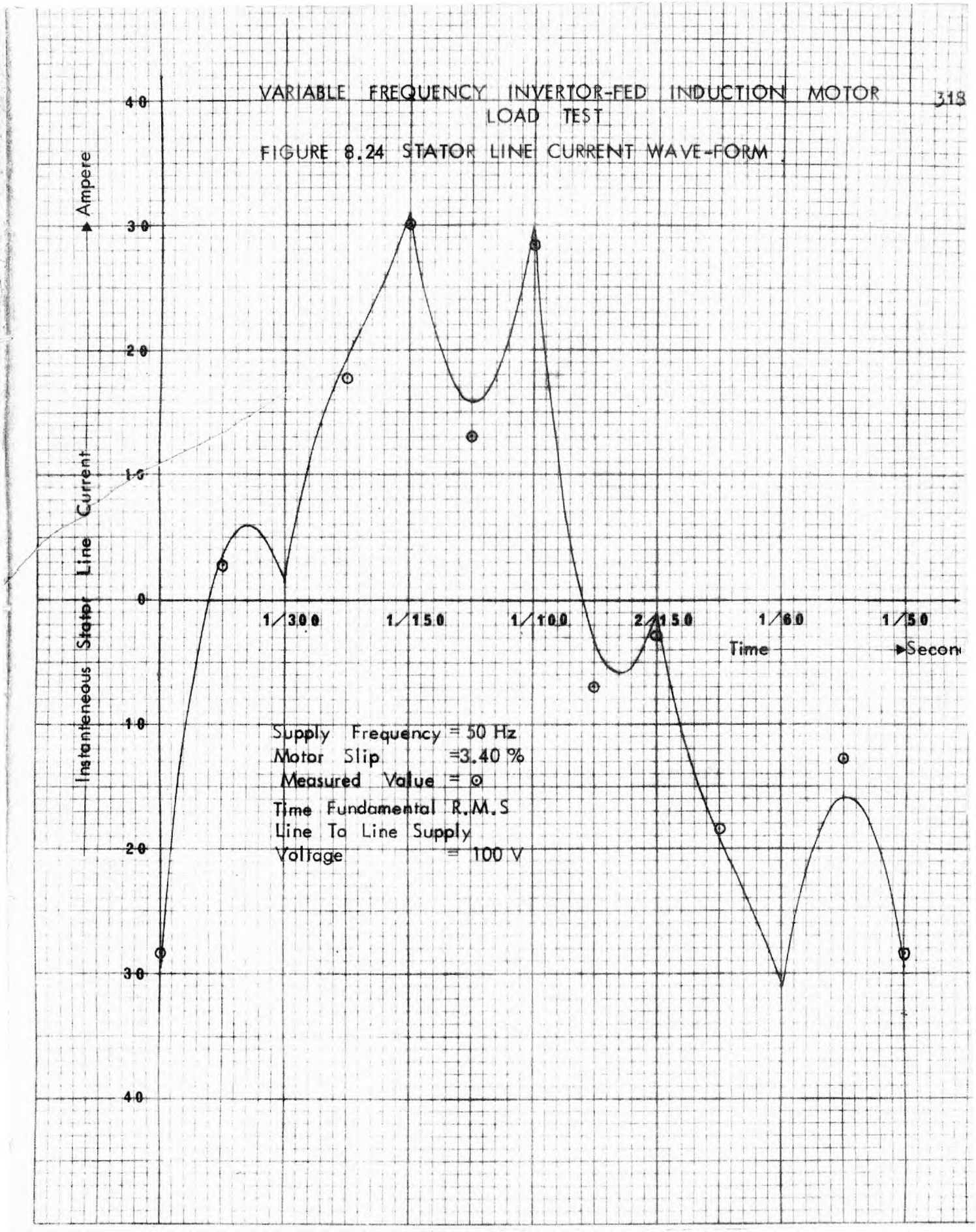

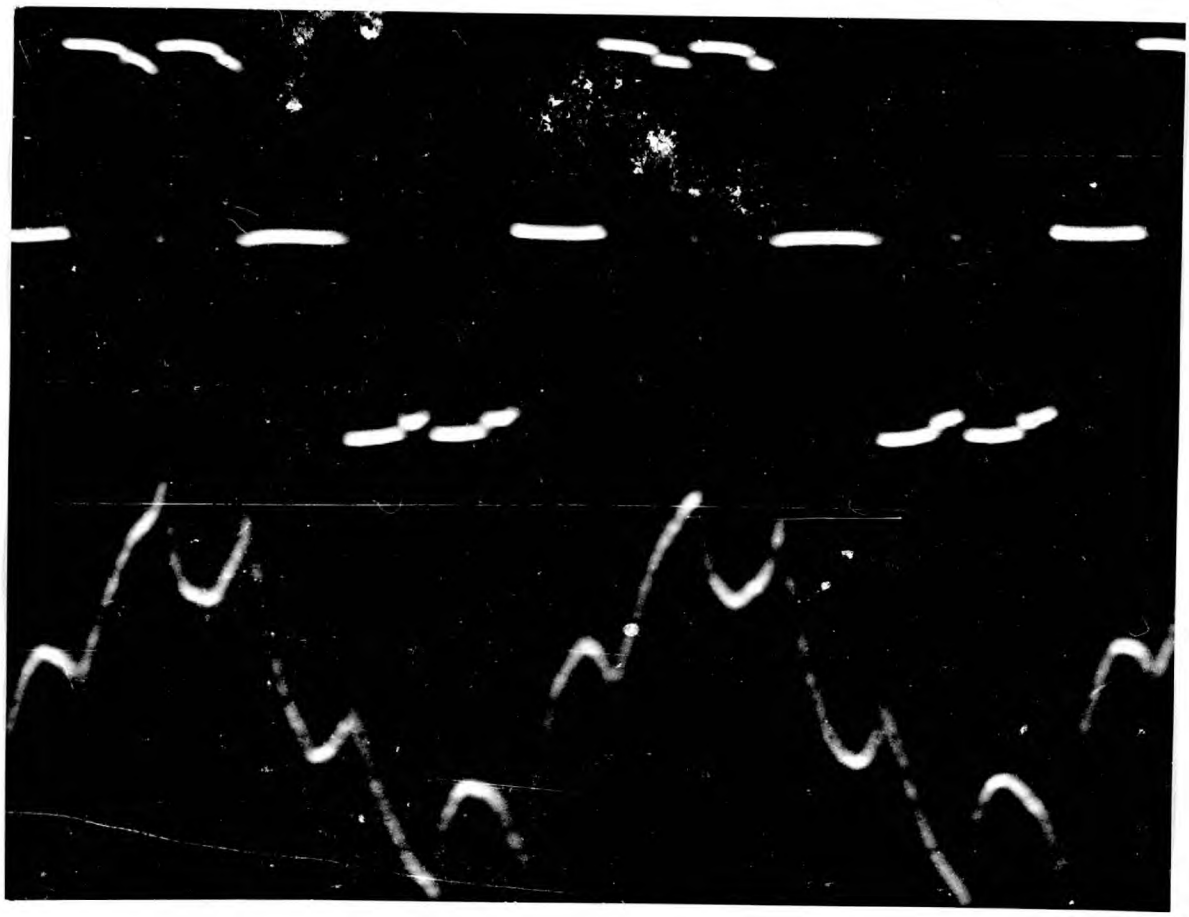

TOP TRACE : LINE TO LINE VOLTAGE : SCALE 54 V/cm

BOTTOM TRACE: LINE CURRENT : SCALE 14.2 A/cm

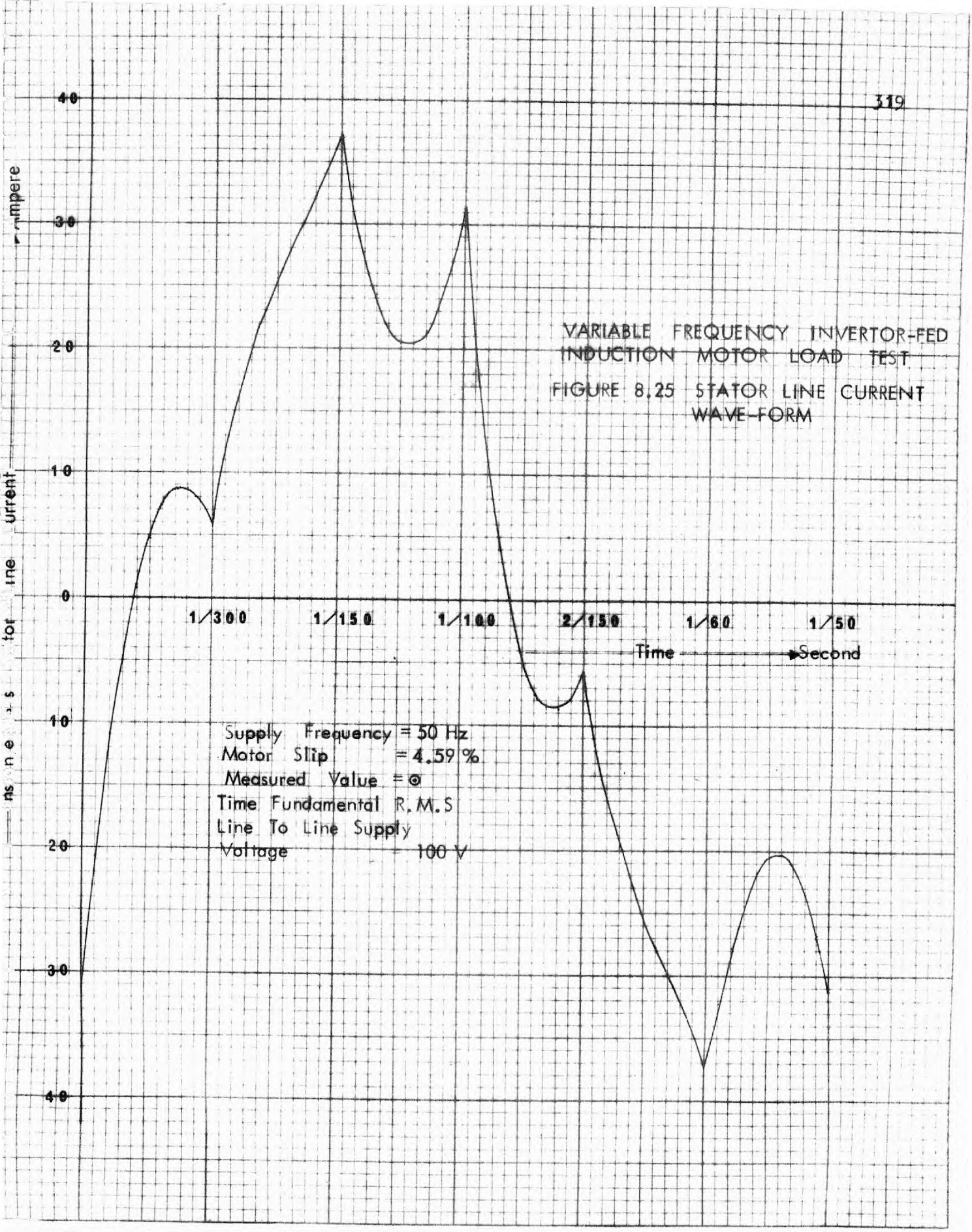

VARIABLE FREQUENCY INVERTOR-FED INDUCTION MOTOR LOAD TEST

FIGURE 8.25 STATOR LINE CURRENT WAVE-FORM

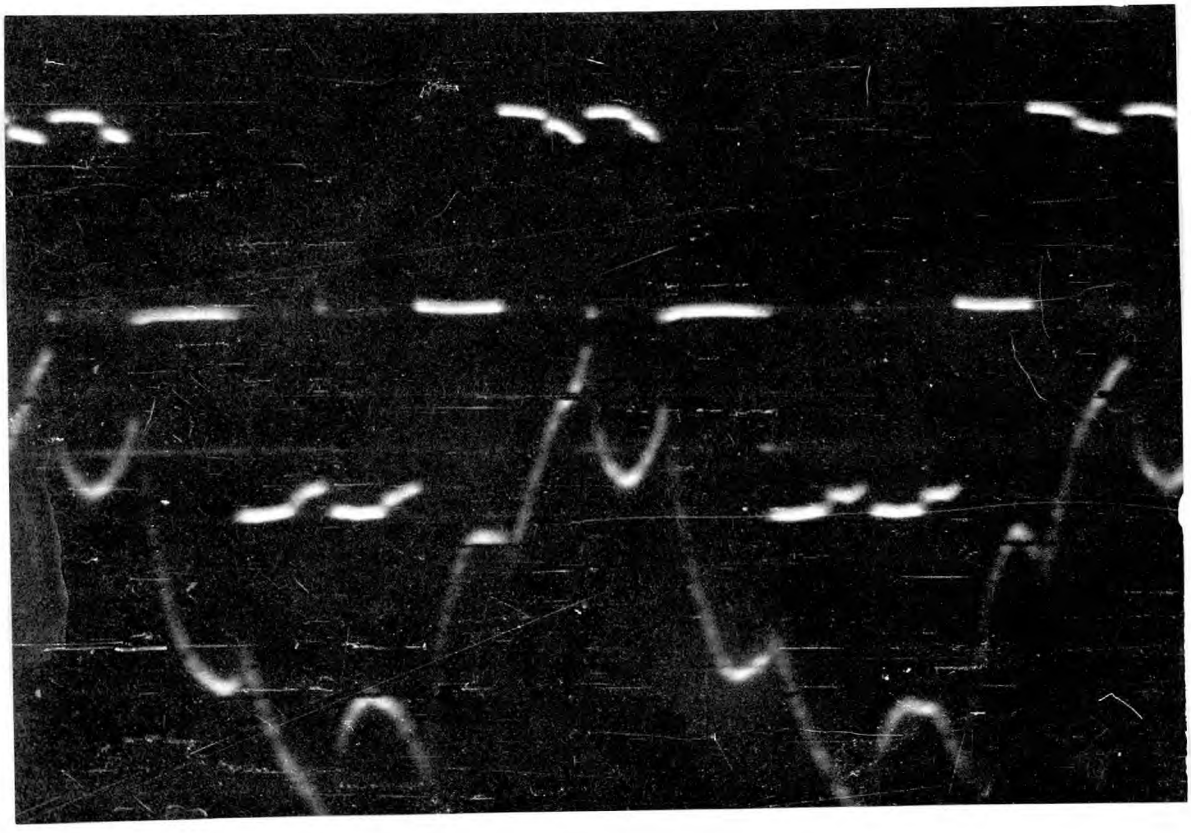

TOP TRACE : LINE TO LINE VOLTAGE : SCALE 54 V/cm

BOTTOM TRACE: LINE CURRENT : SCALE 14.2 A/cm

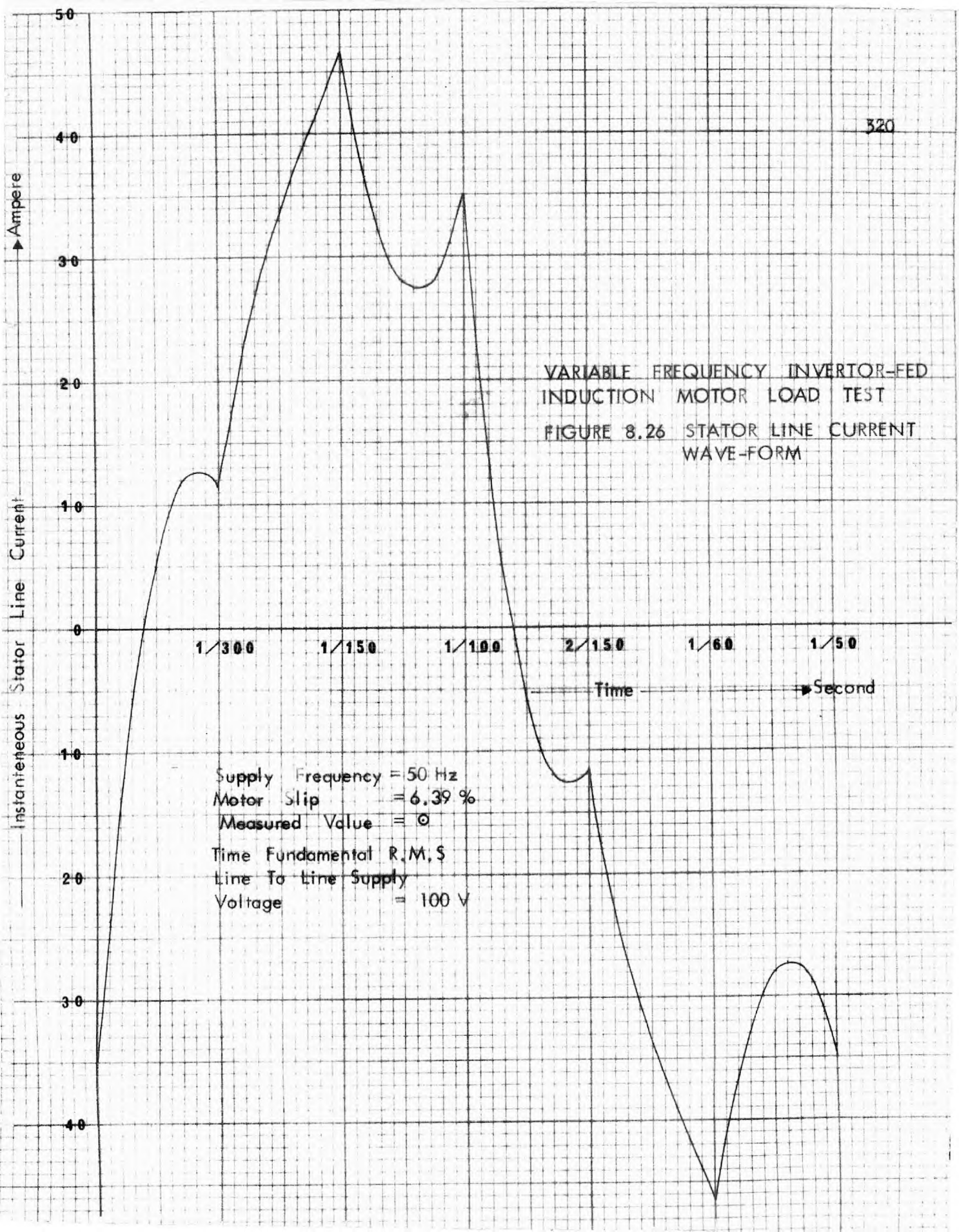

VARIABLE FREQUENCY INVERTOR-FED INDUCTION MOTOR LOAD TEST

FIGURE 8.26 STATOR LINE CURRENT WAVE-FORM

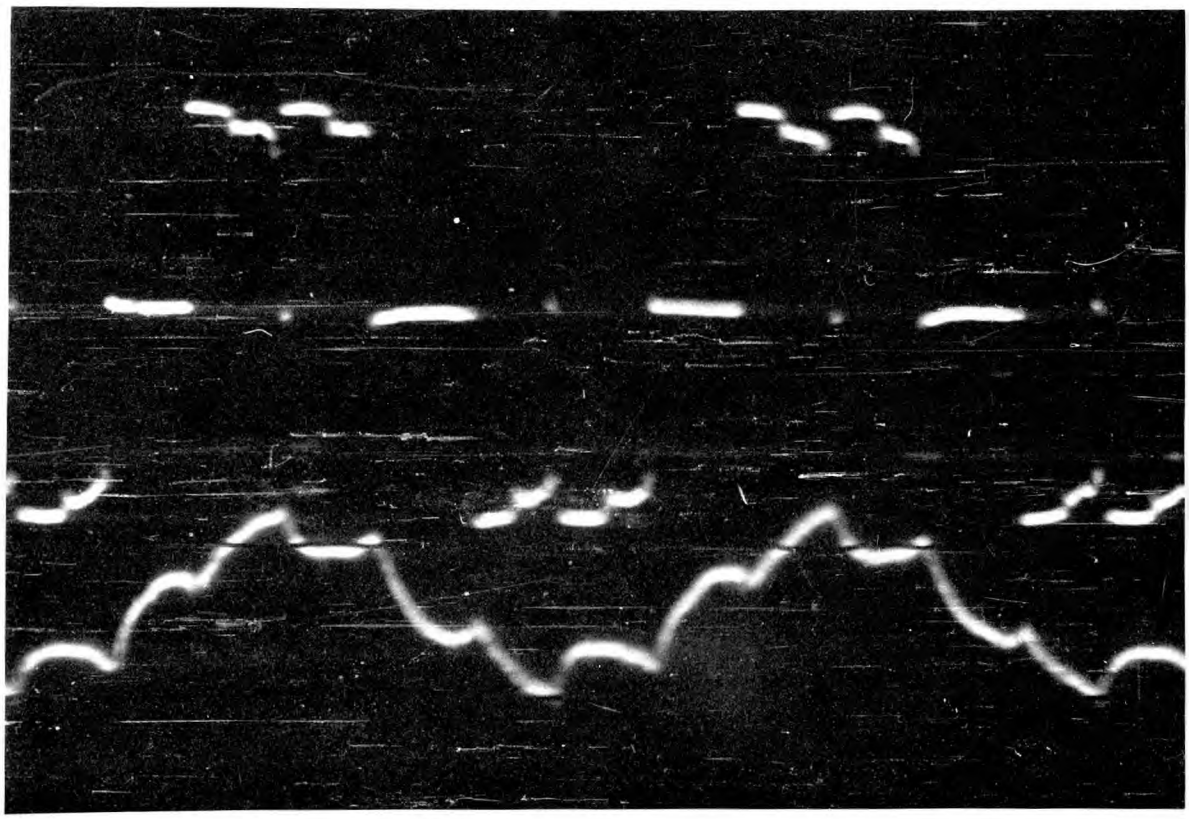

TOP TRACE: LINE TO LINE VOLTAGE : SCALE 54 V/cm

BOTTOM TRACE : LINE CURRENT : SCALE 42.6 A/cm

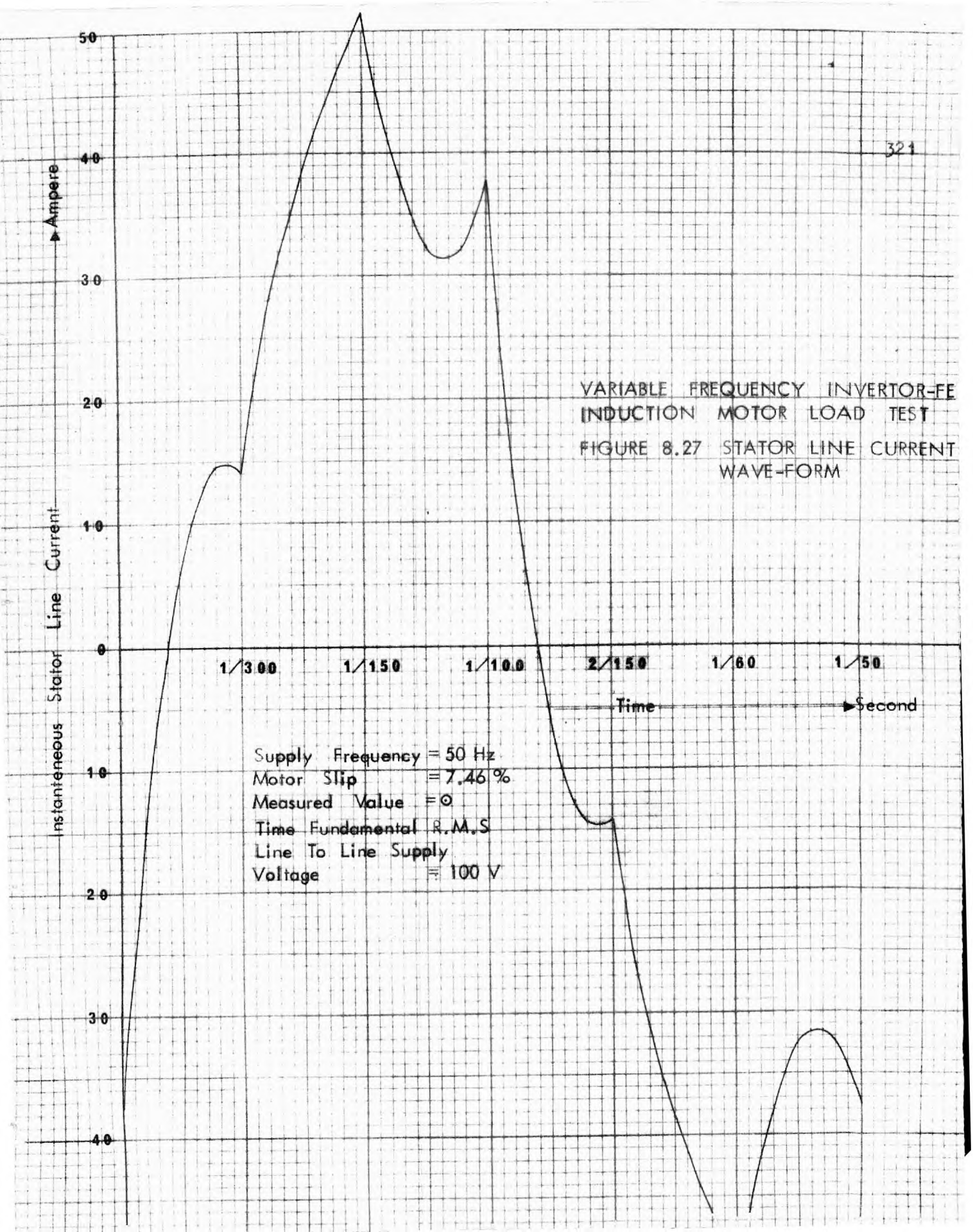

VARIABLE FREQUENCY INVERTOR-FE INDUCTION MOTOR LOAD TEST

FIGURE 8.27 STATOR LINE CURRENT WAVE-FORM

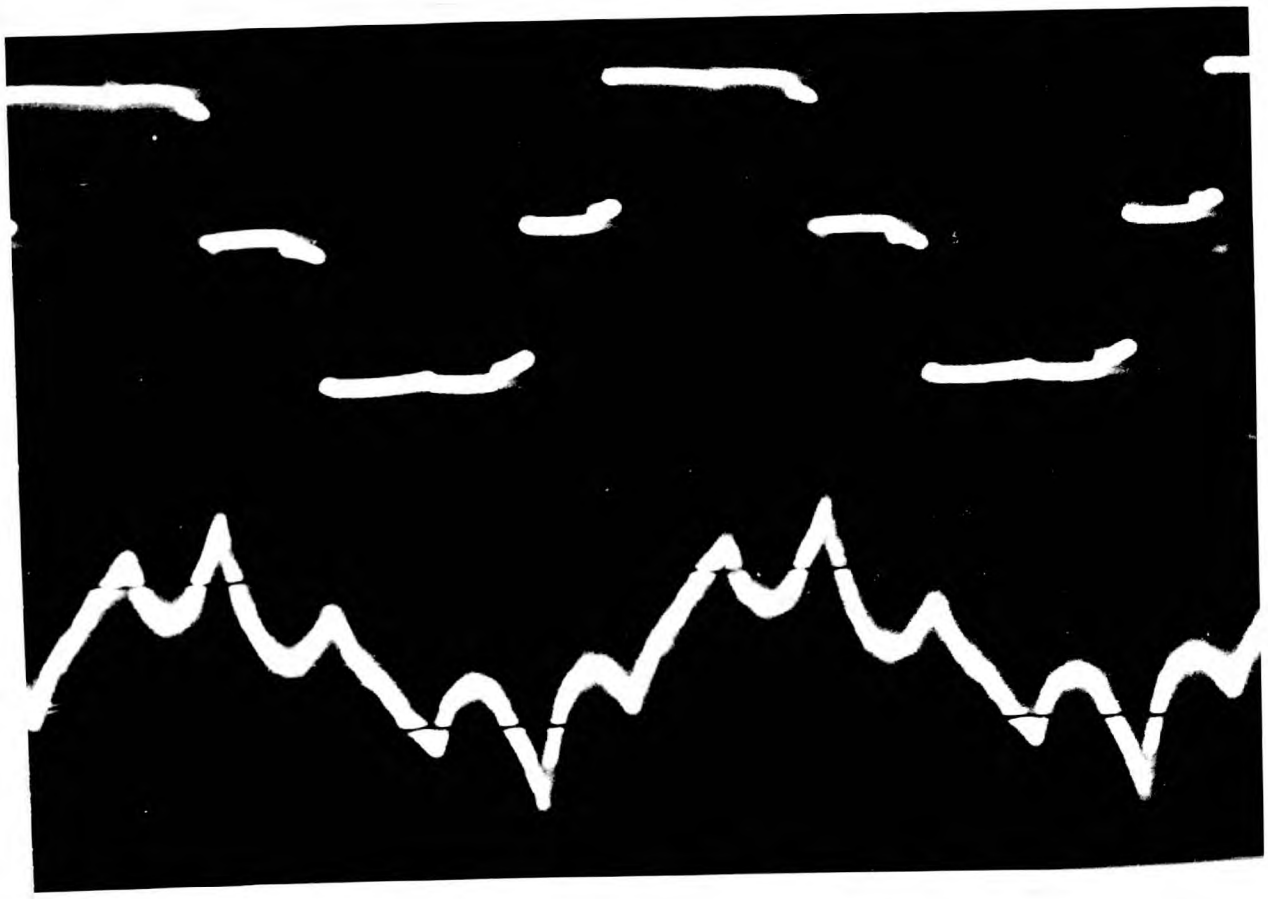

TOP TRACE : LINE TO LINE VOLTAGE : SCALE 54 V/cm

BOTTOM TRACE: LINE CURRENT : SCALE 14.2 A/cm

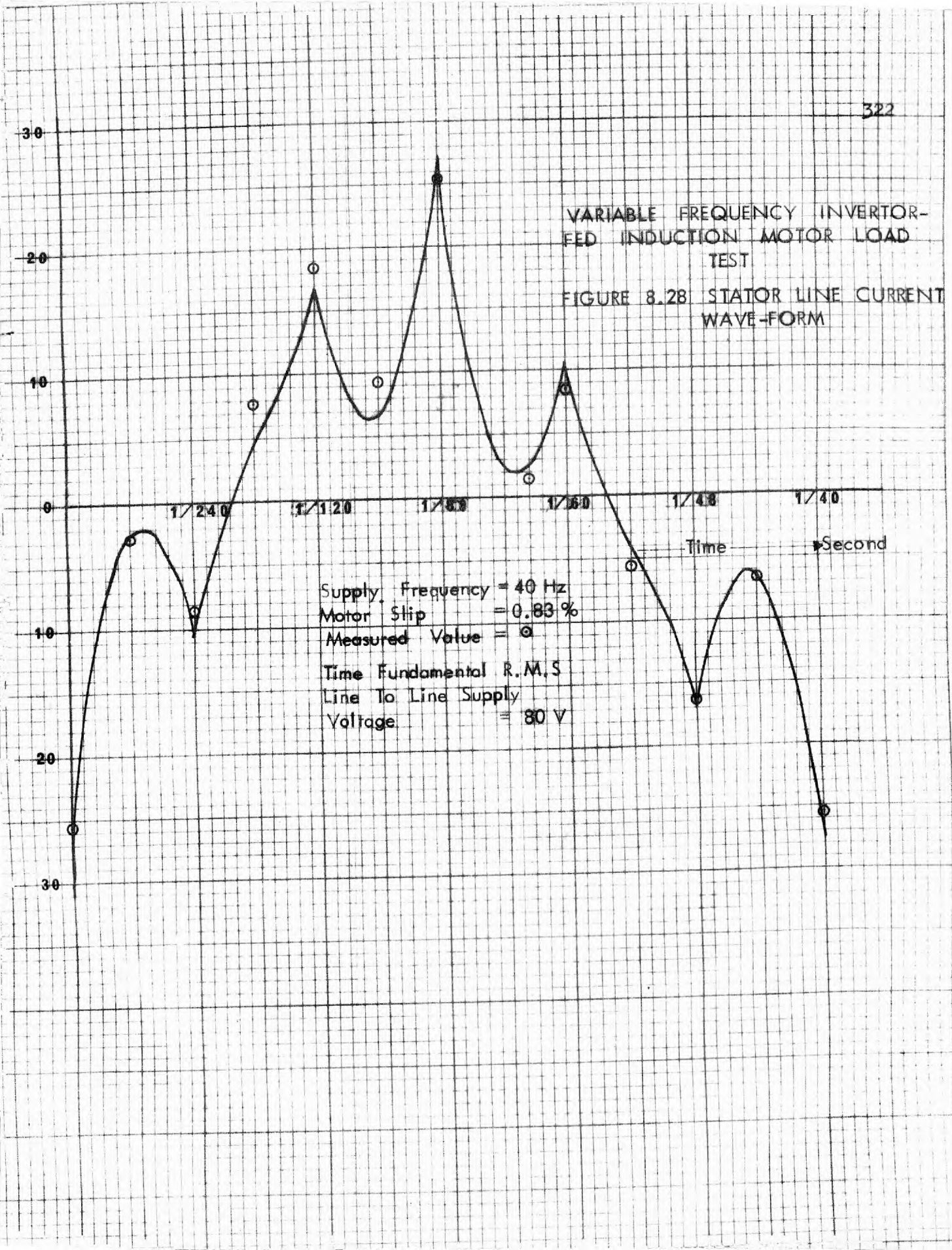

VARIABLE FREQUENCY INVERTOR-FED INDUCTION MOTOR LOAD TEST

FIGURE 8.28 STATOR LINE CURRENT WAVE-FORM

TOP TRACE: LINE TO LINE VOLTAGE : SCALE 54 V/cm

BOTTOM TRACE : LINE CURRENT : SCALE 14.2 A/cm

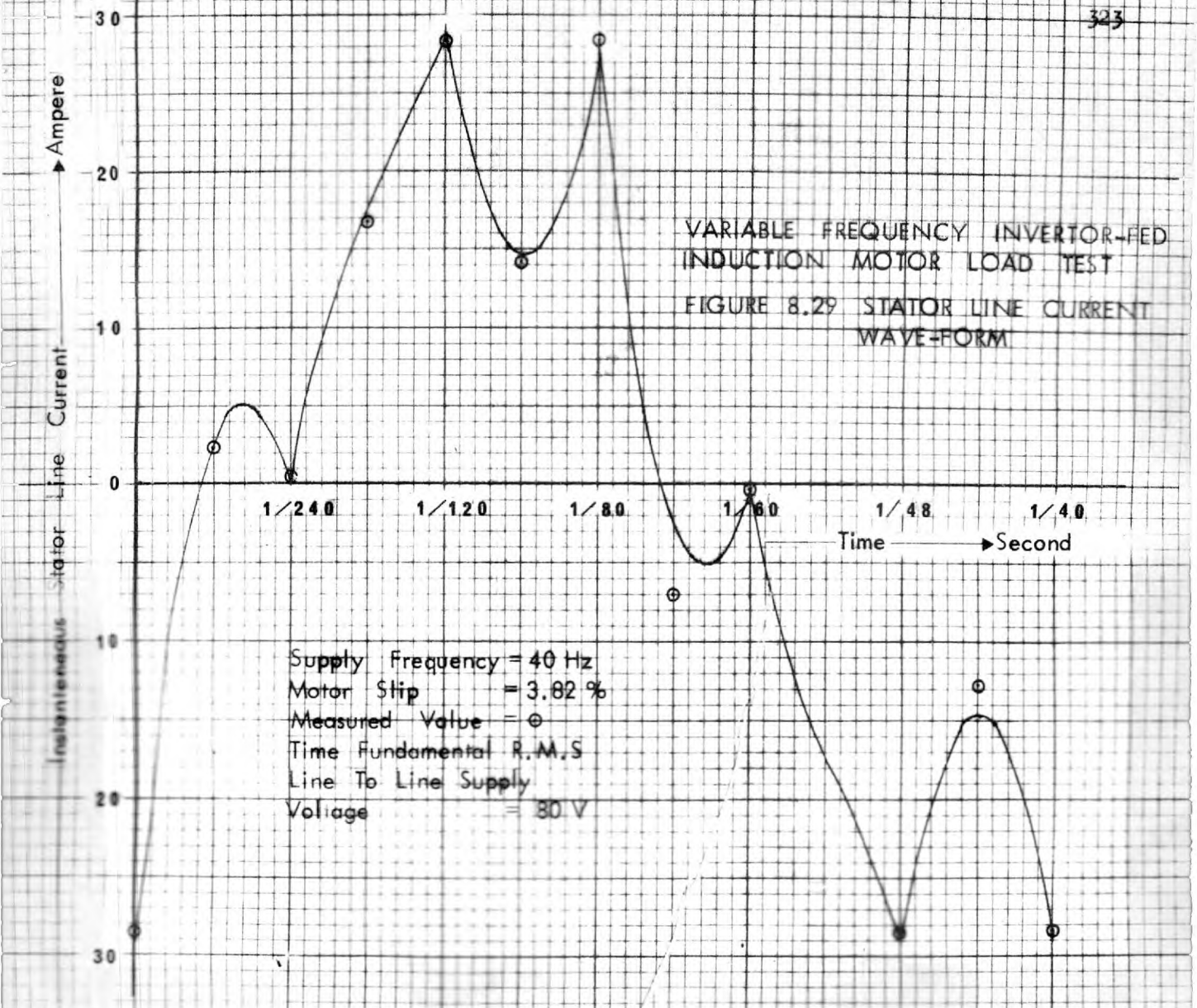

VARIABLE FREQUENCY INVERTOR-FED INDUCTION MOTOR LOAD TEST

FIGURE 8.29 STATOR LINE CURRENT WAVE-FORM

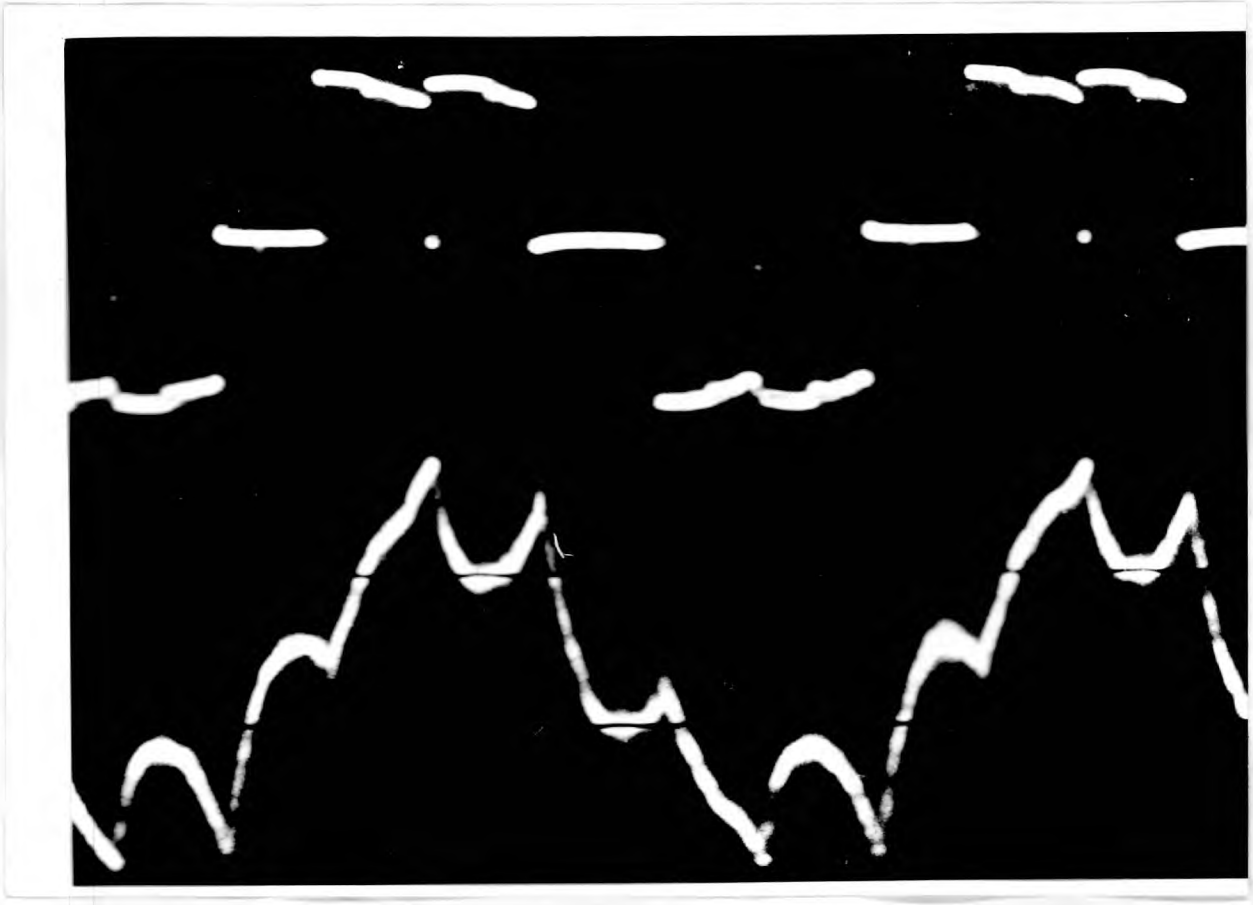

TOP TRACE: LINE TO LINE VOLTAGE : SCALE 54 V/cm

BOTTOM TRACE : LINE CURRENT : SCALE 14.2 A/cm

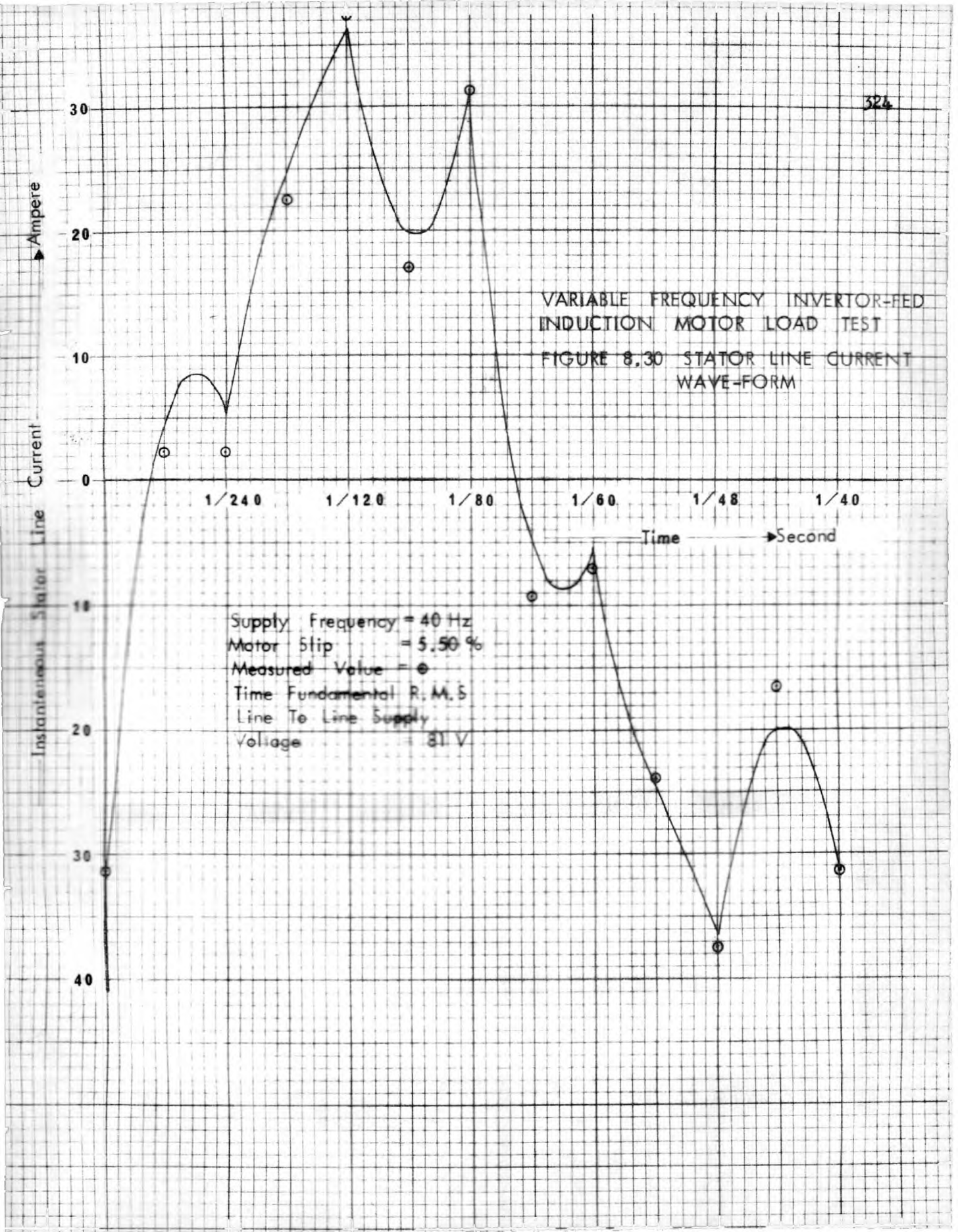

VARIABLE FREQUENCY INVERTOR-FED INDUCTION MOTOR LOAD TEST

FIGURE 8.30 STATOR LINE CURRENT WAVE-FORM

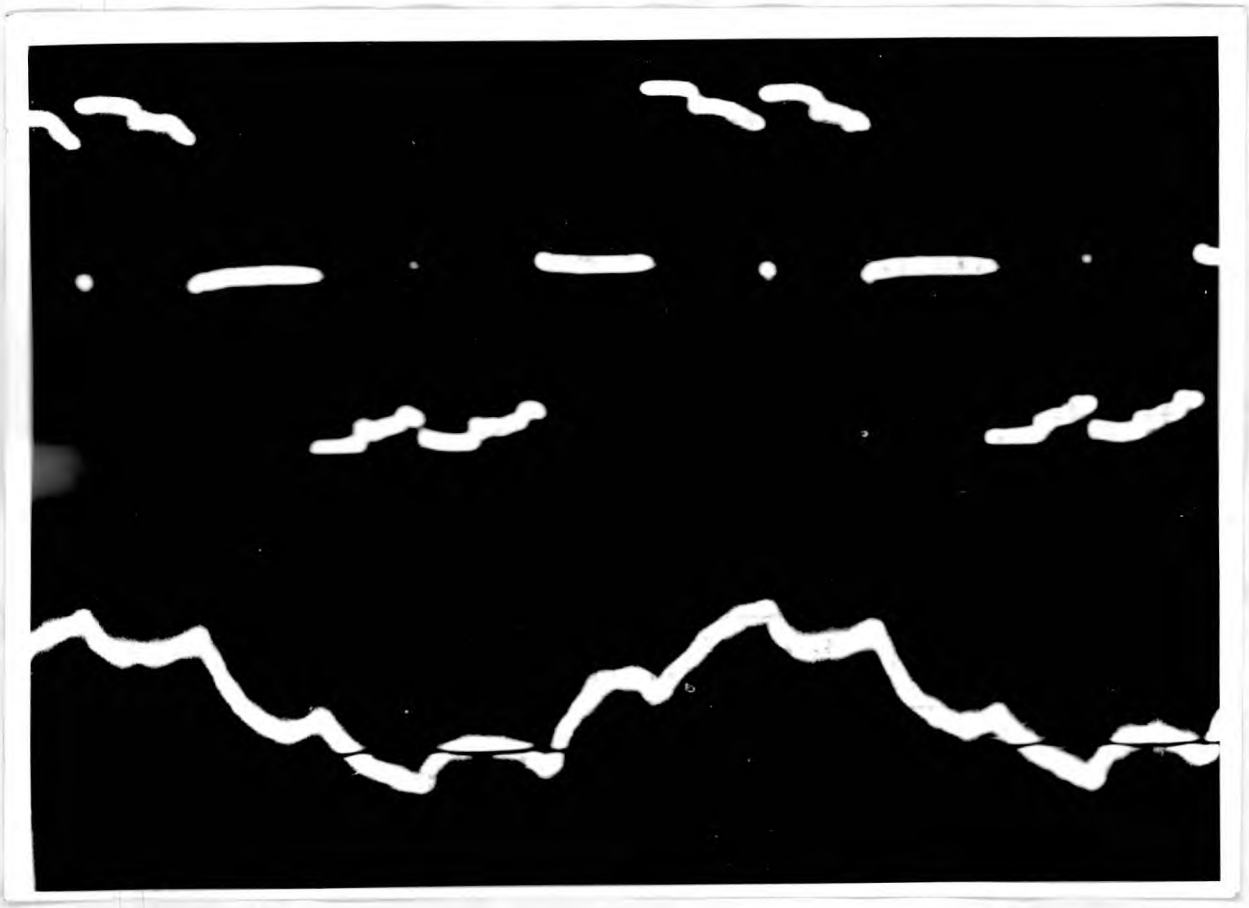

TOP TRACE: LINE TO LINE VOLTAGE : SCALE 54 V/cm

BOTTOM TRACE : LINE CURRENT : SCALE 42.6 A/cm

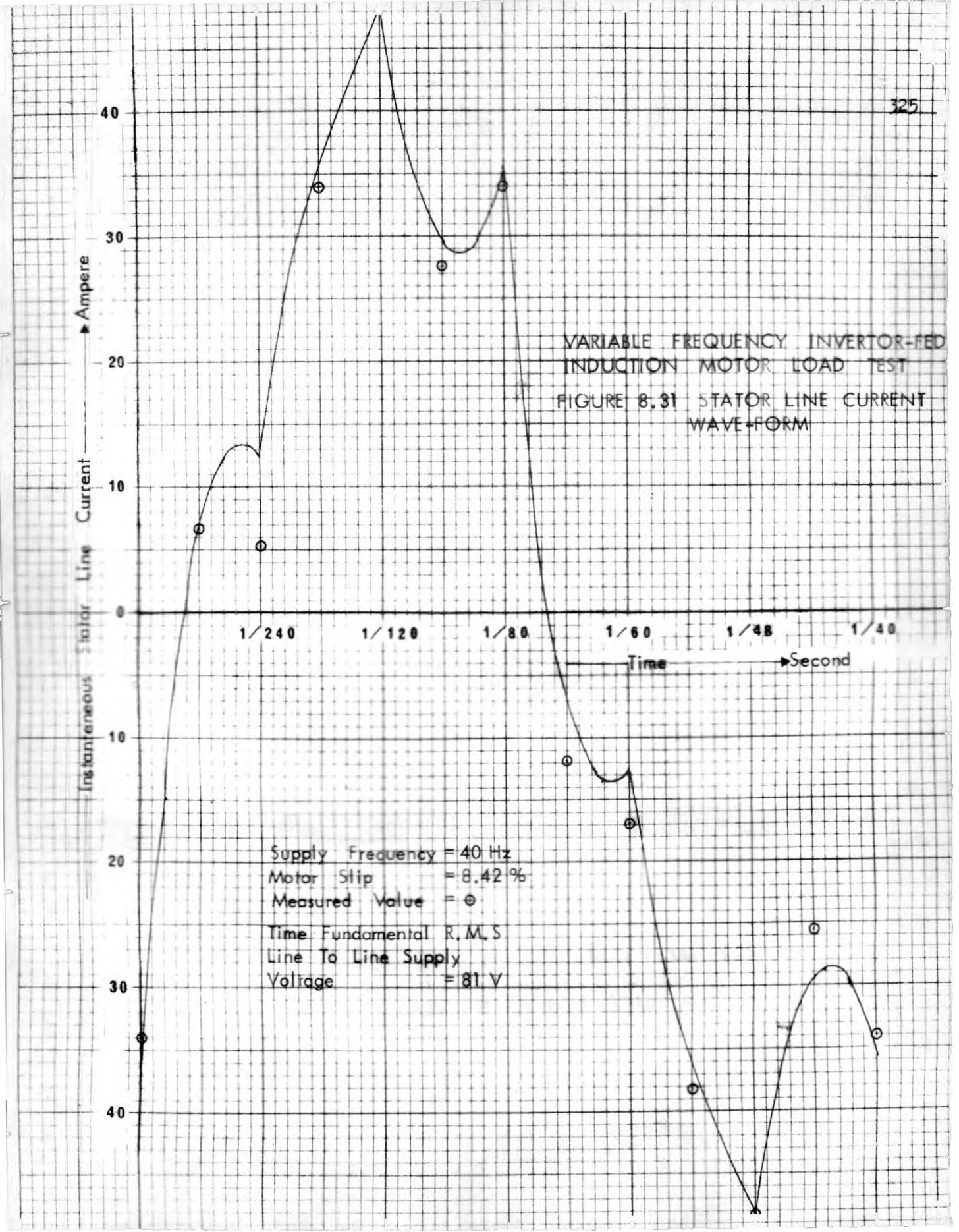

VARIABLE FREQUENCY INVERTOR-FED INDUCTION MOTOR LOAD TEST

FIGURE 8.31 STATOR LINE CURRENT WAVE-FORM

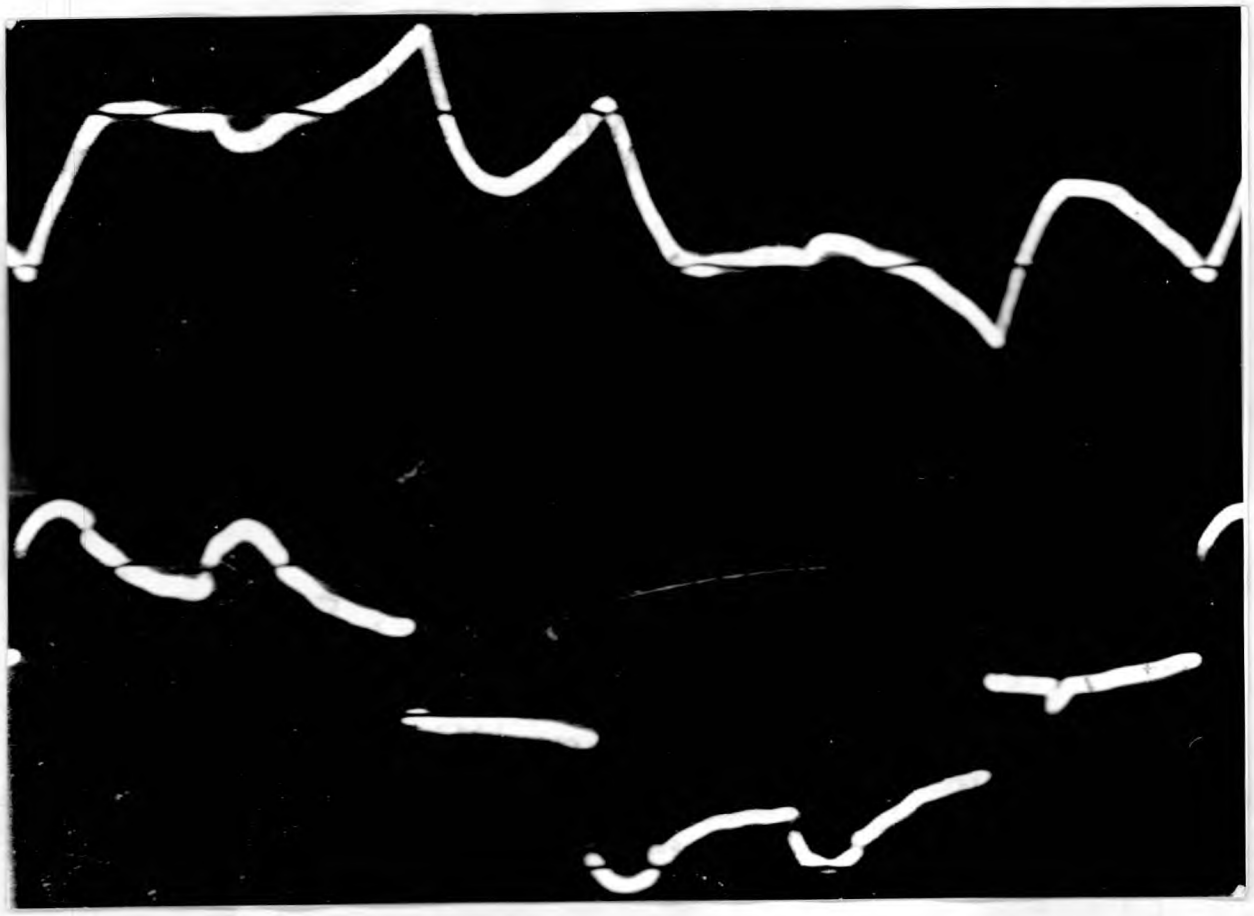

TOP TRACE: LINE CURRENT: SCALE 14.2 A/cm

BOTTOM TRACE: LINE TO LINE VOLTAGE: SCALE 16.2 V/cm

VARIABLE FREQUENCY INVERTOR-FED INDUCTION MOTOR
LOAD TEST

FIGURE 8.32 STATOR LINE CURRENT WAVE-FORM

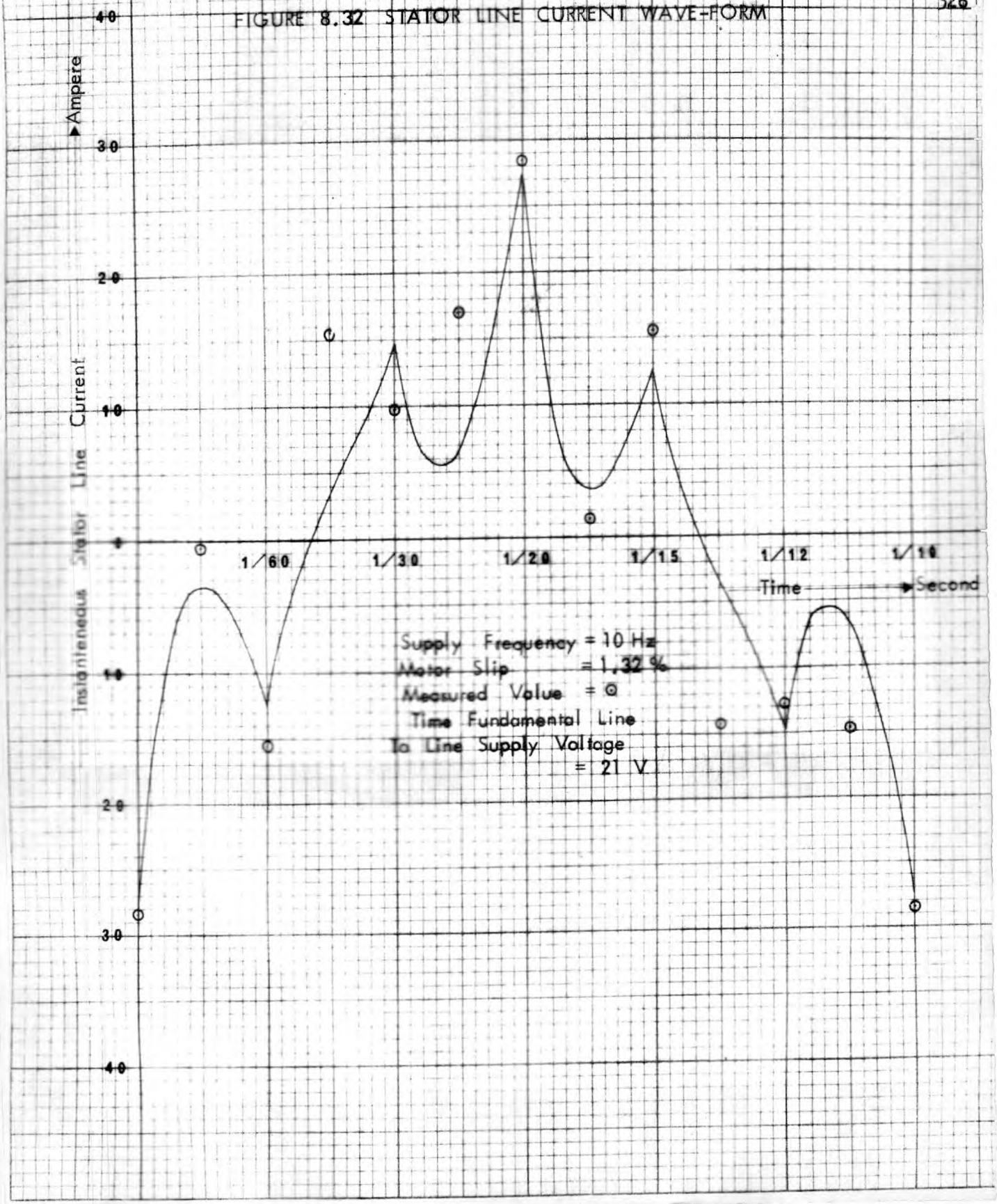

TOP TRACE: LINE CURRENT: SCALE 14.2 A/cm

BOTTOM TRACE: LINE TO LINE VOLTAGE: SCALE 16.2 V/cm

VARIABLE FREQUENCY INVERTOR-FED INDUCTION MOTOR
LOAD TEST

FIGURE 8.33 STATOR LINE CURRENT WAVE-FORM

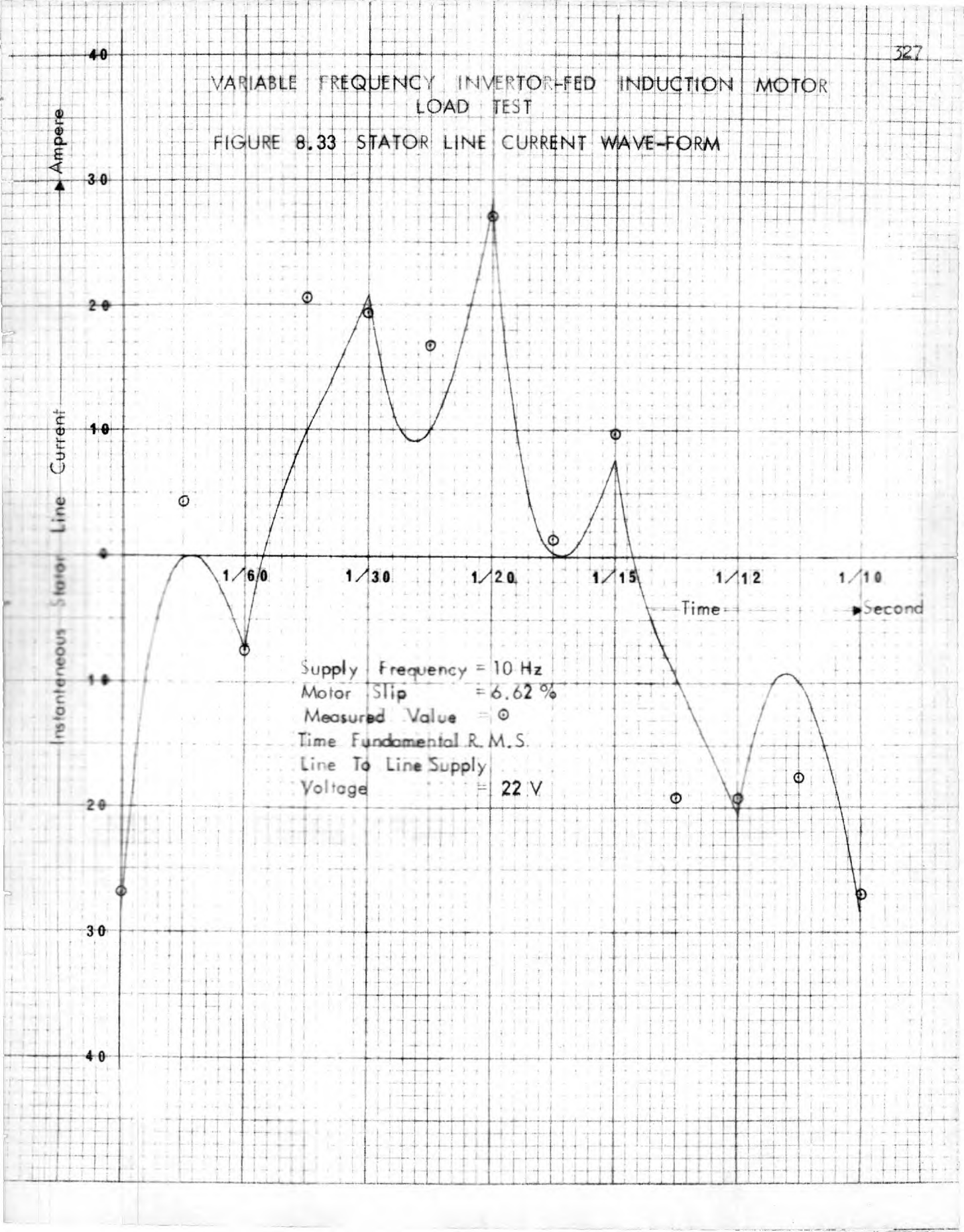

TOP TRACE: LINE CURRENT: SCALE 14.2 A/cm

BOTTOM TRACE: LINE TO LINE VOLTAGE: SCALE 16.2 V/cm

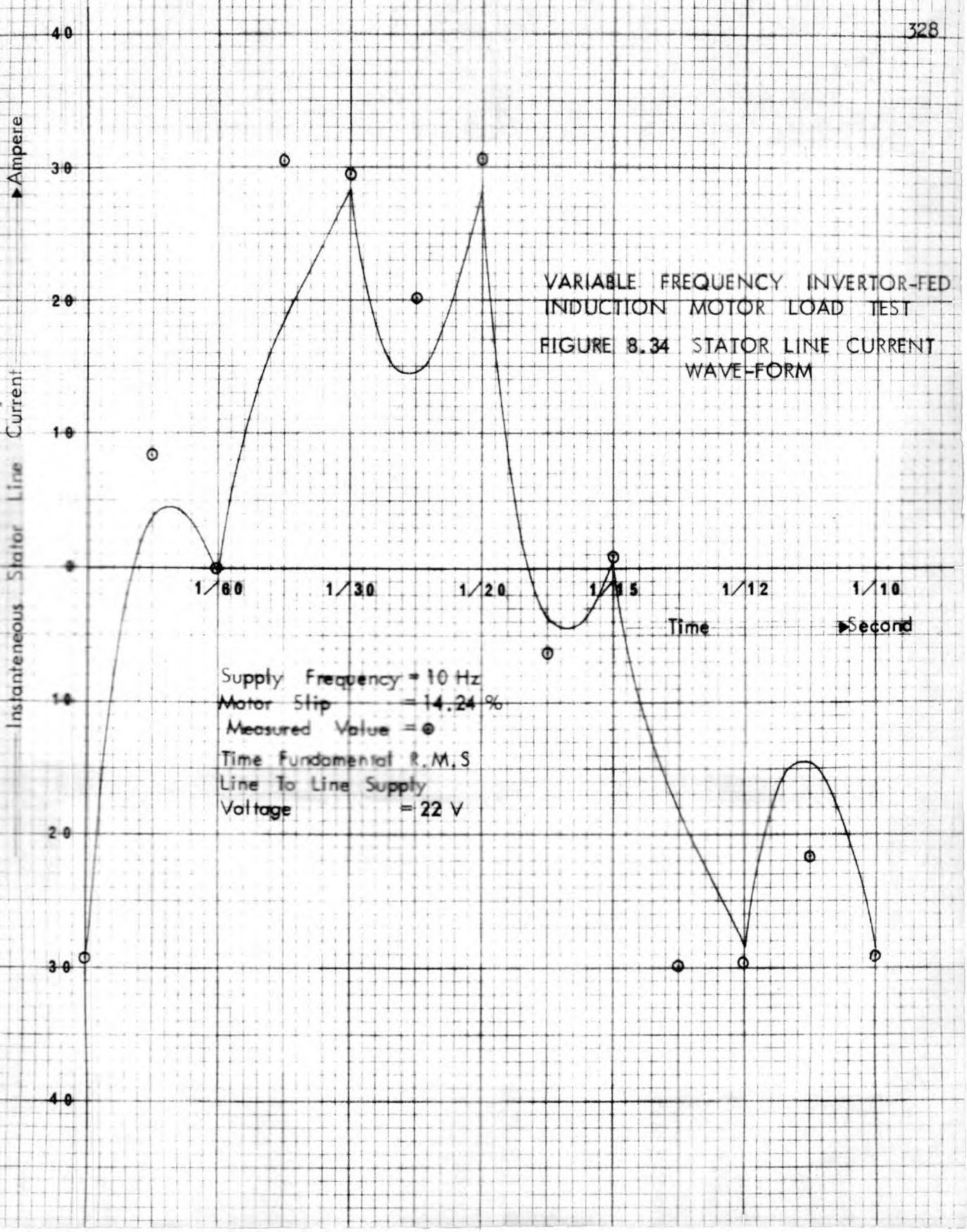

VARIABLE FREQUENCY INVERTOR-FED INDUCTION MOTOR LOAD TEST

FIGURE 8.34 STATOR LINE CURRENT WAVE-FORM

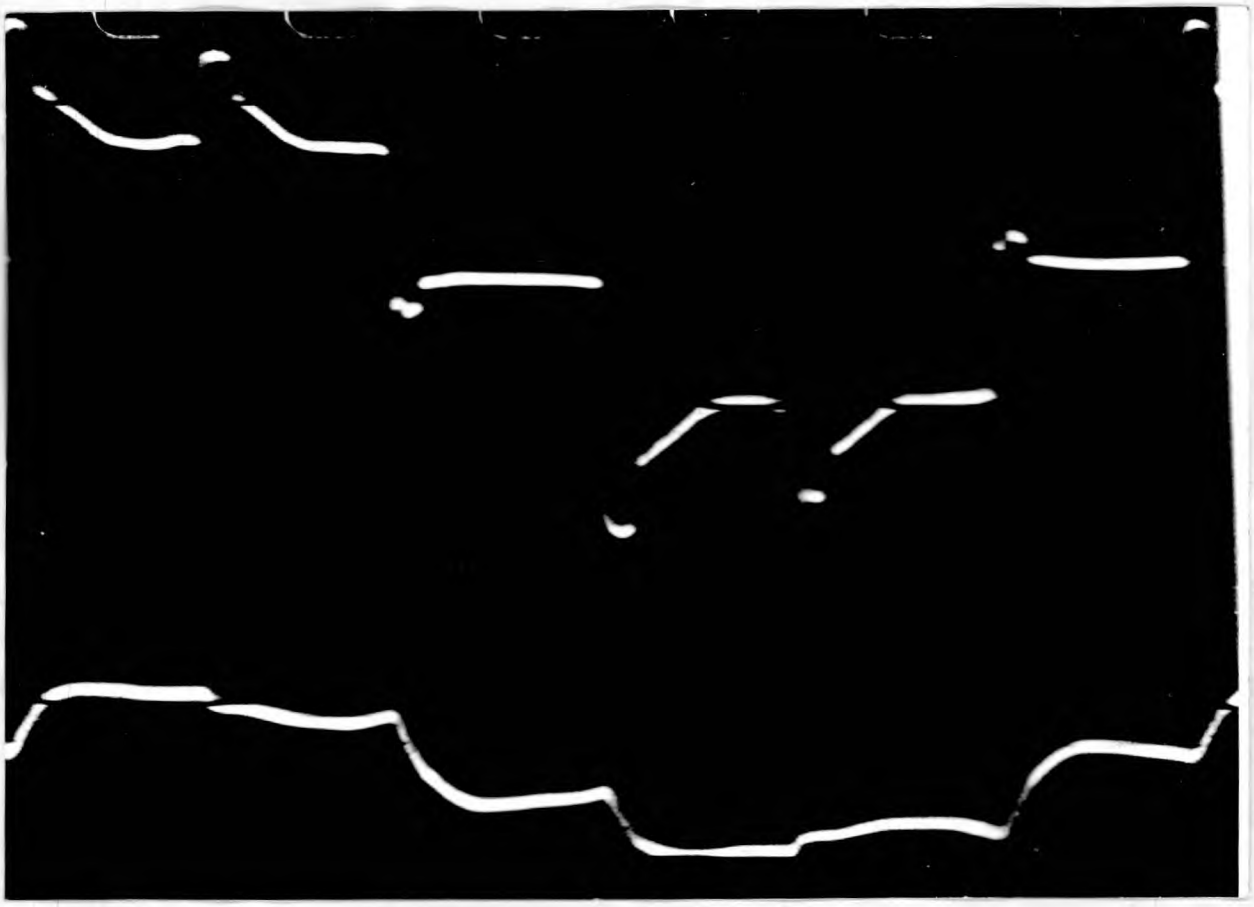

TOP TRACE: LINE TO LINE VOLTAGE : SCALE 16.2 V/cm

BOTTOM TRACE: LINE CURRENT : SCALE 42.6 A/cm

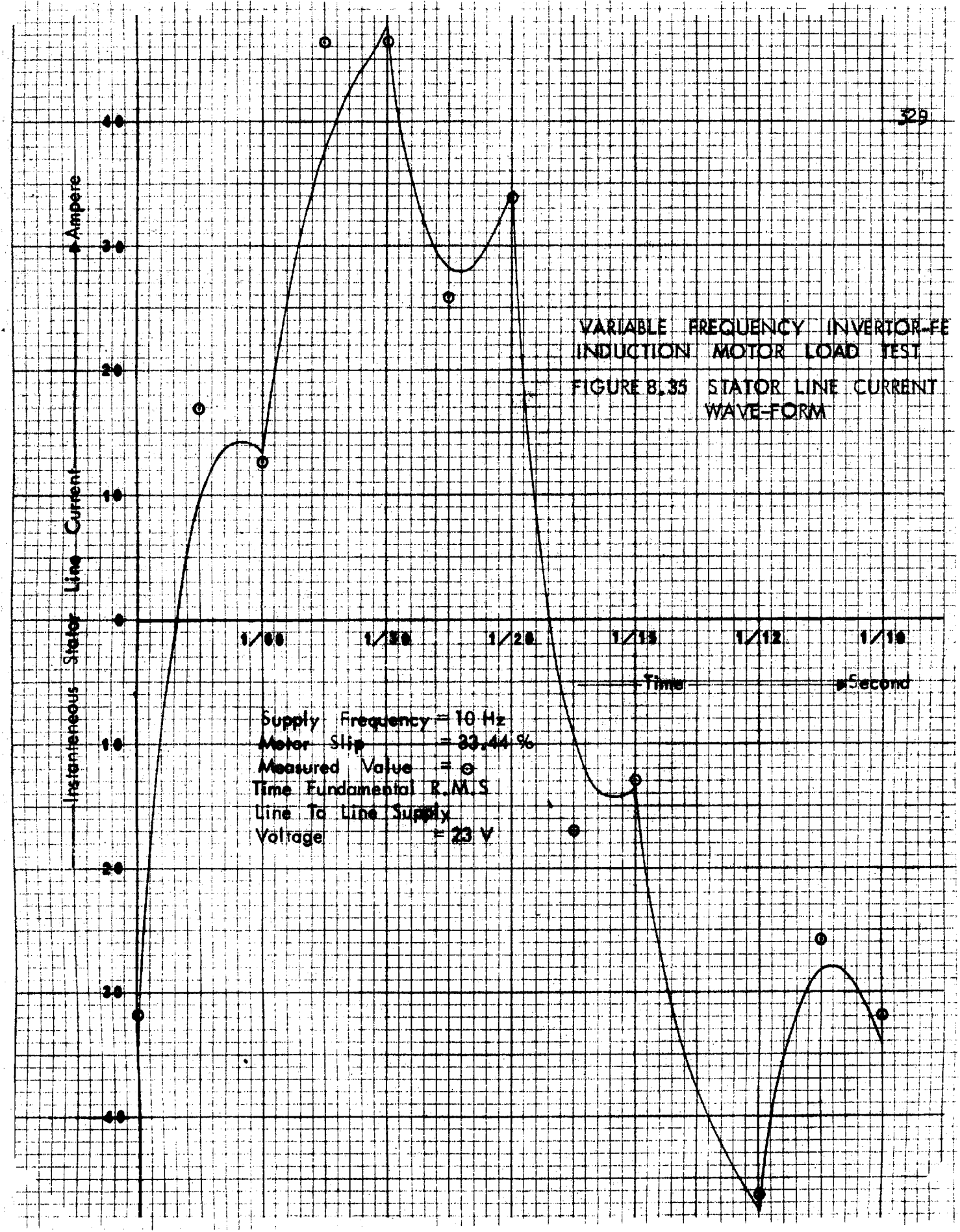

VARIABLE FREQUENCY INVERTOR-FE INDUCTION MOTOR LOAD TEST

FIGURE 8.35 STATOR LINE CURRENT WAVE-FORM

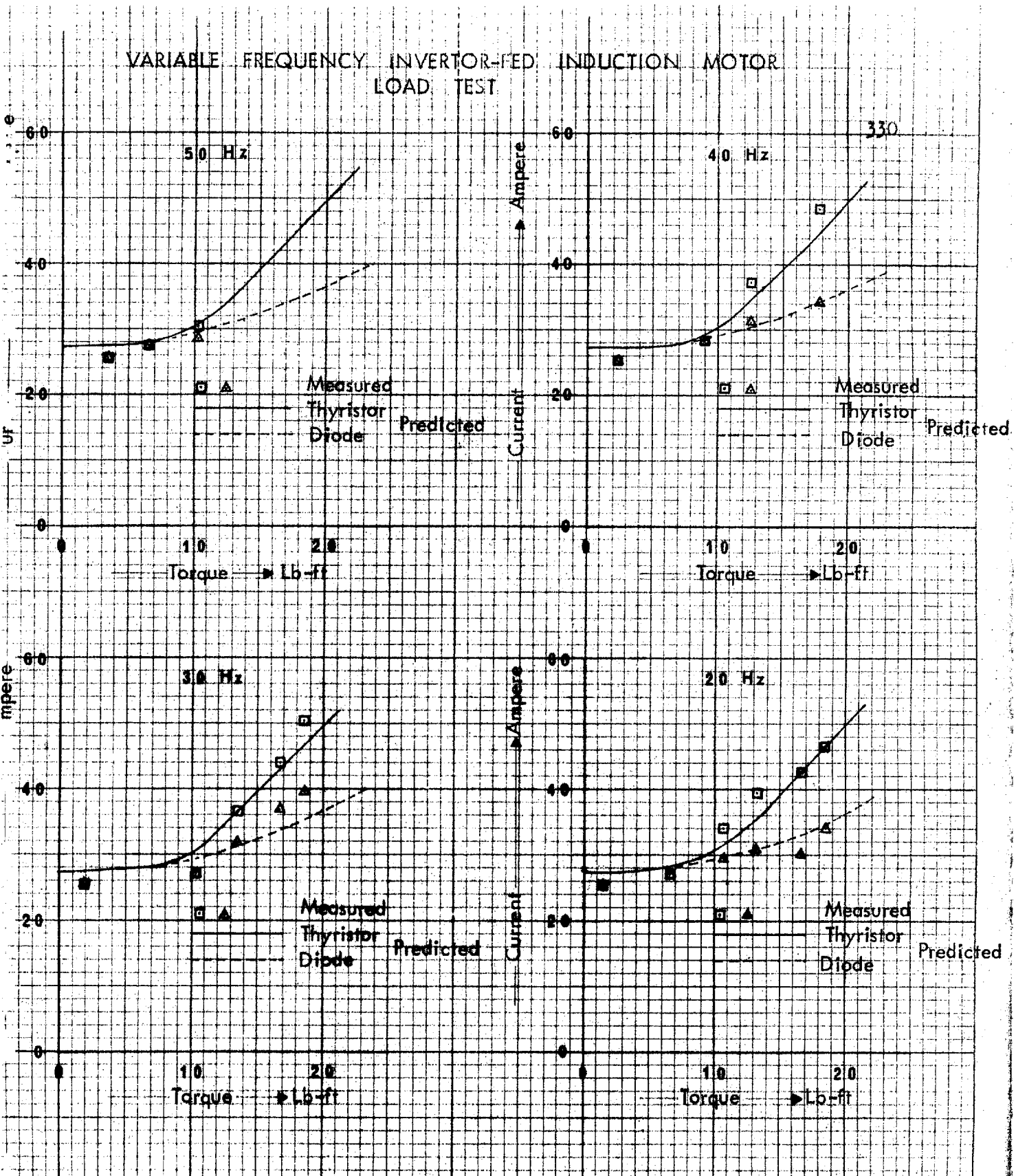

FIGURE 8.36 BRIDGE THYRISTOR & BRIDGE DIODE PEAK CURRENT

VARIABLE FREQUENCY INVERTOR-FED INDUCTION MOTOR LOAD TEST

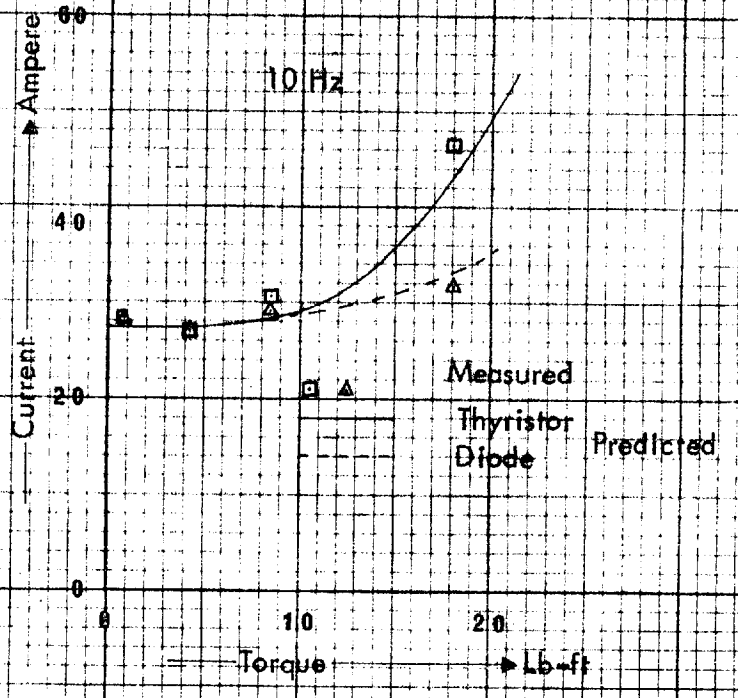

FIGURE 8.37 BRIDGE THYRISTOR & BRIDGE DIODE PEAK CURRENT

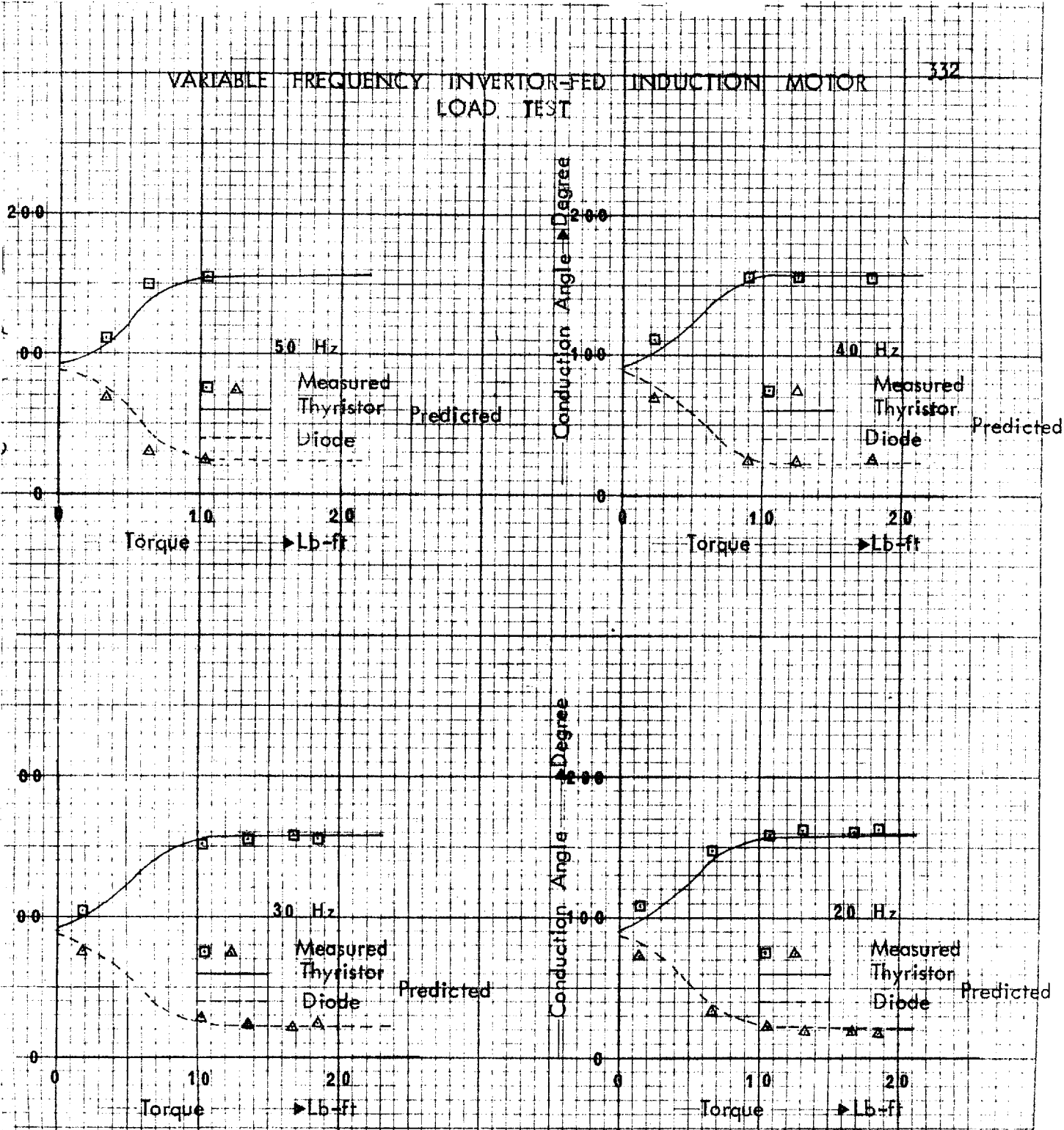

FIGURE 8.38 BRIDGE THYRISTOR & BRIDGE DIODE CONDUCTION ANGLE

VARIABLE FREQUENCY INVERTOR – FED INDUCTION MOTOR
LOAD TEST

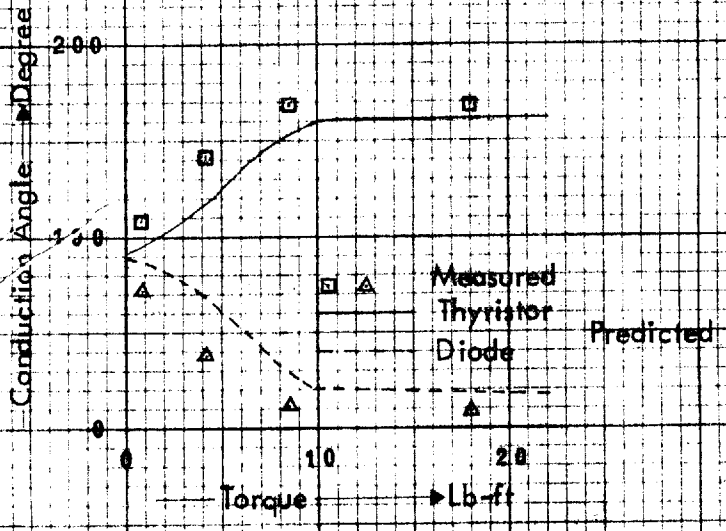

FIGURE 8.39 BRIDGE THYRISTOR & BRIDGE DIODE CONDUCTION ANGLE

VARIABLE FREQUENCY INVERTOR-FED INDUCTION MOTOR
LOAD TEST

FIGURE 8.40 PREDICTED BRIDGE THYRISTOR & BRIDGE DIODE AVERAGE CURRENT

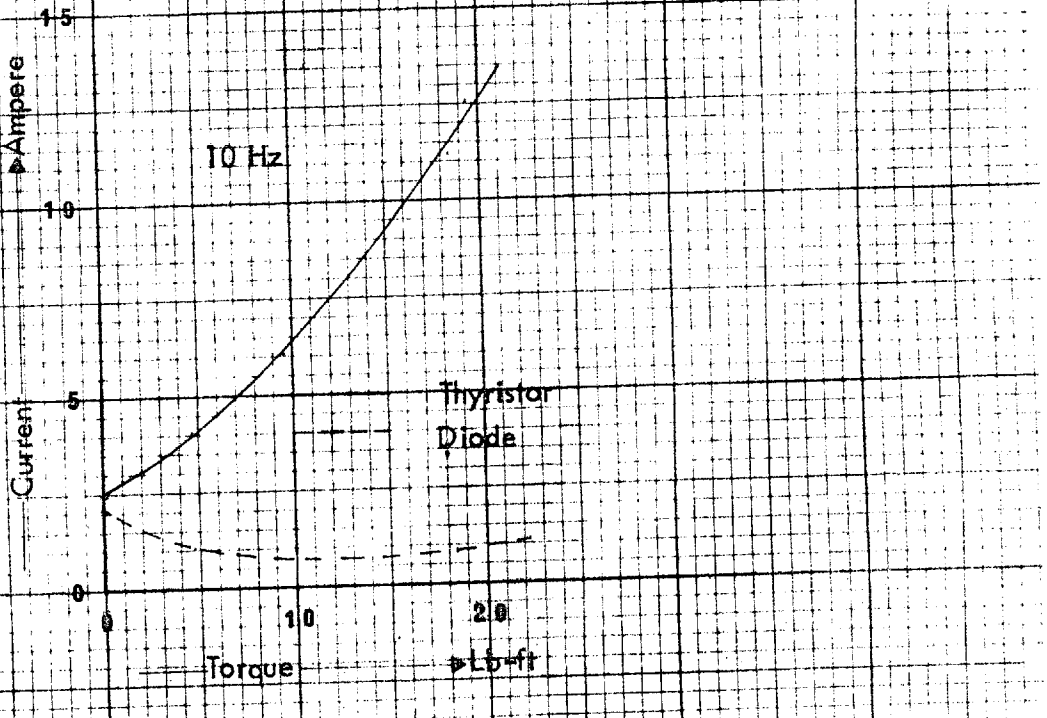

FIGURE 8.41 PREDICTED BRIDGE THYRISTOR & BRIDGE DIODE AVERAGE CURRENT

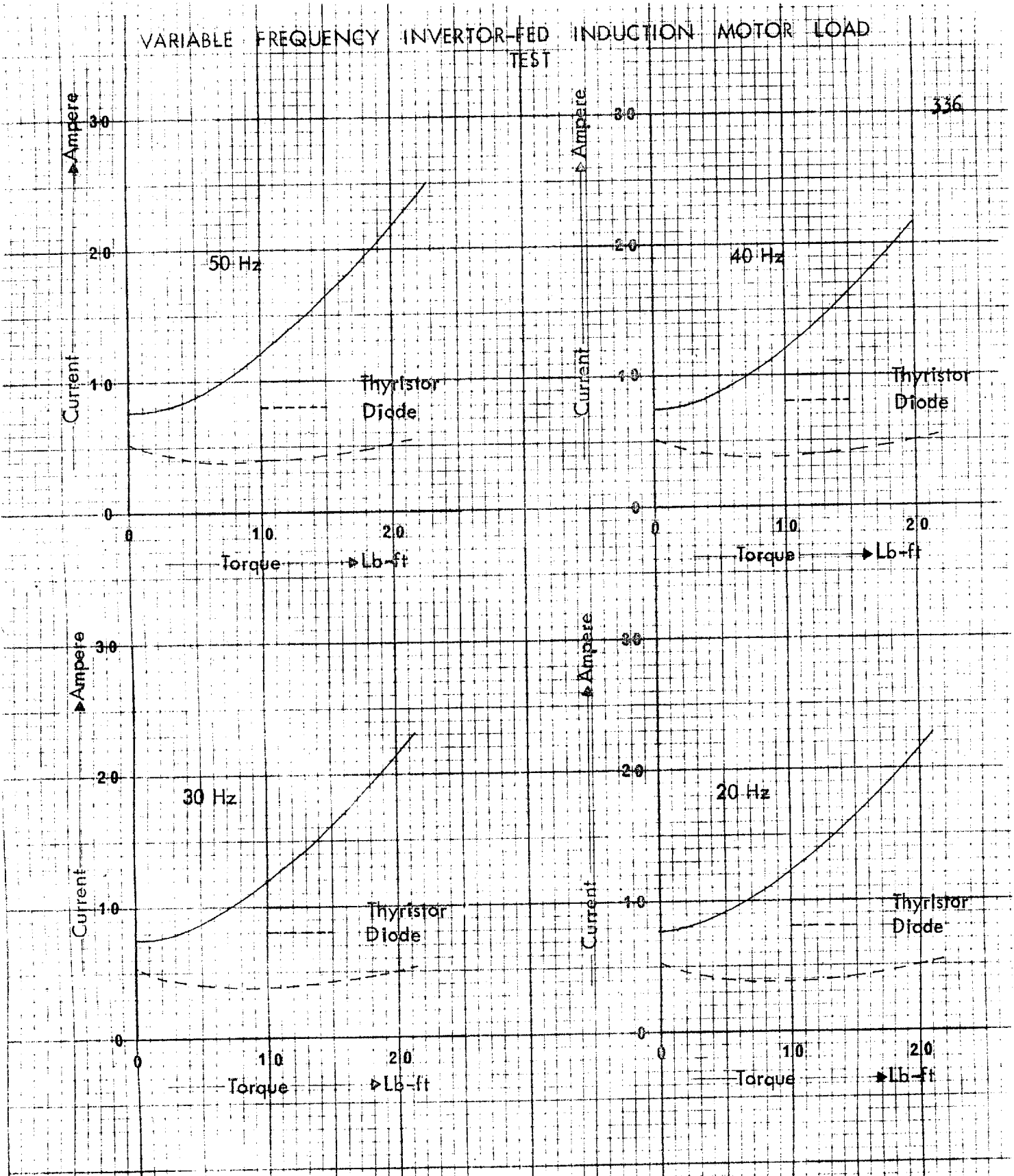

FIGURE 8.42 PREDICTED BRIDGE THYRISTOR & BRIDGE DIODE R.M.S. CURRENT

VARIABLE FREQUENCY INVERTOR-FED INDUCTION MOTOR LOAD TEST

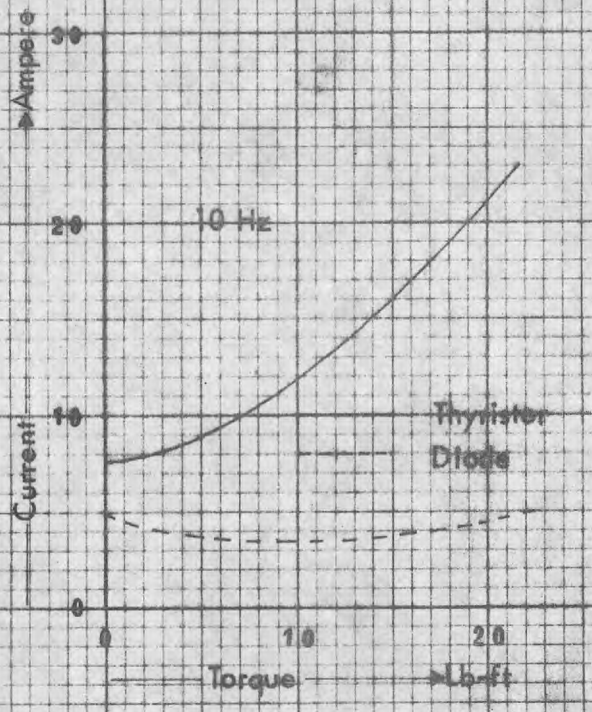

FIGURE 8.43 PREDICTED BRIDGE THYRISTOR & BRIDGE DIODE R.M.S. CURREN

7.27 (after due conversion from Synchronous-watt to Lb-ft.) and shown in figure 8.44. The frequency of torque pulsation was six times that of the invertor supply. The average torque was calculated from this instantaneous torque and is shown in the same figure. Figures 8.45 and 8.46 give the predicted invertor-fed induction motor torque fluctuation as a function of average torque for various constant values of frequencies. The electro-magnetic torque, as measured and predicted by the two methods, is shown in figure 8.47.

8.3.3 Electro-magnetic rotor power output

The electro-magnetic power output of the induction motor was measured as in section 8.2.2. This was predicted by harmonic analysis from equation 6.100 and also by time domain analysis from the following equation

$$P_{2o} = (2\pi 746/33,000) \times NT_{AV} \qquad (8.5)$$

where T_{AV} is the average torque predicted from the time domain analysis (Section 8.3.2) and N is the actual rotor speed in R.P.M. The measured and predicted (by the two methods) rotor power output are shown in figure 8.48.

8.3.4 Electric power input

The power input to the induction motor was measured

VARIABLE FREQUENCY INVERTOR-FED INDUCTION MOTOR
LOAD TEST

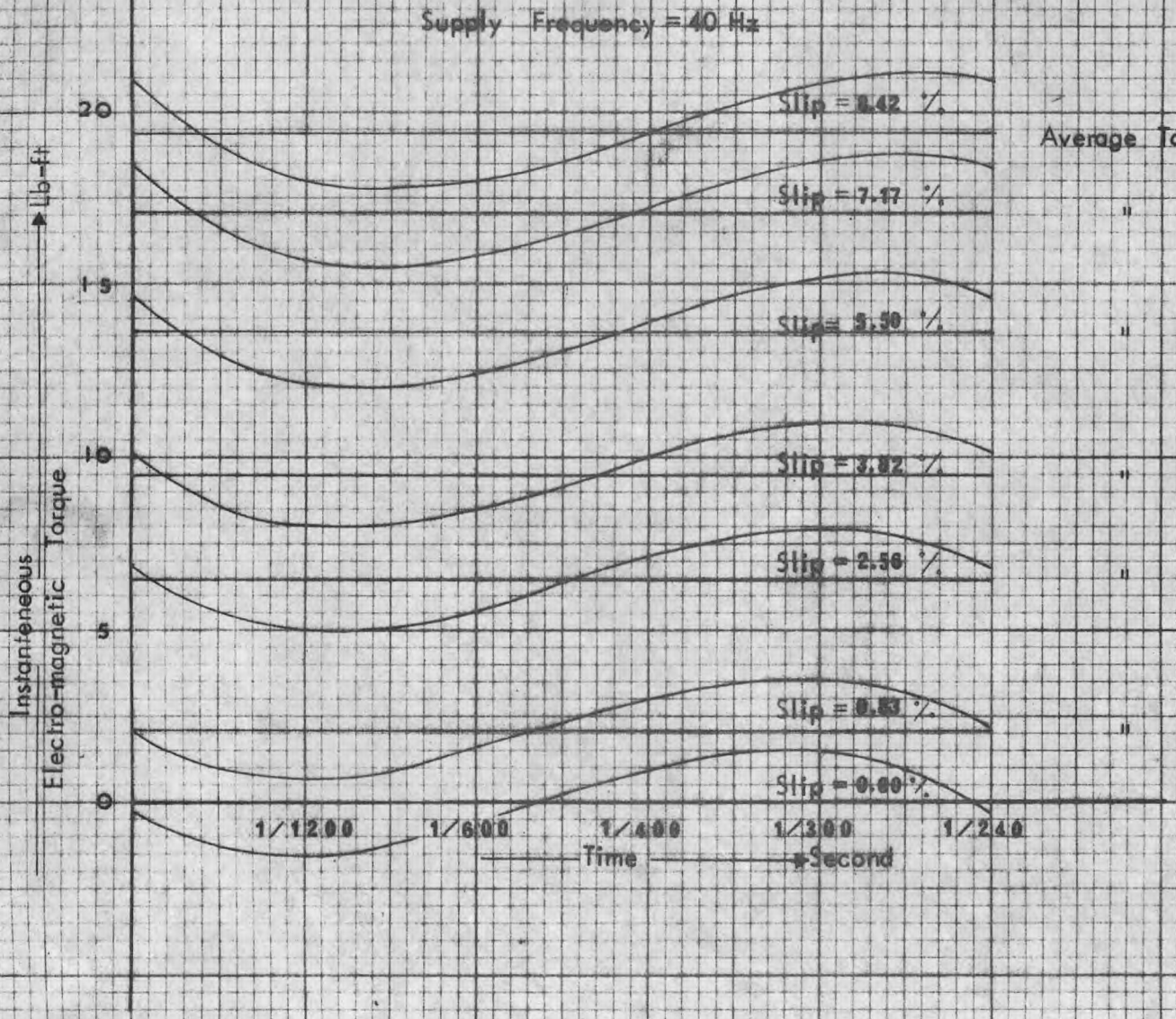

FIGURE 8.44 PREDICTED INSTANTANEOUS AND AVERAGE ELECTRO-MAGNETIC TORQUE

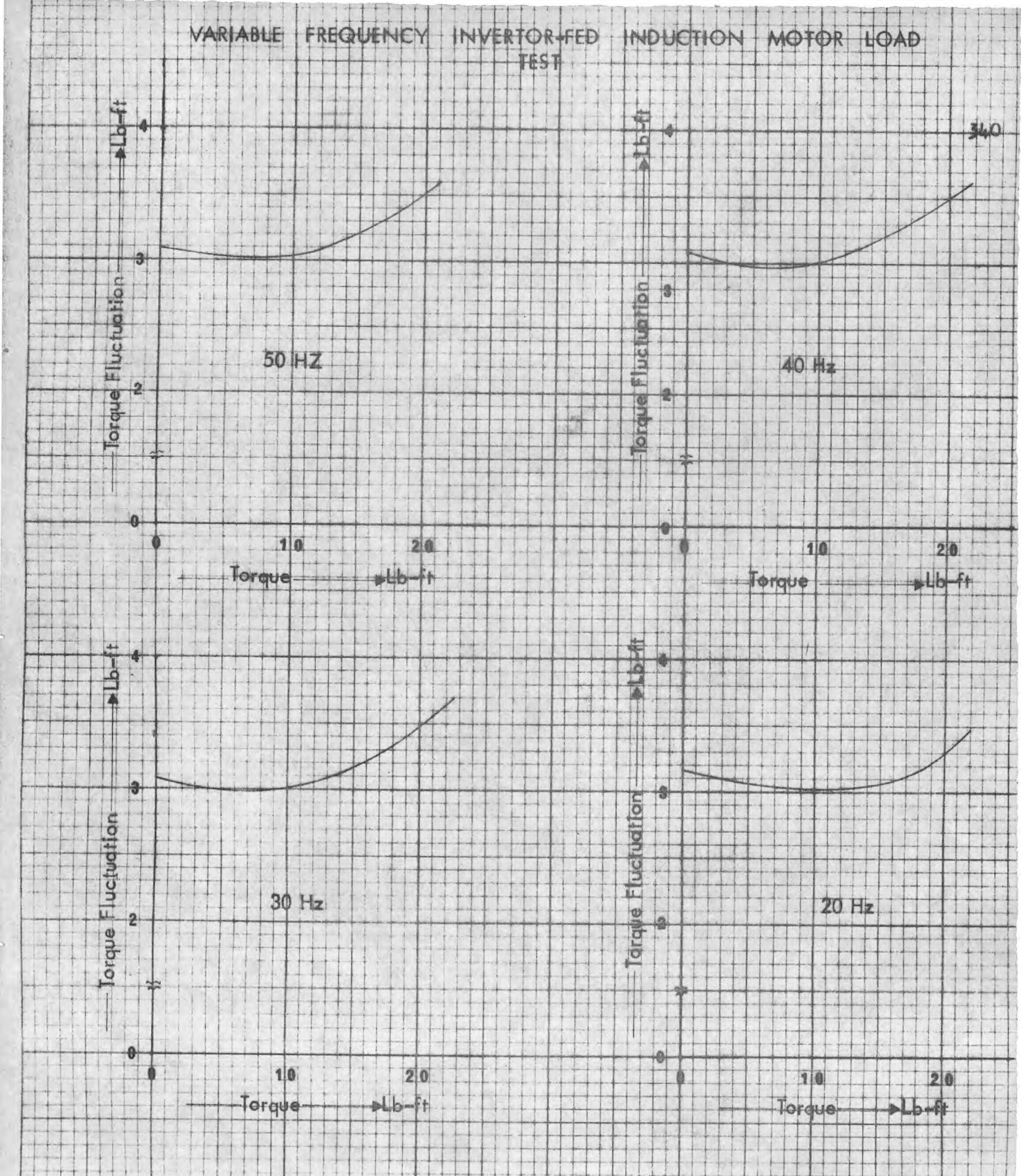

FIGURE 8.45 PREDICTED ELECTRO-MAGNETIC TORQUE FLUCTUATION VS AVERAGE ELECTROMAGNETIC TORQUE

VARIABLE FREQUENCY INVERTOR-FED INDUCTION MOTOR
LOAD TEST

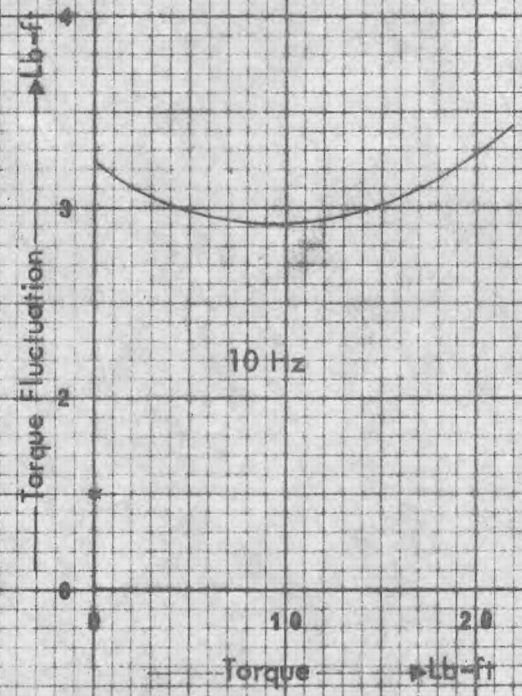

FIGURE 8.46 PREDICTED ELECTRO-MAGNETIC TORQUE FLUCTUATION VS AVERAGE ELECTRO-MAGNETIC TORQUE

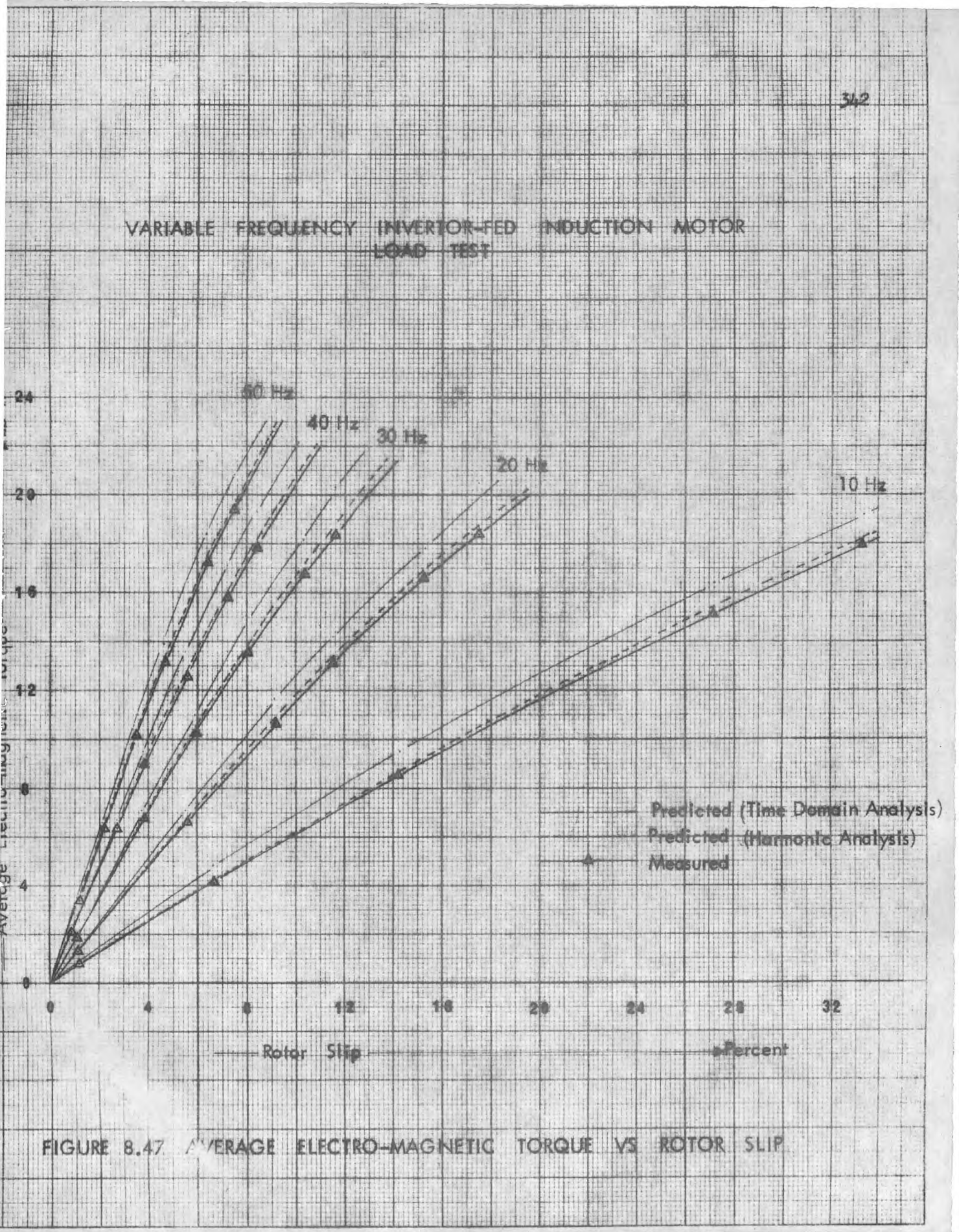

FIGURE 8.47 AVERAGE ELECTRO-MAGNETIC TORQUE VS ROTOR SLIP

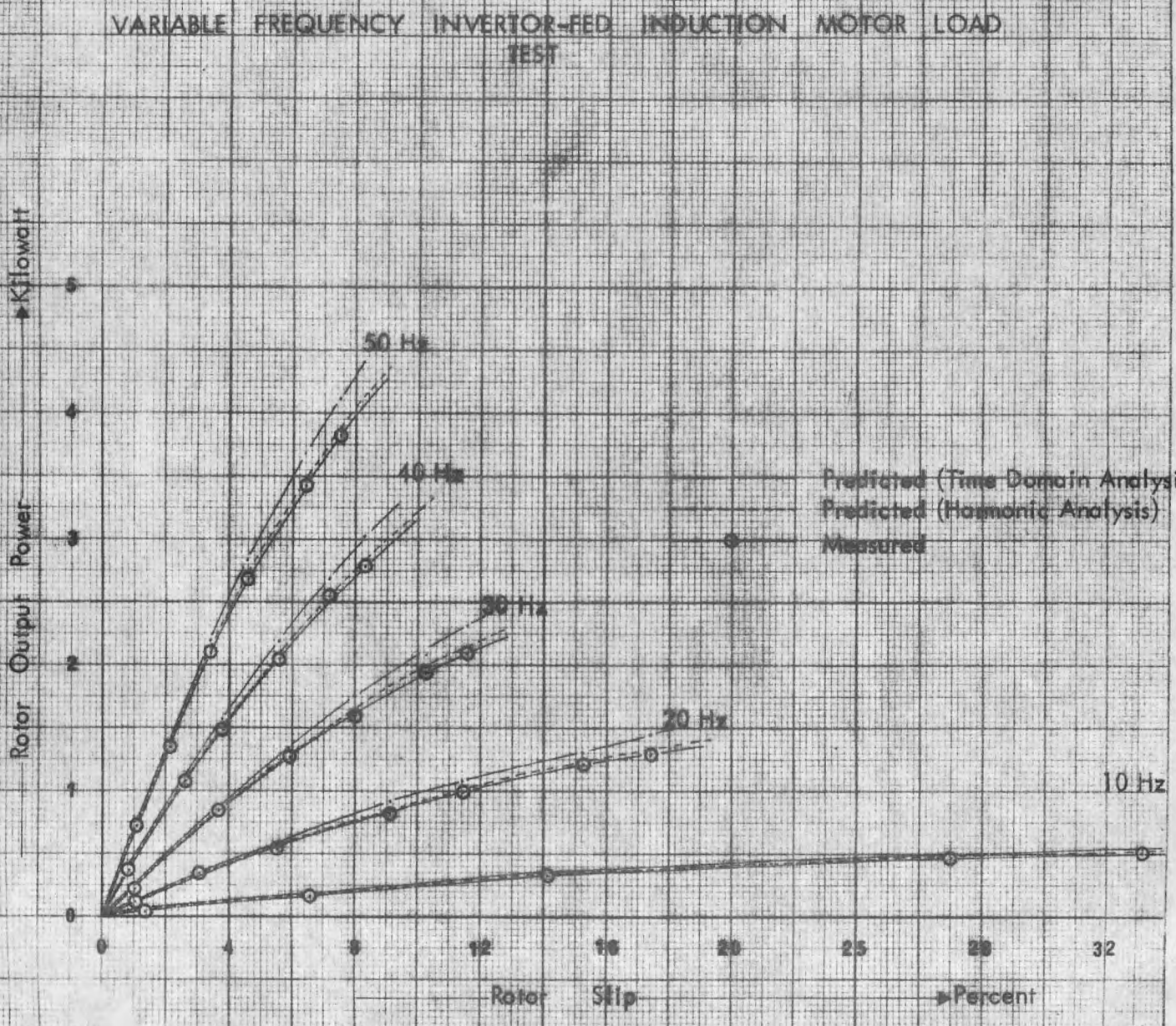

FIGURE 18 ROTOR ELECTRO-MAGNETIC OUTPUT POWER VS ROTOR SLIP

as in section 8.2.4. The input power was predicted by harmonic analysis from equation 6.111. Knowing the instantaneous stator current from time domain analysis and the idealized line to neutral voltage wave-form, the instantaneous power input to stator was calculated. The power input was taken as the average of the instantaneous input power over a cycle. The input calculated in this way does not contain the iron loss due to the assumptions made (Section 7.1). Iron loss was separately calculated from the knowledge of the r.m.s. value of the idealized line to neutral voltage and the iron loss simulating resistance under invertor operation (Section 6.3). This iron loss was then added to the 'input power', so calculated, to determine the corrected input power(Figure 8.49).

8.3.5 Total electro-magnetic loss

The total electro-magnetic loss of the induction motor was measured as in section 8.2.5. It was predicted by harmonic analysis from equations 6.108, 6.104 and 6.94. The r.m.s. value of stator and rotor current along α' reference frame was calculated from the knowledge of instantaneous currents along that reference frame (Equations 7.22 and 7.24). These r.m.s. currents were used to calculate the stator and rotor copper loss. The iron loss was calculated as in section 8.3.4. Summation

VARIABLE FREQUENCY INVERTOR-FED INDUCTION MOTOR
LOAD TEST

FIGURE 8.49 STATOR INPUT POWER VS ROTOR SLIP

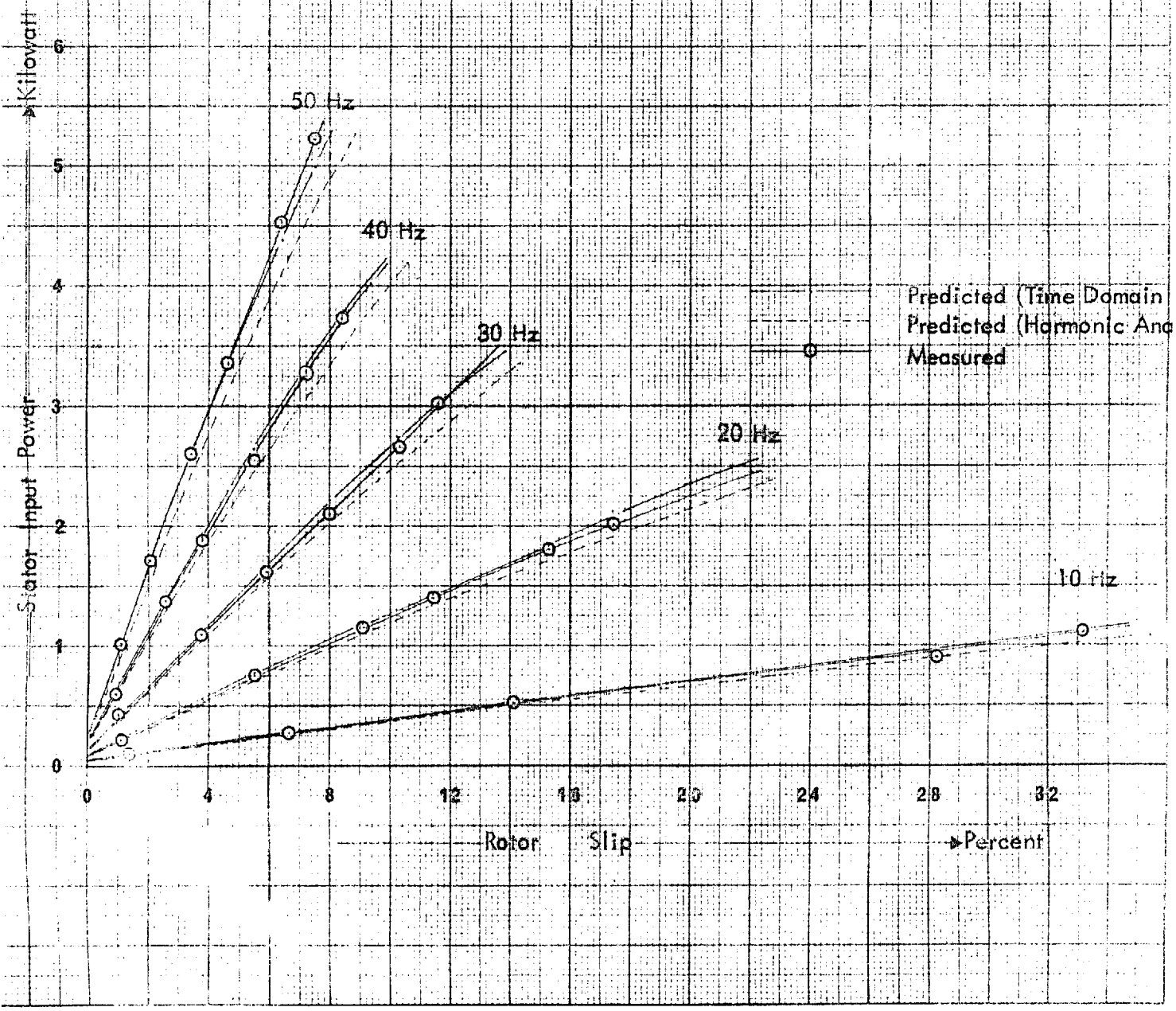

VARIABLE FREQUENCY INVERTOR-FED INDUCTION MOTOR LOAD TEST

FIGURE 8.50 ELECTRO-MAGNETIC POWER LOSS VS ROTOR SLIP

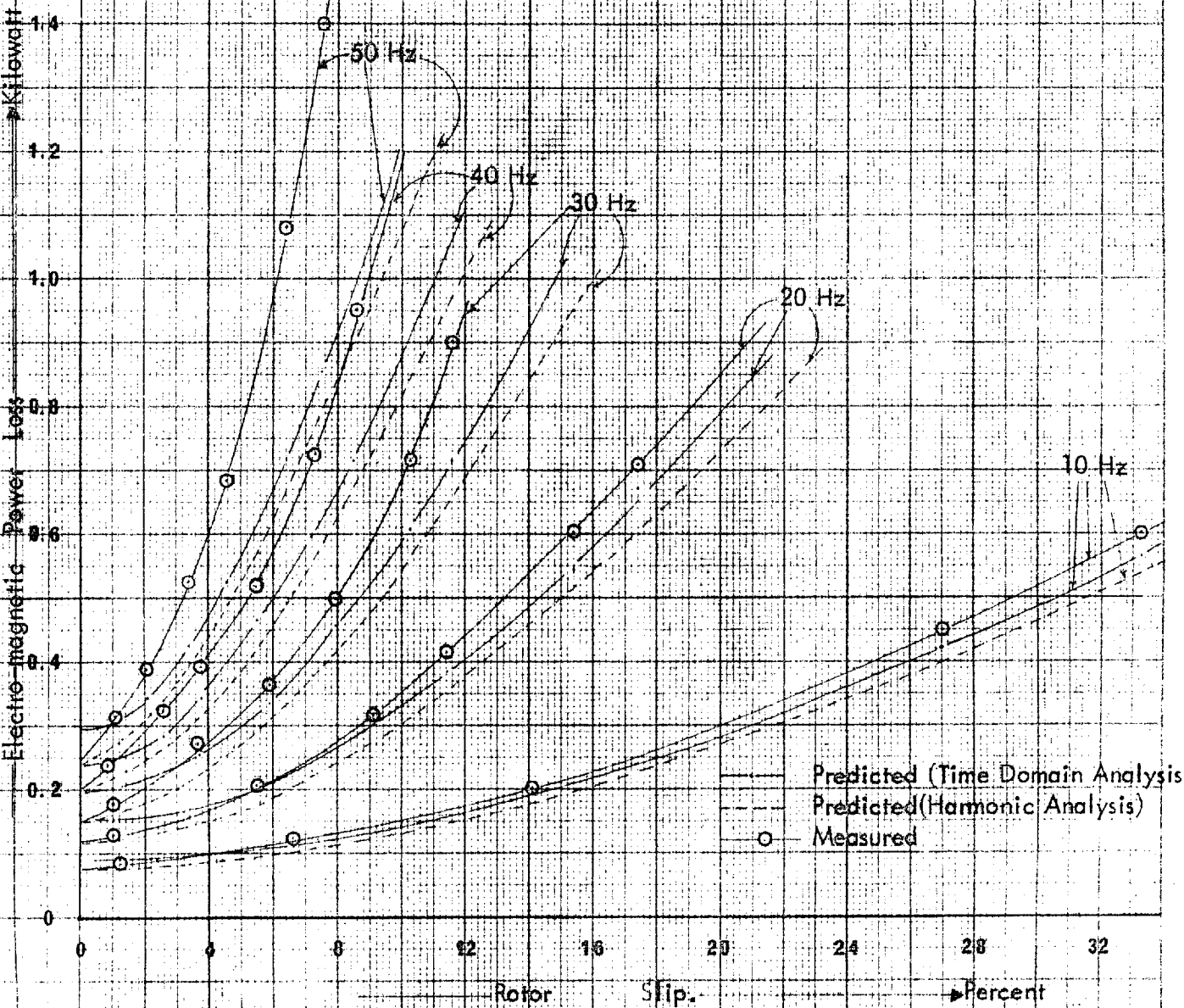

INDUCTION MOTOR LOAD TEST UNDER VARIABLE FREQUENCY EXCITATION

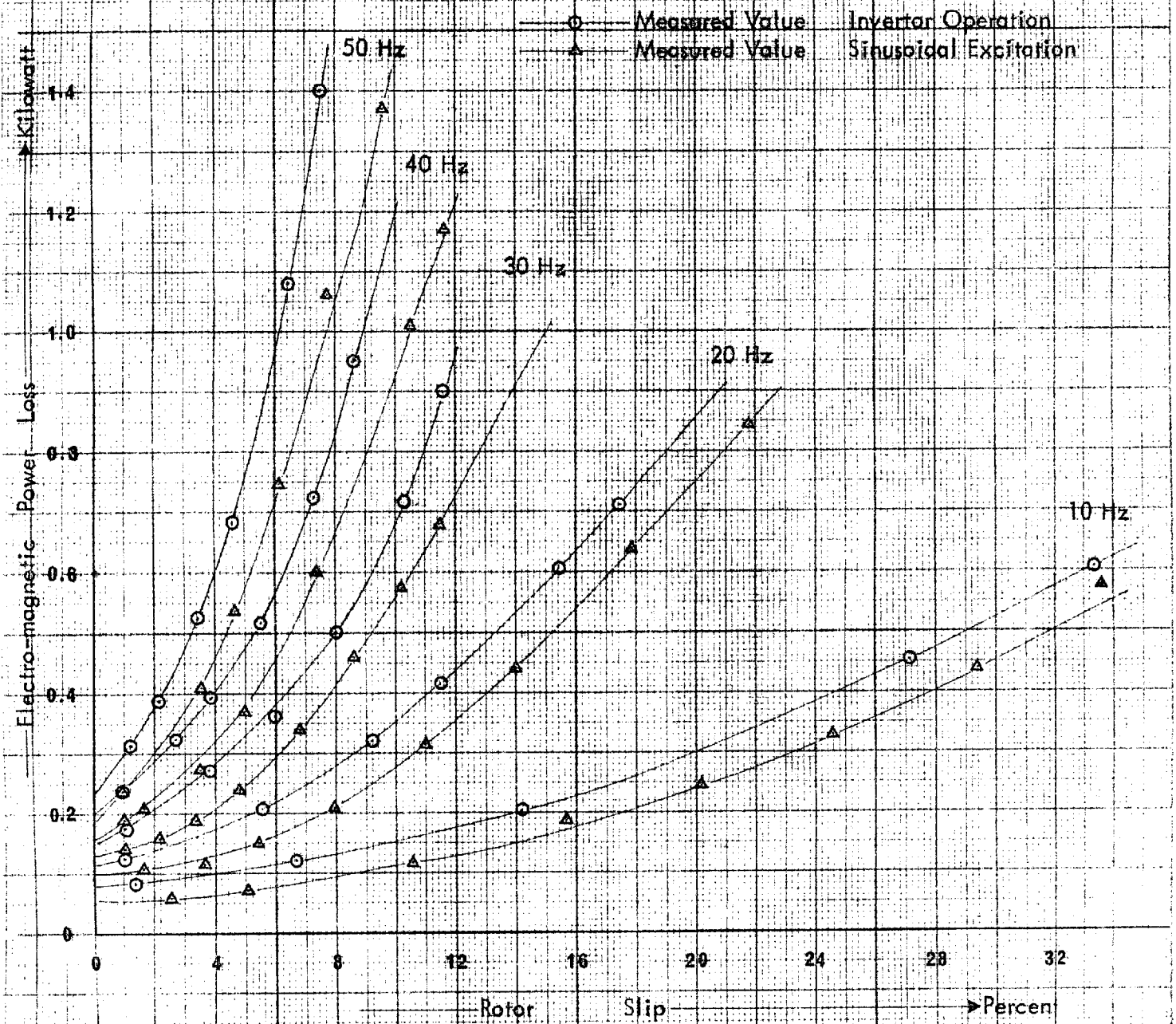

FIGURE 8.51 ELECTROMAGNETIC POWER LOSS VS ROTOR SLIP (MEASURED VALUE)

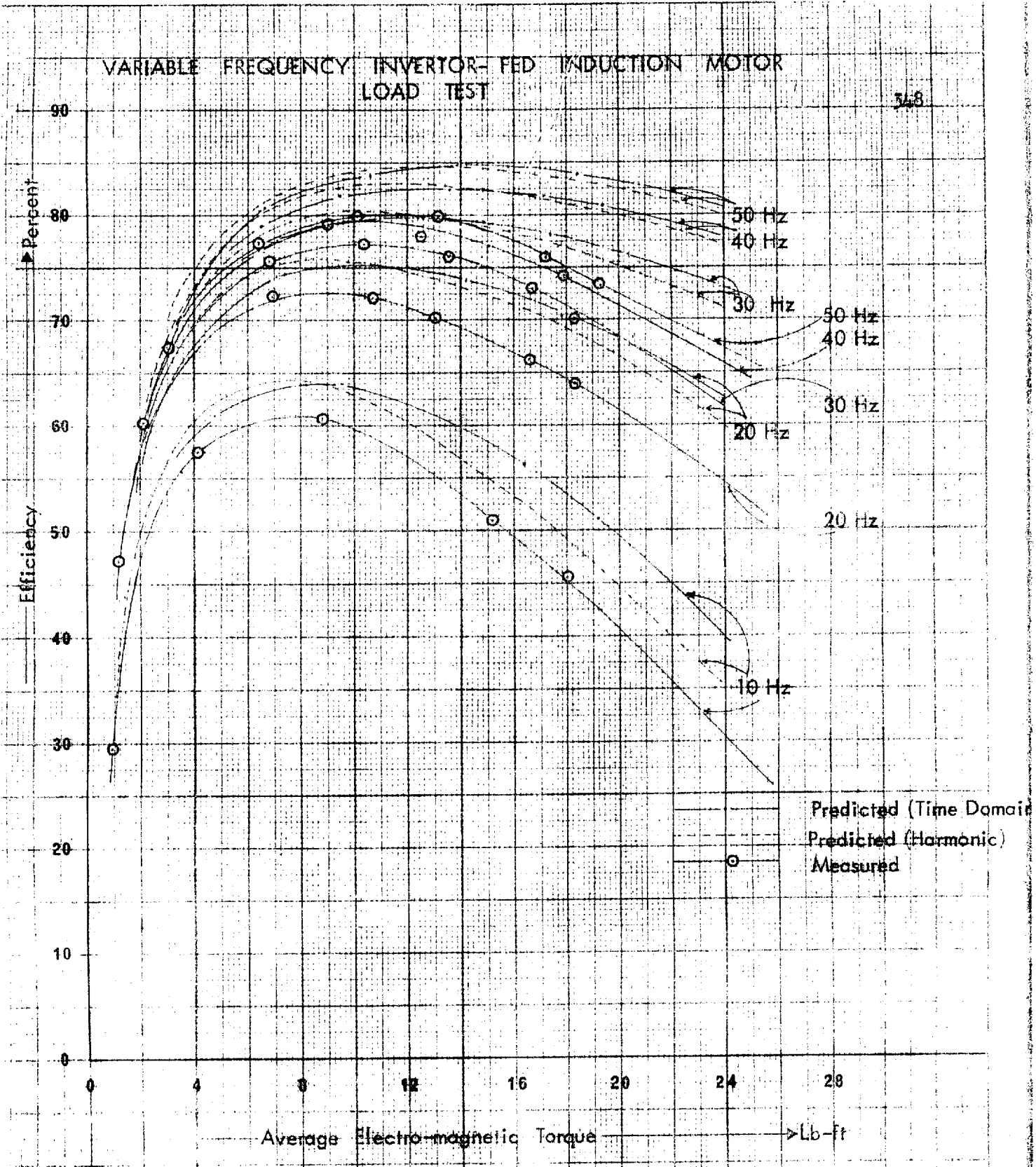

FIGURE 8.52 INDUCTION MOTOR EFFICIENCY VS AVERAGE ELECTRO-MAGNETIC TORQUE

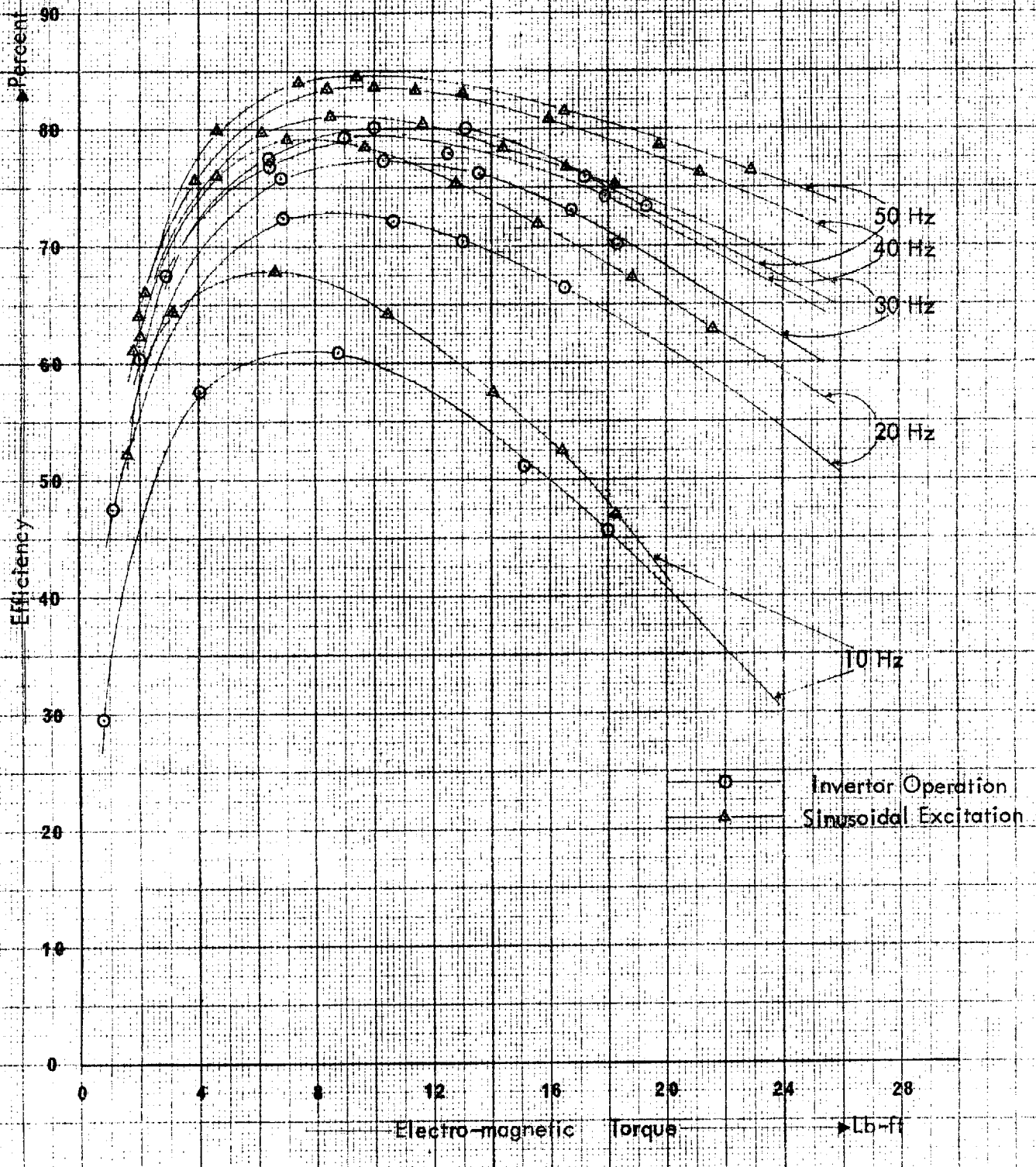

FIGURE 8.53 MEASURED INDUCTION MOTOR EFFICIENCY VS ELECTROMAGNETIC TORQUE

of these three losses is the total electro-magnetic loss as predicted by time domain analysis. The losses as measured and as predicted by the two methods are shown in figure 8.50. Figure 8.51 is given to compare the measured losses under sinusoidal excitation and under invertor operation.

8.3.6 Electro-magnetic efficiency

The electro-magnetic efficiencies were measured as in section 8.2.6. The measured and predicted efficiencies are shown in figure 8.52. The measured efficiencies under sinusoidal excitation and under invertor operation are given in figure 8.53 for comparison.

CHAPTER 9

GENERAL CONCLUSIONS AND DISCUSSIONS

This investigation was directed towards the development of design methods for impulse commutated invertors and the prediction of the behaviour of invertor-fed induction motors.

9.1 Applicability of the Invertor Design Equations to Other Types of Impulse-commutated Invertors

The invertor designed and built for this investigation was of the single D.C. side impulse-commutated type. The principle of operation and circuit configurations of impulse-commutated invertors, in general, have been published elsewhere[1].

Single D.C. side impulse-commutated invertors have high commutation efficiency and require less commutation circuit components and auxiliary supply power than other impulse-commutated invertors. This type of invertor suffers from high rates of forward voltage rise on the thyristors and is suitable for supplying low voltage motors.

Compared with single D.C. side invertors double D.C. side impulse-commutated invertors require, in general, two additional thyristors and more auxiliary supply power but

have lower forward voltage rise on the thyristors[1]. Motors of medium voltage rating can be conveniently fed from invertors of this type.

Individual D.C. side impulse-commutated invertors require, in general, the highest number of commutation circuit components (6 D.C. line chokes, 6 commutation thyristors and 6 D.C. line diodes). The rate of rise of forward voltage across the thyristors are well controlled[1] and the D.C. line chokes receive commutating pulses once per cycle. The auxiliary supply has the lowest power rating as compared with the other two types of impulse-commutated invertors. It is preferable to use this type of invertor for supplying high power and high voltage motors.

The invertor design equations of chapter 2 were developed primarily for single D.C. side impulse-commutated invertors, but can be used, with minor modifications, for the design of double D.C. side and individual D.C. side impulse-commutated invertors. The modification involves only the frequency of commutation. For single D.C. side impulse-commutated invertors the frequency of commutation is 3f, whereas for double D.C. side impulse-commutated invertors it is 6f, and for individual D.C. side impulse-commutated invertors it is f. Modification is required for the evaluation of the following four quantities :-

i) r.m.s. current of commutation thyristors (Section 2.3.7).

ii) Average current of commutation thyristors (Section 2.3.8).

iii) Power rating of auxiliary commutation supply (Section 2.3.9).

iv) Commutation power supplied by the main D.C. supply (Section 2.3.10).

Those impulse-commutated invertors which do not employ a centre-tapped auxiliary supply are basically similar to invertors which employ centre-tapped main D.C. supply reservoir capacitors and a centre-tapped auxiliary commutating supply[1] (e.g. Figure 2.1). The design of the commutation circuit with this variation is best done by first evaluating the values of the commutation circuit components of an invertor of similar type with centre-tapped auxiliary supply and then changing the star-connected commutation circuit capacitors (e.g. C_A, C_B and C_3 of Figure 2.1) to delta, the component values being evaluated by appropriate transformation (star/delta for single D.C. side and individual D.C. side invertors, series-parallel for double D.C. side versions).

9.2 Performance Prediction and Measurement of the Induction Motor when excited from Sinusoidal Source

The equivalent circuit parameters, as determined from no-load and locked rotor tests (Sections 4.3 and 4.4) were used to predict the induction motor performance under variable frequency sinusoidal excitation. The errors of performance prediction are given in table 9.1.

There is a large discrepency between the measured and predicted electro-magnetic losses. These losses were measured by taking the difference between the stator input power and the rotor output power. The stator input power was measured by the two-wattmeter method. The rotor electro-magnetic power was measured by summing the power output of the D.C. loading machine, the armature copper loss of the D.C. machine, and the loss due to brush arc Volt-drop.

This method of measuring the induction motor electro-magnetic power output does not account for the stray load losses of the D.C. machine. As such the measured electro-magnetic losses consist of the true loss and the stray load loss of the D.C. machine. The loss measurement by input/output tests gives a result of poor accuracy.

The wattmeters used to measure the stator input power had an accuracy of $\pm$ 2½% for a frequency range of 0 Hertz to

Table 9.1 ERRORS OF PERFORMANCE PREDICTION (MOTOR EXCITED FROM VARIABLE FREQUENCY SINUSOIDAL SOURCE)

Items	Check Points	Fig. No.	% Error
Stator line current	32% rotor slip and supply frequency of 10 Hertz	8.3	- 2.30
Rotor output power	12% rotor slip and supply frequency of of 30 Hertz	8.4	+ 5.84
Electro-magnetic torque	20% rotor slip and supply frequency of 50 Hertz	8.5	+ 2.97
Stator input power	10% rotor slip and supply frequency of 50 Hertz	8.7	- 3.36
Electro-magnetic loss	9.8% rotor slip and supply frequency 50 Hertz	8.8	- 23.8
Electro-magnetic efficiency	Torque of 22 Lb.-ft. and supply frequency of 50 Hertz	8.9	+ 6.35

$$\% \text{ Error} = \frac{\text{Measured} - \text{Predicted}}{\text{Measured}} \times 100$$

1,000 Hertz. The stray-load loss of the D.C. loading machine was approximately 1% of the input[20]. With an induction motor efficiency of 75% the accuracy of loss measurement is estimated for the worst case (assuming accurate measurement of D.C. loading machine power output) to be:-

$$(1.025\ P_{in} - 0.99\ P_{2o})/P_{in}$$

or

$$(1.025\ P_{in} - 0.99 \times .75\ P_{in})/(4\ \text{loss})$$

or

$$(1.025\ P_{in} \times 4\ \text{loss} - 0.99 \times 4 \times .75\ \text{loss})/(4\ \text{loss})$$

or

45% higher than true loss.

The predicted electro-magnetic loss under sinusoidal excitation is 23.8% lower than that measured and hence the prediction is well within the accuracy of measurement. To investigate the losses a more sophisticated method of measurement must be used where the losses are measured directly[21] and not as the difference of two large quantities.

As the intention in this project was to investigate the performance of an invertor-fed induction motor and the

development of invertor design methods, no attempt was made to investigate the losses in detail. Loss measurement involve a multi-machine system with swinging stators.[21] As time was limited, it was thought that discrepancies between the theory developed in this thesis and practical ~~works~~ tests would provide a basis for further work.

In the electro-magnetic loss prediction, the losses due to slot openings (discussed in Section 5.4) have not been taken into account.

9.3 Performance Prediction and Measurement of Invertor-fed Induction Motor

To predict the induction motor performance when the machine is fed from the invertor, two methods, harmonic analysis (Chapter 6) and time domain analysis (Chapter 7), have been used. The harmonic analyser used to measure the time harmonic content of stator line to line voltage and stator line current, had an accuracy of $\pm$ 5%. The harmonic analysis utilized the measured values of harmonic content of the invertor supply whereas the time domain analysis utilized an idealized voltage wave-form. The actual harmonic contents of the invertor output voltage were in general considerably higher than that of the idealized voltage, and increased as the load on the motor increased and the time fundamental supply frequency decreased.

Table 9.2 shows the harmonic content of the actual (maximum values at selected operating conditions) and the idealized invertor voltage expressed as a percentage of the fundamental.

The worst cases of inaccuracy in the performance prediction by harmonic analysis and time domain analysis are given in table 9.3.

The harmonic currents predicted by harmonic analysis are rather inaccurate although their general variation with rotor-slip agrees with that measured. The harmonic currents on the other hand were predicted by assuming that the equivalent circuit frequency-dependent parameters were linearly dependent on frequency.

This assumption of linear variation of the parameters has no experimental justification at high harmonic frequencies. The eddy current losses which were absent when the motor was tested under sinusoidal excitation over a frequency range of 25 Hertz to 50 Hertz, may be significant at the higher harmonic frequencies. The eddy currents could produce considerable damping effects on the mutual and leakage fluxes, which has the effect of reducing the magnetizing reactance, leakage reactance and core-loss analogue resistance below those calculated from 50 Hertz values, assuming a linear dependence on frequency.

The experimental determination of the equivalent

Table 9.2 HARMONIC CONTENT OF INVERTOR OUTPUT VOLTAGE (INVERTOR-FED INDUCTION MOTOR LOAD TEST)

Order of time harmonics	Check Points	Fig. No.	Harmonic Content	
			Measured	Idealized
			%	%
5^{th}	8% rotor slip and supply frequency 50 Hertz	8.11	31.0	20.0
7^{th}	34% rotor slip and supply frequency 10 Hertz	8.12	25.6	14.29
11^{th}	8% rotor slip and supply frequency 50 Hertz	8.13	18.0	9.09
13^{th}	34% rotor slip and supply frequency 10 Hertz	8.14	12.2	7.69
17^{th}	8% rotor slip and supply frequency 50 Hertz	8.15	12.8	5.88
19^{th}	8% rotor slip and supply frequency 10 Hertz	8.16	13.4	5.26

Table 9.3 ERRORS OF PERFORMANCE PREDICTION (INVERTOR-FED INDUCTION MOTOR LOAD TEST)

Item	At	Fig. No.	Harmonic Analysis ($\frac{\text{Measured-Predicted}}{\text{Measured}} \times 100$)	Time-domain Analysis ($\frac{\text{Measured-Predicted}}{\text{Measured}} \times 100$)
Stator time funda-mental current	8% rotor slip and supply frequency of 50 Hertz	8.17	-2.92%	-
5^{th} harmonic stator current	8% rotor slip and supply frequency of 50 Hertz	8.18	-40.87%	-
7^{th} harmonic stator current	8% rotor slip and supply frequency of 50 Hertz	8.19	-31.7%	-
11^{th} harmonic stator current	18% rotor slip and supply frequency of 20 Hertz	8.20	-35.0%	-

Table 9.3 ERRORS OF PERFORMANCE PREDICTION (INVERTOR-FED INDUCTION MOTOR LOAD TEST)

Item	At	Fig. No.	Harmonic Analysis ($\frac{\text{Measured-Predicted}}{\text{Measured}} \times 100$)	Time-domain Analysis ($\frac{\text{Measured-Predicted}}{\text{Measured}} \times 100$)
13^{th} harmonic stator current	8% rotor slip and supply frequency of 50 Hertz	8.21	-84.5%	-
Peak value of stator current	2.3 Lb.-ft. torque at 40 Hertz	8.36	-	6.6%
	8.5 Lb.-ft. torque at 10 Hertz	8.37	-	-5.94%
Bridge thyristor conduction angle	Torque = 6.51 Lb.-ft. Frequency = 10 Hertz	8.38 8.38	-	-6.66%
	Torque = 4.2 Lb.-ft. Frequency = 10 Hertz	8.39	-	-14.9%
Torque	12% rotor slip 30 Hertz	8.47	+3.2%	+10.6%

Table 9.3 ERRORS OF PERFORMANCE PREDICTION (INVERTOR-FED INDUCTION MOTOR LOAD TEST)

Item	At	Fig. No.	Harmonic Analysis ($\frac{\text{Measured-Predicted}}{\text{Measured}} \times 100$)	Time-domain Analysis ($\frac{\text{Measured-Predicted}}{\text{Measured}} \times 100$)
Rotor output power	18% rotor slip 20 Hertz	8.48	+3.8%	+15.1%
Stator input power	8% rotor slip at 50 Hertz	8.49	-10.2%	-3.7%
Electro-magnetic power loss	7% rotor slip at 50 Hertz	8.50	-39.4%	-35.2%

circuit parameters at higher harmonic frequencies involves no-load tests at high speeds, and is not feasible. Theoretical determination of these parameters from the machine design details should be considered. Correction factors (as functions of the order of time harmonic and time fundamental frequency) could be determined and used to correct the variable frequency equivalent circuit for invertor operation (Figure 6.2).

The above-mentioned reasons, together with increased slot losses at the higher harmonic frequencies, cause a large discrepancy between the measured and predicted electro-magnetic loss of the invertor-fed machine. At a time-fundamental supply frequency of 50 Hertz and a rotor-slip of 7% the electro-magnetic loss, when invertor-fed, was around 40% higher than that for equivalent sinusoidal operation (Figure 8.51). Harmonic analysis (up to the 39^{th} in space and 19^{th} in time are accounted for) predicts only a 4% increment of loss under invertor operation (Figures 8.8 and 8.50). At large loads the time domain analysis gives a closer prediction of the electro-magnetic loss compared to that predicted by harmonic analysis (Figure 8.50). This improved prediction of losses is mainly due to the increased iron loss in the equivalent circuit where the iron loss simulating resistance is

connected at the stator supply terminals. It can also be seen (Figure 8.50) that the measured "zero slip" losses and those predicted by the harmonic analysis are identical, whereas those predicted by the time domain analysis are 16% higher compared to the measured values.

When the induction motor was invertor-fed with a time fundamental frequency of 50 Hertz, and loaded at full-load torque of 19 Lb.-ft., the efficiency was measured to be 73.6%. Under the same loading conditions and supply frequency, but with sinusoidal excitation, the efficiency was measured to be 79.8% (Figure 8.53).

Time domain analysis predicted considerably higher electro-magnetic torque than that predicted by harmonic analysis (harmonic analysis gives the closest prediction). This is considered to be due to two reasons. Firstly, time domain analysis uses an idealized voltage wave-form whose backward rotating harmonic contents are considerably lower than those actually present. Secondly, time domain analysis assumes that the main flux path iron loss does not absorb a part of electro-magnetic power flowing across the machine air-gap.

9.4 Torque Fluctuation of Invertor-fed Induction Motor

The torque fluctuation as predicted by time domain

analysis is shown in figures 8.45 and 8.46. At an average torque of 20 Lb.-ft. (supply frequency 50 Hertz) the torque fluctuation is 17.5% of the average torque. The percentage torque fluctuation increases as the load torque is decreased. The net torque fluctuation remains roughly constant over a certain range of average torque, and increases at high average torques. The torque fluctuation is independent of supply time fundamental frequency except at very low frequencies.

9.5 Bridge Thyristor and Bridge Diode Conduction Angle

From figures 8.38 and 8.39 it is seen that the bridge thyristor and bridge diode conduction angles at zero electro-magnetic torque are almost equal (= 90°) and then rapidly change up to a certain value of average torque, (thyristor conduction angle increasing and that of diode decreasing), and thereafter remains constant. Variation of the supply frequency has only a minor effect on the conduction angles.

9.6 Bridge Thyristor and Bridge Diode Peak Currents

The variation of the bridge thyristor peak current (which is the current at the instant of commutation) with average electro-magnetic torque is shown in figures 8.36

and 8.37. This peak current remains fairly constant up to a certain torque value and then increases rather rapidly with higher torques. For the motor under test the peak current at full-load torque of 19 Lb.-ft. was 182% of its value at zero torque. Variations of supply time fundamental frequency had only a small effect on the peak current.

9.7 Considerations of Design for Invertor-fed Induction Motors

In the author's opinion induction motors, for use with invertors, should be so designed that the peak current remains constant from no-load to full-load. This would considerably reduce both the capital and running cost of the invertors. Further, by this means torque pulsation would also remain at a low value over the whole operating range. It seems that there is a particular set of values for the induction motor equivalent circuit parameters which will give this optimum condition. The digital computer programme devised for time domain analysis is now being modified to calculate the optimal values of the induction motor equivalent circuit parameters in per unit quantities. It is hoped to publish details of this at a later date.

Since the invertor supply consists of various time harmonics, it can be postulated that these time harmonics react with some of the space harmonics of the motor air-gap flux to produce locking torques during the run-up period.

With the supply frequency adjustable the machine was started at a very low frequency and then run-up to the desired speed by gradual increase of supply voltage and frequency. No locking or crawling problem was therefore encountered.

In the experimental work reported no instability problem was experienced due to the main supply reservoir capacitors and the induction motor acting as a resonant L.C. circuit. However, future work on this project might include a thorough investigation of this possibility.

9.8 Further Discussion

A recent paper[22] gave a method for the prediction of instantaneous stator current and torque. The analysis is based on Park's 2-axis equations. (α' reference frame, figures 7.7 and 7.8.) To evaluate the instantaneous current the impedance matrix is inverted and then multiplied by the impressed (instantaneous) voltage. The impressed voltages are then expressed as an infinite series of step voltages. The instantaneous currents in each axis are determined by firstly evaluating the response current for each individual step by a Laplace transformation technique and then summing the response current for each individual step for all the infinite number of past steps.

The paper also gives a shortened method for approximate calculations of the instantaneous stator-line

current and torque. The predicted and measured currents were compared but no measurements were recorded for instantaneous torque. An active analogue circuit was also developed in this paper.

The time domain analysis carried out in chapter 7 departs considerably in the formulation and solution of the differential equations for the stator currents from the method given in the paper[22] referred earlier.

The Park's 2-axis equations given in figures 7.7 and 7.8 were transformed to equations giving hypothetical forward and backward rotating stator and rotor currents (Figure 7.13). The advantages arising from this translation to α" reference frame have been given in section 7.2.3. Having derived the equations giving stator and rotor currents along α" reference frame, the permanently short-circuited rotor reference axes were eliminated. The resulting impedance matrix being diagonal the admittance matrix was evaluated by inspection. The currents were then determined by a Laplace transformation technique which did not require the summation of infinite series (Appendix I). No attempt was made to find a shortened method for approximate calculation of the instantaneous stator-line currents and torques because of the availability of a digital computer. Time domain analysis was extended to predict the complete performance of induction motor under invertor

operation including the prediction of peak, r.m.s., average currents of bridge thyristors and bridge diodes. The conduction angles of the bridge thyristors and diodes were also predicted and compared with measured values.

9.9 Further Work

The prediction of harmonic stator-line currents and electro-magnetic losses in section 9.3 were very inaccurate. A detailed investigation employing an accurate loss measurement method should be carried out.

Further analysis of the invertor-motor combination should be carried out from the D.C. input terminals of the invertor. This would take into account the effect of the D.C. line chokes and also predict the wave-form of the alternating output voltage of the invertor.

Further refinement of analysis could be directed towards making the rotor speed a function of time. Such analysis would be of use at low speeds where the assumption of constant rotor speed is not valid.

The behaviour of the induction motor at the instant of switching on to an invertor supply and also for the few cycles after switching on are also of considerable interest. The equations for these cases would develop (after piece-wise linearization for variable rotor speed) as differential equations, the "initial conditions" of the dependent

variables being determined from another set of difference equations employing the number of lapsed cycles as the independent variable. This has the advantage that the same digital computer programme could be used to determine the induction motor performance during the first few cycles after switching on, as well as the steady-state performance This could be arranged by assigning to the variable denoting the number of cycles a small number or a very large number.

9.10 Final Summary

The invertor commutation circuit design equations and optimization described in chapter 2 has not been previously published and is considered to be original work. The design equations and the commutation circuit design curves (Figures 2.6 and 2.7) allow step-by-step design of single D.C. side impulse-commutated invertors. Application of the equations to other types of impulse-commutated invertor is outlined in section 9.1.

The time domain analysis given in chapter 7 is original although a method of determination of instantaneous line currents and torques had been previously published. The difference between the two approaches is outlined in section 9.8.

This analysis was used to enable calculation of the A.C. line currents and hence the bridge thyristor and diode

average, r.m.s. and peak current, which were required in the invertor design procedure. Time domain analysis was extended to predict the complete behaviour of the invertor-fed induction motor.

It was realized that time domain analysis would have limitations in loss prediction (especially for cage-rotor motors) because it assumes that the stator and rotor are smooth, and also that the air-gap flux is sinusoidally distributed. An idealized stator input voltage wave-form was used.

Harmonic analysis, in time and space, was developed. The determination of the main flux path iron loss (Chapter 6)under non-sinusoidal excitation is also considered to be original work. Although the effect of the form factor of the air-gap voltage on the magnitude of the main flux is given in various text books, no equations leading to the determination of the value of the iron loss analogue resistance for non-sinusoidal excitation are believed to exist. The author claims that the effect of non-sinusoidal excitation on main flux path, eddy current and hysteresis loss, discussed in sections 6.1.1 and 6.1.2 is a contribution to the knowledge of main flux path iron losses under conditions of non-sinusoidal excitation. The effect of non-sinusoidal excitation on load losses due to slot openings, however, was

not investigated because of shortage of time.

The equivalent circuit (Figure 6.2) developed for harmonic analysis in time and space is an extension of a published equivalent circuit (Figure 5.4) for an induction motor excited from a variable frequency sinusoidal source. This published equivalent circuit does not take into account the space harmonics of the machine air-gap m.m.f., which has a pronounced effect on stray load losses, especially for cage-rotor machines.

The prediction of the main flux path iron loss based on the line voltage wave-form showed that an invertor-fed induction motor has lower main flux path iron loss, which led the author to look rather closely into the effect of star/delta connection of the stator coils on the iron loss (Sections 6.2 and 7.8). It was shown that under non-sinusoidal excitation the iron loss must be calculated for line to neutral voltage wave-form and not for line voltage wave-form.

APPENDIX I

SOLUTION OF THE DIFFERENTIAL EQUATION

Equation 7.48 can be rewritten as

$$(p^2 + Bp + C)i = Kv_D(p + D) + jKv_Q(p + D)$$

or

$$(p - R_a)(p - R_b)i = Kv_D(p + D) + jKv_Q(p + D)$$

where R_a and R_b are the roots of the quadratic $p^2 + Bp + C = 0$.

$$\therefore \quad i = \frac{K(p + D)}{(p - R_a)(p - R_b)}v_D + j\frac{K(p + D)}{(p - R_a)(p - R_b)}v_Q \qquad (AI - 1)$$

The sequence currents are therefore composed of two components, one due to the direct axis excitation only, and the other due to quadrature axis excitation only. The solution can be obtained very neatly by utilizing a Laplace transformation technique.

A.I.1 Response Due to Direct Axis Excitation only

The direct axis exciting voltage wave-form is shown in figure 7.6. Denoting the instantaneous direct axis

voltage by v_D, the Laplace transformation of the wave-form for one cycle only is

$$V_{DO}(s) = \int_0^T v_D(t) e^{-st} dt$$

where T is the period of the direct axis voltage.

If $V_{1\ INV}^{RMS}$ is the r.m.s. value of the time fundamental of the idealized invertor output voltage then the height of each step of the direct axis voltage is given by (Figure 7.6 and Appendix II)

$$K_D = \text{Height of each step}$$

$$= \frac{\pi}{(6)^{\frac{1}{2}}3} L_V RMS_{1\ INV}$$

$V_{DO}(s)$ now has the form

$$V_{DO}(s) = K_D \frac{1}{s}\left[1 + e^{-\frac{T}{6}s} - e^{-\frac{T}{3}s} - 2e^{-\frac{T}{2}s} - e^{-\frac{2T}{3}s} + e^{-\frac{5T}{6}s} + e^{-Ts}\right] \qquad (AI - 2)$$

Taking periodicity into account, the Laplace transformation of the direct axis wave-form $V_D(s)$

$$V_D(s) = \frac{K_D}{s(1 - e^{-Ts})}\left[1 + e^{-\frac{T}{6}s} - e^{-\frac{T}{3}s} - 2e^{-\frac{T}{2}s}\right.$$

$$- e^{-\frac{2}{3}Ts} + e^{-\frac{5}{6}Ts} + e^{-Ts}\Big]$$

$$= K_D \frac{T_{DO}(s)}{s(1 - e^{-sT})} \qquad (AI - 3)$$

where

$$T_{DO}(s) = \Big[1 + e^{-\frac{T}{6}s} - e^{-\frac{T}{3}s} - 2e^{-\frac{T}{2}s} - e^{-\frac{2}{3}Ts} + e^{-\frac{5}{6}Ts} + e^{-Ts}\Big] \qquad (AI - 4)$$

= a factor which relates to the wave-form of the direct axis exciting voltage for one cycle only.

The component of current due to direct axis excitation only in the complex s domain is from equations AI - 1 and AI - 3

$$I_D(s) = \frac{K_D K(s + D)}{s(s - R_a)(s - R_b)} \frac{T_{DO}(s)}{1 - e^{-sT}}$$

and in partial fractions is

$$I_D(s) = K_D K\left[\frac{A_1}{s} + \frac{B_1}{s - R_a} + \frac{C_1}{s - R_b}\right] \frac{T_{DO}(s)}{1 - e^{-sT}} \qquad (AI - 5)$$

where the residues

$$A_1 = \frac{-D}{R_a R_b} \qquad (AI - 6)$$

$$B_1 = \frac{R_a - D}{R_a(R_a - R_b)} \qquad \text{(AI - 7)}$$

and $$C_1 = \frac{R_b - D}{R_b(R_b - R_a)} \qquad \text{(AI - 8)}$$

The principal terms of the partial fraction (Equation AI - 5) about the poles $s = R_a$ and $s = R_b$ are

$$A_D(s)_{s=R_a} = \frac{K_D K B_1}{s - R_a} \frac{T_{DO}(s)_{s=R_a}}{1 - e^{-R_a T}} \qquad \text{(AI - 9)}$$

$$A_D(s)_{s=R_b} = \frac{K_D K C_1}{s - R_b} \frac{T_{DO}(s)_{s=R_b}}{1 - e^{-R_b T}} \qquad \text{(AI - 10)}$$

The sum of the two principal terms is

$$A_D(s)_{s=R_a,R_b} = \frac{K_D K B_1}{s - R_a} K_{D1} + \frac{K_D K C_1}{s - R_b} K_{D2} \qquad \text{(AI - 11)}$$

where

$$K_{D1} = \frac{T_{DO}(s)_{s=R_a}}{1 - e^{-R_a T}} \qquad \text{(AI - 12)}$$

$$K_{D1} = \frac{T_{DO}(s)_{s=R_b}}{1 - e^{-R_b T}} \qquad \text{(AI - 13)}$$

The component of current due to direct axis excitation for one cycle is then given by

$$I_{DO}(s) = H(s)V_{DO}(s) - (1 - e^{-sT})A_D(s)_{s=R_a,R_b} \qquad \text{(AI - 14)}$$

where H(s) is the component of current due to direct axis impulse dirac excitation and is from equation AI - 1.

$$H(s) = \frac{K(s + D)}{s(s - R_a)(s - R_b)} \qquad (AI - 15)$$

Substituting equation AI - 15 in equation AI - 14 we obtain

$$I_{DO}(s) = \frac{K_D K(s + D)}{s(s - R_a)(s - R_b)} \left[1 + e^{-\frac{T}{6}s} - e^{-\frac{T}{3}s} - 2e^{-\frac{T}{2}s} - e^{-\frac{2}{3}Ts} + e^{-\frac{5}{6}Ts} + e^{-Ts} \right] - \frac{K_D K B_1}{s - R_a} \times K_{D1}(1 - e^{-sT}) - \frac{K_D K C_1}{s - R_b} K_{D2}(1 - e^{-sT})$$

$$= \frac{K_D K(s + D)}{s(s - R_a)(s - R_b)} - \frac{K_D K B_1}{s - R_a} K_{D1} - \frac{K_D K C_1}{s - R_b} \times K_{D2} + \frac{K_D K(s + D)}{s(s - R_a)(s - R_b)} e^{-\frac{T}{6}s} - \frac{K_D K(s + D)}{s(s - R)(s - R)} e^{-\frac{T}{3}s} - \frac{2K_D K(s + D)}{s(s - R_a)(s - R_b)} e^{-\frac{T}{2}s} - \frac{K_D K(s + D)}{s(s - R_a)(s - R_b)} e^{-\frac{2}{3}Ts} + \frac{K_D K(s + D)}{s(s - R_a)(s - R_b)} e^{-\frac{5}{6}Ts} + \frac{K_D K(s + D)}{s(s - R_a)(s - R_b)} e^{-Ts}$$

$$+ \frac{K_D K B_1}{s - R_a} K_{D1} e^{-sT} + \frac{K_D K C_1}{s - R_b} K_{D2} e^{-sT}$$

(A1 - 16)

Inverting the component of current due to direct axis excitation only for one cycle into the time domain gives

$$\begin{aligned} i_{DO}(t) = {} & K_D K\left[A_1 + B_1 e^{R_a t} + C_1 e^{R_b t}\right] - K_D K B_1 K_{D1} e^{R_a t} \\ & - K_D K C_1 K_{D2} e^{R_b t} + K_D K\left[A_1 \right. \\ & \left. + B_1 e^{R_a(t - \frac{T}{6})} + C_1 e^{R_b(t - \frac{T}{6})}\right] \\ & \times U(t - \tfrac{T}{6}) - K_D K\left[A_1 + B_1 e^{R_a(t - \frac{T}{3})} \right. \\ & \left. + C_1 e^{R_b(t - \frac{T}{3})}\right] U(t - \tfrac{T}{3}) - 2K_D K\left[A_1 \right. \\ & \left. + B_1 e^{R_a(t - \frac{T}{2})} + C_1 e^{R_b(t - \frac{T}{2})}\right] \\ & \times U(t - \tfrac{T}{2}) - K_D K\left[A_1 + B_1 e^{R_a(t - \frac{2}{3}T)} \right. \\ & \left. + C_1 e^{R_b(t - \frac{2}{3}T)}\right] U(t - \tfrac{2}{3}T) + K_D K\left[A_1 \right. \\ & \left. + B_1 e^{R_a(t - \frac{5}{6}T)} + C_1 e^{R_b(t - \frac{5}{6}T)}\right] \\ & U(t - \tfrac{5}{6}T) + K_D K\left[A_1 + B_1 e^{R_a(t - T)}\right. \end{aligned}$$

$$+ C_1 e^{R_b(t - T)}\Big]U(t - T) + K_D K\Big[K_{D1} B_1 e^{R_a(t - T)} + K_{D2} C_1 e^{R_b(t - T)}\Big] \times U(t - T) \qquad (AI - 17)$$

One cycle current response due to direct axis excitation only is

$$0 \leq t \leq \tfrac{T}{6}: \quad K_D K\Big[A_1 + B_1 e^{R_a t} + C_1 e^{R_b t} - B_1 K_{D1} e^{R_a t} - C_1 K_{D2} e^{R_b t}\Big]$$

$$\tfrac{T}{6} \leq t \leq \tfrac{T}{3}: \quad K_D K\Big[2A_1 + B_1 e^{R_a t}(1 + e^{-\frac{T}{6}R_a}) + C_1 e^{R_b t} \times (1 + e^{-\frac{T}{6}R_b}) - B_1 K_{D1} e^{R_a t} - C_1 K_{D2} e^{R_b t}\Big]$$

$$\tfrac{T}{3} \leq t \leq \tfrac{T}{2}: \quad K_D K\Big[A_1 + B_1 e^{R_a t}(1 + e^{-\frac{T}{6}R_a} - e^{-\frac{T}{3}R_a}) + C_1 e^{R_b t}(1 + e^{-\frac{T}{6}R_b} - e^{-\frac{T}{3}R_b}) - B_1 K_{D1} e^{R_a t} - C_1 K_{D2} e^{R_b t}\Big]$$

$$\tfrac{T}{2} \leq t \leq \tfrac{2}{3}T: \quad K_D K\Big[-A_1 + B_1 e^{R_a t}(1 + e^{-\frac{T}{6}R_a} - e^{-\frac{T}{3}R_a} - 2e^{-\frac{T}{2}R_a}) + C_1 e^{R_b t}(1 + e^{-\frac{T}{6}R_b} - e^{-\frac{T}{3}R_b} - 2e^{-\frac{T}{2}R_b}) - B_1 K_{D1} e^{R_a t}$$

$$- C_1 K_{D2} e^{R_b t} \Big]$$

$\frac{2}{3}T \leq t \leq \frac{5}{6}T$: $K_D K \Big[-2A_1 + B_1 e^{R_a t} (1 + e^{-\frac{T}{6}R_a} - e^{-\frac{T}{3}R_a} - 2e^{-\frac{T}{2}R_a} - e^{-\frac{2}{3}TR_a}) + C_1 e^{R_b t} (1 + e^{-\frac{T}{6}R_b} - e^{-\frac{T}{3}R_b} - 2e^{-\frac{T}{2}R_b} - e^{-\frac{2}{3}TR_b})$

$$- B_1 K_{D1} e^{R_a t} - C_1 K_{D2} e^{R_b t} \Big]$$

$\frac{5}{6}T \leq t \leq T$: $K_D K \Big[-A_1 + B_1 e^{R_a t} (1 + e^{-\frac{T}{6}R_a} - e^{-\frac{T}{3}R_a} - 2e^{-\frac{T}{2}R_a} - e^{-\frac{2}{3}TR_a} + e^{-\frac{5}{6}TR_a}) + C_1 e^{R_b t} (1 + e^{-\frac{T}{6}R_b} - e^{-\frac{T}{3}R_b} - 2e^{-\frac{T}{2}R_b} - e^{-\frac{2}{3}TR_b} + e^{-\frac{5}{6}TR_b}) - B_1 K_{D1} e^{R_a t}$

$$- C_1 K_{D2} e^{R_b t} \Big]$$

$T \leq t \leq \infty$: $K_D K \Big[B_1 e^{R_a t} (1 + e^{-\frac{T}{6}R_a} - e^{-\frac{T}{3}R_a} - 2e^{-\frac{T}{2}R_a} - e^{-\frac{2}{3}TR_a} + e^{-\frac{5}{6}TR_a} + e^{-TR_a}) + C_1 e^{R_b t} (1 + e^{-\frac{T}{6}R_b} - e^{-\frac{T}{3}R_b} - 2e^{-\frac{T}{2}R_b} - e^{-\frac{2}{3}TR_b} + e^{-\frac{5}{6}TR_b} + e^{-TR_b}) - B_1 K_{D1} e^{R_a t}$

$$\times(1 - e^{-R_aT}) - C_1K_{D2}e^{R_bt}(1 - e^{-R_bT})\Big]$$

$$= K_DK\Big[B_1e^{R_at}(1 - e^{-TR_a})K_{D1} + C_1e^{R_bt}(1 - e^{TR_b})$$

$$\times K_{D2} - B_1K_{D1}e^{R_at}(1 - e^{-R_aT})$$

$$- C_1K_{D2}e^{R_bt}(1 - e^{-R_bT})$$

$$= 0$$

This demonstrates the validity of the expressions.

(AI - 18)

A.I.2 Current Response Due to Quadrature Axis Excitation only

Following the procedure given in section A.I.1 the current response due to quadrature axis excitation only, for one cycle is

$$0 \leqslant t \leqslant \frac{T}{6}: \quad K_QK\Big[-\{B_1K_{Q1}e^{R_at} + C_1K_{Q2}e^{R_bt} + A_1$$

$$+ B_1e^{R_at} + C_1e^{R_bt}\}\Big]$$

$$\frac{T}{6} \leqslant t \leqslant \frac{T}{3}: \quad K_QK\Big[-B_1K_{Q1}e^{R_at} - C_1K_{Q2}e^{R_bt} + B_1e^{R_at}(-1$$

$$+ e^{-\frac{T}{6}R_a}) + C_1e^{R_bt}(-1 + e^{-\frac{T}{6}R_b})\Big]$$

$\frac{T}{3} \leqslant t \leqslant \frac{T}{2}$: $K_Q K\Big[-B_1 K_{Q1} e^{R_a t} - C_1 K_{Q2} e^{R_b t} + A_1$

$+ B_1 e^{R_a t}(-1 + e^{-\frac{T}{6}R_a} - e^{-\frac{T}{3}R_a})$

$- C_1 e^{R_b t}(-1 - e^{-\frac{T}{6}R_b} - e^{-\frac{T}{3}R_b})$

$\frac{T}{2} \leqslant t \leqslant \frac{2}{3}T$: Same as above. $(\frac{T}{3} \leqslant t \leqslant \frac{T}{2})$

$\frac{2}{3}T \leqslant t \leqslant \frac{5}{6}T$: $K_Q K\Big[-B_1 K_{Q1} e^{R_a t} - C_1 K_{Q2} e^{R_b t} + B_1 e^{R_a t}(-1$

$+ e^{-\frac{T}{6}R_a} + e^{-\frac{T}{3}R_a} - e^{-\frac{2}{3}TR_a})$

$- C_1 e^{R_b t}(-1 + e^{-\frac{T}{6}R_b} + e^{-\frac{T}{3}R_b}$

$- e^{-\frac{2}{3}TR_b})\Big]$

$\frac{5}{6}T \leqslant t \leqslant T$: $K_Q K\Big[-B_1 K_{Q1} e^{R_a t} - C_1 K_{Q2} e^{R_b t} - A_1 +$

$+ B_1 e^{R_a t}(-1 + e^{-\frac{T}{6}R_a} + e^{-\frac{T}{3}R_a}$

$- e^{-\frac{2}{3}TR_a} - e^{-\frac{5}{6}TR_a}) + C_1 e^{R_b t}(-1$

$+ e^{-\frac{T}{6}R_b} + e^{-\frac{T}{3}R_b} - e^{-\frac{2}{3}TR_b} - e^{-\frac{5}{6}TR_b})\Big]$

$T \leqslant t \leqslant \infty$: $K_Q K\Big[-B_1 K_{Q1} e^{R_a t}(1 - e^{-R_a T}) - C_1 K_{Q2} e^{R_b t}$

$\times(1 - e^{-R_b T}) + B_1 K_{Q1} e^{R_a t}(1 - e^{-R_a T})$

$$- C_1 K_{Q2} e^{R_1 t} \left(1 - e^{- R_b T}\right) \Bigg]$$

$$= 0$$

This checks the validity of the equations.

(AI - 19)

Where A_1, B_1 and C_1 are given by equations AI - 6, AI - 7 and AI - 8

K_Q = Height of quadrature axis voltage step.

$$= \frac{1}{3(2)^{\frac{1}{2}}} L_{V_1 \text{ INV}}^{\text{RMS}} \qquad \text{(AI - 20)}$$

$$T_{Q0}(s) = \left[-1 + e^{-\frac{T}{6}s} + e^{-\frac{T}{3}s} - e^{-\frac{2}{3}Ts} - e^{-\frac{5}{6}Ts} + e^{-Ts}\right] \qquad \text{(AI - 21)}$$

$$K_{Q1} = \frac{T_{Q0}(s)_{s=R_a}}{1 - e^{-R_a T}} \qquad \text{(AI - 22)}$$

$$K_{Q2} = \frac{T_{Q0}(s)_{s=R_b}}{1 - e^{-R_b T}} \qquad \text{(AI - 23)}$$

APPENDIX II

HARMONIC ANALYSIS OF INVERTOR IDEALISED OUTPUT VOLTAGE

A.II.1 Harmonic Analysis of Line to Line Voltage

The idealised line to line output voltage with axes axes selected for output voltage is shown in figure 7.5.

The output voltage expressed as a function of angle θ is given by

$$\begin{aligned} f(\theta) &= 0 && 0 \leqslant \theta \quad \frac{\pi}{6} \\ &= \hat{L_V}_{INV} && \frac{\pi}{6} \leqslant \theta \leqslant \frac{5\pi}{6} \\ &= 0 && \frac{5\pi}{6} \leqslant \theta \leqslant \pi \end{aligned}$$

The function so described is an odd function and in accordance with Fourier series

$$f(\theta) = \sum_{\gamma} b_{\gamma} \sin \gamma\theta d\theta$$

where the amplitude b_{γ} of the γ^{th} harmonic is given by

$$\begin{aligned} b_{\gamma} &= \frac{2}{\pi}\int_{0}^{\pi} f(\theta)\sin\gamma\theta d\theta \\ &= -\frac{2}{\pi}(\hat{L_V}_{INV})\ \frac{\cos\gamma\theta}{\gamma}\Bigg|_{\frac{\pi}{6}}^{\frac{5\pi}{6}} \end{aligned}$$

$$= \frac{2}{\pi} \frac{L\hat{V}_{INV}}{} \left[\cos \gamma \frac{\pi}{6} - \cos \gamma \frac{5\pi}{6} \right]$$

Now

$$\cos \gamma \frac{\pi}{6} = \cos \gamma \frac{5\pi}{6} \text{ for even values of } \gamma$$

and

$$\cos \gamma \frac{\pi}{6} = \cos \frac{5\pi}{6}$$

$$= 0 \text{ for triplen values of } \gamma$$

Further

$$\cos \gamma \frac{\pi}{6} - \cos \gamma \frac{5\pi}{6} = (3)^{\frac{1}{2}} \text{ for all values of } \gamma = (6K \pm 1)$$

where K = 0, 1, 2, 3 .... any positive integer.

Therefore the idealised output line to line voltage of the invertor consists time harmonics of the order $\gamma = (6K \pm 1)$ and devoid of any even and triplen harmonics.

The amplitude of the fundamental

$$b_1 = \frac{2(3)^{\frac{1}{2}}}{\pi} L\hat{V}_{INV}$$

The amplitude of the γ^{th} harmonic

$$b_\gamma = \frac{2(3)^{\frac{1}{2}}}{\pi} \frac{L_{V_{INV}}}{\gamma}$$

A.II.2. Harmonic Analysis of Line to Neutral Voltage

Figure 7.5 shows the idealised line to neutral voltage with axes selected for harmonic analysis.

Over a half cycle, the voltage expressed as a function of angle θ

$$f(\theta) = \frac{1}{3} L\hat{V}_{INV} \quad 0 \leqslant \theta \quad \frac{\pi}{3}$$

$$= \frac{2}{3} L\hat{V}_{INV} \quad \frac{\pi}{3} \leqslant \theta \leqslant \frac{2\pi}{3}$$

$$= \frac{1}{3} L\hat{V}_{INV} \quad \frac{2\pi}{3} \leqslant \theta \leqslant \pi$$

Since the function is odd it can be written as a Fourier series

$$f(\theta) = \sum_{\gamma=1} b_\gamma \sin \gamma\theta d\theta$$

where the amplitude b_γ of the γ^{th} time harmonic is given by

$$b_\gamma = \frac{2}{\pi}\int_0^{\pi} f(\theta)\sin\gamma\theta d\theta$$

$$= \frac{2}{\pi}\frac{L\hat{V}_{INV}}{3}\left[\int_0^{\frac{\pi}{3}} \sin\gamma\theta d\theta + 2\int_{\pi/3}^{\frac{2\pi}{3}} \sin\gamma\theta d\theta + \int_{\frac{2\pi}{3}}^{\pi} \sin\gamma\theta d\theta\right]$$

$$= \frac{2}{\pi} \frac{L\hat{V}_{INV}}{3} \left[-\frac{\cos \gamma\theta}{\gamma} \Big|_{0}^{\frac{\pi}{3}} - 2\frac{\cos \gamma\theta}{\gamma} \Big|_{\frac{\pi}{3}}^{2\pi/3} - \frac{\cos \gamma\theta}{\gamma} \Big|_{\frac{2\pi}{3}}^{\pi} \right]$$

$$= \frac{2}{\pi} \frac{L\hat{V}_{INV}}{3\gamma} \left[1 - \cos\frac{\gamma\pi}{3} + 2\cos\frac{\gamma\pi}{3} - 2\cos\frac{2\pi}{3}\gamma + \cos\gamma\frac{2\pi}{3} - \cos\gamma\pi \right]$$

$$= \frac{2}{\pi} \frac{L\hat{V}_{INV}}{3\gamma} \left[1 + \cos\gamma\frac{\pi}{3} - \cos\gamma\frac{2\pi}{3} - \cos\gamma\pi \right]$$

The term

$$\left[1 + \cos\frac{\gamma\pi}{3} - \cos\gamma\frac{2\pi}{3} - \cos\gamma\pi \right] = 0 \text{ for all triplen values of } \gamma$$

$$= ? \text{ for all even values of } \gamma$$

$$= 3 \text{ for } \gamma = (6K \pm 1)$$

where K = 0, 1, 2, 3, etc.

Therefore

$$b_\gamma = \frac{2}{\pi\gamma} L\hat{V}_{INV} \text{ for } = \gamma(6K \pm 1)$$

$$= 0 \text{ for } \neq (6K \pm 1)$$

The amplitude of the fundamental component

$$b_1 = \frac{2}{\pi} L\hat{V}_{INV}$$

A.II.3 R.M.S. Value of the Idealised Line to Line Voltage in terms of its Step-height

Referring to figure 7.5, the r.m.s. value of the idealised line to line invertor output voltage

$$L_{V_{INV}}^{RMS} = \left[\frac{1}{2\pi}\left\{(L\hat{V}_{INV})^2 \frac{2\pi}{3} + (L\hat{V}_{INV})^2 \frac{2\pi}{3}\right\}\right]^{1/2}$$

$$= \left(\frac{2}{3} L_{V_{INV}}\right)^2$$

A.II.4 R.M.S. Value of the Idealised Line to Line Voltage in terms of the R.M.S. Value of its Time Fundamental

From section A.II.1 the amplitude of the time fundamental = $\frac{2(3)^{\frac{1}{2}}}{\pi} L\hat{V}_{INV}$

$\therefore$ R.M.S. value of the time fundamental $L_{V_{1\ INV}}^{RMS} = \frac{(6)^{\frac{1}{2}}}{\pi} L\hat{V}_{INV}$

$$L\hat{V}_{INV} = \frac{\pi}{(6)^{\frac{1}{2}}} L_{V_{1\ INV}}^{RMS}$$

$$L_{V_{INV}}^{RMS} = \frac{\pi}{3} L_{V_{1\ INV}}^{RMS}$$

A.II.5 Average Value of the Idealised Invertor Line to Line Voltage in terms of its Step-height

Referring to figure 7.5,

$$L_{V_{INV}}^{AV} = \frac{1}{\pi}\left\{L\hat{V}_{INV}\ \frac{2\pi}{3}\right\}$$

$$= \frac{2}{3}\ L\hat{V}_{INV}$$

A.II.6 Form-factor of Idealised Invertor Line to Line Voltage

$$\text{Form-factor } {}^{L}K_{f\ INV} = \frac{L_{V_{INV}}^{RMS}}{L_{V_{INV}}^{AV}}$$

$$= \frac{(2)^{\frac{1}{2}}}{(3)^{\frac{1}{2}}}\ L\hat{V}_{INV}\ \frac{3}{2}\ \frac{1}{L\hat{V}_{INV}}$$

$$= (1.5)^{\frac{1}{2}} = 1.225$$

A.II.7 R.M.S. Value of Invertor Idealised Line to Neutral Voltage in terms of Idealised Line to Line Voltage Step

Referring to figure 7.5, the r.m.s. value

$$P_{V_{INV}}^{RMS} = \left[\frac{1}{\pi}\left\{\left(\frac{1}{3}\ L\hat{V}_{INV}\right)^2 \frac{\pi}{3} + \left(\frac{2}{3}\ L\hat{V}_{INV}\right)^2 \frac{\pi}{3} + \frac{1}{3}\left(L\hat{V}_{INV}\right)\frac{\pi}{3}\right\}\right]^{\frac{1}{2}}$$

$$= L\hat{V}_{INV}\left(\frac{1}{3x9} + \frac{4}{3x9} + \frac{1}{3x9}\right)^{\frac{1}{2}}$$

$$= \frac{L\hat{V}_{INV}}{(3)^{\frac{1}{2}}} (6/9)^{\frac{1}{2}} = \frac{(2)^{\frac{1}{2}}}{3} L\hat{V}_{INV}$$

A.II.8 R.M.S. Value of Invertor Idealised Line to Neutral Voltage in terms of its Time Fundamental R.M.S. Value

From section A.II.2, the amplitude of the time fundamental of idealised line to neutral voltage = $\frac{2}{\pi} L\hat{V}_{INV}$.

The r.m.s. value of the time fundamental is then

$$P_V{}^{RMS}_{1\ INV} = \frac{(2)^{\frac{1}{2}}}{\pi} L\hat{V}_{INV}$$

$$\therefore \quad L\hat{V}_{INV} = \frac{\pi}{(2)^{\frac{1}{2}}} P_V{}^{RMS}_{1\ INV}$$

From section A.II.7,

$$P_V{}^{RMS}_{INV} = \frac{\pi}{3} P_V{}^{RMS}_{1\ INV}$$

A.II.9 Average Value of Invertor Idealised Line to Neutral Voltage in terms of Idealised Line to Line Voltage Step

Referring to figure 7.5, the average value

$$P_V{}^{AV}_{INV} = \frac{1}{\pi}\left[\left\{(\tfrac{1}{3})(L\hat{V}_{INV})\right\}\frac{\pi}{3} + \left\{(\tfrac{2}{3})(L\hat{V}_{INV})\right\}\frac{\pi}{3} + \left\{(\tfrac{1}{3})(L\hat{V}_{INV})\right\}\frac{\pi}{3}\right]$$

$$= L\hat{V}_{INV}\left\{\frac{1}{9} + \frac{2}{9} + \frac{1}{9}\right\} = \frac{4}{9} L\hat{V}_{INV}$$

A.II.10 Form-factor of Idealised Invertor Line to Neutral Output Voltage

$$\text{Form-factor } {}^{P}K_{f\ INV} = \frac{P_{V}RMS_{INV}}{P_{V}AV_{INV}}$$

$$= \frac{(2)^{\frac{1}{2}}}{3} \hat{L}_{V_{INV}} \frac{9}{4} \frac{1}{\hat{L}_{V_{INV}}}$$

$$= \frac{3}{2(2)^{\frac{1}{2}}} = 1.061$$

REFERENCES

1. BRADLEY, D.A.; CLARK, C.D.; DAVIS, R.M.; JONES, D.A.: 'Adjustable-frequency invertors and their application to variable speed drives', Proc. I.E.E., 1964, 111, (11), p. 1833.

2. G.E.: 'Thyristor Manual' (a book), 1964.

3. WESTINGHOUSE: 'Thyristor Manual' (a book), 1964.

4. GUTZWILLER, F.W.; SYLVAN, T.P.: 'Power semi-conductor ratings under transient and intermittent loads', A.I.E.E., 1961, January.

5. HAUGE, B: 'Mathematical treatment of the m.m.f. of the armature winding', J.I.E.E., 1917, 55, 489.

6. GRAHAM, Q: 'M.M.F. of poly-phase winding', J.I.E.E., 1927, 46, 19.

7. ALGER, P.L. 'Nature of poly-phase induction motor', (a book), Wiley, 1951.

8. AGARWAL, P.D.; ALGER, P.L.: 'Saturation factors for leakage reactance of induction motors', Trans. A.I.E.E., 1961, 80, p. 1037.

9. POSTONIKOV, N.W.: 'Stray torques and losses from higher harmonics of armature reaction in squirrel-cage induction motors', Elektrichestvo, 1963, No. 7, p. 39.

10. LIWSCHITZ-GARIK, M: 'Electrical Machinery', Vol. II, (a book), Van Nostrand, 1961.

11. RICHTER, R: 'Elektrische Maschinen', Vol. IV, Verlag Birkhauser, 1954.

12. CHRISTOFIDES, N: 'Ph.D. thesis', University of London, 1966, July.

13. WEBER, C.A.M.; LEE, F.W.: 'Harmonics due to slot openings', J.A.I.E.E., 1924, 43, p. 687.

14. APAROFF, B.P.: 'Influence of the slot harmonics on the torque-speed curve of the induction motor', Publ. National Research Institute (Moscow), 1924, 1: 47.

15. HO, H.: 'Induction motor operation under variation of supply frequency', International Journal of Electrical Engineering Education, Vol. I, 1963-64, p. 375.

16. KRON: 'Tensor Analysis', (a book), Dover, 1959.

17. ADKINS, B.: 'Generalized machine theory', (a book), Chapman and Hall, 1957.

18. JEVONS, M.: 'Electrical machine theory', (a book), Blackie, 1966.

19. LAITHWAITE, E.R.: 'Differences between series and parallel connection in machines with asymetric magnetic circuits', Proc. I.E.E., 1965, 112, (11), p. 2074.

20. KOSTENKO, M.; PIOTROVSKY, L.: 'Electrical Machines', Vols. I and II, (a book), Foreign Languages Publishing House, Moscow.

21. CHRISTOFIDES, N.; ADKINS, B.: 'Determination of load losses and torques in squirrel-cage induction motors', Proc. I.E.E., 1966, 113, (12), p. 1995.

22. WARD, E.E.; KAZI, F.I.E.E.; FARKAS, R.: 'Time-domain analysis of the invertor-fed induction motor', Proc. I.E.E., 1967, 114, (3), p. 361.